Apparatus for Simultaneous Measurement of Internal Combustion Engine Ring/Liner Oil Film Thickness and Friction

by

Janice Vivienne Dearlove

S.B., Massachusetts Institute of Technology (1991)
S.B., Massachusetts Institute of Technology (1992)

Submitted to the Department of Mechanical Engineering
in partial fulfillment of the requirements for the degree of

Master of Science in Mechanical Engineering

at the

MASSACHUSETTS INSTITUTE OF TECHNOLOGY

September 1994

Author .....
Department of Mechanical Engineering
August 22, 1994

Certified by .....
Wai K. Cheng
Associate Professor
Thesis Supervisor

Accepted by .....
A. A. Sonin
Chairman, Departmental Committee on Graduate Students

Apparatus for Simultaneous Measurement of Internal Combustion Engine Ring/Liner Oil Film Thickness and Friction

by

Janice Vivienne Dearlove

Submitted to the Department of Mechanical Engineering
on August 22, 1994, in partial fulfillment of the
requirements for the degree of
Master of Science in Mechanical Engineering

Abstract

This thesis reports on the simultaneous measurement of internal combustion engine ring/liner oil film thickness and friction using a reciprocating test apparatus. The design, construction and instrumentation of the apparatus are presented. Friction measurements are compared to rig and in-engine test results previously described in the literature. Observations of the experimental behavior of the test apparatus are detailed. Results are presented from a test matrix of five lubricating oils of viscosity ranging from 38 to 226 cP, at three mean piston speeds of 0.45, 0.67 and 0.89 m/s and at three normal ring pressures of 0.48, 0.95 and 1.9 MPa. The data were highly repeatable and patterns indicative of mixed lubrication and trends towards hydrodynamic lubrication were exhibited. Oil film thickness and friction coefficient results are consistent with the physical understanding of ring/liner lubricant friction behavior.

Thesis Supervisor: Wai K. Cheng
Title: Associate Professor

Acknowledgments

There are many people who have provided joy and humor and have inspired learning in my life these last two years and I fear that I may not adequately acknowledge them.

This research was sponsored by the Consortium on Lubrication in Internal Combustion Engines. Durga Rao and Joseph Aksamit at Ford Motor Company furnished the piston rings and liner samples for the rig, as well as the original design. David Fiedler of Dana Corporation provided the ring etching and ring profile measurements, as well as general information on the piston rings. Philip Burnett of Shell Development Company gave oil data and imparted helpful advice on this project.

Wai Cheng, the advisor for the research presented herein, was approachable, enthusiastic, supportive, honest and always willing to work an idea through. I learned many things from working with him in the laboratory.

Brian Corkum was an invaluable aid in the test rig construction and Viktor Dubrowski did a careful and meticulous job on the L.I.F. machining. On the administrative side, Joan Kenney was extremely helpful and supportive.

I am especially indebted to the students at the Sloan Automotive Laboratory, who have provided advice, research insight and technical experience: Leon Bronchstein, Jonathan Fox, Haissam Haidar, Douglas Hamrin, Peter Hinze, R.B. Laurence, Michael Norris, Bouke Noordzij, Goro Tamai and Richard Versteegh. Special thanks to Tian Tian for his theoretical insights, Mark Lusted for risking limb if not life, Eric Deutsch for his unique and honest friendship and Gatis Bazbauers for coffee breaks and conversation.

Finally, thank you to Mihnea for eight wonderful years. *Te iubesc.*

Dedication

To my father,

for giving me freedom to define my dreams and faith in my ability to achieve them.

Contents

List of Figures

List of Tables

Chapter 1

Introduction

1.1 Motivation

The focus of this work is the experimental measurement of friction and oil film thickness between the ring and liner of an internal combustion engine, utilizing a reciprocating test rig. The internal combustion engine was first developed in 1860 by Jean J. Lenoir and is still used to power modern day automobiles. Main issues in the development of the internal combustion engine have included: improved quality of engine emissions, greater engine power density, increased engine durability and improved engine efficiency. This last issue can be approached by considering the ability of a particular engine to utilize the fuel energy available to it and, naturally, affects the third issue of durability. A more quantitative measurement of engine efficiency is the product of two quantities: the fuel conversion efficiency of the engine, η_f and the mechanical efficiency, η_m. The latter is defined as the ratio of the brake, or usable, power to the indicated power [1, p.49] In other words, a mechanical efficiency index of one means that all the mechanical energy released from combustion is transferred to usable power to drive the automobile transmission system. Mechanical efficiency can also be expressed as one minus the ratio of total friction power to gross indicated power, where total friction power is power other than that transferred to the automobile wheels, such as: engine rubbing friction, pumping work and power to drive the engine accessories. Typical automobile spark ignition engine mechanical efficiencies

are in the neighborhood of 0.7, depending on load and speed, indicating a significant loss of power to friction. This can dictate a variety of improvements to engine efficiency, such as altering the combustion process to produce greater available energy and indicated power or decreasing the magnitude of friction power. The latter is the motivation for this research.

Total friction power is an all-encompassing term. Its components have been studied and it has been found [1, p.713] that the piston-crank assembly has the greatest contribution to the total friction (approximately 50%). The piston-crank assembly friction is dominated by the ring/liner friction, which constitutes approximately 25% of the piston-crank assembly friction.

Thus, if two identical cars, one without ring/liner friction, were to be driven under the same conditions (such as: speed, load, and road route), the car without ring/liner friction would have one-eighth less total friction and a corresponding increase in brake power of 14%. In addition, without friction or wear, the engine would have a longer life.

It is the goal of this research to recognize the role of ring/liner friction in engine power loss and the consequent importance of understanding the mechanisms of ring/liner friction in a detailed qualitative and quantitative manner.

1.2 Approach

The approach herein is to simultaneously measure the ring/liner friction and the oil film thickness in a reciprocating test rig. This research will focus on isolating the friction contribution of a single ring and liner so that there are no secondary factors, such as the friction of the piston skirt, second ring or oil control ring, affecting the experiment. This is best achieved through use of a rig which simulates the ring/liner interaction outside of the engine. However, the results should be applicable to actual engine conditions and so it is desired to reproduce those conditions, such as ring and liner material surface finishes, stroke length, temperature, engine speed, and lubricant properties. It should also be recognized that a test rig will not be able to realistically

reproduce the cyclic gas loading on the piston ring. A test apparatus is less expensive and less time-consuming than full engine tests and can provide initial results cheaply and quickly before further, more extensive engine tests are performed.

1.3 Background

1.3.1 Definitions

Figure 1-1 shows a schematic of an internal combustion engine liner and reciprocating apparatus. The piston moves up and down within the liner in the axial direction through a mechanical link to a connecting rod, which is mounted on the revolving engine crankshaft. The direction from the center of the piston out towards the liner is referred to as the radial direction and the direction following the curvature of the liner, the circumferential direction. Figure 1-2 diagrams the ring/liner interface in the presence of a lubricating film. The point along the liner at which the lubricant contacts, or wets, the ring is called the inlet, and the axial location is denoted by x_1. The thickness of the lubricant is represented by $h(x)$ and, under the ring, the minimum oil film thickness is h_0. The lubricant exits from under the ring at the outlet, x_2, and the region under the ring, between the inlet and outlet is termed the subring region.

1.3.2 Friction

The role of mechanical friction has previously been studied extensively. This section offers some technical background for a detailed and thorough discussion of results. The ring is pushed against the liner in the radial direction by the combustion gas pressure loading and the ring tension. The latter is also known as the elastic pressure, which is produced by the spring-like nature of the ring material, compressed to fit in the liner. Typical ring tension is 0.2 MPa and typical radial gas pressure during firing is 1 to 2 MPa. The force exerted by the ring radially on the liner is generally referred to as the ring load, normal force, normal load, F_{normal} or F_N. This produces

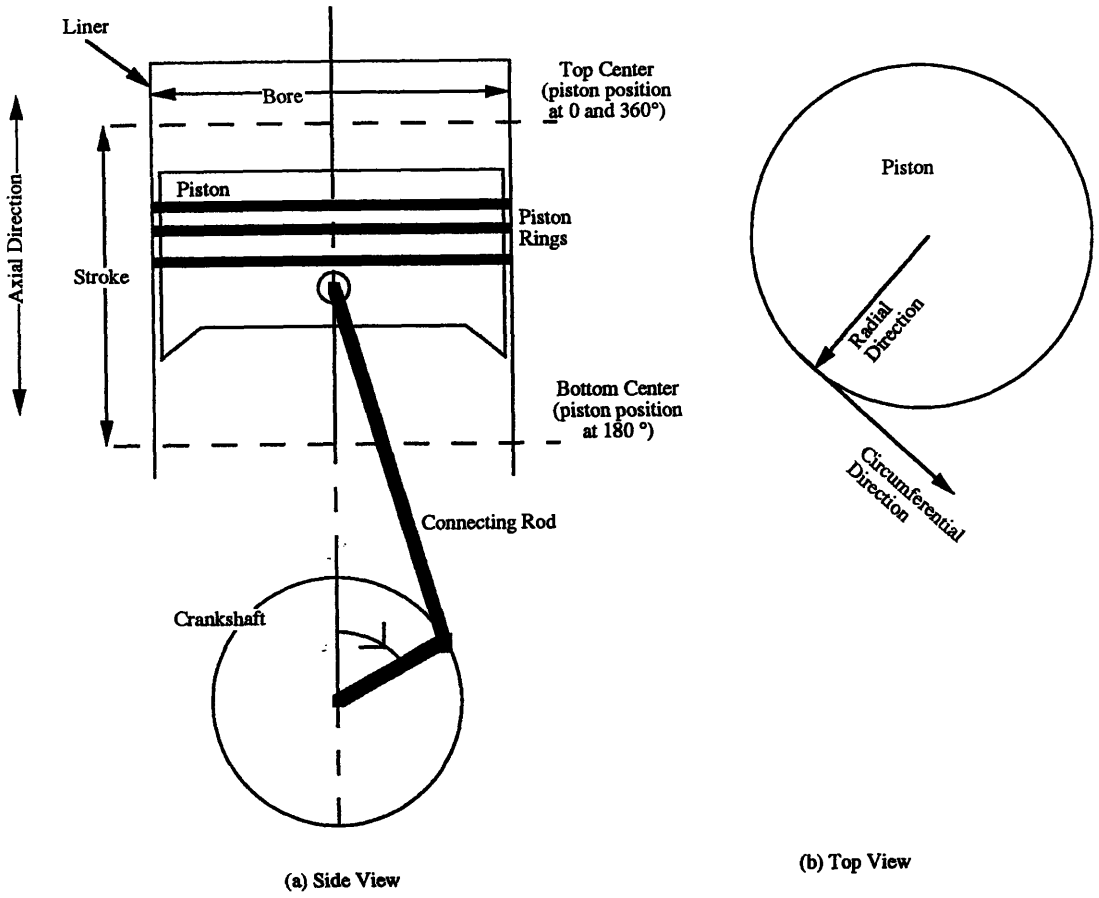

Figure 1-1: Schematic of the Engine Liner, Piston and Connecting Rod

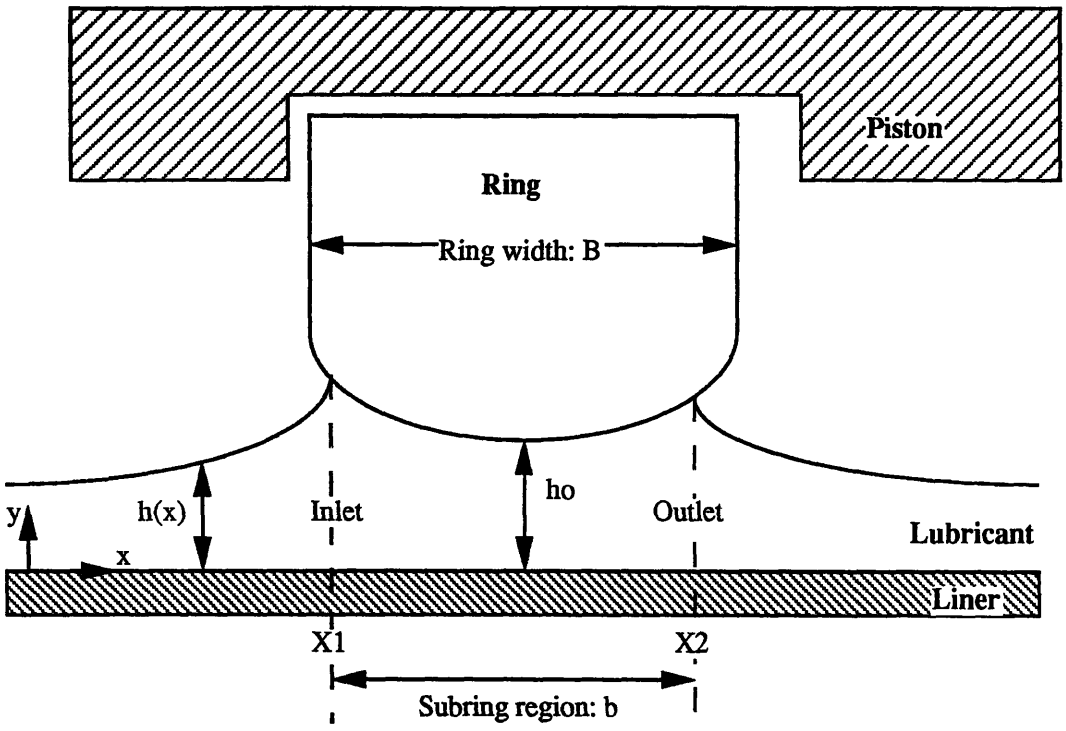

Figure 1-2: Terminology of Ring/Liner Interaction

a friction force in the direction opposite to that of sliding motion, denoted by $F_{friction}$ or F_F. These forces are illustrated in Figure 1-3. The ratio of the friction force to the normal force is the friction coefficient, C_f.

$$C_f = \frac{F_F}{F_N} \tag{1.1}$$

The value of C_f depends on the relative sliding velocity, lubricant viscosity, normal pressure (the normal load divided by the area of contact) and the width of the lubricant over which sliding occurs, known as the sliding pad width. The dependence is generally illustrated in a Stribeck diagram, in which the coefficient of friction is plotted on the vertical axis with a logarithmic scale against a dimensionless parameter, the Sommerfeld Number, $\frac{\mu U}{\sigma c}$, viscosity times sliding speed divided by loading pressure times the width of the sliding pad. An example is shown in Figure 1-4. The first regime, boundary lubrication, operates at a friction coefficient of the order of 0.1, and indicates conditions of wear, or solid friction (metal to metal contact). In this

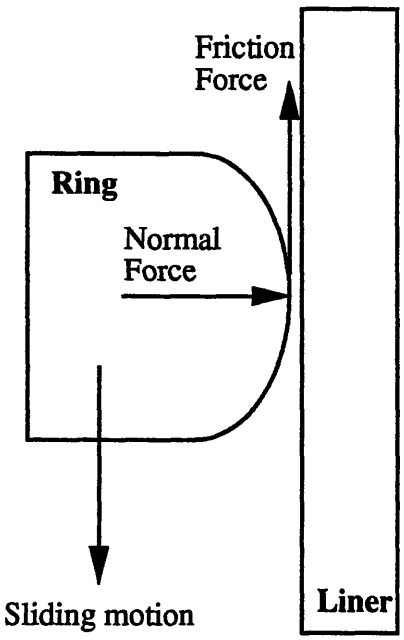

Figure 1-3: Forces in the Ring/Liner Interaction

regime, the coefficient of friction is roughly independent of speed. The third regime is hydrodynamic lubrication where the two sliding surfaces are completely separated by the lubricating film. The corresponding friction coefficient is 0.001 to 0.005. It is independent of the surface material and is generally accepted to be related to a power of the Sommerfeld number. The transition between these two regimes is called mixed lubrication, and has properties corresponding to those of both hydrodynamic and boundary lubrication. It has been found that ring/liner friction operates in all three regimes [2].

1.4 Related Research

1.4.1 Friction

Ring/liner friction experimental research comprises both non-engine test apparatus and in-engine experiments. The latter have focused on adapting production engines

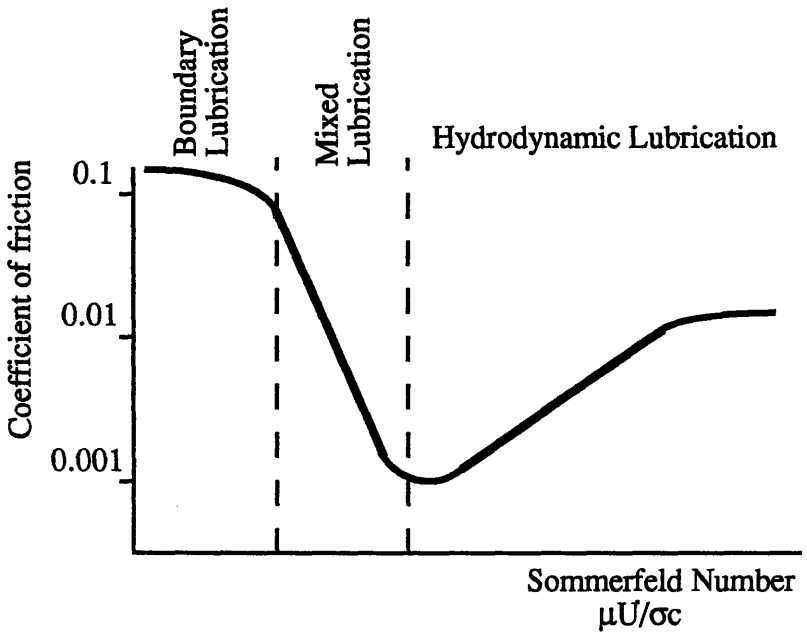

Figure 1-4: Stribeck Diagram

for friction measurements. A test procedure using a floating liner, first developed by Taylor and Forbes, was used by Yoshida et. al. [3], in which a single cylinder diesel engine liner is altered. The liner responds to the friction force exerted by the piston and rings, allowing for transmission of the friction force to two transducers mounted on opposite sides of the liner to the block. This is shown in Figure 1-5.

Similarly, Gauthier et. al. [4] studied friction losses in a single cylinder diesel engine adapted with a floating liner, in which the liner was isolated from the block and cylinder head with three force sensors located between the bore and block to capture all the force components on the liner. A drawing is shown in Figure 1-6. The zero friction force points at dead centers were used to locate the endstrokes. Results were presented for motored and fired conditions and for varying viscosities and speeds. The results obtained from varying viscosity display the role of boundary friction, which was observed in data taken at 500 rpm, both at stroke end and center. It was concluded that a minimal viscosity is necessary for hydrodynamic lubrication for the range of operating conditions.

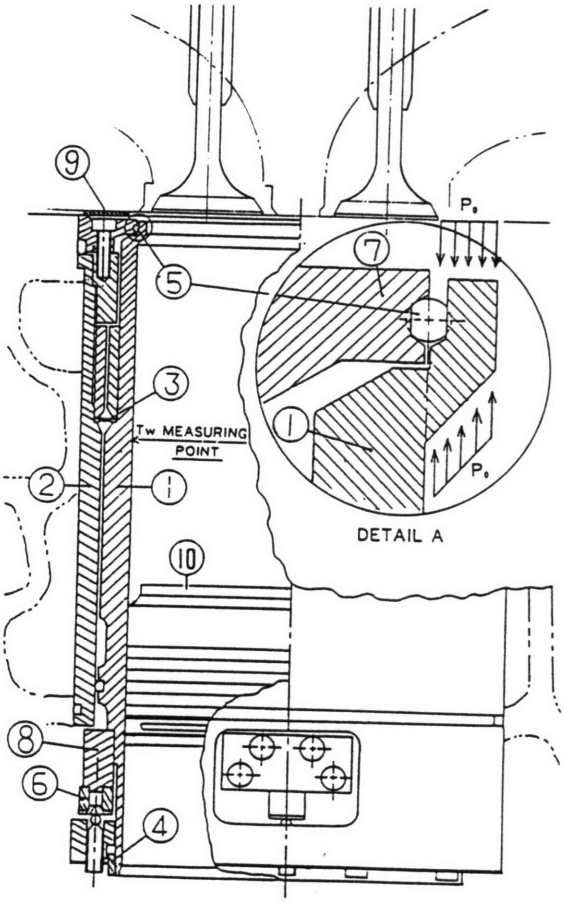

1. CYLINDER LINER
2. LINER SUPPORT
3. LATERAL STOPPER (UPPER SIDE)
4. LATERAL STOPPER (LOWER SIDE)
5. GAS SEAL O-RING
6. PIEZO PICKUP
7. O-RING HOLDER
8. PIEZO PICKUP HOLDER
9. HEAD GASKET
10. PISTON

Source: SAE Paper 900589

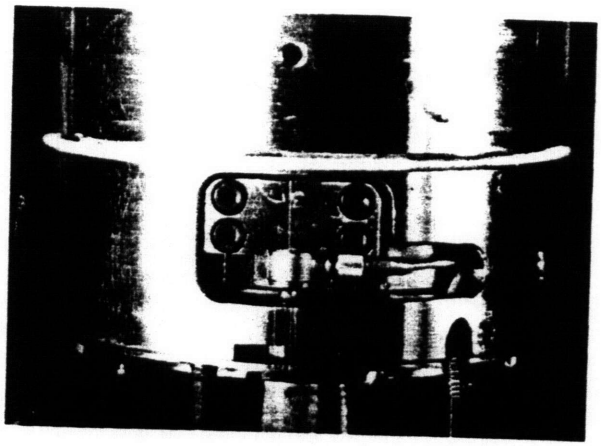

Figure 1-5: Movable Liner Test Apparatus

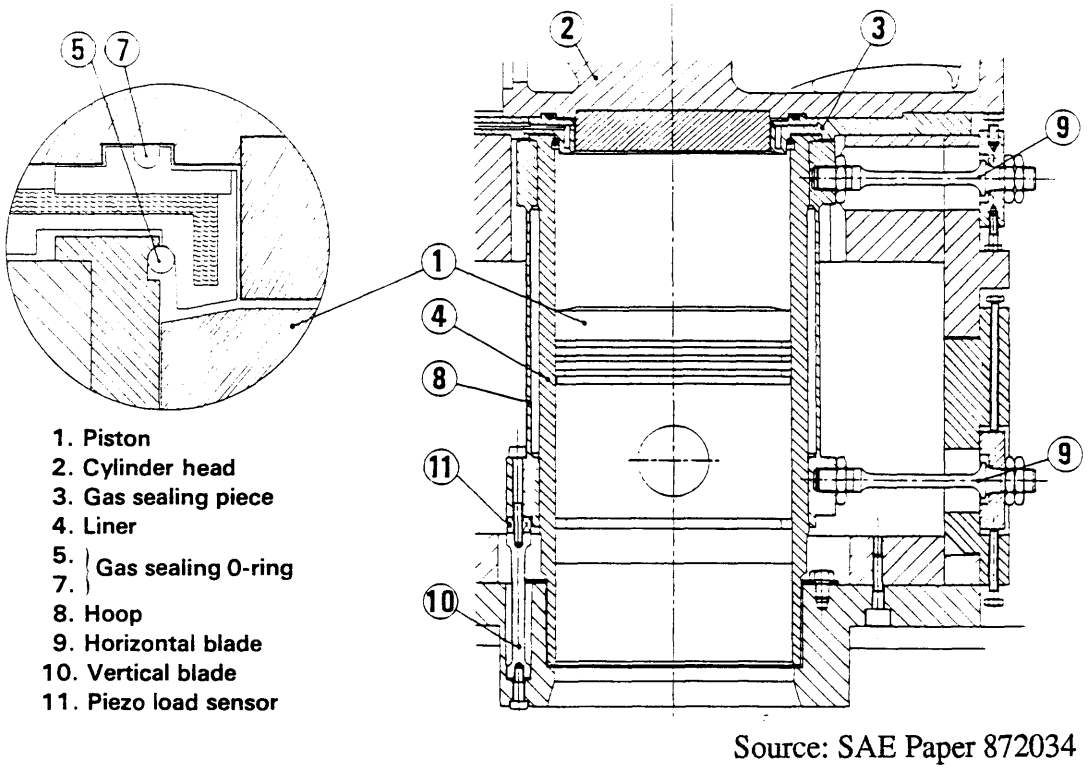

Figure 1-6: Floating bore

A later version of the floating liner, designed to be less susceptible to structural vibration, is the fixed sleeve method [5]. The design is shown in Figure 1-7. One cylinder of a production engine was modified for friction force measurements and the engine was operated under motored and fired conditions. The liner of one cylinder was replaced by two concentric sleeves, held together at the base by a pair of lock nuts. The outer sleeve replaced the liner and the inner sleeve was slightly below the engine head, which left a rim subject to gas pressure during the engine operating cycle. This gas pressure and the friction force were measured by sixteen pairs of strain gauge bridge circuits on the inner and outer surfaces of a narrow section of the outer sleeve. The use of a pressure transducer allowed for cancellation of the gas pressure force. Although there were modifications to the cylinder, the use of the fixed sleeve method allowed for optimal replication of actual engine conditions. This paper has several findings. First, major differences in magnitude between motored and fired results were found to occur at the beginning of the power stroke, but the results were similar in shape and magnitude for the rest of the cycle. Friction was

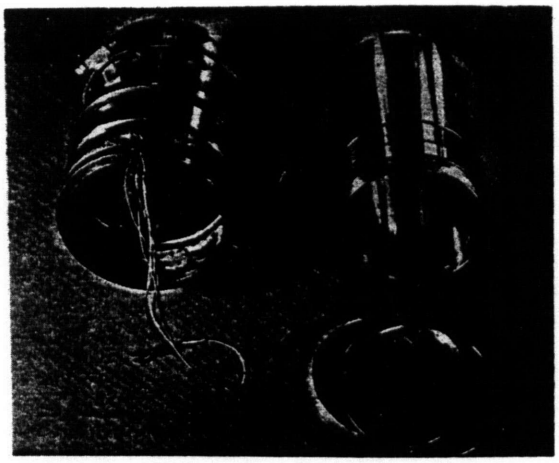

(a)

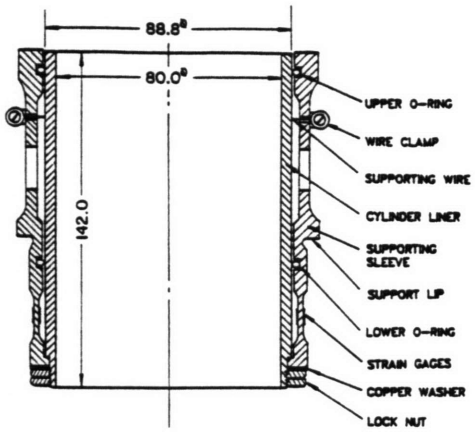

(b)

Source: SAE Paper 880571

Figure 1-7: Fixed Sleeve Experimental Design

not significantly changed as the engine speed was varied from 850 to 2,000 rpm. However, friction behavior did vary with lubricant and coolant temperature. At an oil temperature of 35° C, the friction was higher at midstroke and lower at endstroke than the friction measured at higher temperature. This was attributed to increased viscosity at lower temperature and thus increased hydrodynamic drag at midstroke. The liner surface finish was also found to affect friction, when machined and honed liner friction results were compared. Additionally, the rings were successively removed from the piston to investigate individual effects. These tests were conducted with the engine motored at 500 rpm. It was found that oil control ring friction dominates the ring pack and surmised that removal of the oil control ring resulted in larger amounts of oil left on the liner during engine operation and therefore gave a hydrodynamic characteristic to friction of the top and second ring alone. This analysis was conducted without instrumentation for measuring the radial load of the ring on the liner and thus derivation of the friction coefficient. Assumptions about lubrication regimes were made on the basis of the friction curve shape.

These adapted-engine experiments have the advantage of being able to closely replicate engine (including firing) conditions, such as speed and liner temperature, but do not allow for separation of friction effects of the piston body from the effects of

individual piston rings under normal engine operating conditions. This separation can be achieved through the use of a test rig, some examples of which are described below.

A test apparatus for measuring friction generally consists of: a mechanism for providing reciprocating motion to a ring holder, which functionally replaces the piston, a rig simulating the ring/liner interaction and an oil feed system. Ting [2, 6] describes a test apparatus in which a horizontal liner sample is moved in a reciprocating motion, by use of a slider crank mechanism. The apparatus has a realistic stroke length. A stationary ring segment is held against the liner segment by weights applied to the arm supporting the ring segment as shown in Figure 1-8. The oil is fed by a drip mechanism. The rig allows for simultaneous normal and friction force measurement, and direct sliding velocity measurement. The main purpose of the apparatus is to understand the behavior of the instantaneous piston ring friction coefficient, through use of a modified Stribeck diagram. The results presented were gathered at room temperature, for engine rotational speeds of 100 to 500 rpm, ring contact loads of 40 to 80N, fully flooded lubricant conditions, new bore/ring specimens, a single ring and oils 5W30 and SAE50. Ting's results include friction coefficients of 0.01 to 0.05 and friction force and friction coefficient traces similar to those of current literature.

A similar test apparatus, developed by Hartfield-Wünsch et. al. [7] uses a modified Cameron-Plint High Frequency Friction Tester to investigate engine cylinder component friction and wear. This is shown in Figure 1-9. A section of cylinder liner is fixed horizontally, immersed in an oil bath of 5W30 oil and heated from below to $120°C$. A top ring segment is held in a fixture, shown in part b of the figure, and moved horizontally in a reciprocating motion by a scotch-yoke mechanism, at a rotational speed of 600 revolutions per minute and a stroke length of 10 mm. A spring balance loads the ring against the liner. This is the only reference found which addresses ring conformance to the liner curvature. The ring holder is built to allow the ring to conform to the liner. There are three pins in the ring holder. The load is applied through the center pin and the two outer pins restrain the ring in the fixture. This allows the ring to self-align to the liner curvature. The arrangement is difficult to evaluate

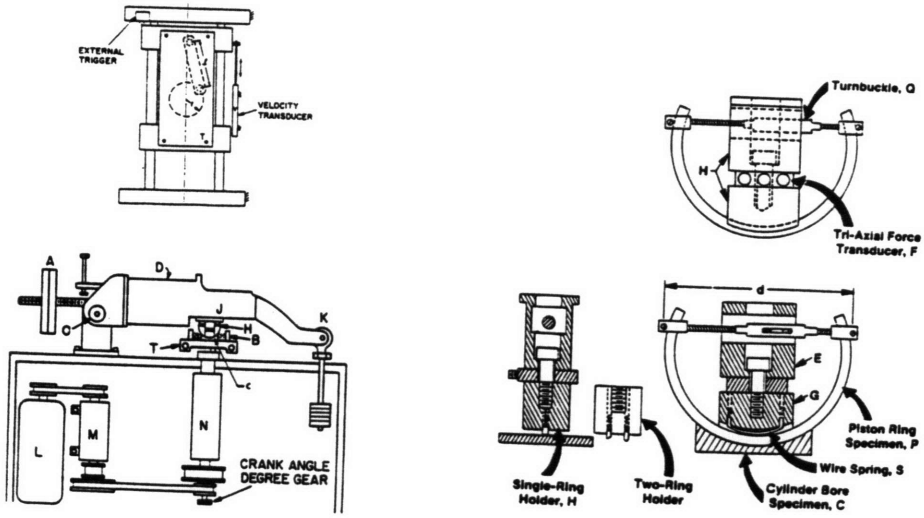

(a)

(b)

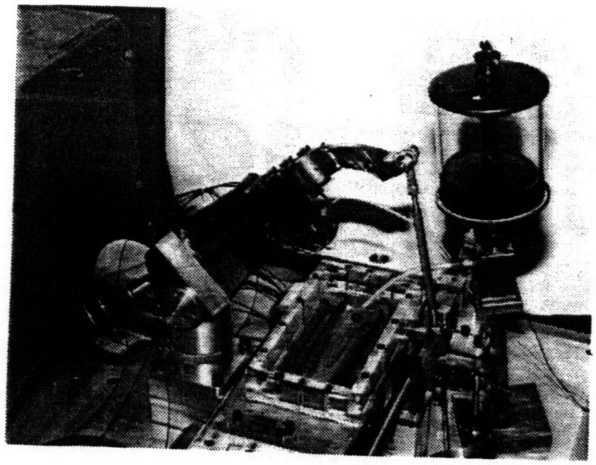

(c)

Source: SAE Paper 930685

Figure 1-8: Reciprocating Test Rig

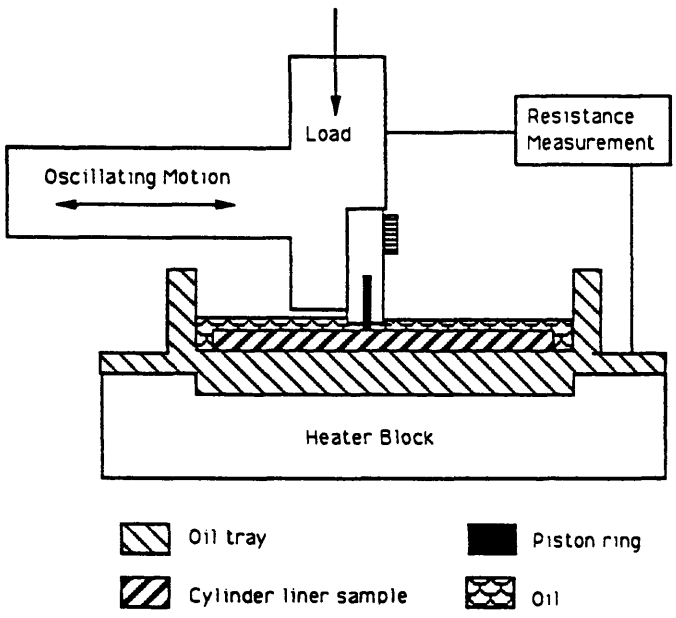

Source: SAE Paper 932693

Figure 1-9: Bench Wear Test

because the conformance is not quantitatively measured. Because this apparatus is used primarily for wear tests, a worst case situation (corresponding to the beginning of the power stroke) of 80N, or 7 MPa pressure, normal load was used.

The bench tester, EMA-LS9, [8] was constructed by Slone et. al. to simulate friction and wear for testing of new diesel engine lubricants, liners and rings under several speed, temperature and loading conditions. The rig is unique for its use of an oil spray onto the liner, rather than a drip or immersion system. The spray mechanism is a water-cooled stainless steel pipe system carrying a pressurized air and oil mixture, driven by a peristaltic pump, providing control of the feed rate to the liner. A schematic of the rig is shown in Figure 1-10. The ends of a complete piston ring are held together by pins in a disk shaped holder, which is driven by a motor and reciprocates to rotational speeds of up to 700 rpm, for a stroke of 25.4 mm. The holder is loaded by two liner segments, placed 180° apart, of 38 mm length and 7 mm width. They are pressed against the ring through a pressurized air cylinder and lever arm. The friction force is measured about the liner-air cylinder pivot and the instantaneous friction coefficient is measured using the load supplied by the air

cylinder as the normal load. The rig temperature is varied using an oven containing electric heaters around the liner samples and ring. The temperature is measured using thermocouples placed in the oven, although not in the liner samples. The oven has a temperature range from room temperature to 550°C. Because the paper emphasizes wear results, there are few friction results available for comparison. However, for a standard ring, liner and lubricant at room temperature, load of 85.4N and engine speed of 268 rpm, the average friction coefficient measured is 0.04. The tests were run over several hours and it was found that the friction coefficient varied over a time scale of minutes. Over a liner/ring break-in process, the friction coefficient dropped steadily until it reached a steady state. Additionally, the friction coefficient was found to vary depending on the lubricant supply. Initially, there were differences in the oil feed systems for each sample. When the systems were equalized, the friction coefficients were identical. This experiment assumes that the air cylinder exerts the same force from each side and that the equal forces, when transmitted to the ring through the apparatus lever and connections, results in the same force applied to both sides of the ring. It is difficult to judge this assumption with the information given on this bench test, but, if the assumption is valid, then it leads to self-alignment of the liner samples' axes and the ring holder axis of motion, which is a significant advantage.

The papers available on test rigs do not discuss the lubricant behavior. While this can be thoughtfully derived or hypothesized, the oil film behavior is essentially unknown.

1.4.2 Oil Film Thickness

A review of the literature in this field reveals that there are three primary methods used for direct experimental measurement of oil film thickness. Grice and Sherrington [9] measured piston ring/liner oil film thickness utilizing transducers based on capacitance and inductance measurement methods, using a single cylinder diesel engine fitted with eighteen capacitance transducers and one inductance transducer. Tests were run for the full four-ring pack under motored and fired conditions, for engine speeds 900 to 1600 rpm. The lubricant film thicknesses under the top ring were on the

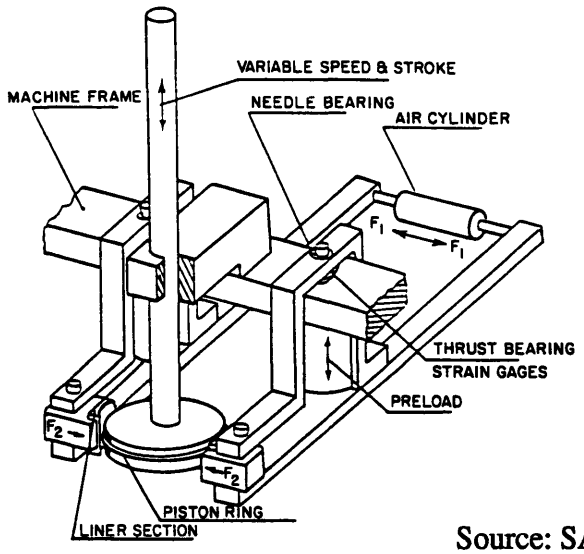

Source: SAE Paper 890146

Figure 1-10: Bench Tester: EMA-LS9

order of 9 to 10 μm and increased at lower speeds. For the top ring, some instabilities of oil film behavior were inferred from the non-repeatability of ring traces at constant speed and this was attributed to secondary piston motion, lateral movement of the ring (ring tilting in the groove) and ring circumferential motion. Since the goal of the research was to investigate the ring location of maximum pressure change in the top ring subring region, the project also focused on the most likely location for top ring instability. The calibration procedure is not discussed. However, it is probable that calibration of the transducers can be performed independent of the engine, thus giving a fairly robust calibration.

Optical methods, namely thin-film interferometry, have been used by Wakuri et. al. [10] in 1981 on a test bench, shown in Figure 1-11 similar to that of the friction rigs, in which a circular slider simulating a ring is moved against a flat optical plate. The oil film thickness is measured by studying the light and dark patterns of interferograms generated by a streak camera.

Laser Induced Fluorescence (L.I.F.) was investigated by Ting as early as 1979 [11] and subsequently, many researchers have used this experimental technique, in which a laser signal is directed at a dyed lubricant. The dye emits a fluorescence signal at a known wavelength proportional to the volume of oil and thus the oil film thickness

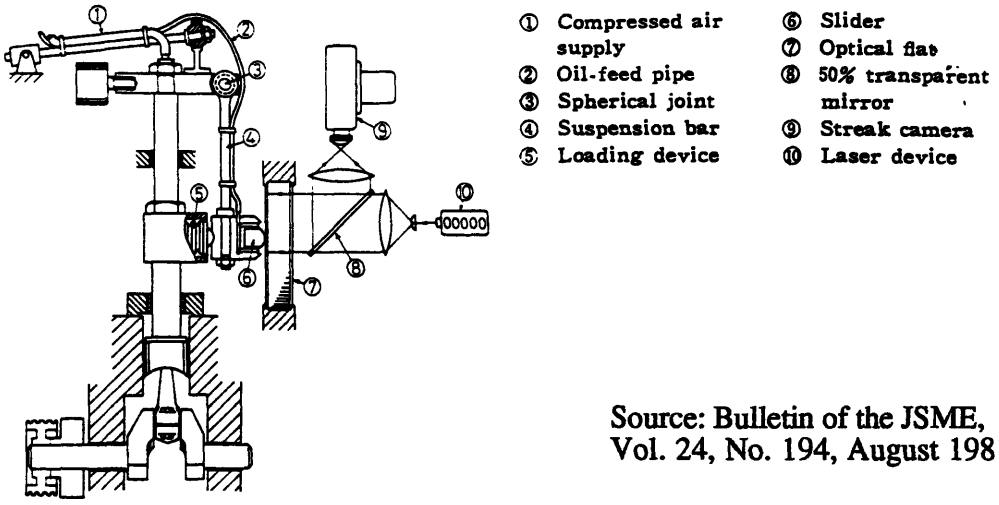

Figure 1-11: Use of thin-film interferometry for observation of oil film thickness.

on the liner. L.I.F. has been significantly advanced at the M.I.T. Sloan Automotive Laboratory [12]. Past applications have involved installation of quartz L.I.F. windows flush with the engine liner, to allow passage of the laser signal to the oil and subsequent measurement of the fluorescence signal. This makes the L.I.F. data collection fundamentally different to that of friction data, since the window can only be mounted at a specific, stationary liner location, limiting the film thickness measurement to a fixed axial and circumferential position, while the friction data is collected for the complete stroke. The window was mounted close to midstroke, where there is high speed and typically low film thickness and friction close to the hydrodynamic lubrication range, and at endstroke, where there is low speed and high friction, typically characterized by boundary lubrication. The development of the L.I.F. apparatus is well described and detailed in [13, 14, 15].

Additionally, L.I.F. was used by Brown et. al. [16] to measure the liner/ring oil film thickness in a single cylinder firing diesel engine. While the basic design is similar to that of M.I.T.'s, there are two important differences. The laser signal was directed to activate the natural fluorescence of the oils (15W40 and 10W30), rather than a dye and the calibration of the L.I.F. signal was performed using a bench-top calibration cell. Results from calibration *in-situ*, using grooves of known depth in the piston skirt

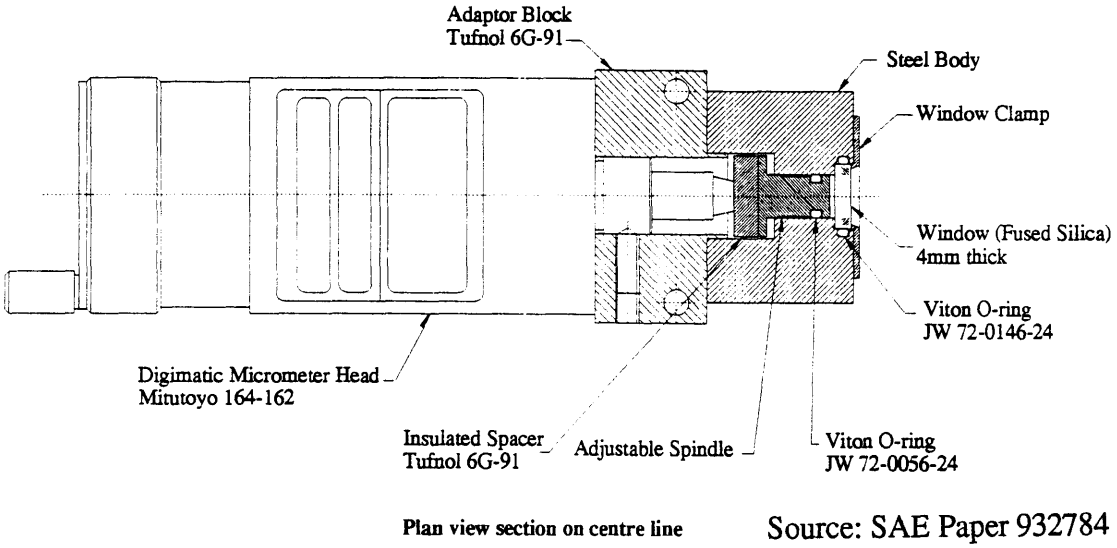

Figure 1-12: Calibration Cell

and top ring, were unreliable and the grooves were under-filled with oil or filled in a random manner, as a result of the engine oil flow. The calibration cell is shown in Figure 1-12. The L.I.F. apparatus is directed at a calibration compartment filled with oil, where the separation of the compartment walls is of known distance. The error associated with this method was estimated at 5 to 8%. The results presented are for operation of the entire ring pack and show clear trends of oil film thickness under the rings dependent on oil flow through the ring pack. The minimum oil film thickness under the top ring as it passed 123° from top center, varied between 1 and 3 μm, at 1200 rpm engine speed. This thickness may be dependent on conditions of the entire ring pack, such as geometry and oil flow.

In addition to the experimental aspects of engine friction and oil film thickness, there is an abundance of literature on theoretical models. For example, Yoshida et. al. derived the oil film thickness under the top ring corresponding to their friction measurements using theoretical considerations. The M.I.T. Laser Induced Fluorescence oil film thickness measuring technique was used for the research described herein. The system is available, well understood and there is resident expertise and a base of knowledge, as well as in-engine data for comparison of experimental results.

1.5 Objective

Based on the review of research to date, there is a need for a test apparatus for measuring friction which also confirms realistic engine conditions in terms of lubricant behavior, particularly oil film thickness. In cases when film thickness has been considered, it has been indirectly derived rather than experimentally measured.
The objective of this research is to simultaneously measure ring/liner friction and oil film thickness using a test apparatus which simulates conditions of an internal combustion engine. The test results will provide a mechanism for understanding the proximity of the apparatus lubrication conditions to actual engine tribology and will provide background when compared to current research friction results. It will also allow understanding of friction and oil film thickness behavior.
The future use of this test rig will also allow for analysis of methods for achieving reduced friction and subsequent friction power loss, engine economy benefits, as well as the design of new lubricants, such as low-friction oils.

1.6 Thesis Outline

This thesis will report research results in the following order:

1. Description of the test apparatus
2. Description of the instrumentation necessary for oil film thickness and friction measurements
3. Explanation of data processing
4. Presentation of trial results and subsequent lessons learned and incorporated into the research
5. Presentation of test conditions and data results
6. Analysis of results
7. Comparison to theoretical results and current research results

The conclusion will comprise a discussion of the apparatus capabilities as implied by this research, as well as suggestions for rig improvement and future research.

Chapter 2

Experiment

The purpose of the test apparatus is to simultaneously measure oil film thickness and friction in the area between the ring and piston liner. Figure 2-1 shows the concept of the experiment. It is desired to replicate the actual engine conditions, such as speed, load, temperature and lubricant flow between the ring and the liner. Samples of the actual ring and liner materials were used for preservation of geometry, metallurgy and surface finishes. The ring sample was held by a ring holder in such a way that it moved in a reciprocating motion emulating that found in an engine. The liner sample was mounted in such a way that a load cell could measure the friction exerted by the ring on the liner and the behavior of the oil film between the ring and the liner could be studied.

This chapter will detail the experimental setup, instrumentation and procedure. The first section describes the engine drive system, the ring and liner samples, the apparatus for mounting the liner segment and the ring sample mounting hardware. The next section details the instrumentation and the last section reviews the procedure used for data processing.

2.1 Experimental Apparatus

The design of the rig described herein is based on that of an existing apparatus for comparative friction measurements at Ford Motor Company. The Ford apparatus

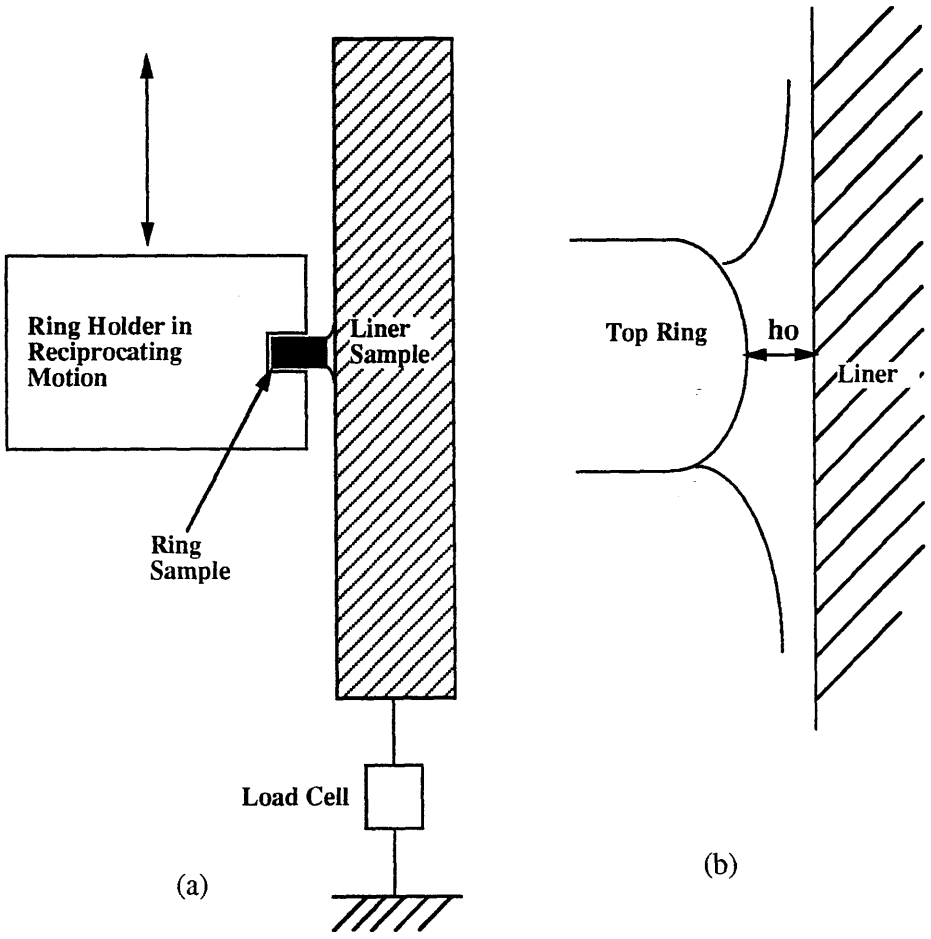

Figure 2-1: Experimental Concept

Type	Single Cylinder, Horizontal Crankshaft, Air Cooled, Spark Ignition, Overhead Valves
Lubrication System	Gerotor Pump, Paper Filter
Power	10.5 kW, 14 hp @ 3600 rpm
Peak Torque	28.9 N-m (21.3 lbf-ft)
Bore	87 mm (3.43 in)
Stroke	67 mm (2.64 in)
Typical Application	Lawn Tractor
Modifications	Retained reciprocator, inertia balancer and lubrication system.

Table 2.1: Kohler Engine General Information

mechanism for mounting the liner and ring samples was almost directly incorporated into the M.I.T. rig, and was subsequently modified for oil film thickness measurements.

2.1.1 Engine and Driving System

A commercial spark ignition, single-cylinder engine was used as the source of the reciprocating motion for the ring sample. The engine is a Kohler Command 14-horsepower, four-cycle internal combustion engine. Table 2.1 provides general information. The stroke, which directly corresponds to the ring sample stroke is 67 mm, which is slightly shorter than that of a typical automobile engine ($\approx$ 90 mm).

In order to transfer the motion of the engine piston to the ring sample, the head of the engine was removed, with the short block remaining. The lubrication system

was retained, as well as the camshaft and gear for balancing of the crankshaft. The piston, rings, connecting rod apparatus and crankcase were kept.

The engine was motored by a DC dynamometer. Since the heavy ring holder mechanism exerts a large load on the piston, possibly stressing the wrist pin or connecting rod or unbalancing the crankshaft, it was decided to initially run the engine at low speeds of 100 to 600 rpm. The dynamometer has a listed speed range of 10 to 3600 rpm. The coupling between the dynamometer and engine was a pulley and belt system with a ratio of 9:1 speed reduction. Two 3:1 identical pulley and belt systems were used, so that, in the future, one pulley and belt system could be reversed to gain a 1:1 speed ratio from engine to dynamometer. This was designed for potential future high speed experiments.

Figure 2-2 is a drawing of the assembled driving system, mounted on a test bed. The dynamometer directly drives the right pulley and belt system, which is mounted on an intermediate shaft and pillow block, connecting to the second pulley and belt system, which is directly coupled to the engine crankshaft. Photographs of the constructed system are shown in Figure 2-3. In (a), the dynamometer is on the right and the engine, with the test apparatus mounted on top, is to the left of the photograph. The mounting of the test rig is shown in more detail in (b).

2.1.2 Experiment Ring and Liner Samples

Since it is desired to replicate engine conditions whenever possible, materials from an actual engine were used for the ring and liner samples. For the set of experiments described in this thesis, new rings and liners from a Ford Motor Company production engine were used. It is also possible to use worn samples of the same geometry.

The liner is made of cast-iron and the inner surface is polished and honed. Its length is 131.5 mm and the bore is 90.2 mm. The sample was cut at Ford using electrical discharge machining, to minimize bore distortion from the cutting process. The sample was cut for a circumferential sector of approximately 56°, which results in a width of approximately 5 cm. The back of the liner sample was then machined at the center, to provide a flat mounting surface. The top and second rings are

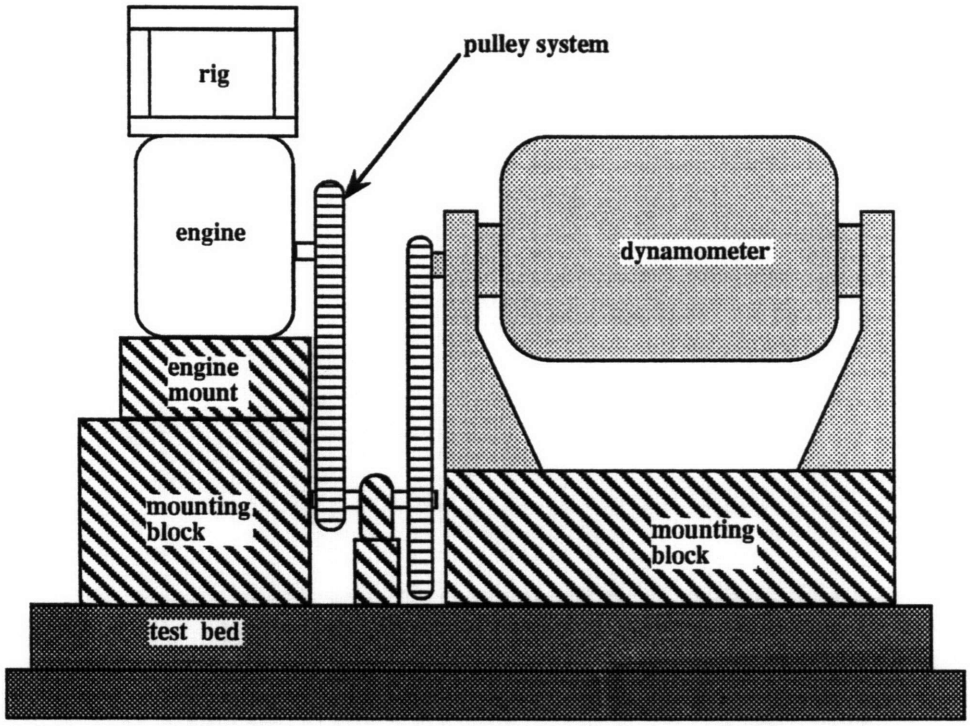

Figure 2-2: Test Apparatus Driving System

manufactured from coiled steel wire which is heat treated for shape retention. There is a coating on the ring surface which contacts the liner, to improve the ring wear and durability characteristics. Both rings have thicknesses of 0.058 inches and widths of 0.161 inches and therefore are interchangeable in the ring holder. The ring is cut so that the center of the ring sample is opposite from the ring gap, for even ring curvature, at approximately $\pm 90°$ from the ring gap. The ring and liner samples are drawn in Figure 2-4, and information about the dimensions is summarized in Table 2.2. For calibration purposes, a groove was etched on the sliding surface of the ring. This will be discussed further in the section on Experimental Procedure.

2.1.3 Liner and Load Cell Apparatus

The fixture for the liner sample is supported by a load cell, attached to a fixed stationary structure, for measurement of the friction exerted on the liner. The concept is shown in Figure 2-5. Upwards motion decreases the distance between the two ledges

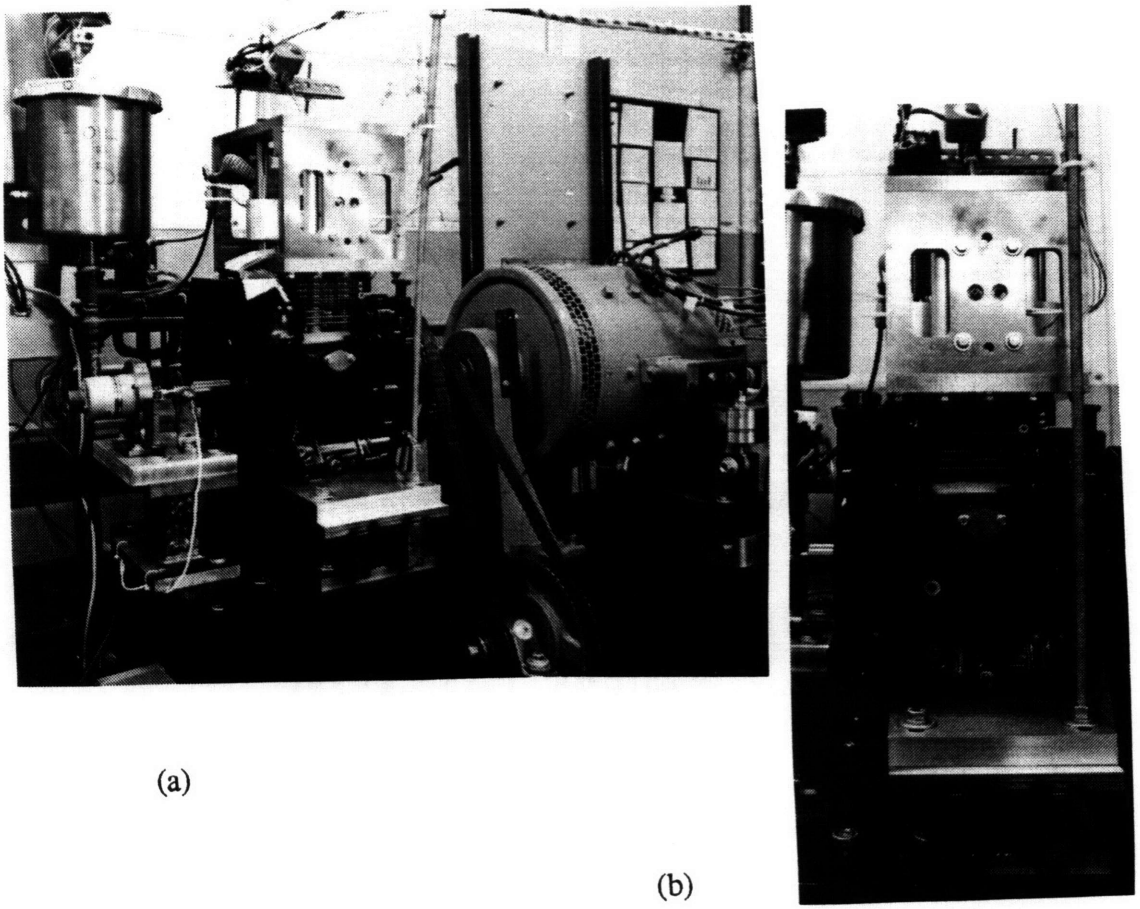

(a)

(b)

Figure 2-3: Photographs of the Driving System

Source	Ford 4.6L engine 90.2mm (3.552") bore x 90.0mm (3.543") stroke
Liner Segment	Length: 5.176", Width: approx. 2" (approx. 56° of liner) Cut at Ford using E.D.S. (minimization of bore distortion)
Ring Segment	Top & Second Ring Thickness: 0.058", Width: 0.161"

Table 2.2: Ring and Liner Sample Dimensions

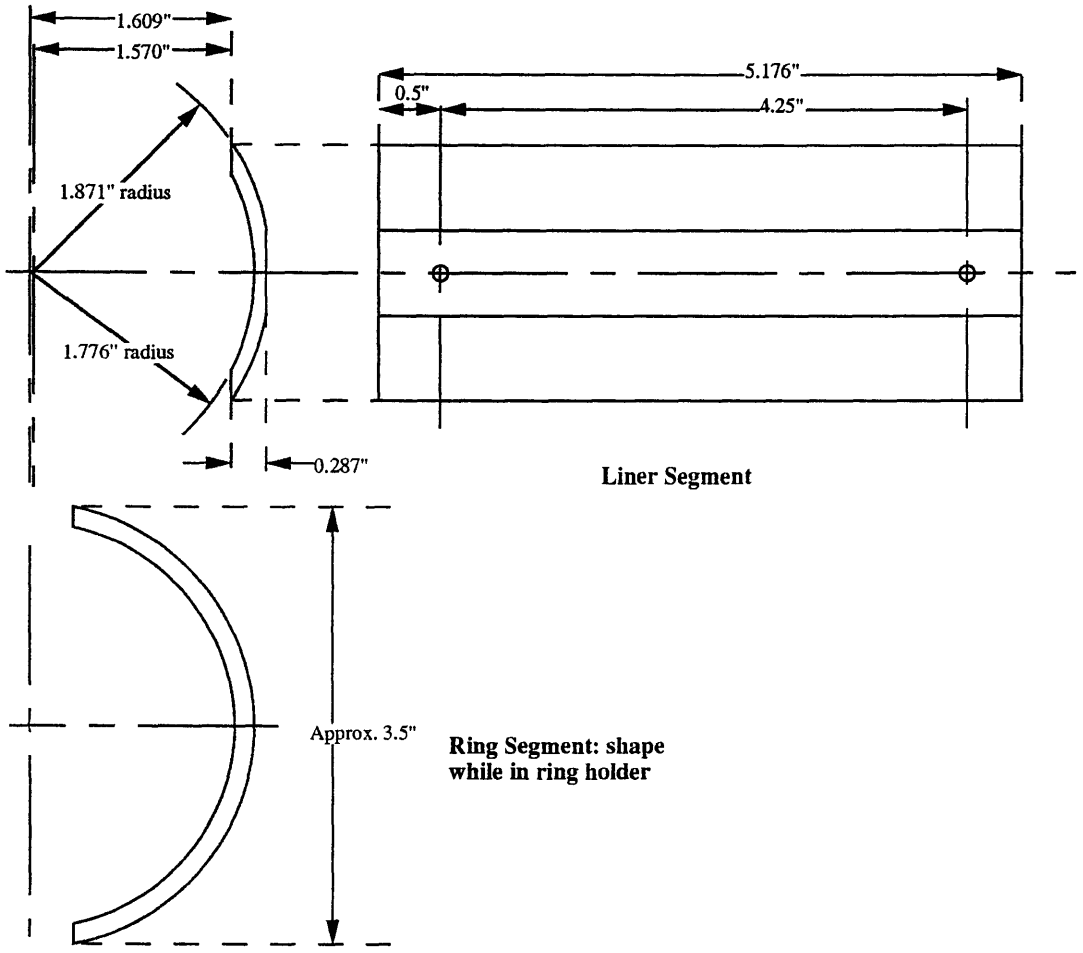

Figure 2-4: Ring and Liner Sample

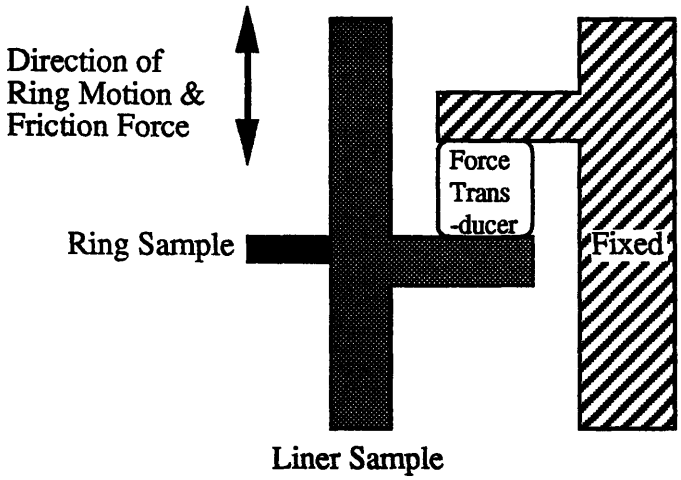

Figure 2-5: Load Cell Apparatus Concept

supporting the load cell, exerting a compressive force on the load cell. Downward motion expands the ledge distance, exerting an expansion force on the load cell. A photograph of the side view of the assembled test apparatus is displayed in Figure 2-6.

The four test apparatus walls provide a fixed structure and additionally, a mounting surface for instrumentation. The bottom wall is mounted on top of the engine through the holes regularly used for mounting the cylinder head. In the original Ford design, two liner samples were used, one as a baseline and the other for comparative friction measurements. In this design, only one liner sample was used. A photograph of the front and rear views of the load cell apparatus mounting in the side wall is shown in Figure 2-7. The load cell fixture is slid in a groove along the stationary side wall until the circumferential center of the liner sample matches that of the ring sample. It is fixed in place by four bolts through the side wall and two placement pins, which are visible in (a). Figure 2-8 shows the load cell apparatus removed from the side wall and reversed. The load cell and thermocouple mountings are clearly visible. The construction of the load cell apparatus is shown in Figure 2-9, which displays the disassembled apparatus, with front and rear views. In (a), the liner sample is displayed on the left, the piston sleeve friction mount is placed in the center and the load cell fixture is on the right. In (b), the piston sleeve friction mount ledge which supports the bottom surface of the load cell through a bolt is visible. A matching

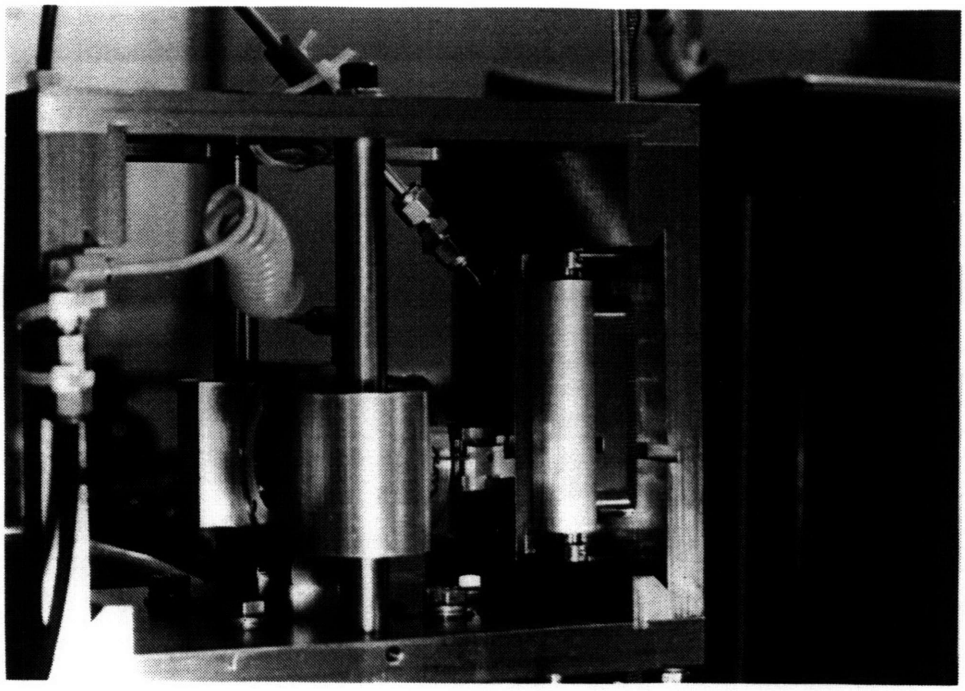

Figure 2-6: Side View of the Test Apparatus

ledge to support the top surface of the load cell is part of the load cell fixture. The liner sample is mounted on the front of the piston sleeve friction mount, for direct translation of the friction force from the liner to the load cell. To prevent mechanical stress or shear on the load cell from the normal load, which is particularly worrisome if the ring sample motion is slightly off axis, the load cell fixture and piston sleeve friction mount are designed to allow two rods to hold the apparatus together. The rods are fitted to the load cell fixture through a set screw, groove and snap rings and are shown in both (a) and (b). The rods move within the piston sleeve friction mount on linear bearings. The two ledges for supporting the load cell were placed to allow for unobstructed passage of L.I.F. instrumentation. Figure 2-10 is a photograph of the top view of the load cell apparatus, showing the liner mounting. The center screw is attached to the load cell, whose outline is faintly visible.

2.1.4 Ring Holder and Support Apparatus

The purpose of the ring holder apparatus is to push the ring sample against the liner sample with a controlled radial force during apparatus operation. The ring normal

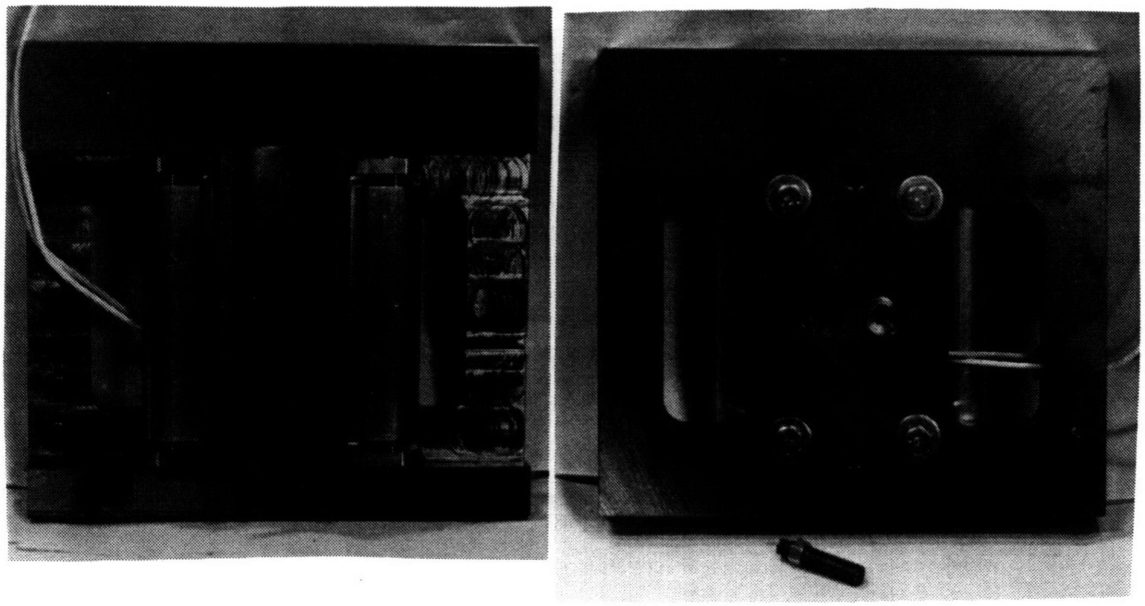

(a) (b)

Figure 2-7: Front and Rear Views of the Load Cell Apparatus in the Side Wall

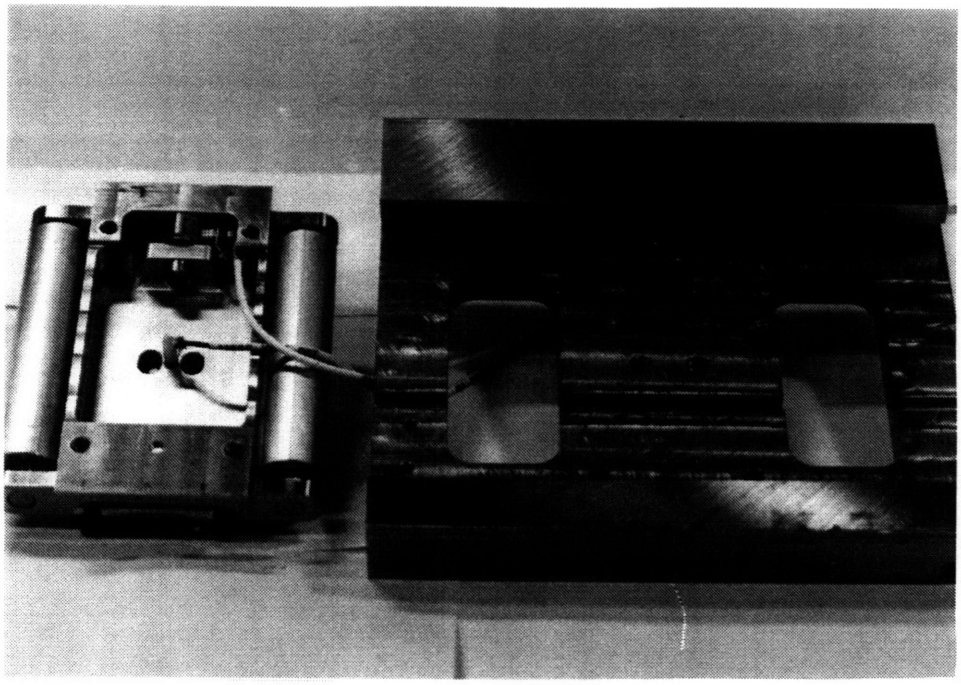

Figure 2-8: Load Cell Apparatus removed from the Side Wall

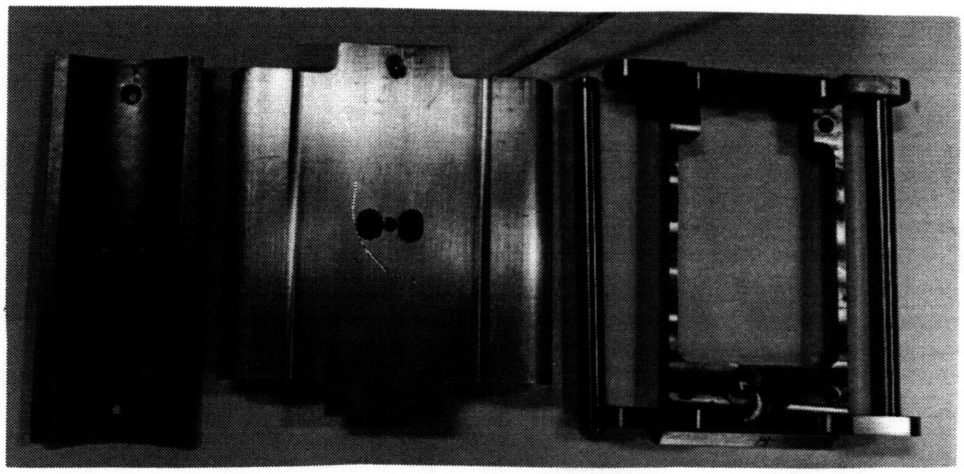

(a)

Liner Sample Piston Sleeve Friction Mount Load Cell Fixture

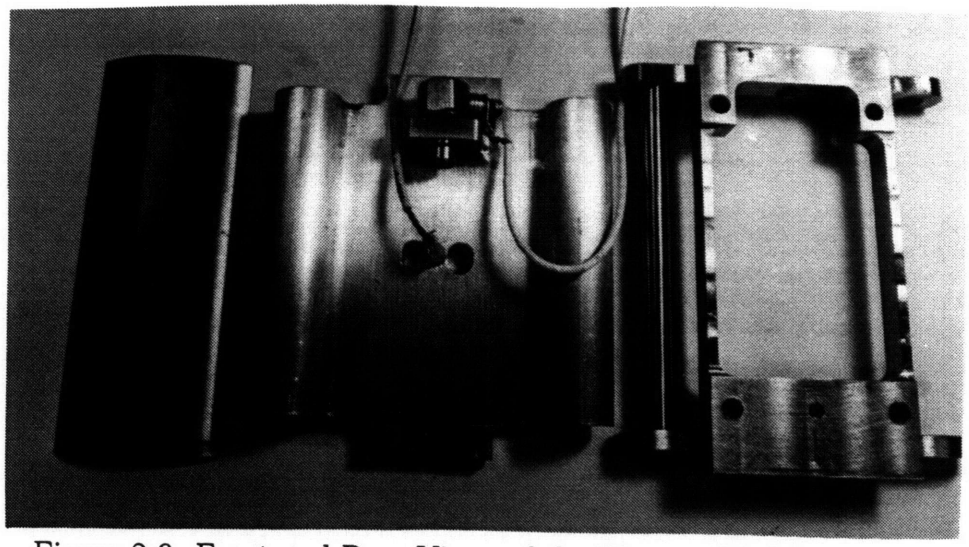

(b)

Figure 2-9: Front and Rear Views of the Disassembled Load Cell Apparatus

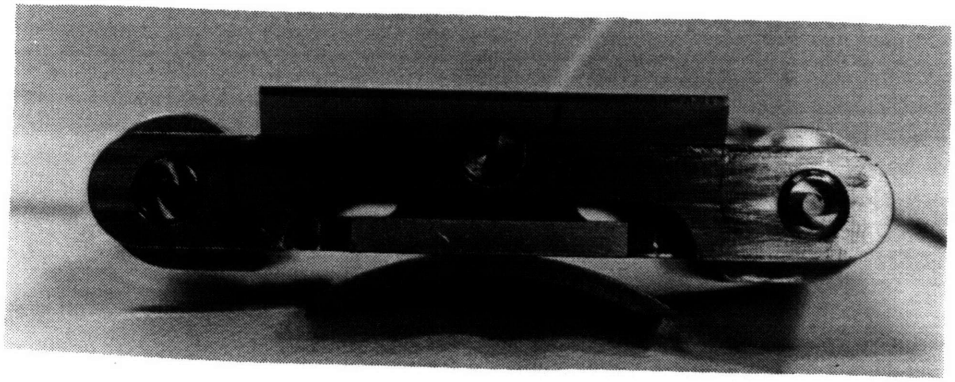

Figure 2-10: Load Cell Apparatus, Top View

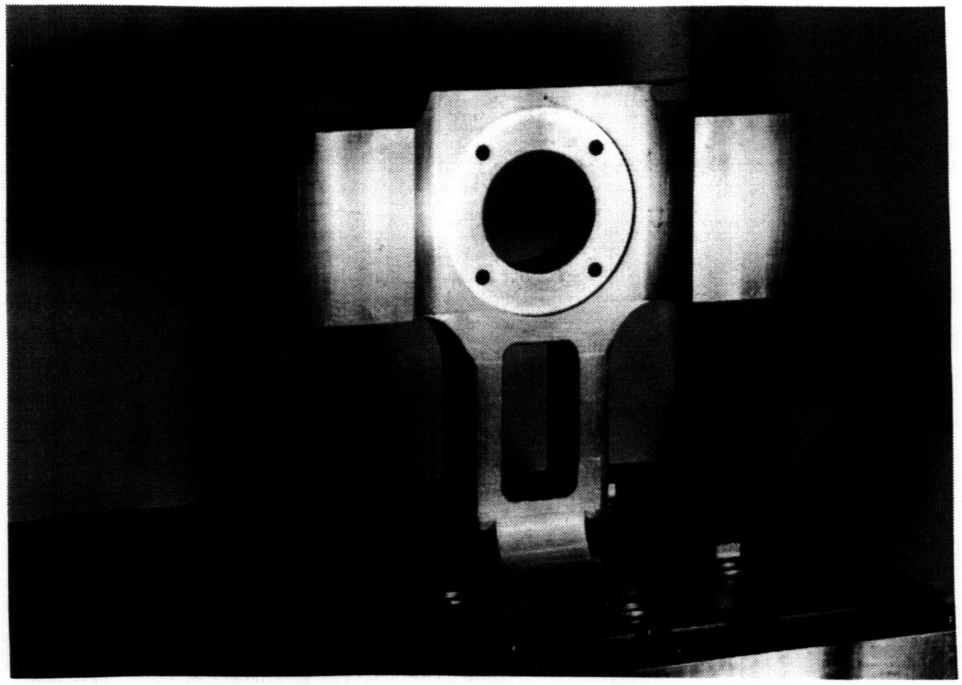

Figure 2-11: Reciprocator

force of a production engine has a cyclic variation generated by the engine firing cycles, but this is difficult to reproduce in the test apparatus described herein. The reciprocating motion is provided by a connecting piece, the reciprocator, photographed in Figure 2-11. The base of the reciprocator is bolted to the top of the Kohler engine piston, so that it moves with the piston. This mounting is shown in detail in Figure 2-12. Holes were machined in the reciprocator to remove unnecessary material and to lighten the inertial load on the engine reciprocating apparatus. Two hardened rods placed parallel to the piston motion were press-fit between the top and bottom walls to guide the motion of the reciprocator. Two linear bearings were slip-fit into the sides of the reciprocator and held in place with snap-rings. A bearing and rod are shown in Figure 2-13.

The ring holder apparatus is photographed in Figure 2-14. Part (a) shows the assembled apparatus and part (b) displays the disassembled components. The radial ring pressure is applied by an air cylinder mounted on the flat circular surface of the reciprocator, which pushes the ring holder towards the liner segment. The normal force on the ring is proportional to the air pressure applied by the air cylinder. A ring guide,

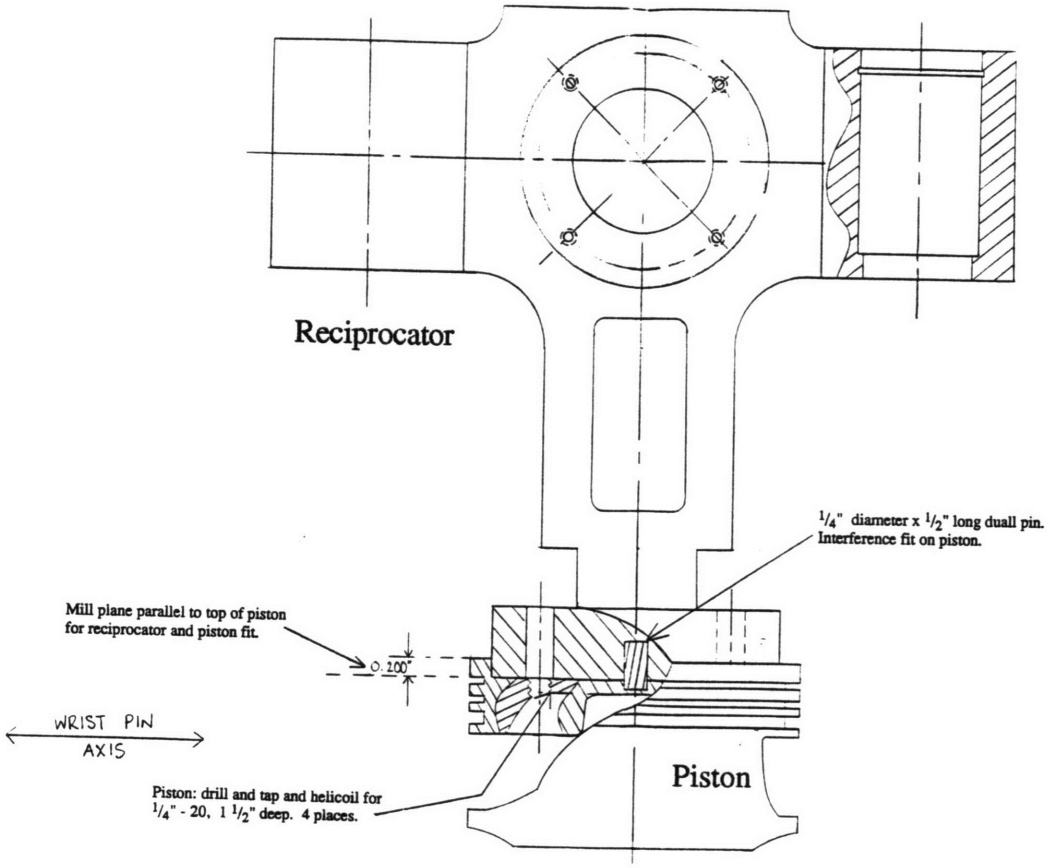

Figure 2-12: Reciprocator Mounting on Piston

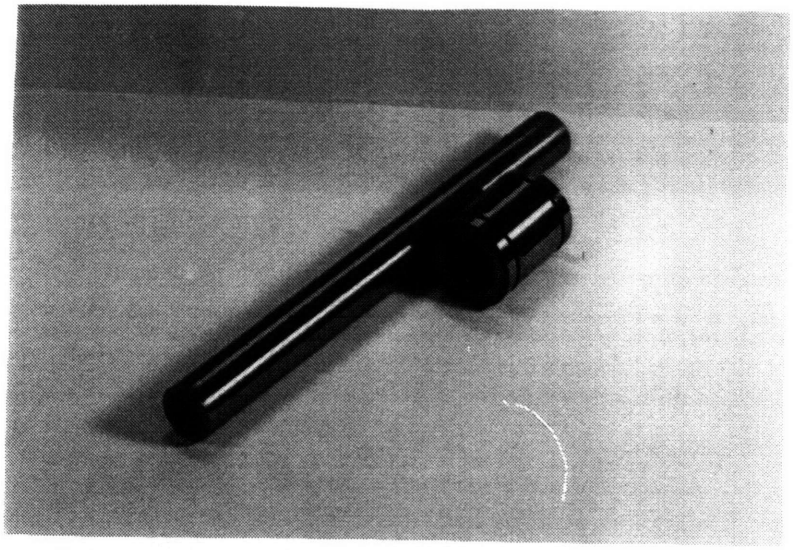

Figure 2-13: Rod and Bearing for Reciprocator

drawn in Figure 2-15, is bolted through two holes onto the bar of the air cylinder and therefore moves forward with the bar. A ring holder is slid between the upper and lower ledges of the ring guide. These ledges are in the direction perpendicular to the friction force and prevent twisting of the ring holder and thus the ring due to the reciprocating motion. The lower and upper ledges are designed to be asymmetric, so that the ring holder cannot be inserted upside down. The ring holder is drawn in Figure 2-16. The back surface of the ring holder has a bore hole for placement of a transducer, which can measure the force exerted on the ring holder by the ring guide, which is the normal force on the ring sample. A through-hole is machined in the ring holder for passage of the load cell wire. The front surface is machined to imitate the ring groove of a piston. The clearance of the groove is one thousandth of an inch larger than the ring thickness. On each side of the ring guide, two ledges constrain the ring sample to the radius of the liner sample. There are two set screws which are in a radial direction to the ring. When the set screws are turned, they push against the ring sample, allowing for slight adjustment of the ring radius. The ring sample is slid into the ring holder.

2.2 Instrumentation

The parameters (inputs) and measurements (outputs) of the experiment are displayed in Figure 2-17. The variables which can be controlled or varied are: oil type, engine speed, normal force, ring geometry and oil feed mechanism. The oil type determines the oil viscosity and the ring geometry refers to the ring profile. Outputs of the test apparatus are: friction force, coefficient of friction, oil film thickness and liner temperature.

Further details of the instrumentation of these variables are shown in Figure 2-18. A side view of the rig is drawn, with the friction force and normal force load cells mounted, respectively, in the liner sample support apparatus and ring holder. Oil film thickness and liner temperature are measured from the back of the liner sample support apparatus. The ring position and engine speed are measured from the engine

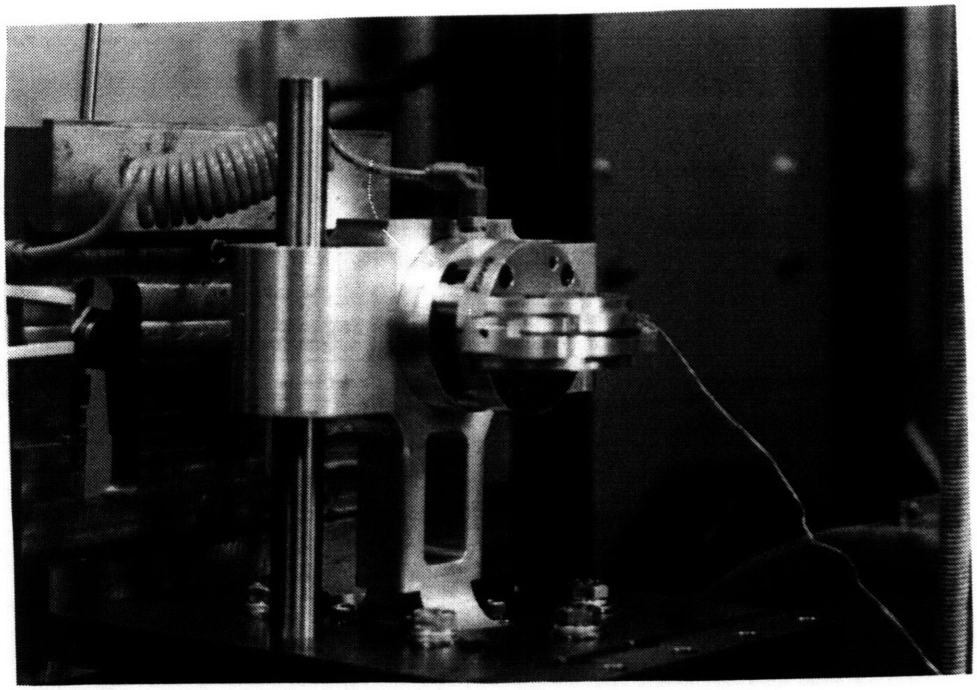

(a)

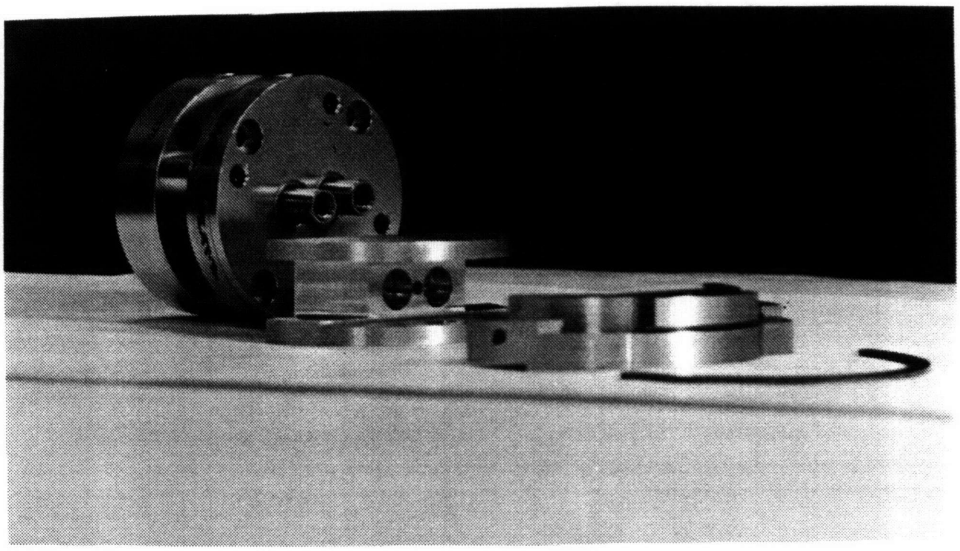

(b)

Figure 2-14: Assembled Ring Holder Apparatus

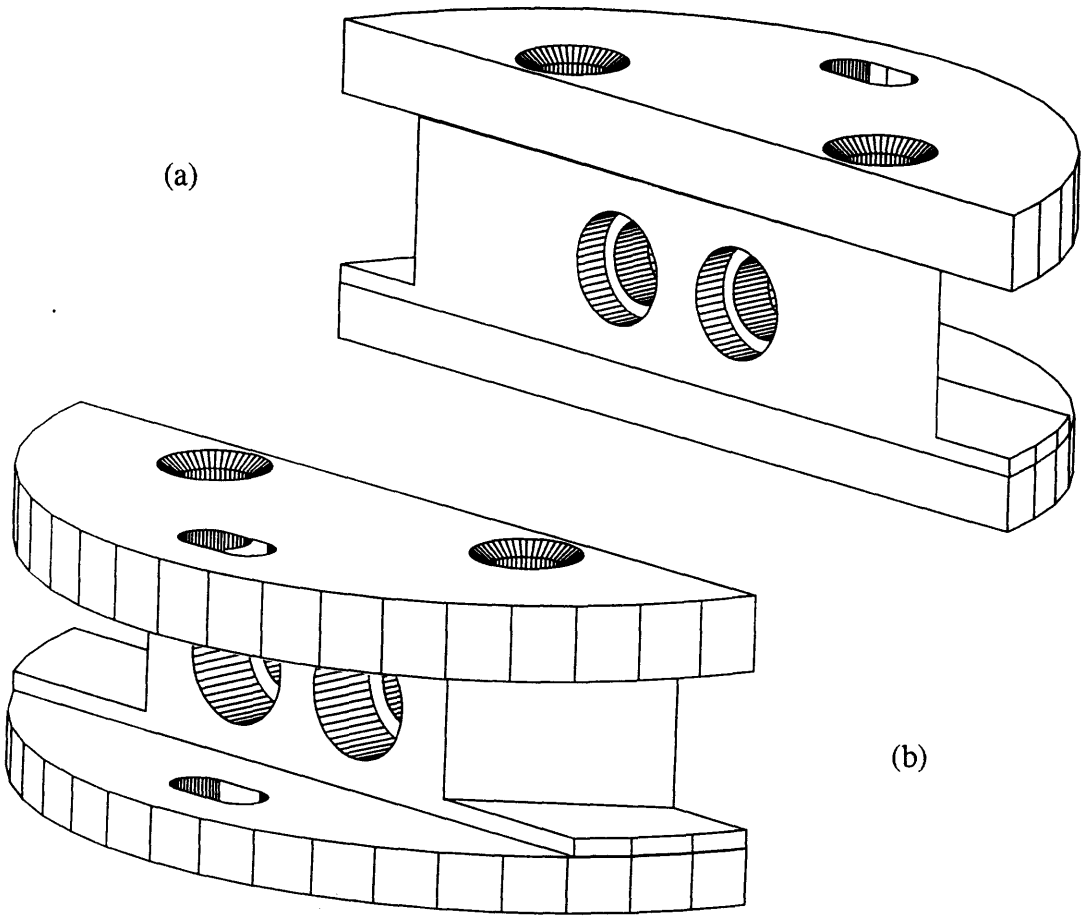

Figure 2-15: Ring Guide

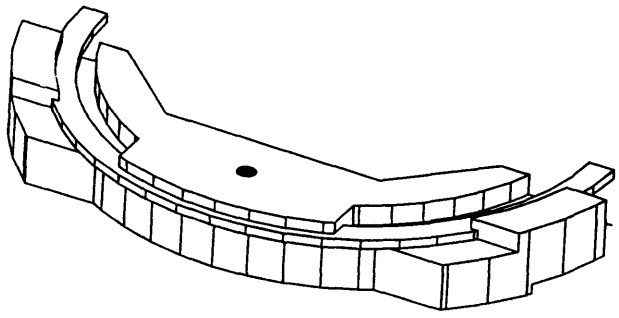

Figure 2-16: Ring Holder

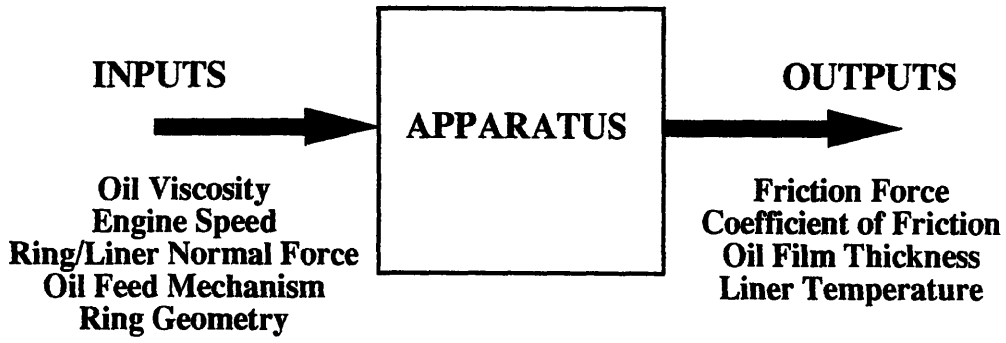

Figure 2-17: Test Apparatus Inputs and Outputs

crankshaft using a shaft encoder and a tachometer. The oil film thickness, shaft encoder signal, friction force and normal force data are fed to a data acquisition system, which samples and digitizes the data and records it. The instrumentation hardware is summarized in Table 2.3.

2.2.1 Ring Sample Linear Position and Engine Speed

The rotational position of the crankshaft is measured using a shaft encoder attached through a flexible coupling to the engine crankshaft, visible in Figure 2-3. The shaft encoder provides impulses triggering the data acquisition system to sample data. The shaft encoder has a resolution of 7,200 data points per revolution. In other words, every 0.05°, the shaft encoder emits a signal to the data acquisition system. The shaft encoder resolution is diagrammed in Figure 2-19.

The rotational speed of the engine crankshaft is measured using a magnetic pick-up coil and a gear attached to the engine crankshaft. The speed is manually recorded from a tachometer in revolutions per minute.

2.2.2 Ring Sample Normal Force

The normal force is measured by a strain gage transducer mounted in the rear of the ring holder. A Sensotec miniature button load cell was used, which is slip fit into the mounting hole. The button protrudes from the load cell, and the ring guide front surface pushes against the button, exerting the normal force on that area. The

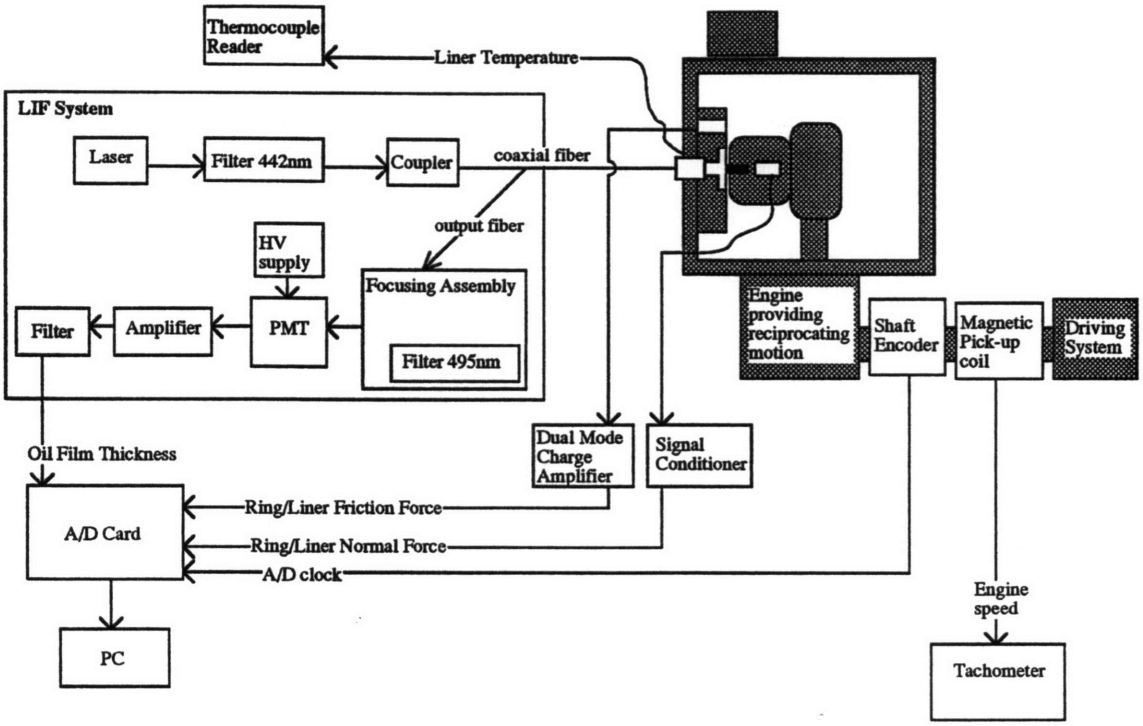

Figure 2-18: Test Apparatus Instrumentation Schematic

Crank Position and Rotational Speed	BEI Motion Systems Company Model H25 Incremental Optical Encoder Model No. H25EF1SS7200T5AZ8830LEDEM18 Minarik Visi-Tach Model No. VT-1-115V
Normal Force	Sensotec Model 13 Subminiature Load Cell Daytronic Model 9171 Strain Gage Conditioner Model 9515A Digital Indicator Model 9005 Mainframe
Friction Force	Kistler Piezotron Load Cell Model No. 9712A5 Kistler Dual Mode Amplifier Model 504E
Liner Temperature	Thermocouple Wire Type K Digital Temperature Indicator Omega Model 199

Table 2.3: Instrumentation Hardware

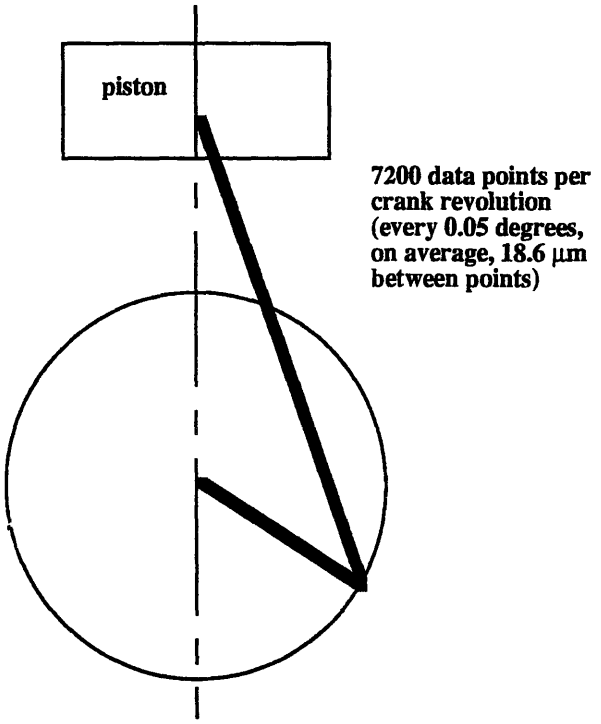

Figure 2-19: Shaft Encoder Resolution

transducer capacity is 100 lbs in compression, and it is pre-calibrated to output 2.1711 mV per input volt. A strain gage conditioner provides an excitation voltage to the transducer and calibrates and amplifies the output signal. This was fed to a digital indicator which allowed for an instant manual readout of normal force for setting the air pressure. The signal was also fed to the data acquisition system, so that the instantaneous normal force could be collected.

2.2.3 Ring/Liner Friction Force

The friction force is measured by a transducer placed between the load cell fixture and piston sleeve friction mount. A Kistler piezotron load cell was used, which has a full scale load capacity of 5 lbf in both tension and compression. It is pre-calibrated at 892 mV/lbf. The load cell was connected to a Dual-Mode Amplifier, which activates the transducer and amplifies the output signal, set on a medium time scale. The amplifier output was fed to the data acquisition system.

2.2.4 Liner Sample Oil Film Thickness

Figure 2-18 shows the details of the L.I.F. system. The laser light is filtered and coupled to an optical fiber connecting to the L.I.F. probe, shown in the lower part of Figure 2-7, part (b). The probe is located near the oil film and focuses the light on the oil film, which is doped with a fluorescent dye. Passage of the light through the liner is achieved by installing a quartz window in the liner. The fluorescence signal is collected through the same fiber, filtered, focused and directed to a photomultiplier tube, which converts the light signal to volts. This data is then sent to the data acquisition system. Further details, including equipment description, procedure for oil dyeing and signal collection, are given in [17].

Two quartz windows were installed in the liner sample at a position close to midstroke, each approximately 0.25 inches, or 8° from the circumferential center. This axial position was chosen because it is the region of highest velocity and thus greatest power loss to friction, and because data from the same L.I.F. system is available for comparison. The windows and holes for passage of the L.I.F. signal are visible in Figure 2-9. The dimensions of the windows are drawn in Figure 2-20 and a three-dimensional view is shown in Figure 2-21. The front surface has the curvature of the liner, so that it does not disturb the oil flow on the liner, or, at worst, minimally disturbs the oil flow. The dimensions of the window were chosen to optimize the tradeoff between maximal area for passage of the laser signal and minimal area for non-disturbance of oil flow. The step in window diameter allows for a rear surface for glueing the window to the liner without blocking the laser signal.

Figure 2-22 displays the mounting of the windows and L.I.F. probe in the liner sample support apparatus. The figure shows a cross section at midstroke of the liner sample, mounted on the piston sleeve friction mount and load cell fixture, which are located in the side plate, in the position for operation of the rig. The holes for the windows were machined in the liner sample. The liner sample was then mounted onto the load cell apparatus and side plate and the window holes were used as centering holes for through holes in the piston sleeve friction mount and side plate. It was important that

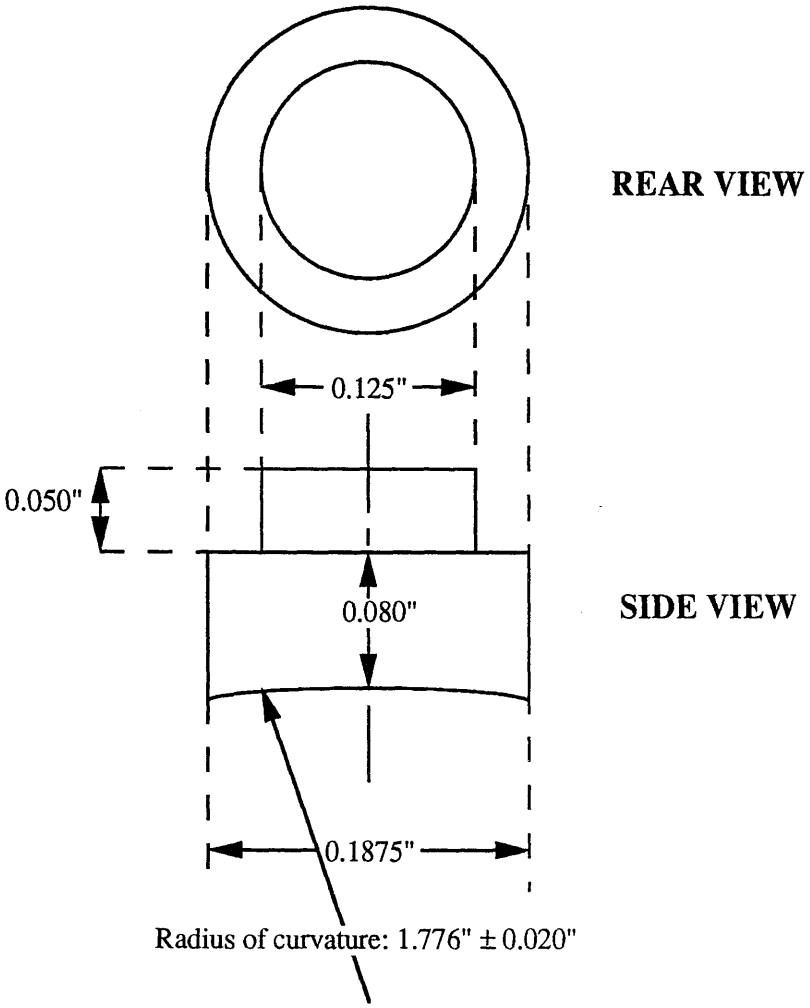

Figure 2-20: L.I.F. Quartz Window Dimensions

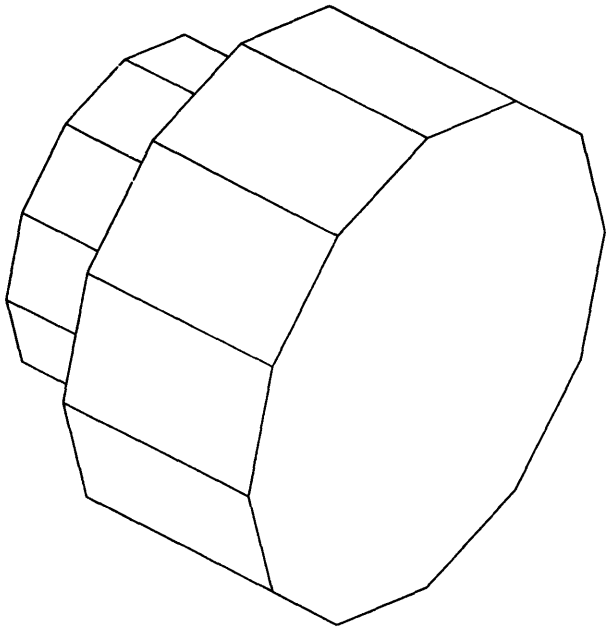

Figure 2-21: L.I.F. Quartz Window Three-Dimensional View

the laser signal not be interrupted and consequently, the through holes were oversized to allow for slight movement of the piston sleeve friction mount. The movement of the piston sleeve friction mount, as well as the lack of supporting material were criteria for choosing the side plate as the probe mount. The location of the probe supporting material far from the liner sample was a concern since the end of the probe may be exposed to engine vibration. The focusing probe is screwed into the threaded mounting. A coupling allows for fitting of the fiber optics cable into the focusing probe. The exact positioning of the probe from the L.I.F. window determines the focus of the laser signal on the oil. The procedure involves running the test apparatus and observing the L.I.F. signal on an oscilloscope. The probe is then turned until the signal is maximized and then it is locked in position using a locknut. The laser power supply input is then adjusted so that the maximum values of the L.I.F. trace are slightly less than 10 V, which is the maximum input to the data acquisition system. The laser signal is transmitted through four parts of the test apparatus, which must be re-aligned every time the rig is disassembled and reassembled. This requires very careful handling of the reassembly as well as re-calibration of the L.I.F. signal.

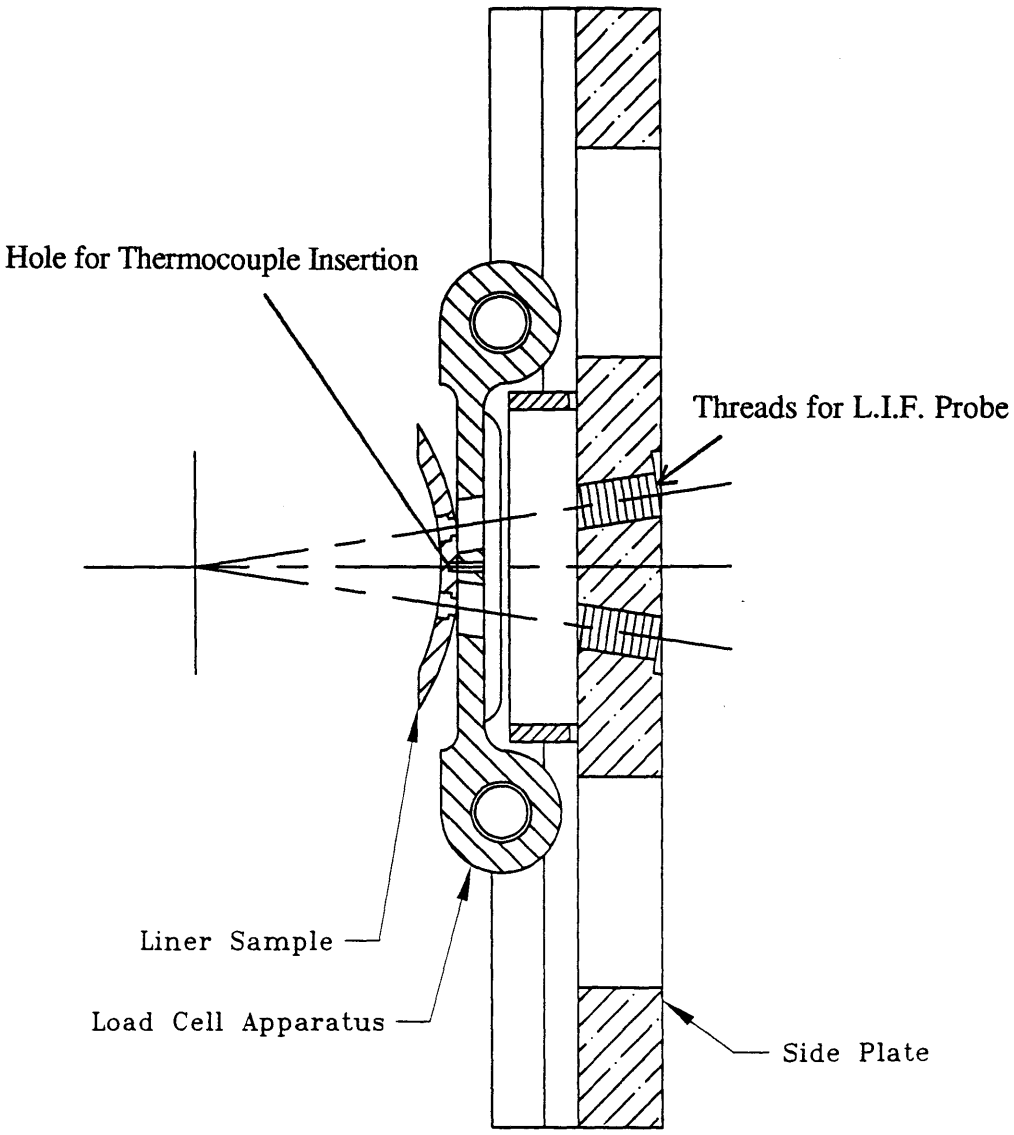

Figure 2-22: L.I.F. Window and Probe Mounting: Cross Section.

2.2.5 Liner Temperature

The liner temperature was measured using thermocouple wire inserted in the back of the liner between the two quartz windows, as shown in Figures 2-9 part (b) and 2-22. The bared wires were locked into an indent in the liner rear surface by a customized plastic screw. Although the wire did not contact the liner surface, it was located less than one sixteenth of an inch from the liner surface. The wire was fed back through the load cell apparatus and connected to a thermocouple reader for an analog display of temperature in degrees Celsius.

2.2.6 Oil Feed System

During the course of the apparatus construction and initial testing, two different oil feed systems were used. The first was a drip system, which was easily assembled and allowed for preliminary measurements. The second system was a controlled oil injection system, an effort to obtain more precisely controlled oil film thicknesses, typical of those of firing spark ignition engines. The second is similar in nature to that used by Slone et. al. [*ibid.*].

Drip Oil Feed System

The preliminary oil feed system consisted of a 100 ml oil-filled burette mounted on the top wall of the rig. A valve on the burette base controlled oil flow. The oil trickled down from the burette to the liner by gravity, similar to the oil drip system employed by Ting [*ibid.*]. This oil feed system, although simple and easy to use for a variety of oils, did not provide precise control of the oil thickness on the liner. The valve was essentially a binary control and, in general, the liner was over-flooded with oil. However, the system was very useful, allowing for preliminary measurements of friction force, normal force and oil film thicknesses.

Pulsed Oil Injection System

A new oil feed system was designed and constructed to provide better control of oil flow and oil film thickness. This mechanism consists of repeated single-pulse oil injection, in which oil is pumped from a reservoir through a nozzle which sprays the oil onto the liner sample, as shown in Figure 2-6. A schematic of the oil feed system is shown in Figure 2-23. From the reservoir, the oil is filtered and then pumped through a stainless steel pipe to a nozzle. A solenoid valve, located in the pipe just prior to the nozzle, opens and closes according to an electrical pulse from a signal generator. The signal can be varied in terms of duration and frequency, allowing for control of the number of pulses in time and the amount of oil injected per pulse, as diagrammed in Figure 2-24. Various nozzles were tried. The most successful was a modified syringe nozzle, which has a large enough cross section to allow flow of a fluid as viscous as engine oil, but a small enough cross section to provide a jet of oil. Typically, in an automobile engine, the oil splashes up onto the hot liner from the motion of the piston and the connecting rod. While the way in which the oil reaches the liner is difficult to duplicate, it is hoped that the final product, the spreading of the oil on the liner, is similar to that found in an automobile engine. Additionally, in an automobile engine, the oil splashes up onto the liner from the bottom of the liner. The geometry of this test apparatus is such that it is not an easy task to mount the oil feed system. The best mounting is one which utilizes the stationary top wall of the apparatus. This allows for positioning of the nozzle close to the liner, so that most of the oil reaches the liner. The oil exits the nozzle in a stream, rather than a spray, and, from the nozzle placement, contacts the liner at the circumferential center, just above top center. The stream can contact the liner in several ways, diagrammed in Figure 2-25. The first, (a), shows inadequate pump pressure, where the oil fluid does not have enough pressure to reach the liner and instead drips down from the nozzle. The third, (c), diagrams the fluid behavior when the pump pressure is too high. The oil hits the liner and a large fraction bounces off the liner, down onto the rig, or onto the ring holder. Some oil does remain on the liner. The second picture, (b), shows

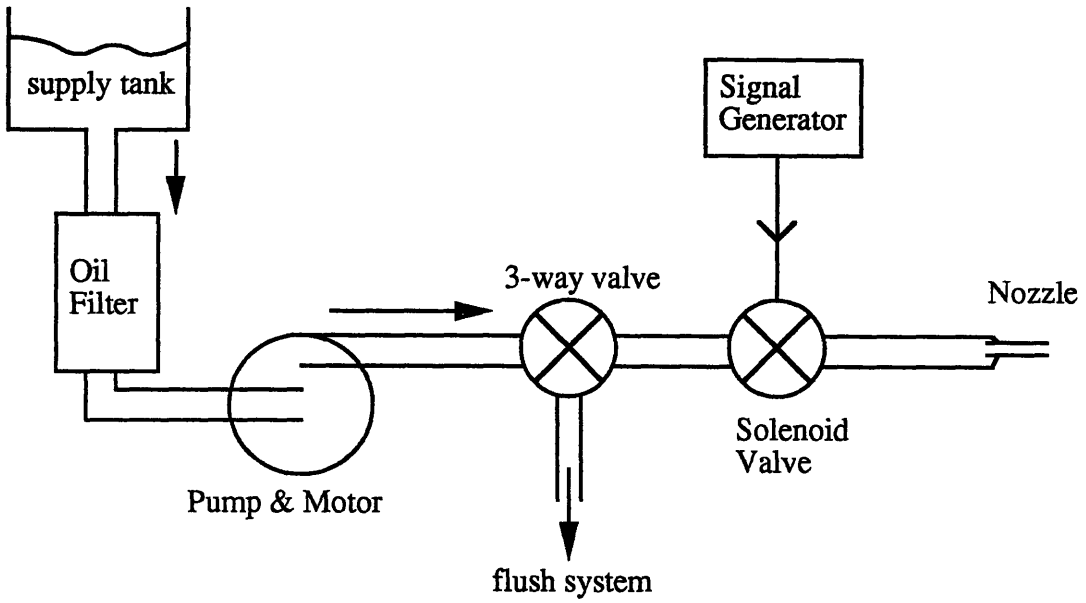

Figure 2-23: Oil Feed System Schematic

the ideal situation, with the pump pressure optimized to spray just to the liner. Most of the oil remains on the liner. However, this situation is very difficult to achieve in practice. The system is actually closer to the situation shown in (c), where there is some oil loss as a result of the high stream pressure.

2.2.7 Data Acquisition System

The Data Acquisition System (DAS) used was one employed in conjunction with previous L.I.F. experimentation. More information is available in [18]. Three channels of data, as well as the shaft encoder signal, were input to the DAS. Channel 0 was the friction force signal, channel 1, the normal force signal, and channel 2 was the L.I.F. signal. The DAS system software does not allow for collection of three channels, so four channels were recorded, with channel 3 discarded during data analysis.

The analog to digital (A/D) converter transforms the channel input voltages to 12 bit (4096 levels) of digital data. For this case, the L.I.F. signal was set to vary between 0 and 10 Volts and the friction force load cell emitted a positive and negative voltage for compression and tension, so a range of ± 10 V was set. The resolution is thus 5

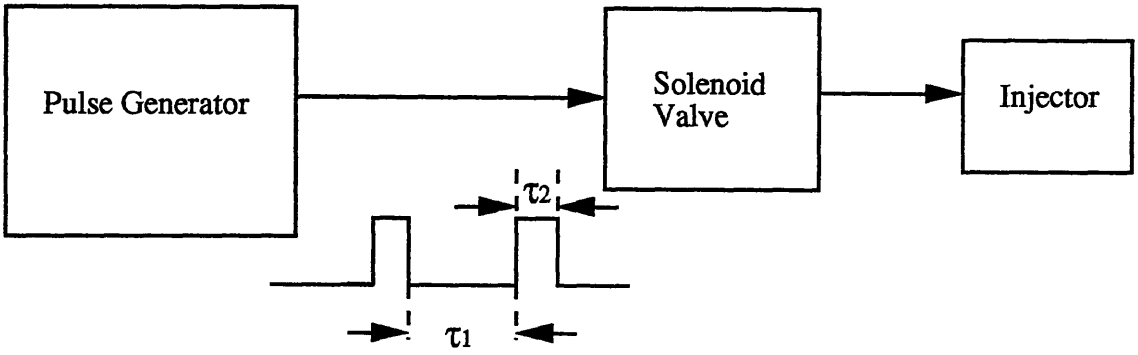

τ1: pulse spacing: frequency of valve opening
τ2: pulse width: valve open duration

Figure 2-24: Oil Feed System Schematic: Pulse Duration and Frequency Control

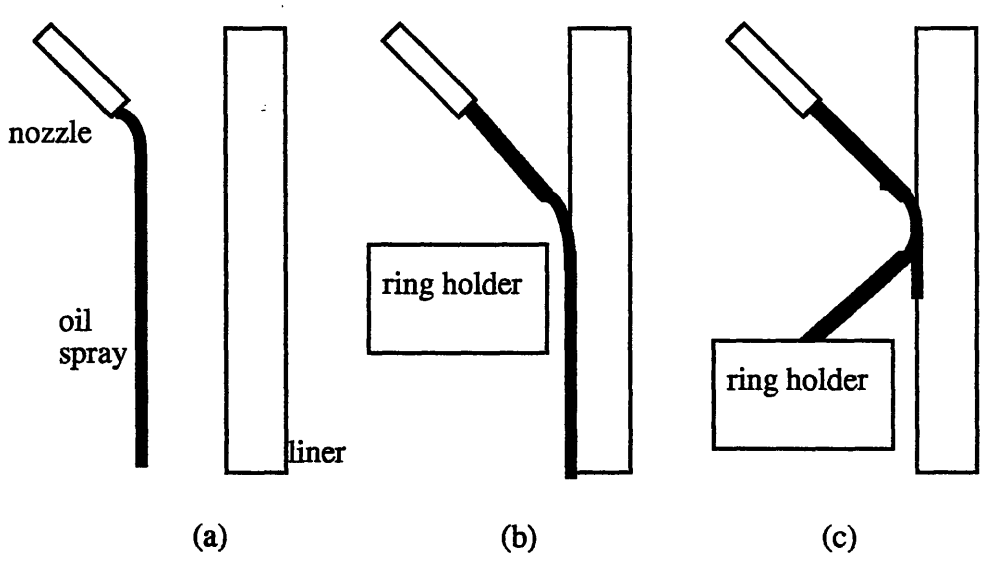

Figure 2-25: Oil Feed System Spray Patterns

Number of samples	288,000
Clock	External
Channel	0&1&2&3
Range	±10V
Trigger on	digital edge
Start	after pos
Offset	0

Table 2.4: DAS software inputs

mV.

The user inputs to the DAS software program are listed in Table 2.4. The shaft encoder sent 7,200 data points per revolution, the number of input channels was four and the number of cycles for sampling was usually set at ten. This gave a total number of 288,000 samples. It was desired to average the data over several cycles, however, the size of output data files were usually very large, placing a limitation on the amount of collectible data. The choice of ten cycles reflected the compromise.

The software output was in ASCII format of four columns of data, each column containing the data for one input channel and each row signifying the crank angle difference between sampling.

2.3 Experimental Procedure

This section describes how the raw data gathered by the data acquisition system and the analog displays was processed into calibrated and useful results for analysis and comparison.

2.3.1 Calibration of Friction and Normal Forces

The friction force signal was converted to Newtons using the calibration constant provided by the manufacturer. The normal force signal was calibrated by applying weights to the load cell and observing the digital output on the oscilloscope. The

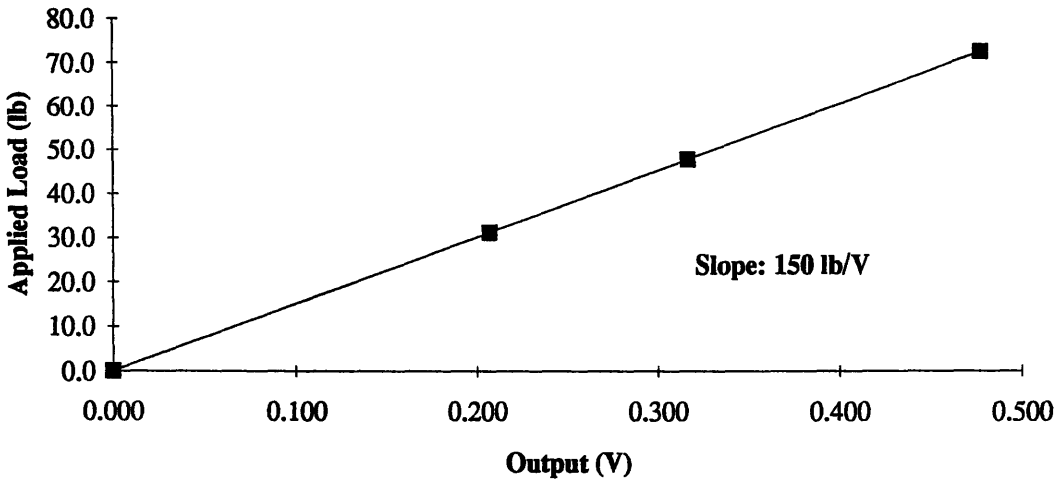

Figure 2-26: Calibration of the Normal Load Cell

data set is graphed in Figure 2-26. The points correspond very well to a straight line, with zero offset. The slope of the line was used as the new calibration.

2.3.2 Calculation of Friction Coefficient

The friction coefficient was calculated from the ensemble averaged friction and normal force cycles. In order to obtain instantaneous friction coefficient values, the coefficient was calculated for the entire average cycle, using equation 1.1.

2.3.3 Calibration of Oil Film Thickness

The standard method for converting the L.I.F. signal to distance is to match a physical marking of known depth on the piston to the equivalent trace in the L.I.F. signal. In [12], the piston skirt machining marks allowed for calibration of the L.I.F. signal. However, this strategy is difficult to apply to the test apparatus because of the use of a single ring and the absence of a piston and easily visible oil control ring. It was decided to mark the top ring itself, for active calibration. Technicians at Dana Corporation etched two top rings at circumferential positions corresponding to the L.I.F. window locations and provided Talysurf profiles of the resulting grooves. The groove chosen for experimentation, shown in Figure 2-27 was the most centered in the ring profile and has a width of approximately 150 μm and a depth of 25 μm, which is

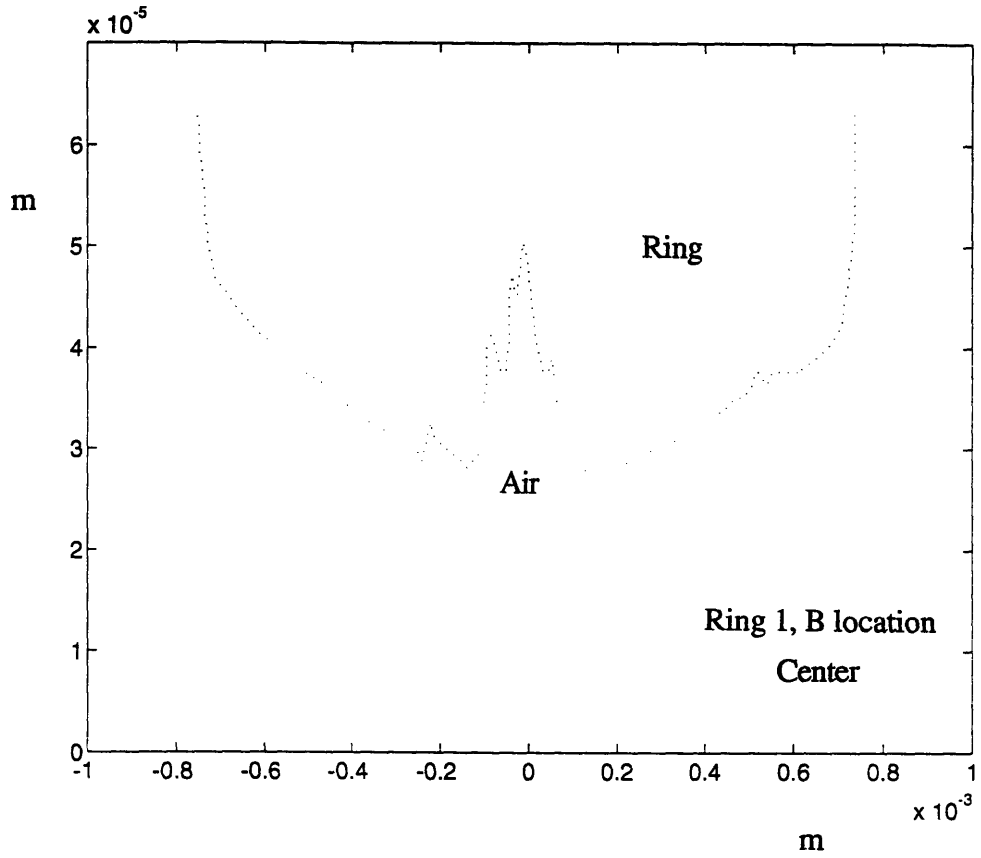

Figure 2-27: Talysurf Profile of the Ring used in experimentation.

of the order of the desired oil film thicknesses. It was hoped that the Talysurf profile could be superimposed on the L.I.F. signal.

2.3.4 Location of Top Center

The shaft encoder pulsing is known to be 7200 points per revolution. This translates to the data having been sampled every 0.05°. A crank angle vector of 7200 points incrementally increased by 0.05° was made to represent this, so that data could be plotted against crank angle. The calibrated averaged friction force trace was plotted against the crank angle vector, and the zero points, where the friction force was zero, were located using an iterative process. The first zero was found to be at 4.625°. The second zero follows the first zero by 180°. These results were reflected in a new crank angle vector. To determine which zero corresponded to top center, the apparatus was turned by hand and the friction trace observed on the oscilloscope. As

the ring moved downwards, the signal was positive, and became negative when the ring reversed direction.

2.3.5 Calculation of Linear Position and Velocity

The crank angle was converted to linear distance along the liner using formula 2.5 of [1, p.44],

$$s = a\cos\theta + (l^2 - a^2\sin^2\theta)^{\frac{1}{2}} \tag{2.1}$$

where θ is the crank angle, a is the crank radius and equal to half the stroke length, l is the length of the connecting rod, and s is the distance from the crankshaft axis of rotation to the piston pin axis. In order to have the linear distance defined relative to top center, this was adjusted to:

$$d = a + l - [a\cos\theta + (l^2 - a^2\sin^2\theta)^{\frac{1}{2}}] \tag{2.2}$$

The stroke length is given as 0.067 m and the connecting rod length was measured at 0.11309 m.

The linear sliding velocity, U, was calculated by taking the time derivative of equation 2.2 above, yielding,

$$U = \frac{2\pi}{60}V\sin\theta\left[a + \frac{a^2\cos\theta}{(l^2 - a^2\sin^2\theta)^{\frac{1}{2}}}\right] \tag{2.3}$$

where V is the crankshaft rotational velocity in rpm.

2.3.6 Calculation of the Sommerfeld Number

The Sommerfeld Number was defined earlier as $\frac{\mu U}{\sigma c}$. The viscosity of the oil, μ was provided by the manufacturer, Shell, for temperatures 40 ° Celsius and 100 ° Celsius. Although these are applicable to engine operating conditions, they were too high for the test apparatus, which runs at room temperature. For each of the oils provided, the viscosity was graphed against temperature, and linearly extrapolated to the desired

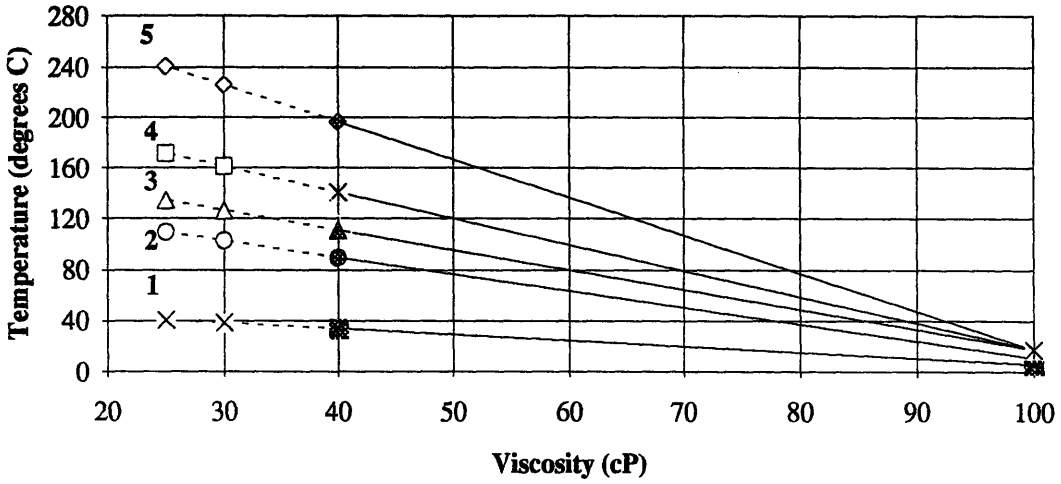

Figure 2-28: Extrapolation of Viscosity to Room Temperature

value, as shown in Figure 2-28. The calculation of the sliding velocity, U, has been described earlier. Physically, the Sommerfeld Number should use the minimum oil film thickness h_0 as the sliding pad width, or reference length. The limitations of the L.I.F. measurements, however, only provide the measurement of film thickness at the quartz window location, estimated at 81° from top center, at midstroke. For the Sommerfeld number for the data in a cycle, b, the ring width, is substituted as the reference length. The normal pressure, σ, is the normal force divided by the area of contact. This was calculated as the ring thickness times the length of contact, estimated at 2.9 cm, resulting in a $4.2 \times 10^{-5}\ m^2$ area. This is probably high, and the normal pressure is probably smaller as a result. The ring profile curvature would not contact the liner over the entire ring width, unless the ring was well worn-in.

The experimental procedure was written into code, using the software MATLAB, chosen because of the software's capability to handle large arrays. A flowchart of the program logic is shown in Figure 2-29. A copy of the actual code is shown in Appendix A.

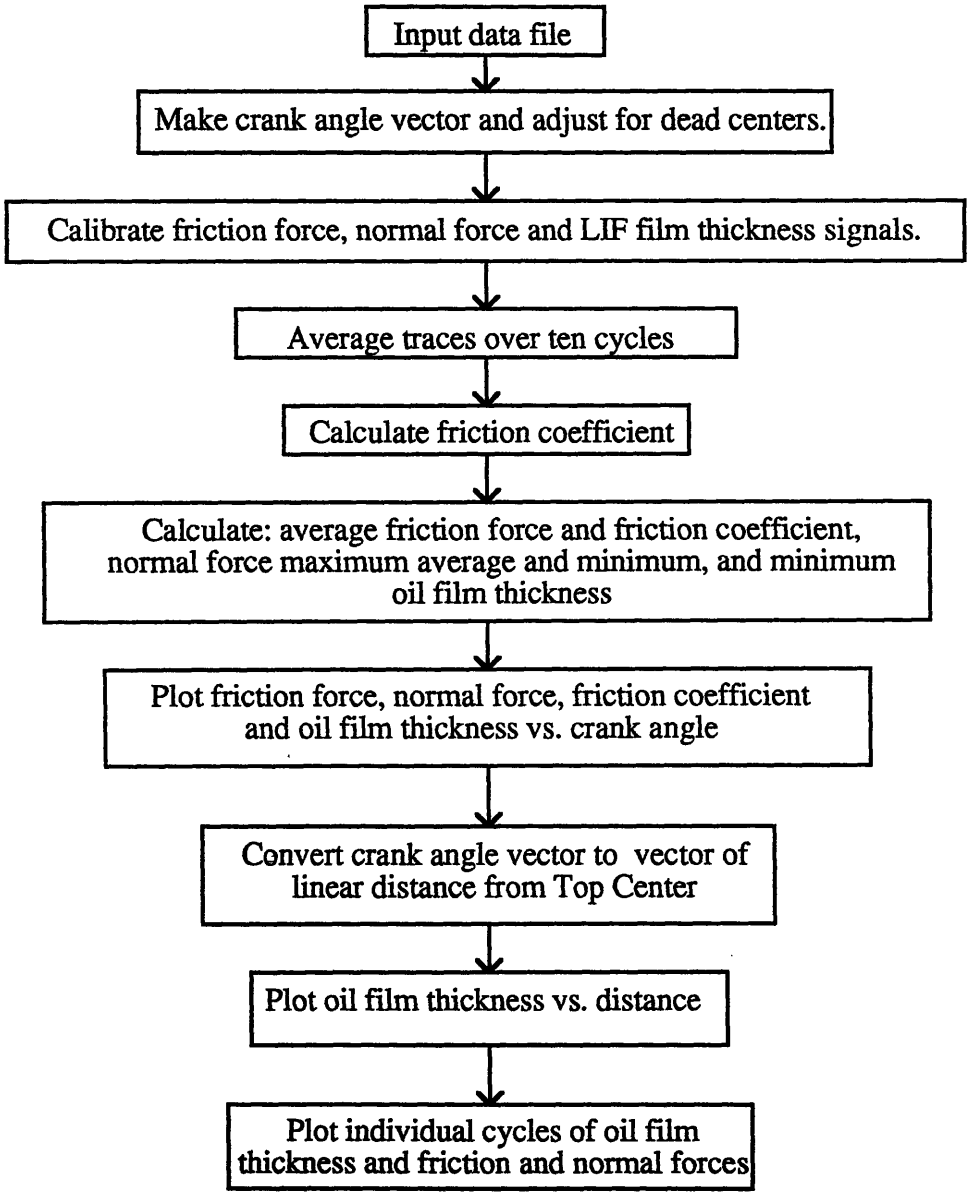

Figure 2-29: Flowchart of the Code embedding the Experimental Procedure

Chapter 3

Observations of Test Apparatus Behavior

This chapter describes typical results obtained from equipment operation, and discusses the issues resulting from the initial runs. Results from a complete data matrix will be presented in the next chapter. Trial tests were run, under varying conditions of load, speed and oil viscosity. The friction force, normal force and oil film thickness signals were found to be repeatable and consistent with the expected behavior and value range. The oil film thickness was found to decrease with load and increase with speed. The main issues for action and discussion were: variation in normal force, effects of quartz windows on friction, conformance of the ring fit to liner curvature, reciprocator/liner axis alignment, ease of apparatus disassembly, linear bearing friction contribution, oil film temporal behavior and oil film thickness calibration.

3.1 Normal Force Variation

Figure 3-1 displays a normal force trace, averaged over ten cycles, taken under test conditions of 210 rpm and 46 N average normal load, using a 10W50 oil. The normal load is not constant throughout the cycle and varies significantly, from a maximum of 58 N to a minimum of 40 N. This variation is repeated for each individual cycle and is highest at low loads. It was hypothesized that the cyclical variation is a result

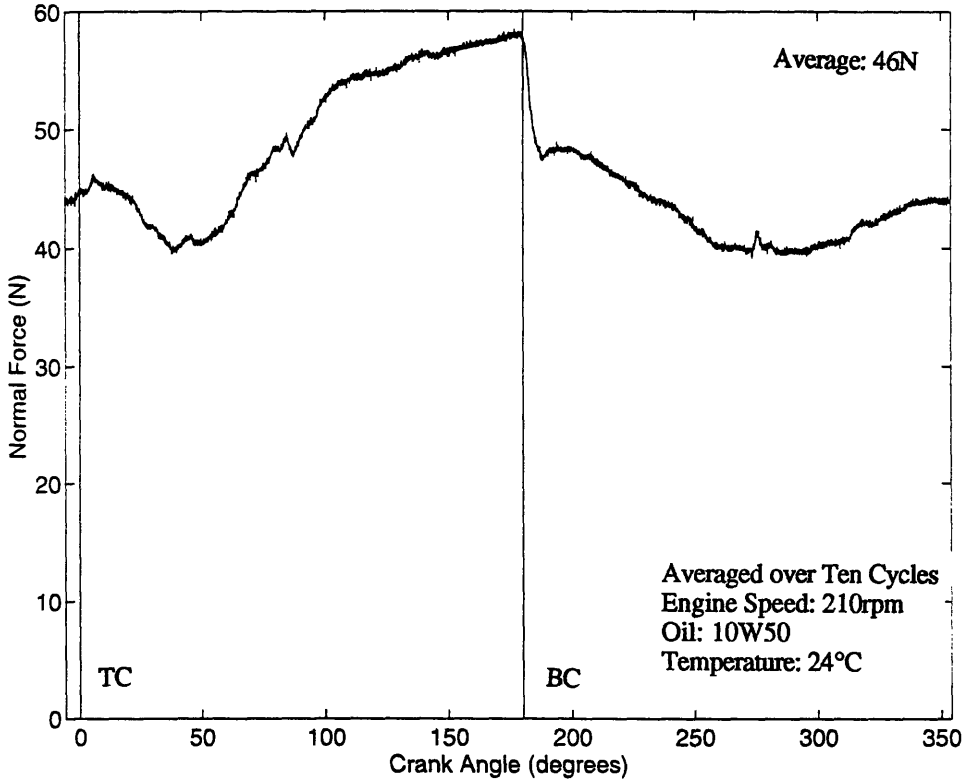

Figure 3-1: Sample Normal Force Trace

of the ring guide/ring holder geometry, shown in Figure 3-2 and photographed in Figure 3-3. The normal force transducer is positioned against the front surface of the ring guide and slip-fit into a bore hole in the rear surface of the ring holder so that the normal force is transmitted through the protruding button on the load cell. The surface area of the button is approximately 9 mm^2, positioned between two surfaces, each approximately 500 mm^2. It is probable that the load cell and thus the ring holder rotates about the button during the stroke. The motion is constrained by the corners of the ring holder. As a result, there may be more contact points than through the button of the load cell, so that not all the normal force is transmitted through the load cell itself. The variation in Figure 3-1 neglects the redistribution of the normal load between the load cell and the other contact points.

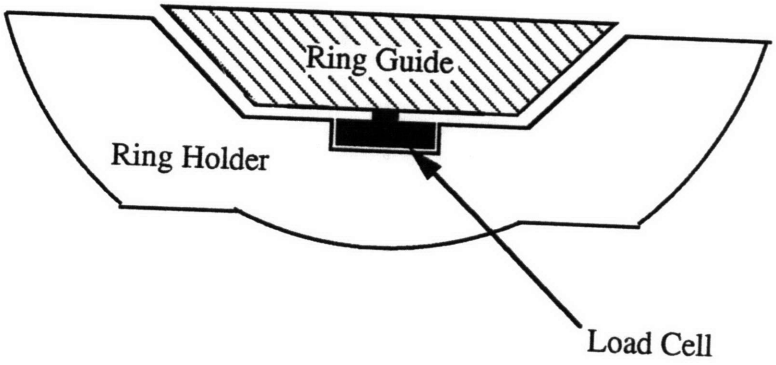

Figure 3-2: Schematic of the Normal Force Load Cell Positioning

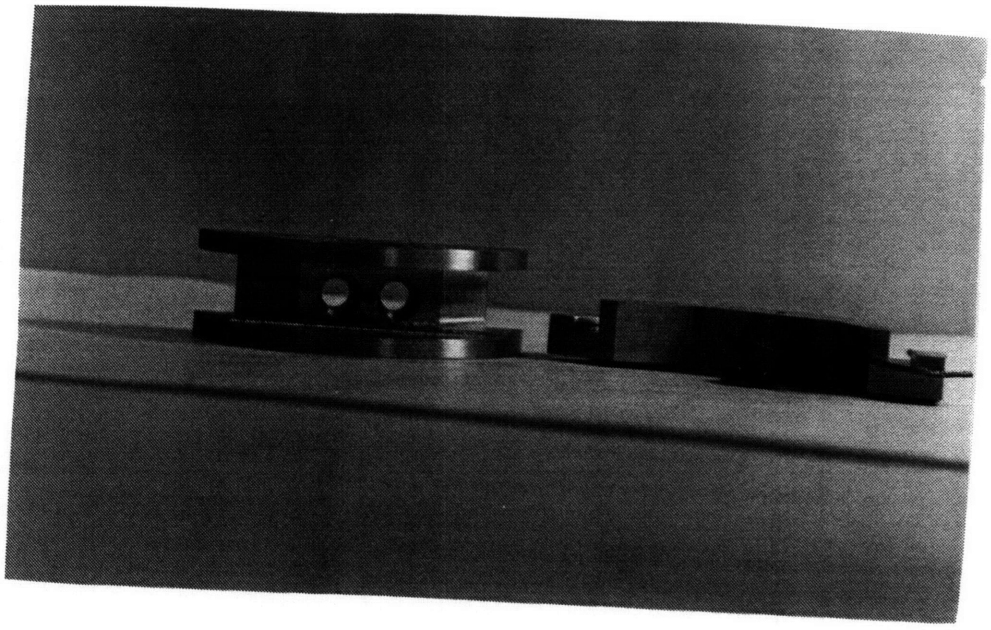

Figure 3-3: Photograph of the Normal Force Load Cell, positioned between the front surface of the Ring Guide (left) and the rear surface of the Ring Holder (right).

3.2 Effects of L.I.F. Quartz Windows on Friction

In a hydrodynamic lubrication regime, the friction force will not be dependent on the surface finishes of the two sliding materials. However, preliminary friction force results showed a change in friction behavior at the axial location of the quartz windows. Figure 3-4 displays an averaged friction force trace at 210 rpm engine speed and approximately 46 N normal force. For both strokes, there is a large spike at the quartz window location, where there is dramatic change in surface finish. Effects from the presence of L.I.F. windows appeared consistently in all trial friction force measurements. This provokes two concerns. First, the rig is not operating under hydrodynamic lubrication and input conditions may have to be altered. Second, the quartz windows may be affecting lubricant flow. Figure 3-5 shows a cross-section of the liner sample at the axial location of maximum window diameter. The window to liner length ratio is approximately 20% but may be higher if the ring is not contacting the complete length of the liner.

Additionally, the liner was machined and the windows glued into the liner with the objective of having the window curvature flush with that of the liner, in order to both minimize the effect of the windows of lubricant behavior and to reduce any offset in oil film thickness measurements. For evaluation purposes, the position of the window in the front surface of the liner sample was measured by using a stationary dial indicator, and moving the liner sample in the axial direction. The results are shown in Figure 3-6. The dial indicator had a precision of 0.00005 inches. The window on the left when facing the liner front surface was cocked in its mounting with the top side lower than the liner surface and the bottom side 0.0001 inch higher. The right window appeared to be uniformly lower than the liner surface, by 0.0001 inch. Both offsets are on the order of previously measured minimum oil film thicknesses, and it is not unreasonable to surmise that this may affect the oil film behavior.

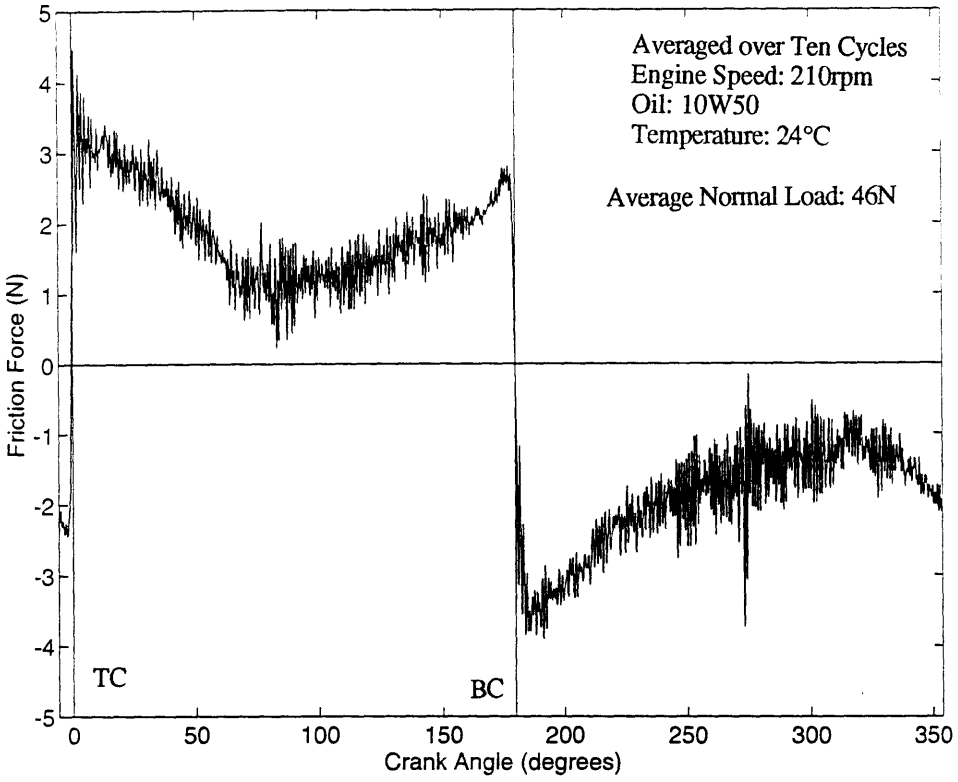

Figure 3-4: Sample Friction Force Trace

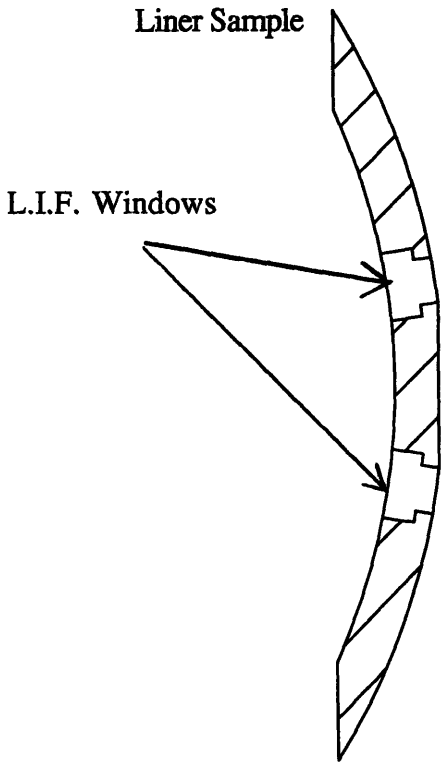

Figure 3-5: Cross section of the Liner Sample, showing L.I.F. Quartz Windows.

3.3 Ring Conformance to Liner Curvature

The ring/liner non-conformance first became noticeable upon observation of the oil spreading. The oil pattern, after the ring had passed over it, was not axially symmetric and there tended to be clumps of oil or oil streaks. In addition, the ring holder, when moving towards the liner sample, tended to hit one side of the liner first, as shown in Figure 3-7. This drawing compares the ideal situation, where the ring curvature conforms to that of the liner at every circumferential point, to the actual situation. To investigate this issue further, the test rig was cleaned of oil and the engine was turned by hand until the ring was positioned in front of the windows. Then a low normal force simulating ring elastic pressure was applied and a miniature light bulb placed under the ring holder. The ring/liner conformance was then studied from above the test apparatus. The ring curvature appeared to match the liner curvature better on one side than on the other as expected and could be adjusted to match part of the curvature but not all of it. This has implications for determining the contact

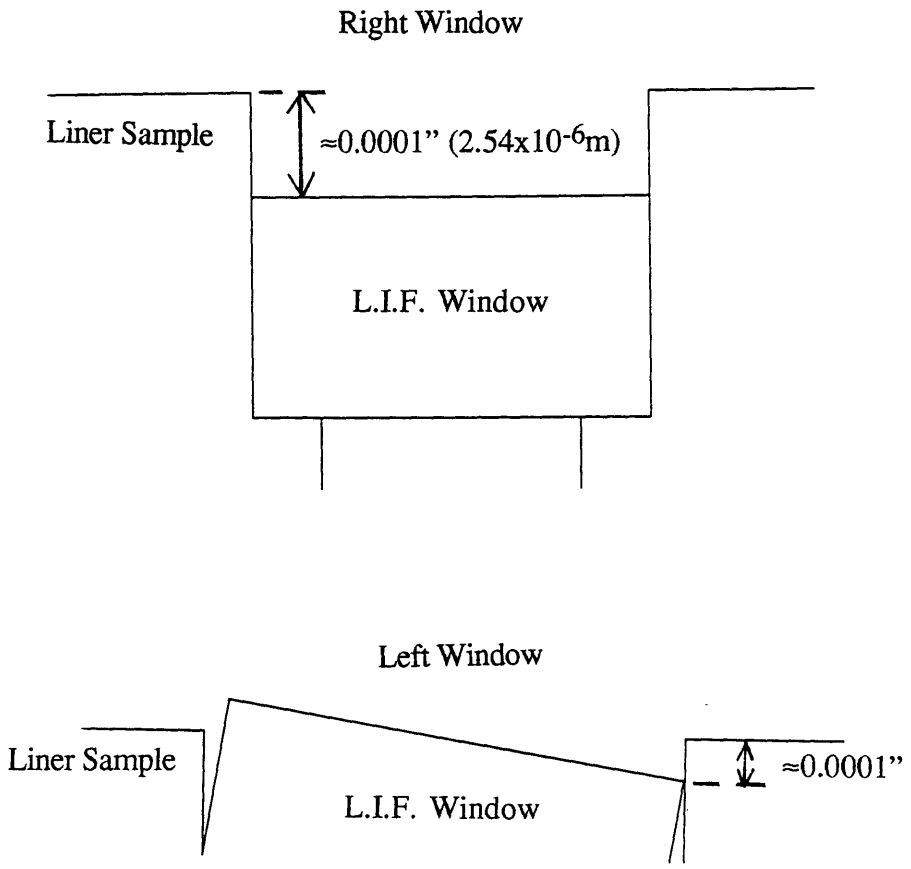

Figure 3-6: Ring/Liner Axis Alignment.

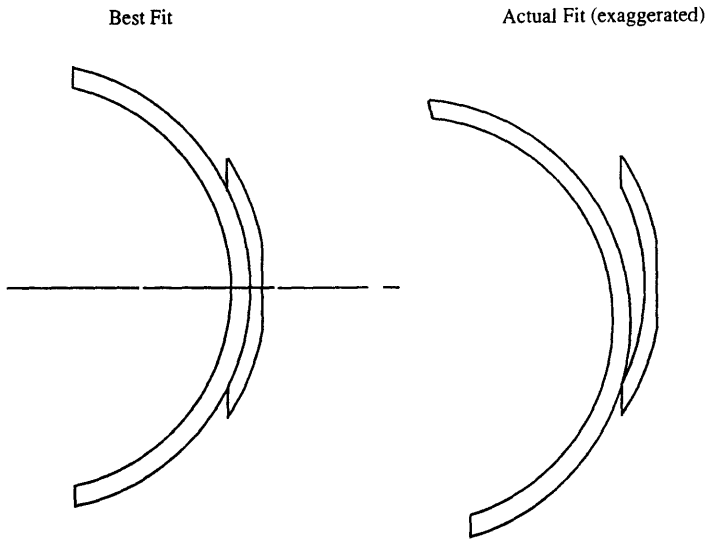

Figure 3-7: Ring/Liner Ideal and Actual Fits.

area and for understanding the lubricant flow. The ring/liner non-conformance could be a result of normal bore distortion in an engine liner, where the liner curvature is not perfectly cylindrical, and it could also be a result of the process used to cut the liner sample. It is possible that the liner, when cut, distorts to a larger and non-uniform radius. This is not an easy problem to solve, especially since the ring holder only allows for maximum ring radius adjustment to that of the pre-cut liner sample radius. Because it is difficult to adjust the liner sample radius, it was decided to alter the ring holder design.

The re-design is shown in Figure 3-8 and photographed in Figure 3-9. The two side ledges were milled off and the inner groove, which controls the ring radius, was machined from 1.776 inches to a larger radius of 1.781 inches. Two machined pieces replaced the ledges and are screwed down to the ring holder and reinforced with helicoil inserts. This re-design provided a slightly better fit, which is shown in Figure 3-10. The ring segment curvature matches at the center and at the extreme sides of the liner sample. but in-between, there is some non-contact, and light can be clearly seen shining through the gaps. The radial gap size was estimate at 0.002 inches, which is an order of magnitude larger than typical minimum oil film thicknesses. It was decided to adjust the ring radius in the ring holder until the ring curvature matched that of the liner in the area near the quartz windows, which are the critical locations. The resulting oil spreading leaves a small streak in the center and at the sides. This is the best fit for this axial position and the liner segment curvature may also be distorted axially. It is difficult to judge the severity of this problem, which is usually not discussed in the literature.

3.4 Ring/Liner Axis Alignment

The problem discussed in the previous section highlighted another potential issue associated with the rig design. The axis of motion of the ring is determined by the engine piston movement. This may not be parallel to the axial direction of the liner segment, which is determined by the liner sample fit to the load cell apparatus and the

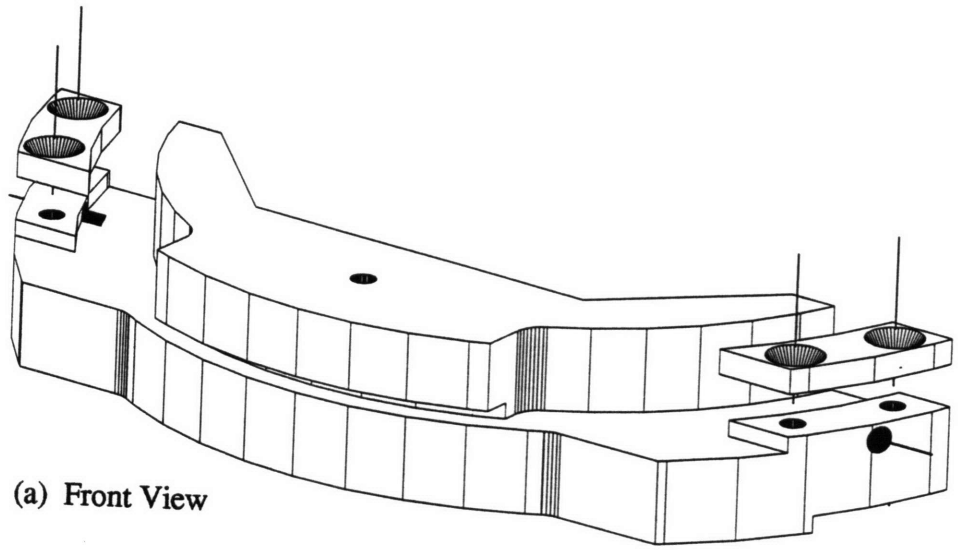

(a) Front View

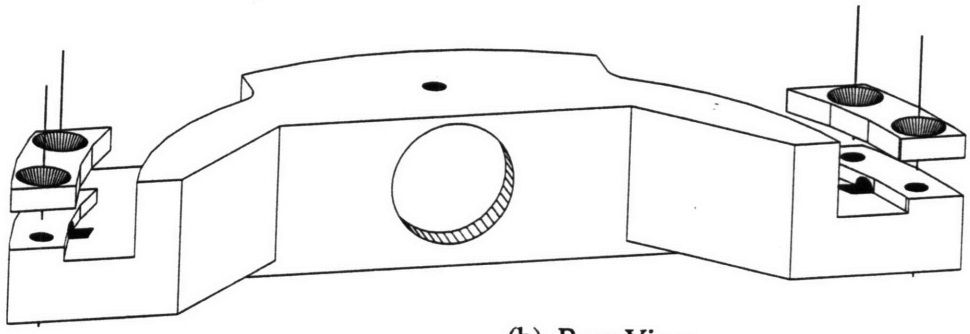

(b) Rear View

Figure 3-8: New Ring Holder Design.

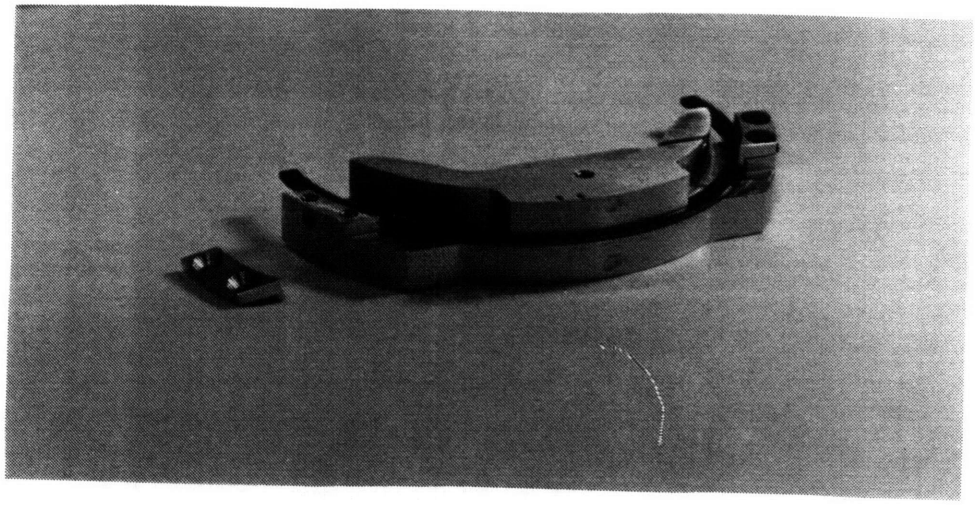

Figure 3-9: Photograph of the redesigned Ring Holder.

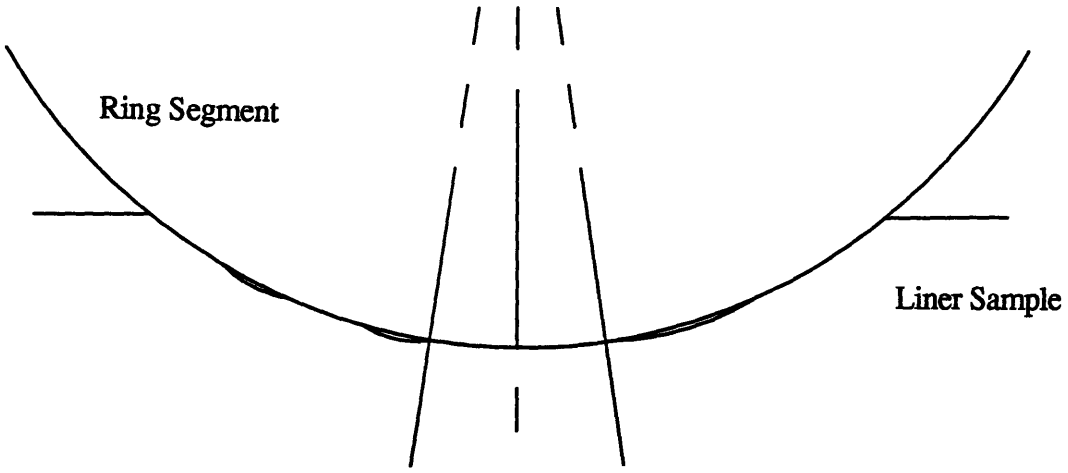

Figure 3-10: Fit of Ring Curvature to that of the Liner Segment.

consequent fit to the test apparatus walls. Moreover, disassembly and reassembly of the rig results in a new liner sample axis. The problem was assessed by mounting a dial indicator on the reciprocator and positioning the indicator end on the liner segment. The engine was hand turned and the distortion of the indicator visually traced and recorded at 20° intervals. The distortion at the circumferential center was examined and the procedure reiterated at two positions, in front of the windows as shown in Figure 3-11, which also displays the results in graphs of measured distortion against axial position. The liner segment appears to be tilted away from the reciprocator at the top and towards the reciprocator at the bottom. This seems to be the sole direction in which the axes are misaligned and confirms that the ring conformance will vary from that measured at midstroke but may not vary circumferentially as a result of changes in liner sample alignment.

3.5 Apparatus Disassembly

Trial testing of the rig demonstrated the difficulty of accessing the ring and ring holder. While the ring holder is not physically attached to anything, it cannot be extracted without first removing the blocking liner sample and load cell apparatus. This is a concern because the total time for this disassembly and reassembly is approximately two hours. A simple re-design was implemented, which reduced the assembly time to

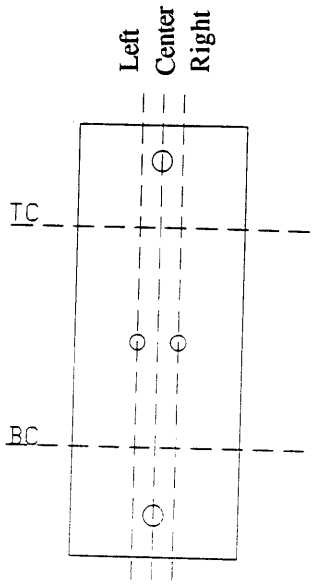

(a) Liner Sample Measurement Locations

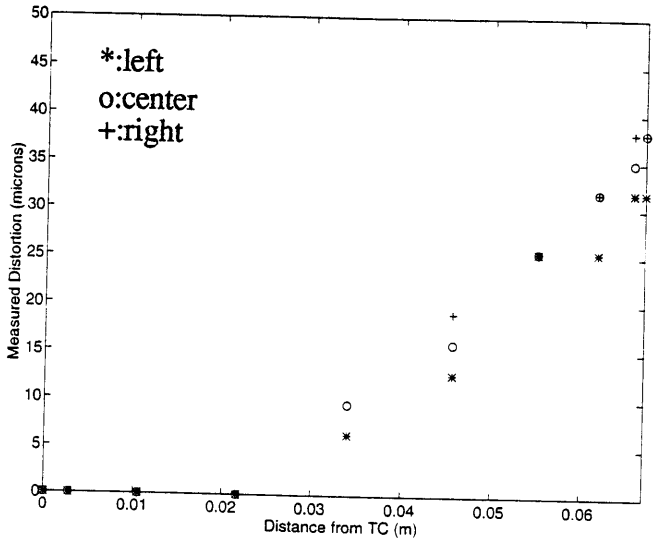

(b) & (c): Liner Distortion with Axial Position, at Three Circumferential Positions

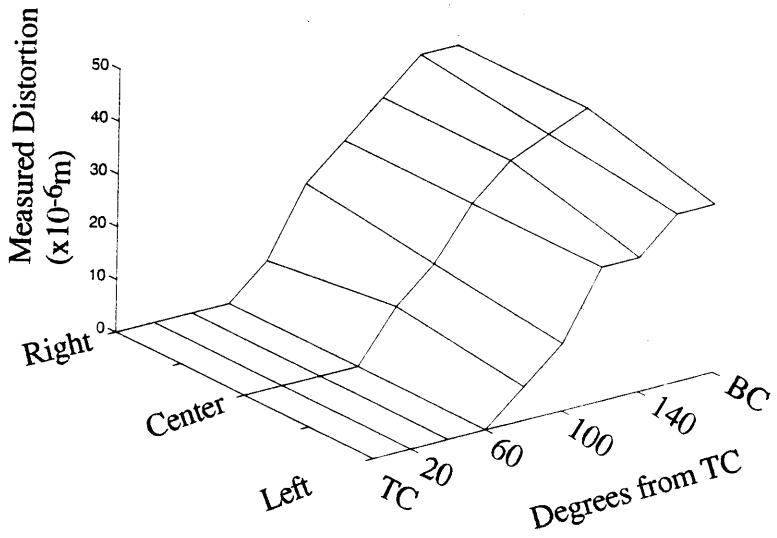

Figure 3-11: Liner/Ring Axis Alignment

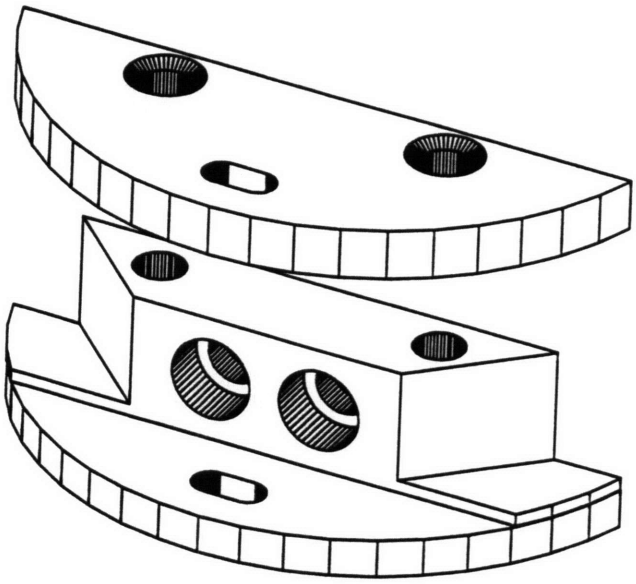

Figure 3-12: Re-design of the Ring Guide for Improved Access to the Ring Holder.

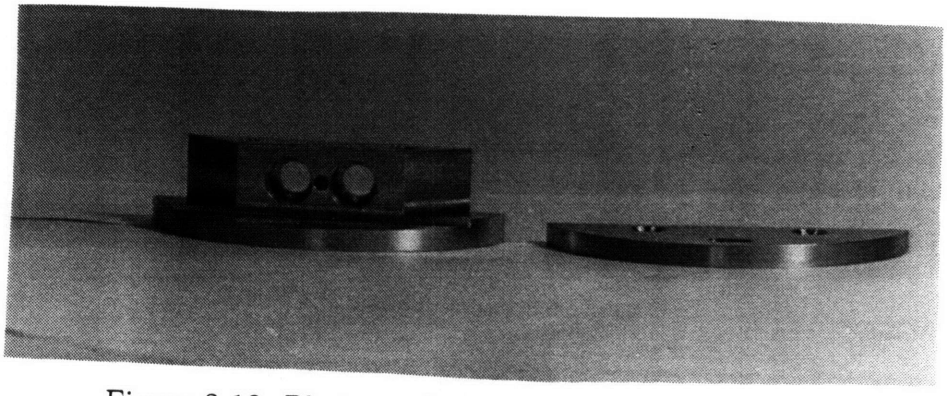

Figure 3-13: Photograph of the redesigned Ring Guide.

five minutes. This is shown in Figure 3-12 and photographed in Figure 3-13. The top ledge of the ring guide was milled off and a replacement piece was machined which is attached through two flathead screws into helicoil inserts. Removal of the ring holder became a simple process of removing the ring guide ledge and lifting up the holder. This also additionally allowed for easier cleaning of and oil removal from the test apparatus.

3.6 Bearing Friction Contribution

Linear bearings were installed in the reciprocator and the load cell apparatus. After approximately an hour of engine operation, score marks appeared on the reciprocator rods, caused by the balls of the larger linear bearings. The effects of the smaller linear bearings in the load cell apparatus were more difficult to discern because the rods are obscured by the equipment but it became a concern that they were contributing to the friction force measured by the load cell. To assuage this concern, the bearings of the load cell apparatus were replaced and the shafts were replaced by rods of smaller diameter. The new equipment appeared to move more easily and there were no visible scratch-marks from vigorous manual movement of the shafts. Unfortunately, the friction force and friction coefficient did not noticeably change.

3.7 Temporal Oil Film Thickness Behavior

The pulsed injection oil feed system was run through some trial tests, both to observe the oil flow to the liner and to examine the oil behavior on the liner. It was found that the oil feed pulsed too much oil to the liner, even at the lowest setting of pulse width of five ms and pulse spacing of one second, which produced a volume flow rate of oil onto the liner of 7.5 mL per minute.

Under these conditions, a large amount of oil was bouncing away from the liner and a visual inspection of the liner showed complete flooding of the liner. It was decided to send a single pulse of oil to the liner and, using an oscilloscope, observe the oil film thickness, focusing on the trace around the ring. An oil thinning pattern was observed, where, defining time zero as the time of the single oil pulse, the oil thickness trace assumed a shape similar to the one shown in Figure 3-14. In the first few seconds, the overall trace would rapidly increase in size and then, over the course of half a minute, reached a steady state, in which the trace did not change further, for a period of observation of over half an hour. The mass of oil to the right of the ring, labeled Δy, was studied over several runs at engine speeds of 300, 400 and 600

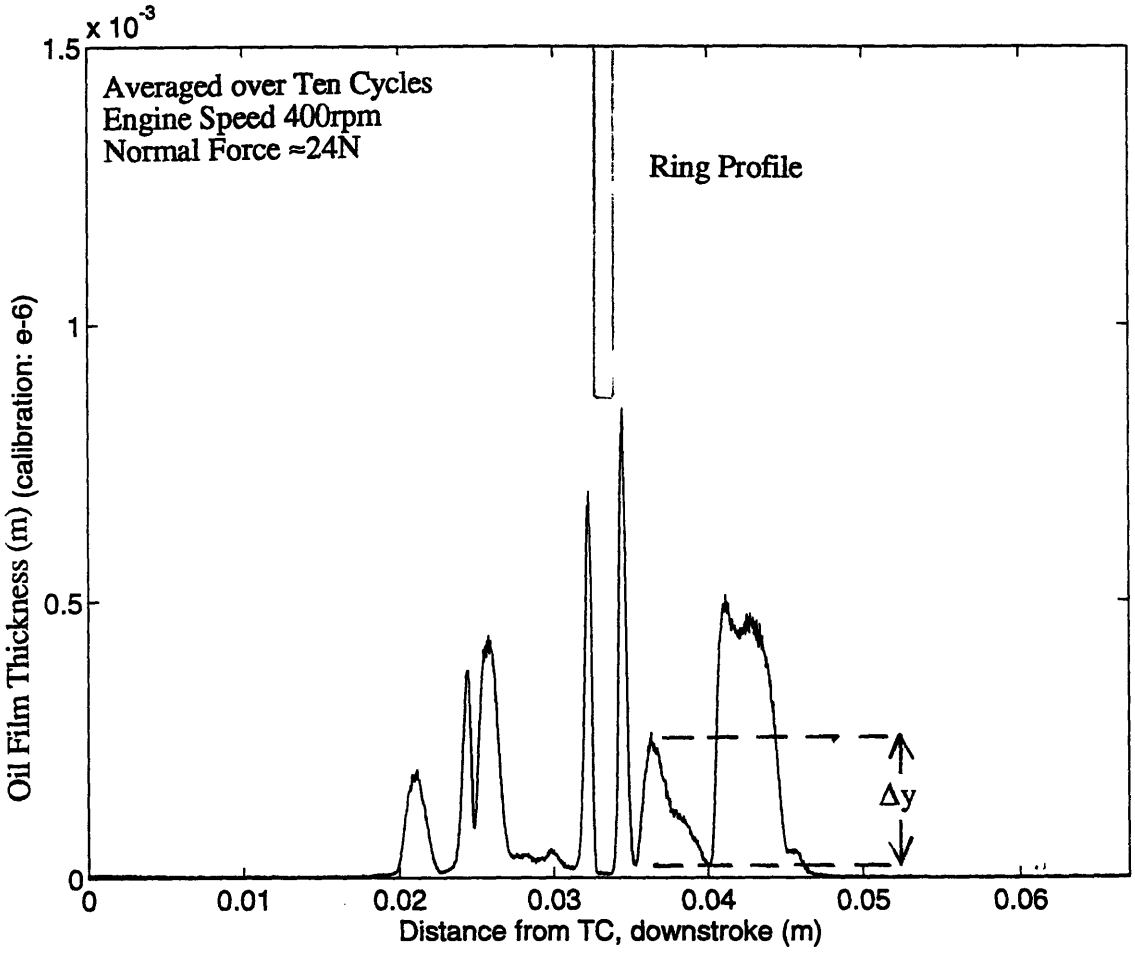

Figure 3-14: Sample Oil Film Thickness Trace.

rpm, approximately 20 N normal load and pulse width of 40 ms. The oil thinning is displayed in Figure 3-15. It was hypothesized that the pulsed oil initially increased the oil mass around the ring and then, reflected in the transition to steady state, some amount was shaken off by engine vibration and ring reciprocating motion and some oil flowed down the liner due to gravity. At steady state, the oil film behavior on the liner is solely determined by the ring/liner interaction and oil properties.

3.8 Oil Film Thickness Calibration

In preliminary trials, the calibration of the L.I.F. signal was found to be very challenging. The calibration factor affects the oil trace shape in both the vertical and horizontal directions. If the factor is halved, then, for the same distance from Top

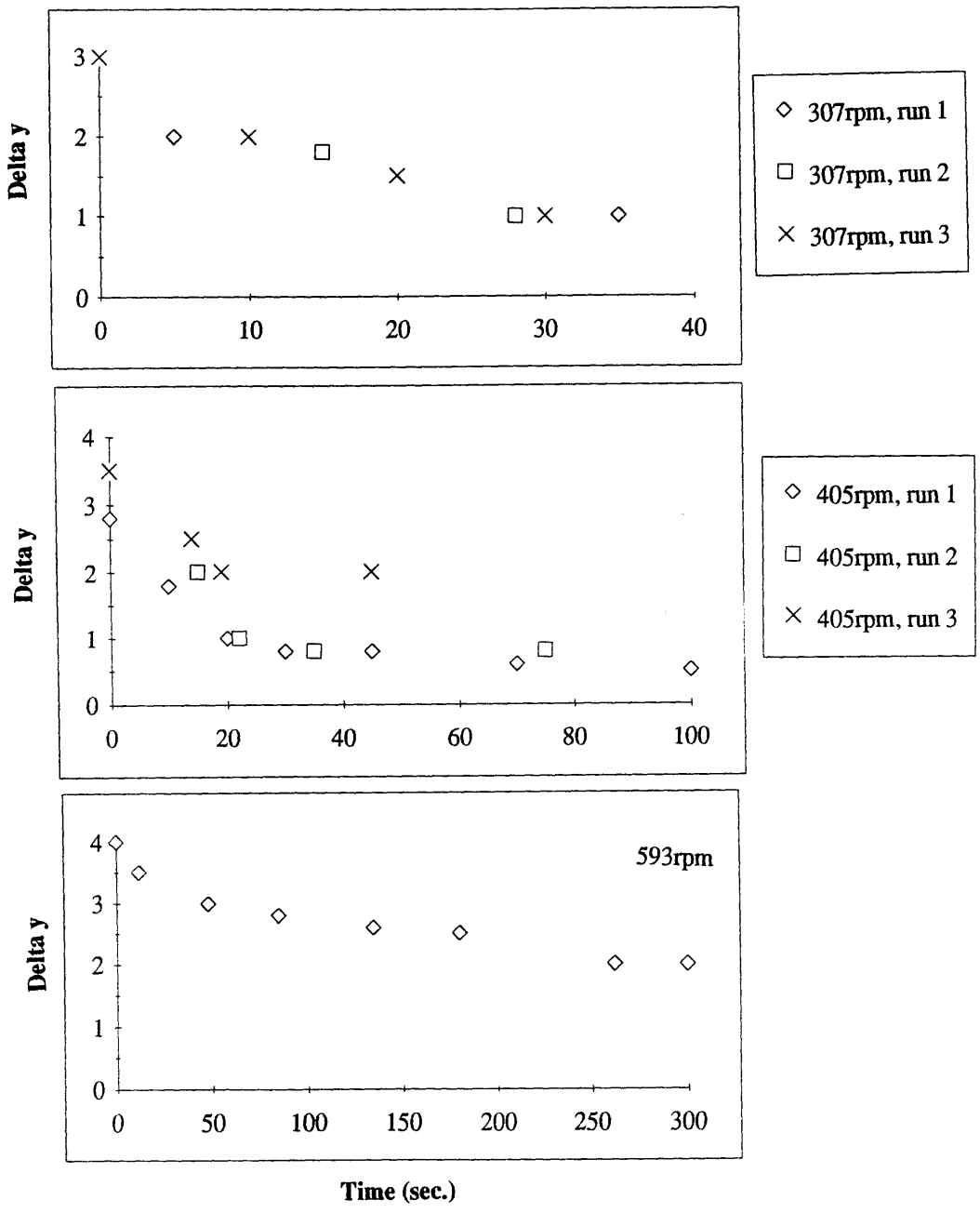

Figure 3-15: Oil Thinning over time.

Center, the height of the oil film thickness is halved and the curvature is flattened. Figure 3-16 shows two oil film thickness traces, taken at 400 rpm, multiplied by the same calibration factor. The left graph, (a), was taken using the drip oil feed system and the right graph (b) is a result of a single oil pulse. In both graphs, the Talysurf ring profile is diagrammed as the dotted line, and is shown to be larger than the oil trace around the ring, a physically impossible situation, although in (a), the actual ring groove matches the groove depth of the oil trace. If, in (a), the calibration is altered until the ring widths are matched, the groove markings of the oil trace are flattened out. In (b), the groove mark is completely absent from the oil trace. The groove was inspected using a microscope and it was found to have been worn down from apparatus operation. Since it can no longer be reliably used for calibration, the only recourse is to recalibrate so that the ring widths are matched.

This chapter has outlined some of the initial data and resulting issues and assessed the main problems and corresponding revisions. The completion of preliminary testing allowed for data collection which is described in the next chapter.

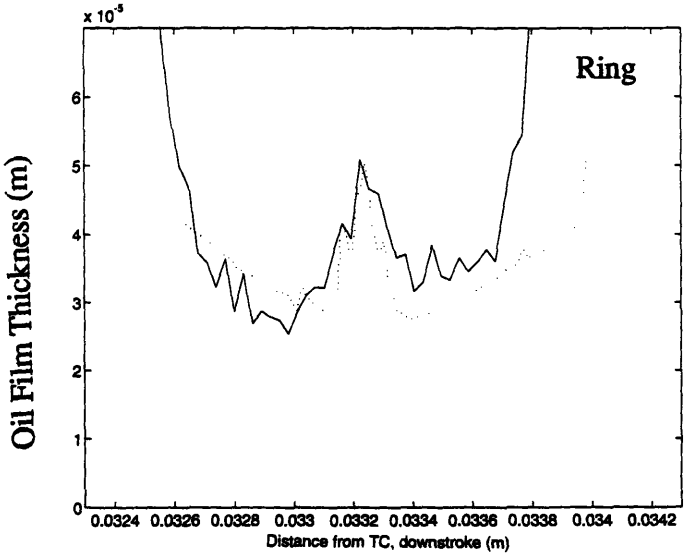

(a) 400rpm
Normal Force ≈14N
L.I.F. calibration: 10^{-6}

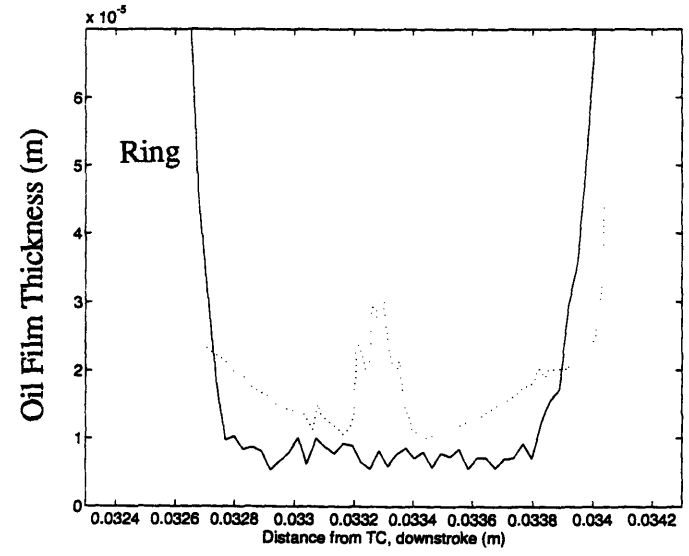

(b) 400rpm
Normal Force ≈24N
L.I.F. calibration: 10^{-6}

Figure 3-16: Two Sample Calibrations of Oil Film Thickness Traces.

Chapter 4

Experimental Data and Analysis

The matrix of test conditions for each data set is shown in Table 4.1. A total of forty-five data sets were taken, where oil type, normal load and engine speed were varied. Each data set included: instantaneous friction force, normal force and L.I.F. signal values. Five oil types were used, providing a viscosity range, at 30°C, of 38 to 226 cP. Three normal load test conditions were chosen. The lowest value of approximately 15 N represents a typical ring force due solely to ring elastic pressure. The two higher values represent the presence of gas pressure behind the ring. Three engine speeds were chosen. The preliminary results indicated increased noise with higher engine speeds such as 400 and 600 rpm, while the results at 200 rpm are relatively noise-free. The highest speed, 600 rpm, is at the limit of the dynamometer capability. For a stroke of 0.067 m, the corresponding mean piston speeds for 200, 400 and 600 rpm are, respectively, 0.45, 0.67 and 0.89 m/s.

The data was collected in order of test number. The raw data is given in Appendix B. This includes: the oil thinning data, oil type, engine speed, liner temperature and applied normal load. The raw data, collected as described in the *Experimental Procedure* section, is also listed, and includes: friction force, instantaneous normal force, friction coefficients and minimum oil film thickness. This chapter will first present the measurements of the system inputs: liner temperature and normal load. Next, typical results will be presented for oil film thickness, friction force and coefficient and general trends will be examined. Specific graphical results for oil film

Data Set	Oil Viscosity at 30°C (cP)	Normal Load (N)	Engine Speed (rpm)
1	38.2	15	200
2	(Oil #1)		400
3	10W		600
4		40	200
5			400
6			600
7		80	200
8			400
9			600
10	102.7	15	200
11	(Oil #2)		400
12	SAE30		600
13		40	200
14			400
15			600
16		80	200
17			400
18			600
19	126.5	15	200
20	(Oil #3)		400
21	10W50		600
22		40	200
23			400
24			600
25		80	200
26			400
27			600
28	161.2	15	200
29	(Oil #4)		400
30	10W50		600
31		40	200
32			400
33			600
34		80	200
35			400
36			600
37	226.0	15	200
38	(Oil #5)		400
39	SAE50		600
40		40	200
41			400
42			600
43		80	200
44			400
45			600

Table 4.1: Matrix of Test Conditions.

thickness and friction will be presented and analyzed. Repeatability will be discussed, as well as oil film thickness calibration and verification of experimental procedure.

4.1 Variation in Experimental Inputs

A typical set of graphs of normal loads for the same oil is given in Figure 4-1. Moving left to right across the page gives increased load, and moving down the page gives increased engine speed. The cyclical variation in the normal load, as discussed in Trial Results, is obvious under each condition. For the lowest load, increased speed leads to greater variation in normal load and increased load leads to reduced noise. The traces for the two higher loads are very similar to each other and show minor variation with increased speed. The extremes of the averaged normal load were measured and are included in the figure. The worst case is at high speed, where the small normal load and air pressure against the liner cannot be steadily maintained, leading to extremes of 80% above the average and 63% below the average. It is possible that the variation in normal load is substantial enough to cause variation in the friction force behavior. There is a consistent difference between the upstroke and the downstroke normal loads. The downstroke normal force at midstroke is always less than that of the upstroke normal force at midstroke. However, this should not affect the friction coefficient.

It was difficult to set the air pressure exactly at the desired normal load, because of the inaccuracy of the air pressure system and the cyclical variation of the normal load. Figure 4-2 shows the accuracy of the normal load setting in order of the desired normal loads. The actual normal load averages, maximums and minimums for each data set are displayed. The lowest load has a high average (5N above the desired average of 15N) and high percentage deviation. This may reflect the inability of the air pressure cylinder to apply a constant, steady load at a low normal load and to maintain that load under engine vibration and movement. These high variations in normal load were kept in mind when comparing friction and L.I.F. results for a given normal force.

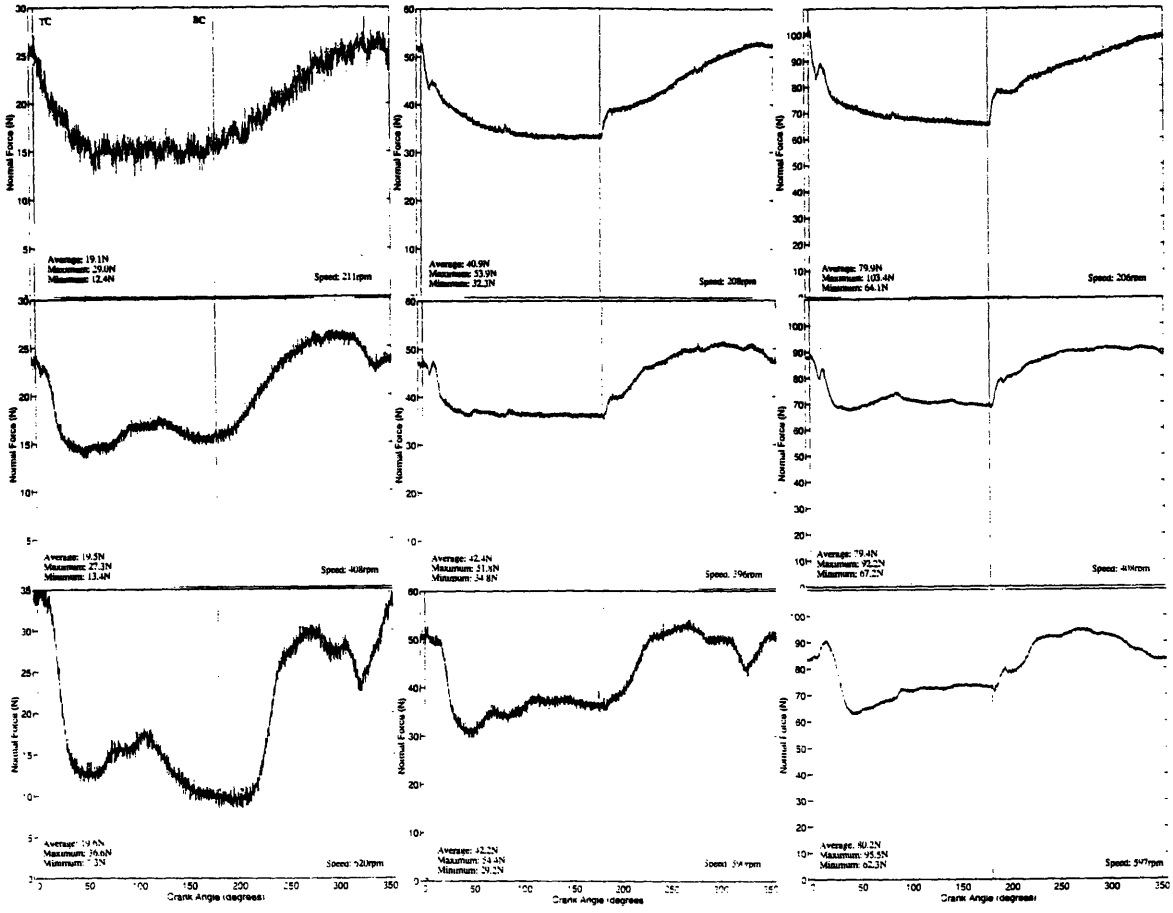

All graphs are averaged over Ten Cycles. oil 4 (10W50)

Figure 4-1: Instantaneous Normal Force averaged over Ten Cycles

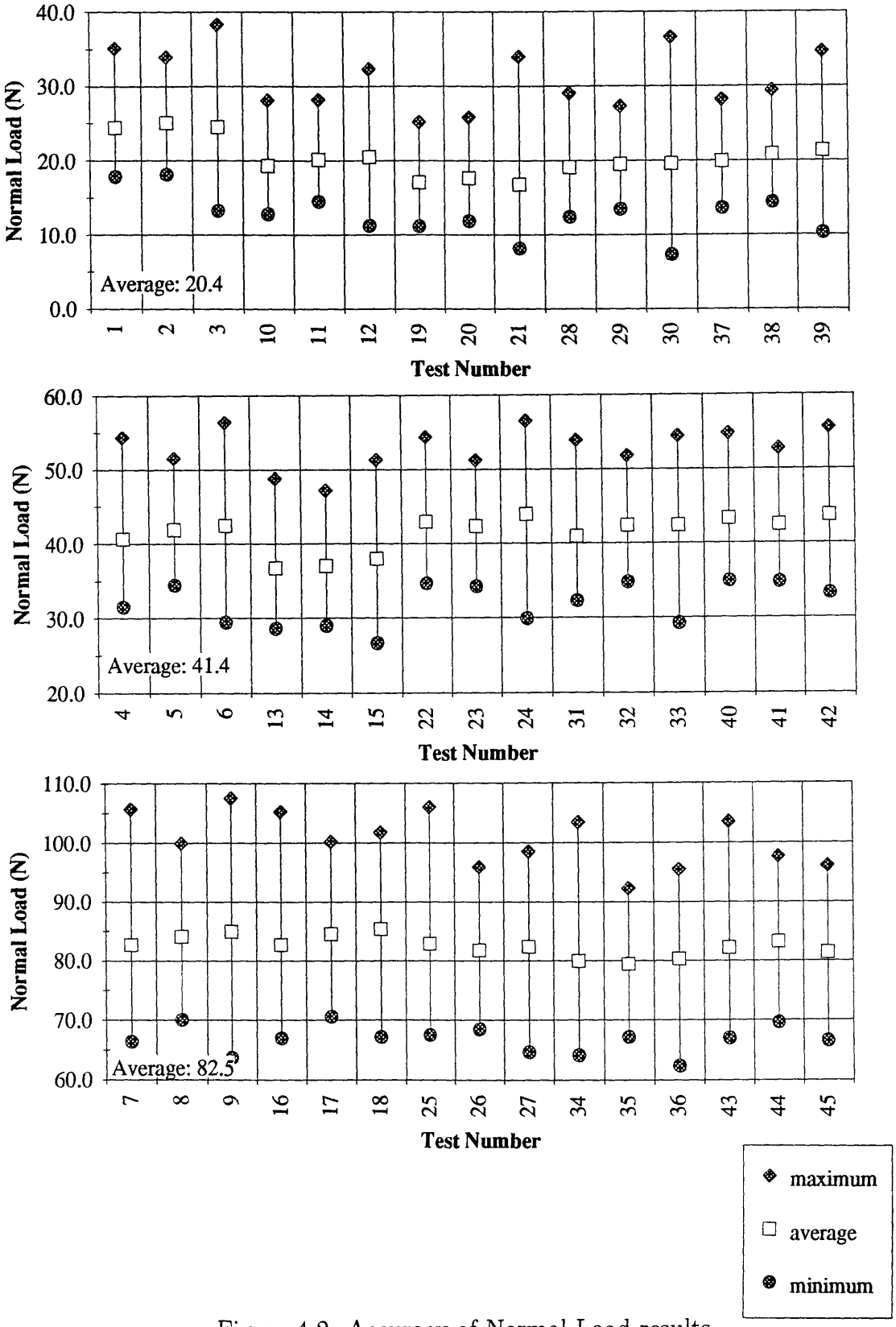

Figure 4-2: Accuracy of Normal Load results.

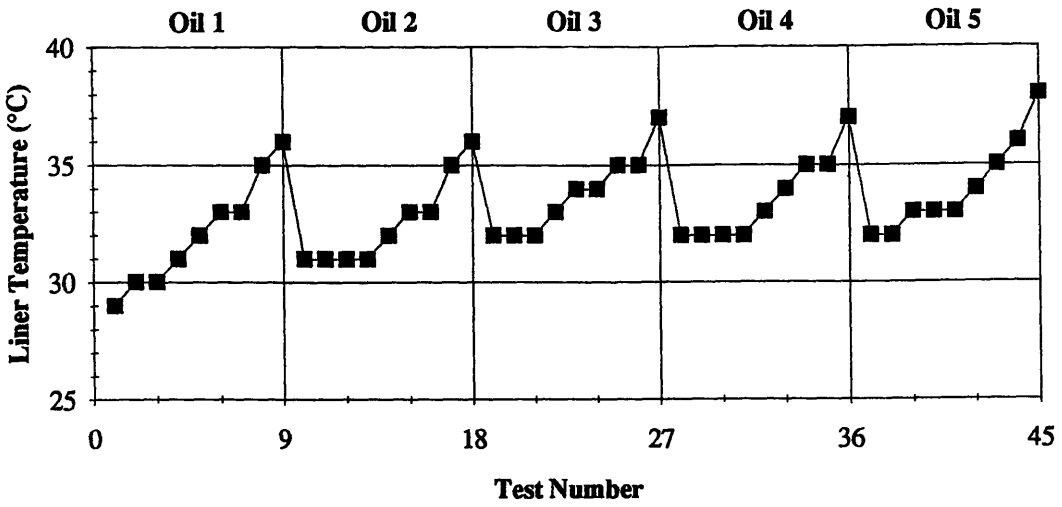

Figure 4-3: Variation of Liner Temperature during Testing

As expected, there were variations in the liner temperature from one data set to the next. Figure 4-3 shows the liner temperature for each test. The temperature increase is steady through each set of tests. This was partly a result of ambient temperature differences, but was mainly due to heating caused by the ring motion against the liner, indicating some heat generation and transfer as a result of friction. This was concluded from the rise in temperature with increased continuous testing and the decrease in temperature when the rig was allowed to rest between data sets while the oil was changed.

It was observed that the motor and pump of the oil feed system also heated up with continuous use. Both became hot to the touch. This became a concern because it was thought that the temperature increase might be transferred to the oil itself, thus affecting the oil viscosity in an unknown manner. However, a touch of the stainless steel pipes of the oil feed system close to the nozzle revealed no significant difference from room temperature, suggesting that whatever heat had been transferred to the oil by the pump, it was lost while flowing through the pipes. The measured liner temperature was assumed to be the temperature of the oil and was used to calculate oil viscosity as discussed in *Experimental Procedure*.

4.2 Results

Typical friction force graphs, for one oil with variation in load and speed, are given in Figure 4-4. There are some similarities with the normal force traces. There is significant noise in the signal. The worst case is at low load, high speed, with high noise, perhaps as a result of the variation in normal load. On each graph, two averages are given. The average includes one stroke and the midstroke average is applicable to the center of the stroke, as defined in the *Experimental Procedure*. The noise increases with engine speed and decreases with applied normal force. In all of the graphs, there is an increase in friction at endstroke, particularly top center and a plateau at midstroke. The presence of the quartz window, marked by the sudden, quick change in friction force, is noticeable in all the traces. The shape also varies with load. This will be discussed when considering the friction coefficient, where the influence of the normal load shape is normalized.

The curve shapes vary little, for the same speed and load conditions, from oil to oil. Exceptions include Oil 3 (10W50) at low speed and low load, where the quartz window does not affect the downstroke friction trace, although it is dramatically visible on the upstroke. For the same oil, at medium load and low speed, the effects of the L.I.F. window are once again not visible, except on the upstroke. This is a promising indication of hydrodynamic lubrication. Both graphs are shown in Figure 4-5. Another set of exceptions arise from the friction traces of Oil 5, where there are suggestions of a 'crown' in the center of the stroke, where the friction force is greatest at endstroke, decreases, and then increases slightly at midstroke. This suggests a transition between lubrication regimes, and is shown in Figure 4-6.

Typical friction coefficient results are shown in Figure 4-7. In general, the curves are similar to those of friction force, for the same speed and load, with differences resulting from fluctuations in the normal force. The friction coefficient values range from approximately 0.09 at endstroke to 0.05 at midstroke, on average, although there are friction coefficients close to 0.02 at midstroke. The lower values are indicative of transition among lubrication regimes. As in the friction force diagrams, two averages

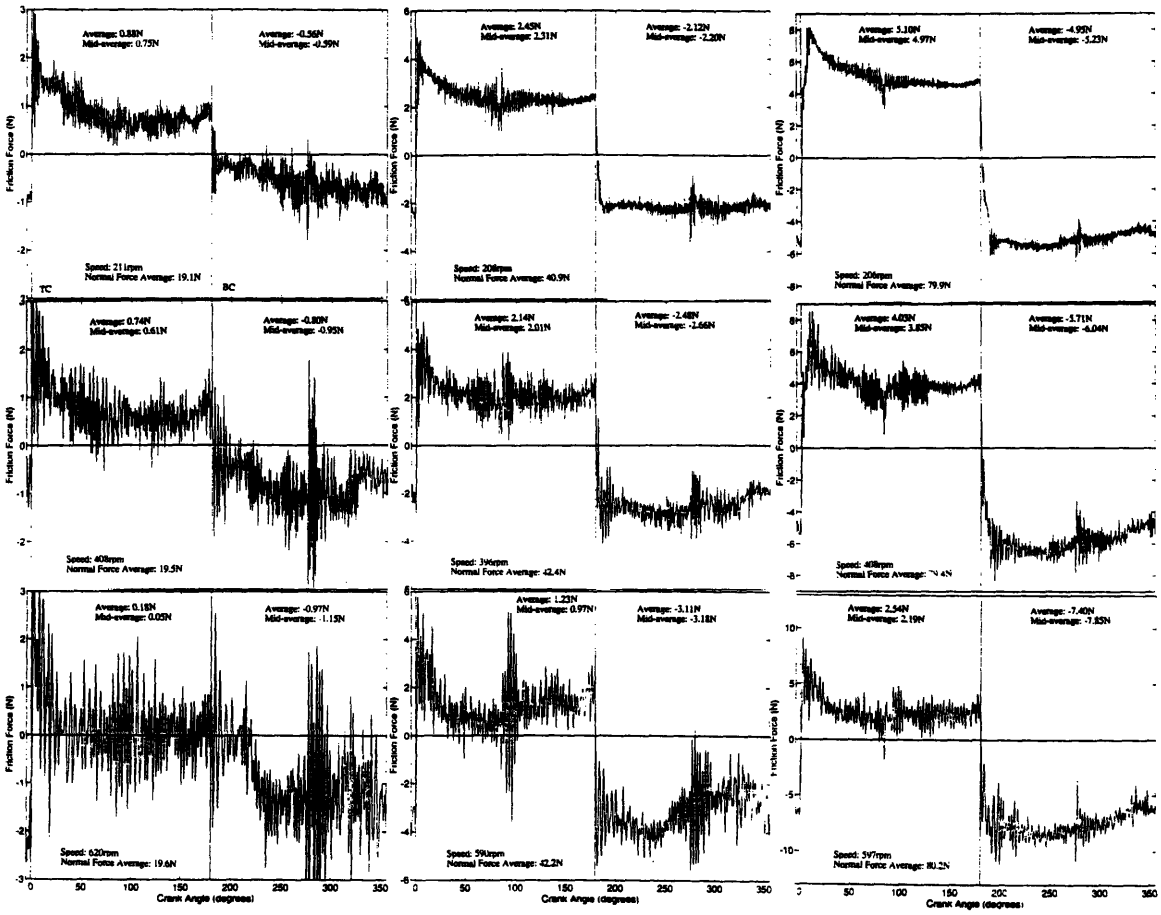

All graphs are averaged over Ten Cycles. oil 4 (10W50)

Figure 4-4: Instantaneous Friction Force

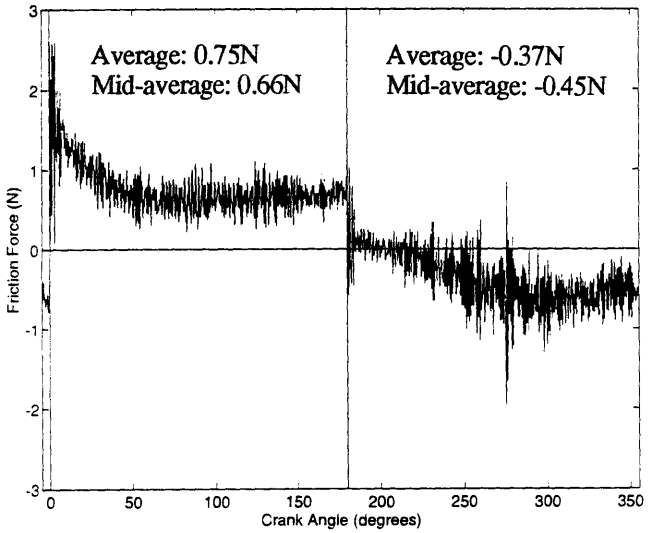

Speed: 209rpm
Normal Force Average: 17.1N

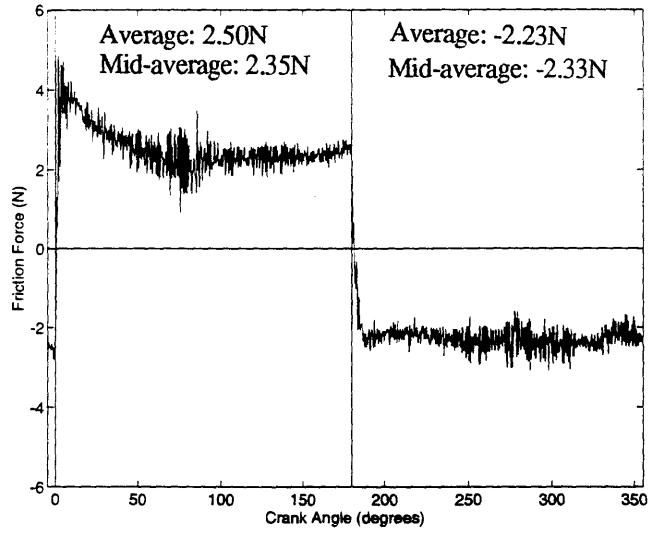

Speed: 207rpm
Normal Force Average: 43.0N

Both graphs are averaged over Ten Cycles. oil 3 (10W50)

Figure 4-5: Notable Friction Force Traces

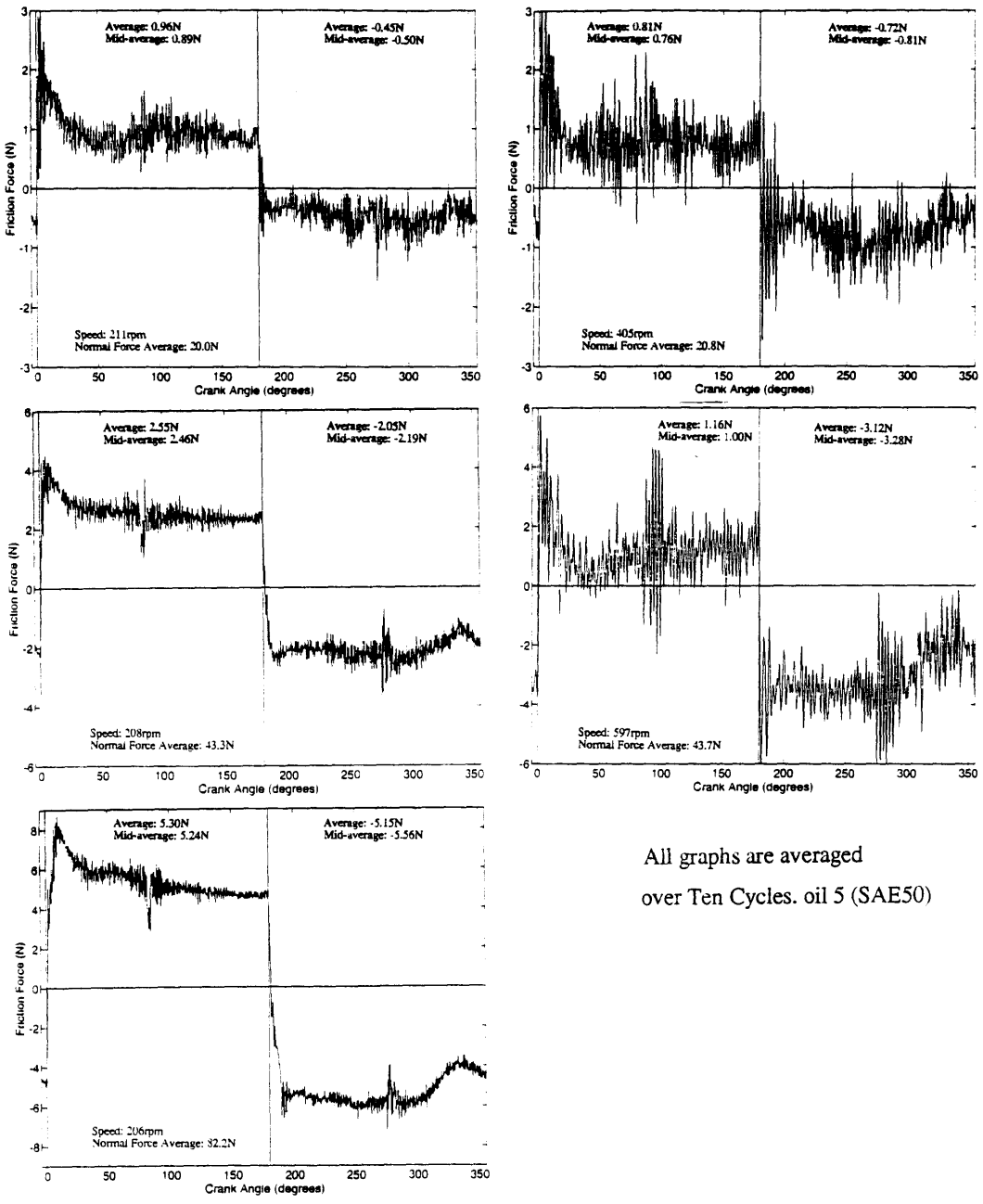

All graphs are averaged over Ten Cycles. oil 5 (SAE50)

Figure 4-6: Notable Friction Force Traces

are given for each stroke. The friction coefficient varies by at most 0.01 between the overall curve average and the midstroke average. This is true of all the forty-five data sets collected. The midstroke friction coefficient average will be used to compare between data sets. There are differences between up- and downstroke friction coefficient averages, which is also visually apparent. These are most prominent at high speeds. These trends are also consistent throughout the data set, leading to the conclusion that the ring/liner friction is different for downstroke and upstroke. This may be due to the ring being cocked differently in the up- and downstrokes. For consistency, the downstroke friction coefficient will be used for comparison between data sets. The curve shapes and values shown in Figure 4-7 are typical of all the oils for the same load and speed. Appendix C shows the friction coefficient graphs for oils 1, 2, 3 and 5. The exceptions are again produced from use of Oil 5, and shown in Figure 4-8. Again , there are trends suggesting lubrication regime transition away from endstroke. Another notable exception is the medium load, low speed graph of Oil 3, shown in Figure 4-9, in which the presence of the L.I.F. quartz window, as noted in the friction force trace, is not visible.

Figure 4-10 shows the variation of the friction coefficient on load for the three engine speeds, with marked lines of constant viscosity. The results for the two lower speeds are very consistent. The friction coefficient increases with normal force. At the highest speed, oils number 1, 3 and 4 demonstrate similar trends, but oils number 2 and 5 do not change substantially with load. The order of the constant viscosity lines is not maintained from one speed to the next, except that oil number 1, the least viscous, consistently has a high friction coefficient and, at high load, oil number 5 consistently has a low friction coefficient. Figure 4-11 displays the dependence of the friction coefficient on engine speed, along lines of constant viscosity for the three normal loads. In this case, the relationship is very clear and repeatable. For each load, the friction coefficient decreases with engine speed. In all but one case, oil 1 has the highest friction coefficient. The relationship between friction coefficient and engine speed is maintained even at low load, high speed, which shows some instability, consistent with previous observations of low load, high speed data. This

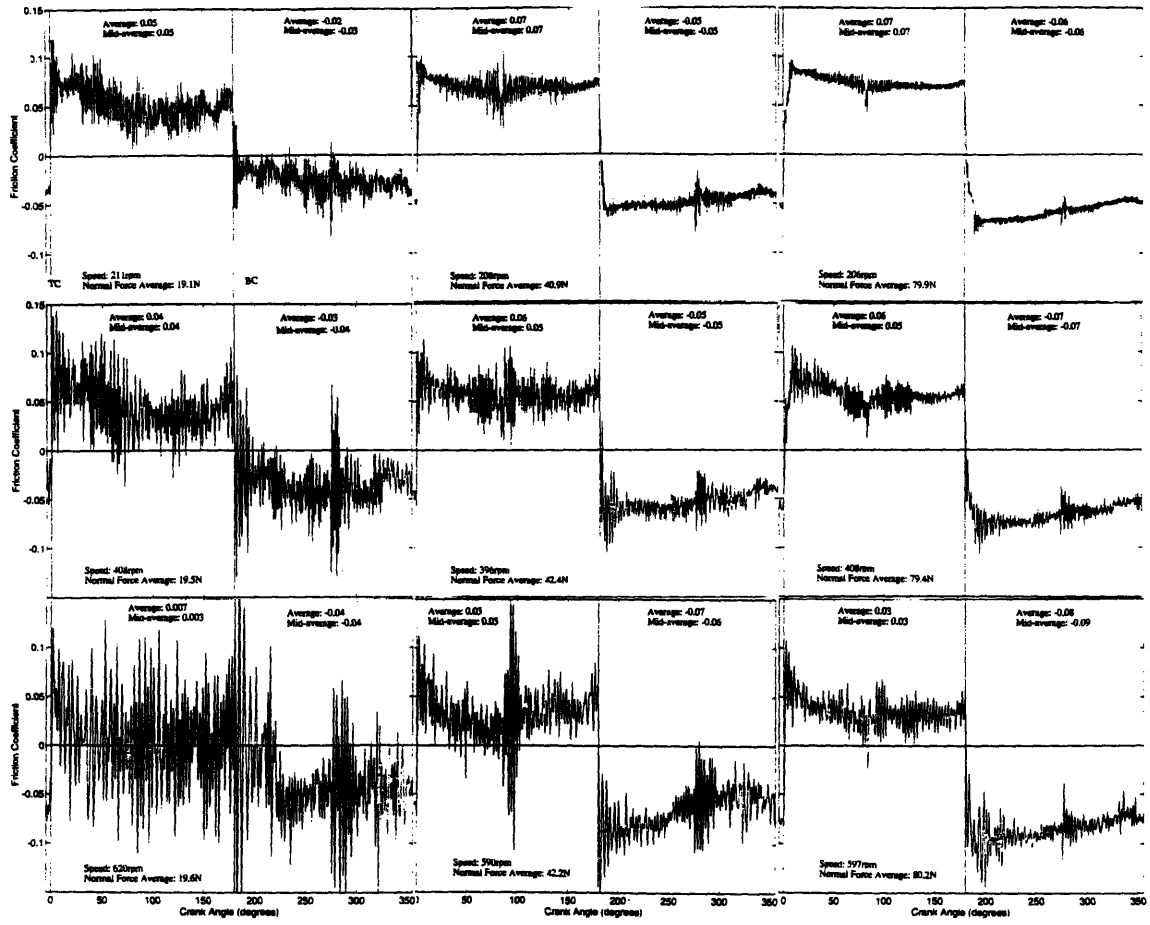

All graphs are averaged over Ten Cycles. oil 4 (10W50)

Figure 4-7: Instantaneous Friction Coefficient

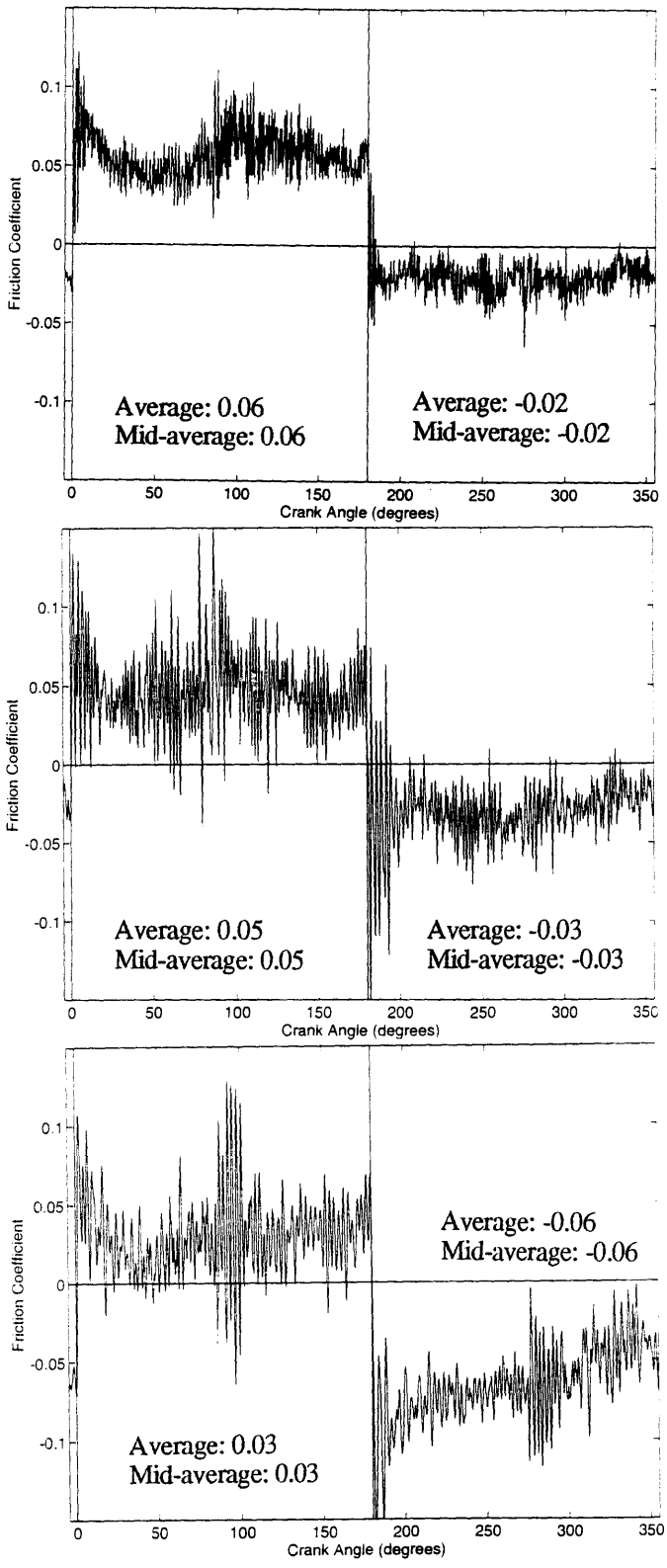

Speed: 211rpm
Normal Force Average: 20.0N

Speed: 405rpm
Normal Force Average: 20.8N

Speed: 597rpm
Normal Force Average: 43.7N

All graphs are averaged over

Ten Cycles. oil 5 (SAE50)

Figure 4-8: Friction Coefficient Traces, exhibiting Possible Lubrication Regime Change.

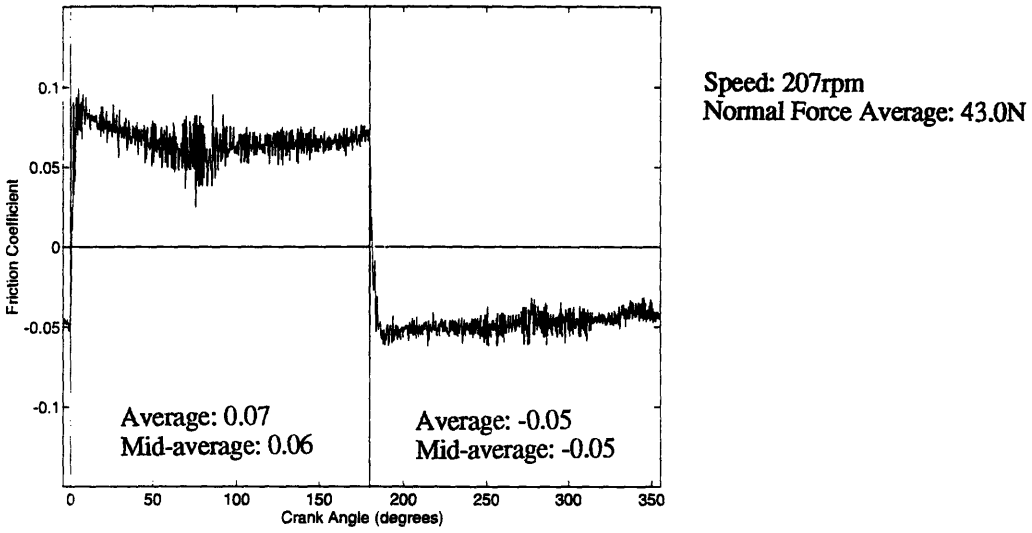

Figure 4-9: Friction Coefficient Upstroke Trace, showing no Quartz Window Effect

indicates that the lubrication regime is not boundary lubrication, in which the friction coefficient would be independent of speed. It is probably mixed lubrication, where, for the same viscosity and load, the friction coefficient decreases with sliding speed, as demonstrated in the Stribeck diagram.

Typical oil film thickness results of averaged oil film thickness over one cycle are shown in Figure 4-12. The L.I.F. signal was calibrated from the ring width, since this was easier to match than the ring profile. Since the groove in the ring was not discernible, it could not be used for reliable calibration. Figure 4-13 shows a comparison of different calibrations. It is apparent that for the lowest calibration, 2×10^{-7}, the ring width is too small and for the largest, 5×10^{-7}, the ring is seemingly filled with oil, a physically impossible situation. A calibration between 3×10^{-7} to 3.5×10^{-7} would be physically plausible. The calibration 3×10^{-7} appeared to be the best fit and was used consistently throughout the data set. This gives the calibration an approximately 20% certainty when calibrating from the ring width. From this calibration, and the match shown, it is difficult and perhaps foolhardy to draw conclusions about the ring wetting and detailed oil film behavior. There were traces, such as that shown in Figure 4-14, where it appeared that there was ring wetting and inlet and outlet points. This became clearer at a higher calibration which provides an excellent fit to

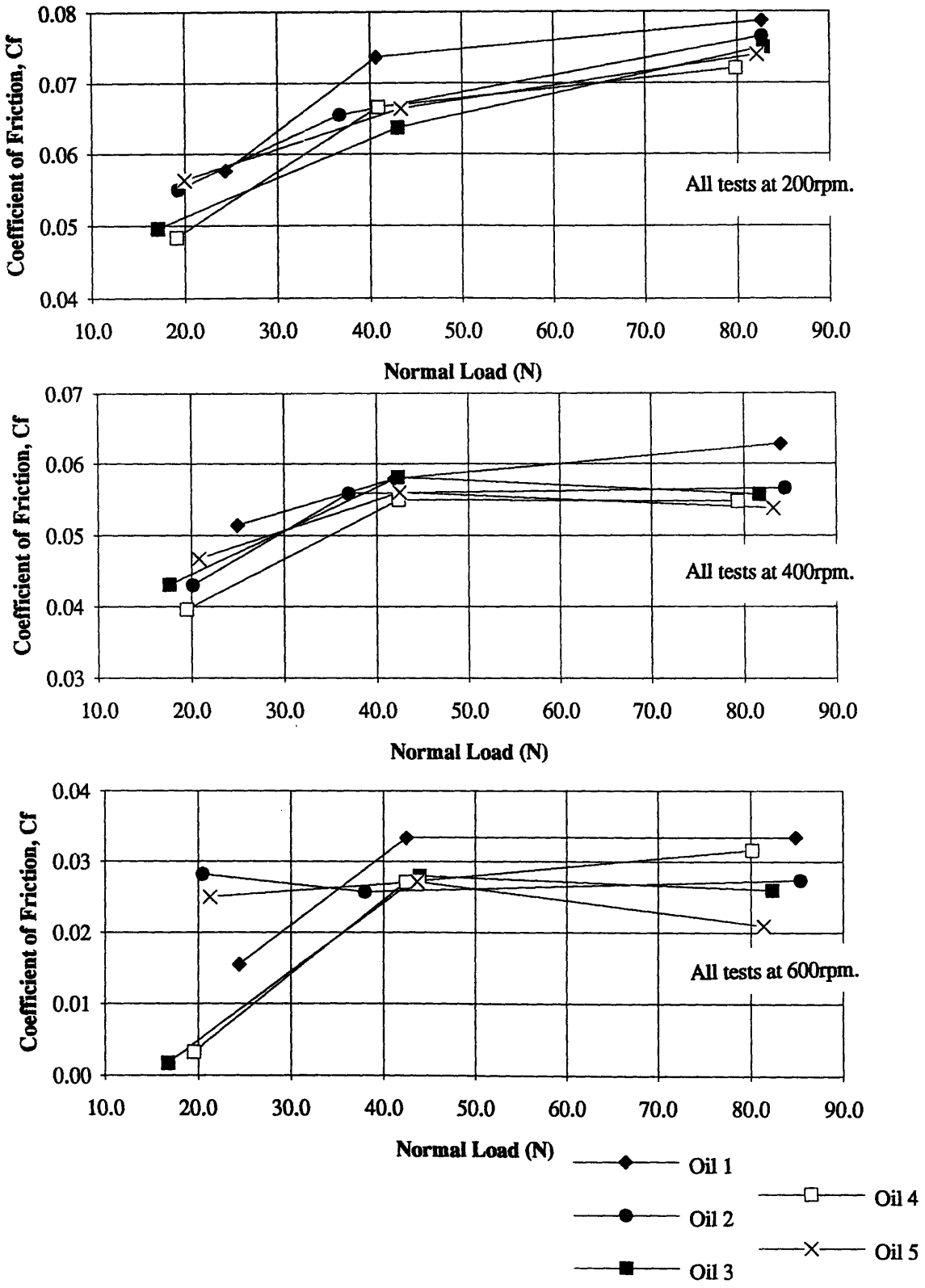

Figure 4-10: Mid-downstroke Friction Coefficient vs. Normal Load, along lines of constant Viscosity for Three Engine Speeds.

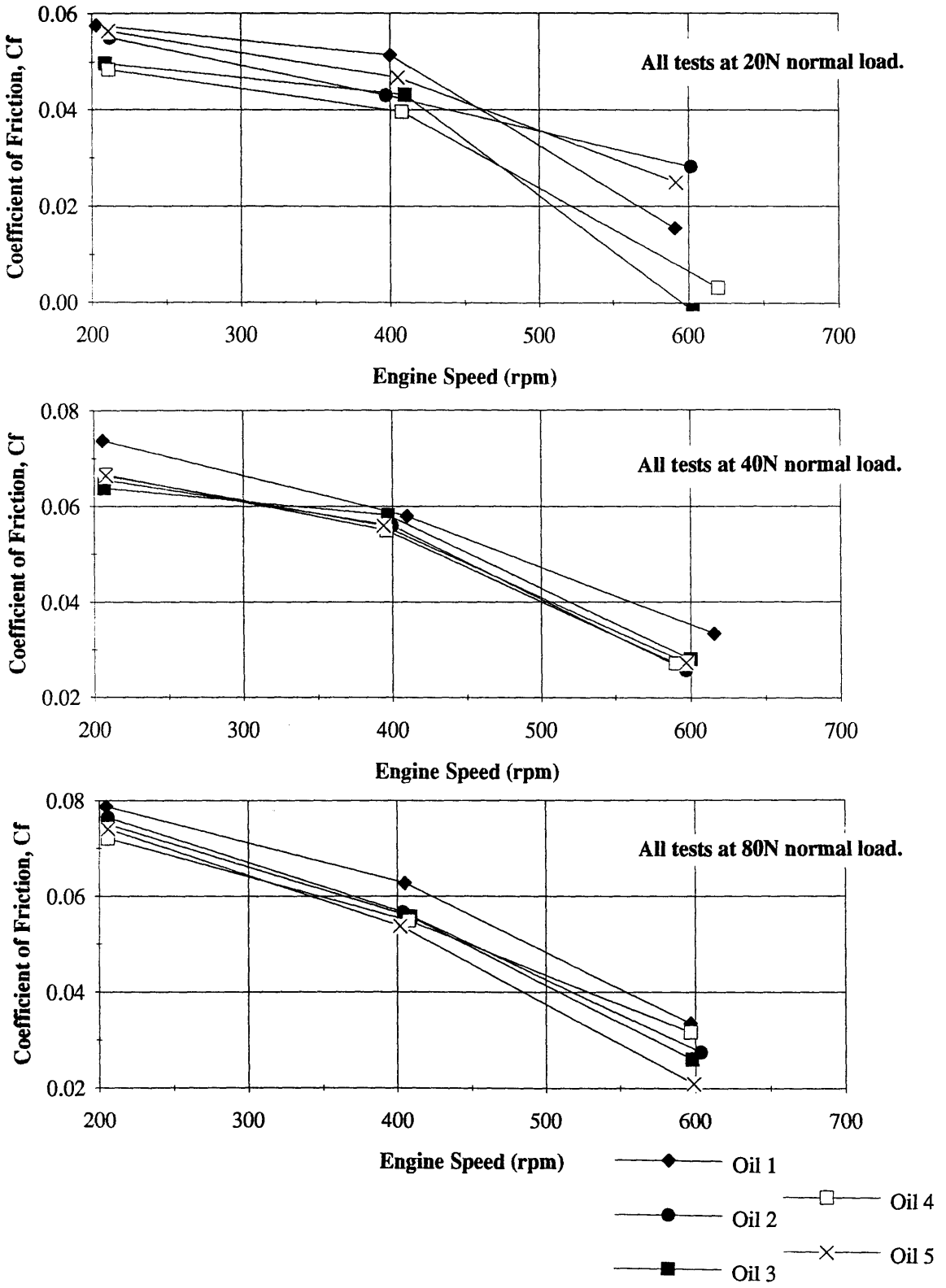

Figure 4-11: Mid-downstroke Friction Coefficient vs. Engine Speed, along lines of constant Viscosity for Three Normal Loads.

the ring curvature. However, this was not consistent for all L.I.F. traces and the ring width is clearly not matched.

From the L.I.F. calibration comparison in Figure 4-13, the sides of the ring shown in the L.I.F. signal are not parallel, while the ring sides are indeed physically parallel. This adds doubt to the calibration, since the ring width can only be matched at one vertical location. The chosen point was the edges of the Talysurf traces, which are clearly parallel, rather than far away from the area of interest, the subring region. For the reasons outlined above, it is preferable to think of the oil film thickness in relative terms, as points for comparison.

The ring wetting is clearly discernible in all the graphs of Figure 4-12. The down- and upstroke traces are almost mirror images of each other. The region around the ring was magnified and is shown in Figure 4-15, confirming the L.I.F. window location at approximately 81° from Top Center. This graph was generated for every data set, to check the assumption for defining minimum oil film thickness, described in the *Experimental Procedure*, of the subring region located between 80° and 82° from Top Center. A visual inspection of all the graphs showed this to be a valid assumption. This process also allowed for an investigation of ring wandering from test to test. This was found to be minor and there were no trends of deterioration during testing. The crank angle was converted to linear distance as described in *Experimental Procedure*. The downstroke trace is shown in Figure 4-16. Again, the ring wetting is very clear. The general shape of the oil around the ring is consistent from one condition to the next, with a large clump of oil present before the ring passes the window, a cavity and then oil wetting around the ring, followed by two smaller clumps of oil. It is difficult to specifically interpret the oil thickness pattern. One interpretation by Deutsch [12], who used the same L.I.F. system, is that the oil around the ring is oil sitting on the piston, or, in this case, the ring holder. Even if the oil is sitting on the holder, which is at a radial distance of approximately 1 millimeter from the liner, the oil will still fluoresce and emit a signal when activated. Further credibility is lent to this interpretation by the fact that the oil thickness covers about 29 millimeters for all the graphs, and the ring holder has a thickness of 25.4 millimeters. Oil has

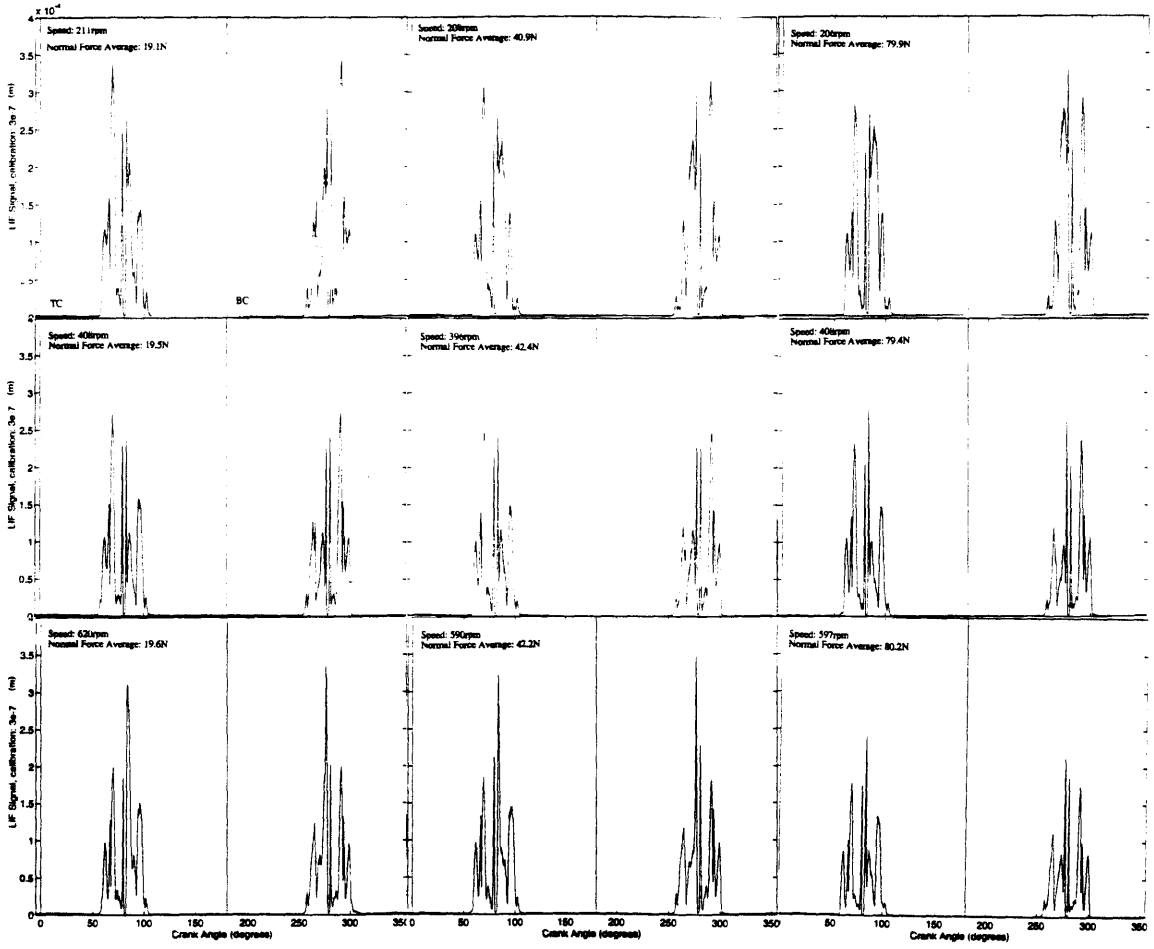

All graphs are averaged over Ten Cycles. oil 4 (10W50)

Figure 4-12: Oil Film Thickness over one Cycle

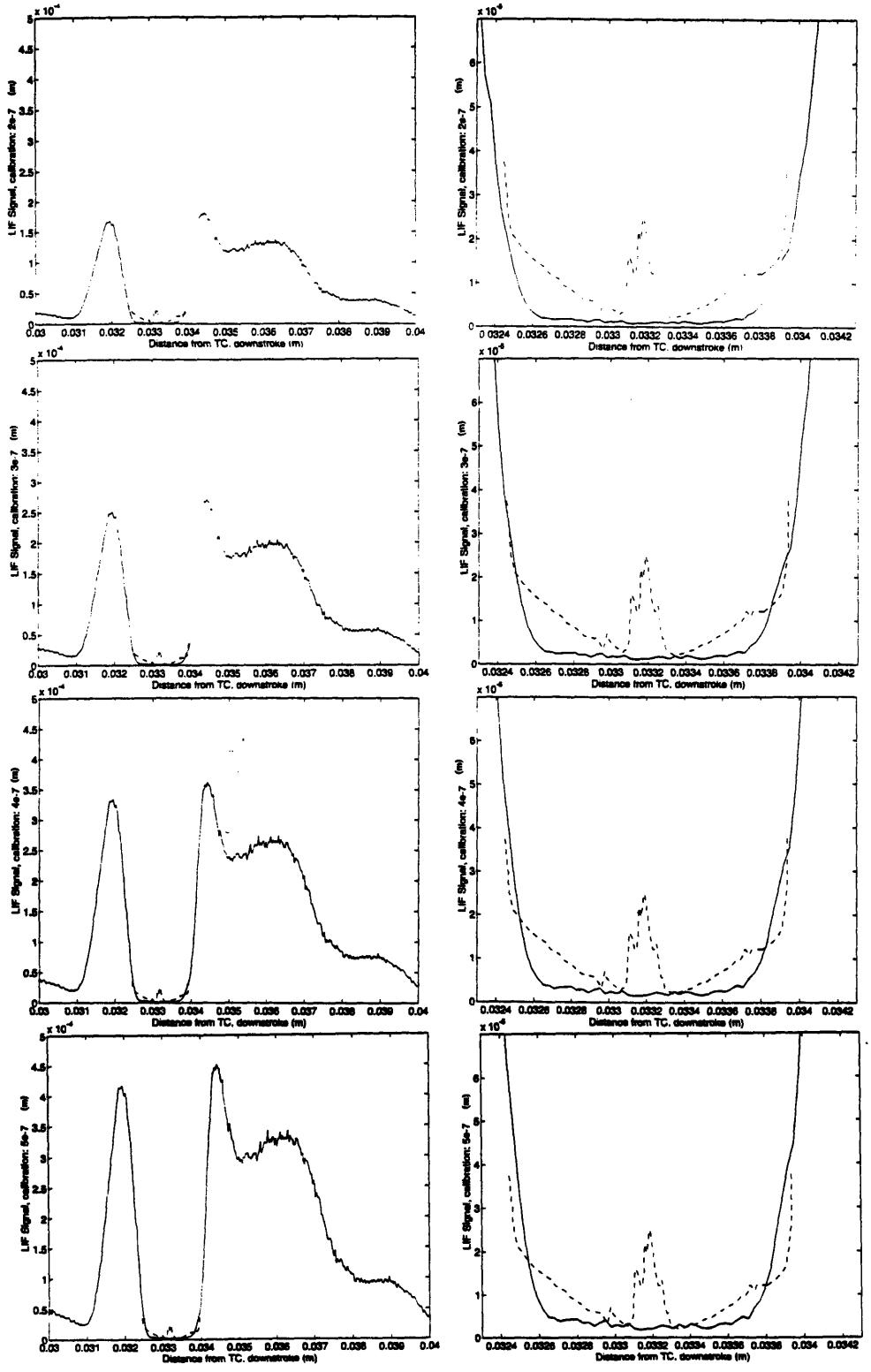

Figure 4-13: Comparison of Different Oil Film Thickness Calibrations

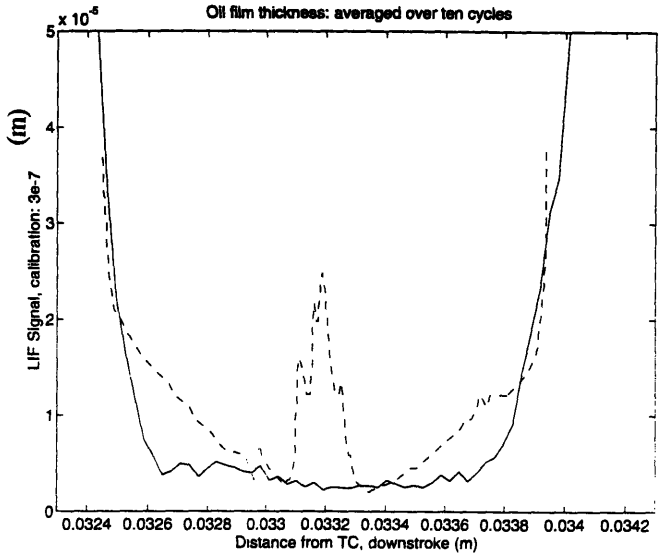

(a) Calibration matched to Ring Width

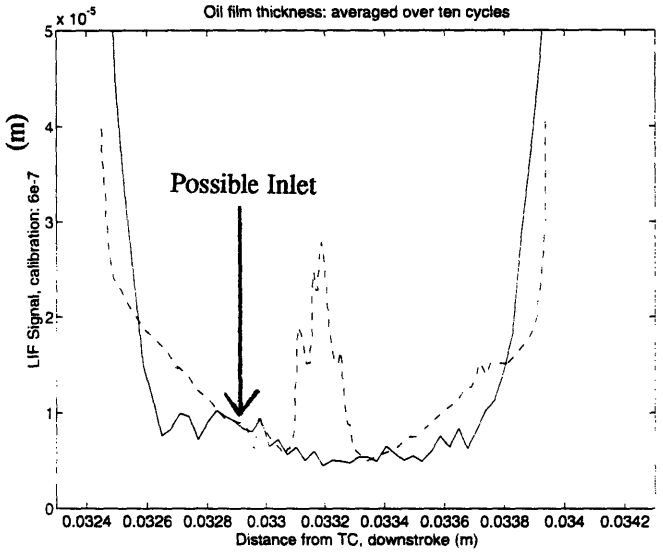

(b) Calibration matched to Ring Curvature

Both graphs display the same data set: oil 2 (SAE30) at low load and low speed.

Figure 4-14: Comparison of Two Oil Film Thickness Calibrations

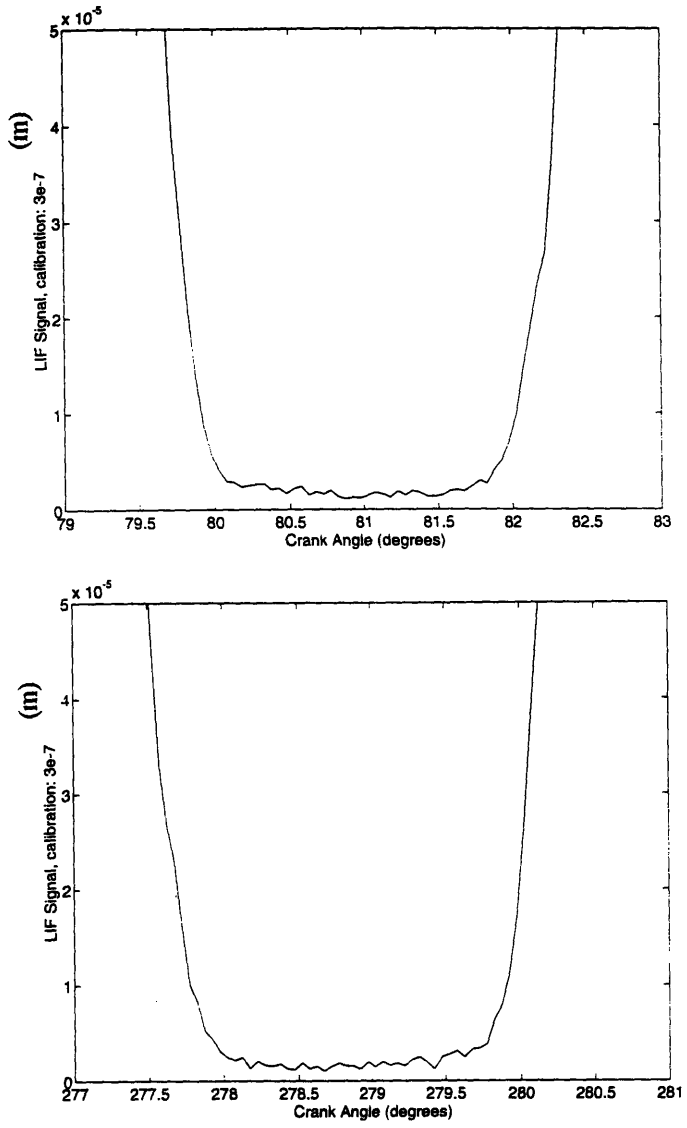

The traces are averaged over Ten Cycles.
Both graphs display the same data: oil 4 (10W50) at low speed and low load.

Figure 4-15: Oil Film Thickness in the Subring Region

been observed on the top and bottom lip of the ring holder, which would increase this thickness. Although it is difficult to observe the oil flow during the experiment, due to the laser beam presence, both before and after the tests, considerable lubricant presence was observed over the ring holder, the ring and the entire rig itself, as well as within crevices on the ring holder, such as the groove holding the ring to the liner curvature. The oil thickness curve does not change in size or shape with increased load but does change with increased speed. One possible explanation for this is that, at higher speeds, less oil is able to remain on the holder and more is shaken off before the oil film stabilizes. These trends are consistent independent of oil type. Appendix D shows the oil film thickness profiles for oils 1, 2, 3 and 5.

Typical traces of the downstroke subring region, with the imposed Talysurf ring profile (dashed line) are shown in Figure 4-17. In all the cases, the Talysurf profile ring width matches the oil wetting ring width. The general shape of the curve changes slightly but not significantly from one condition to the next. These curves are similar through the complete data set. For a more thorough analysis, the downstroke and upstroke minimum oil film thicknesses were determined and are shown in Figures 4-18 and 4-19, against load along lines of constant viscosity, for the three engine speeds. It is difficult to discern a clear relationship between either up or downstroke oil film thickness and normal force, at any speed. Oil 5 consistently has the largest oil film thickness. This suggests that the higher viscosity of the oil causes higher film thicknesses. This matches the thinking that, for lift generated under a hydrodynamic wedge, the lift force is proportional to the velocity times the viscosity divided by the lubricant thickness. For conditions of constant lift and engine speed, an increase in the viscosity will result in a thicker oil film. In most of the cases, oil 1 has the lowest film thickness but this trend does not have the consistency of that of oil 5. At the two higher speeds, the film thicknesses of oils 2, 3 and 5 always decrease with increased load, indicating that, as the normal force increases, it squeezes out more oil, thus decreasing the film thickness. Oils 1 and 4, for the higher speeds, decrease at the lowest load, peak at 40N and then decrease. This behavior is difficult to interpret. At 200 rpm, the behavior is varied and also difficult to translate to a meaningful

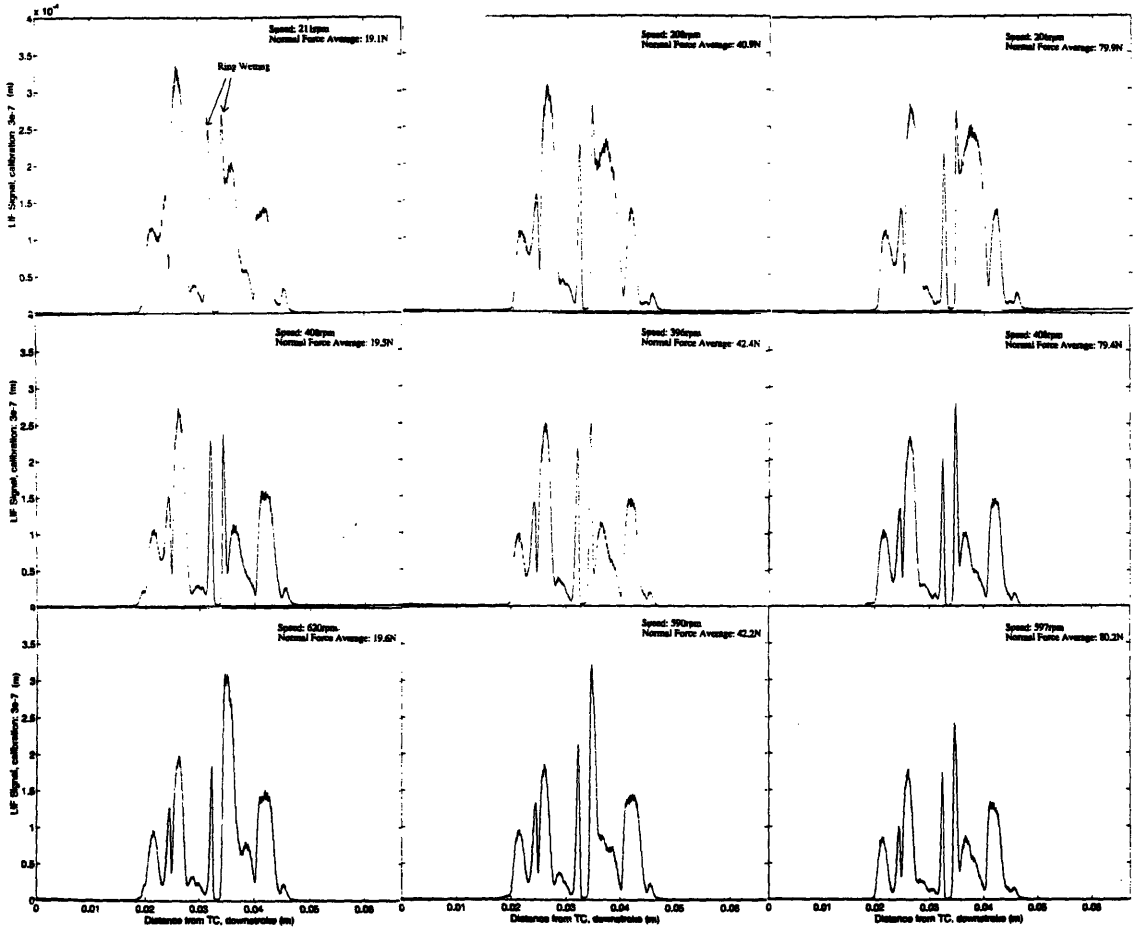

All graphs are averaged over Ten Cycles. oil 4 (10W50)

Figure 4-16: Downstroke Oil Film Thickness vs. Distance from Top Center

physical situation. It may be that the high variation noted at the low load in Figure 4-2 produces a different lubrication mechanism under the ring. Another possible source of unreliability is the temperature change with time, noted earlier. This alters the viscosity which was shown to affect film thickness, but should be a minor effect since the change in viscosity is small compared to the absolute viscosity.

The dependence of minimum oil film thickness on engine speed is graphed in Figures 4-20 and 4-21. Like the previous set of graphs, there are no clear consistent trends . The highest viscosity oil always has the highest minimum film thicknesses and the lowest viscosity oil usually corresponds to the smallest film thickness. At the highest load, all the oils have decreasing oil film thickness with increased speed. At medium load, the trends for up- and downstroke have different behavior and, at low load, minimum film thickness for oil 1 clearly decreases with speed, while oils 2, 3 and 5 appear to increase film thickness with speed.

To understand the nature of the friction regimes in the experiment, the Stribeck diagram for instantaneous friction coefficient vs. Sommerfeld number was generated for the data sets which were considered to be most likely to have reached hydrodynamic friction behavior. These included: oil 4, at high load and high and low speeds and low load and medium speed, and oil 5, at low speed and all three loads. The resulting Stribeck diagrams are shown in Figure 4-22. There is significant noise in the graphs, due to the noise in the friction and normal force measurements. Most of the graphs for oil 4 have a flat trace, indicating lubrication in the boundary or mixed regimes. There is one half-stroke, for the traces of oil 5, which has a promising curvature, which slopes down and then up, perhaps indicative of hydrodynamic lubrication.

Additionally, Stribeck diagrams were generated for the complete data collection, using midstroke friction, velocity and film thickness data. These are shown in Figure 4-23. The trends are unclear for the upstroke, but the downstroke diagrams show a pattern of decreasing friction coefficient with increasing Sommerfeld Number. This indicates boundary, or, at best, mixed lubrication regimes. Figure 4-24 displays the downstroke Stribeck diagram, in which the data is separated by oil type. In each diagram, this relationship is very clear, confirming that conditions of hydrodynamic lubrication

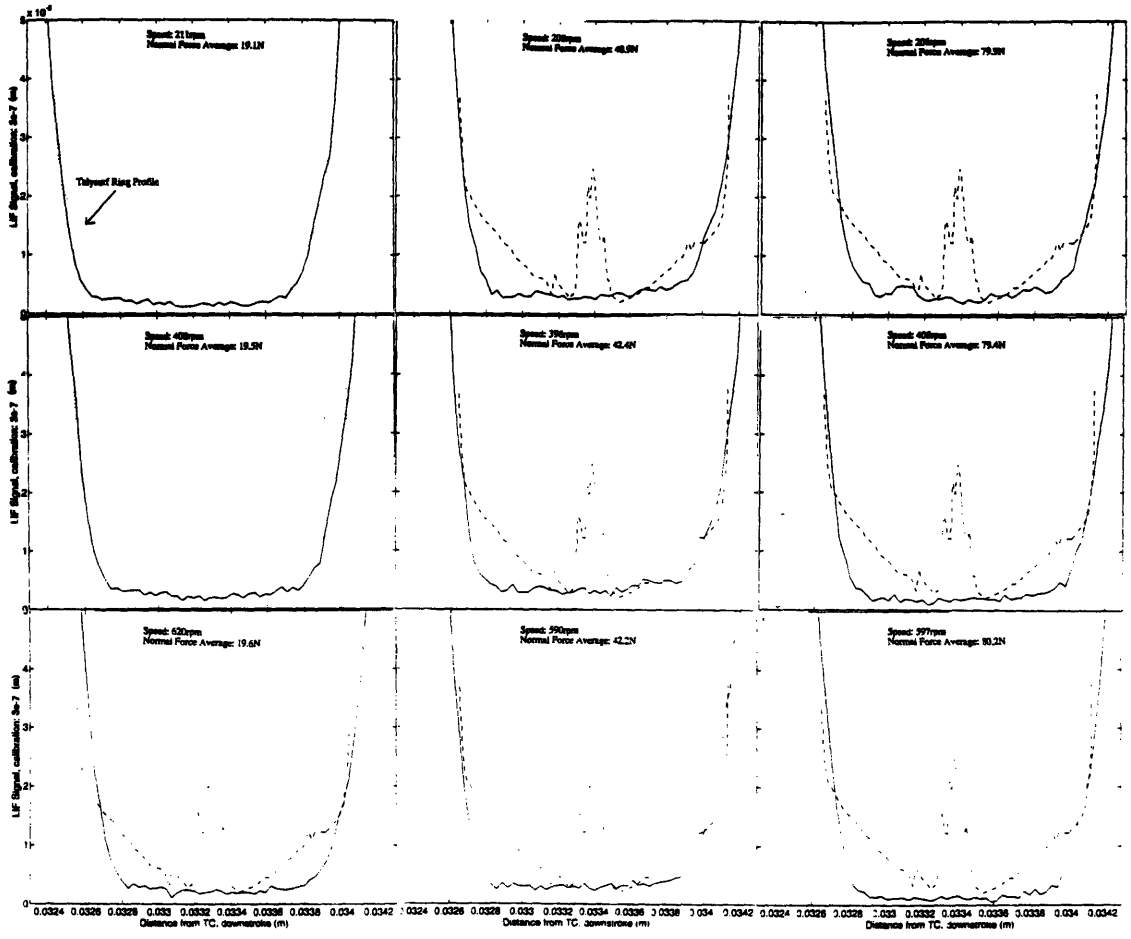

All graphs are averaged over Ten Cycles. oil 4 (10W50)

Figure 4-17: Oil Thickness Downstroke Sub-Ring Region, with imposed Talysurf Ring Profile (dashed line)

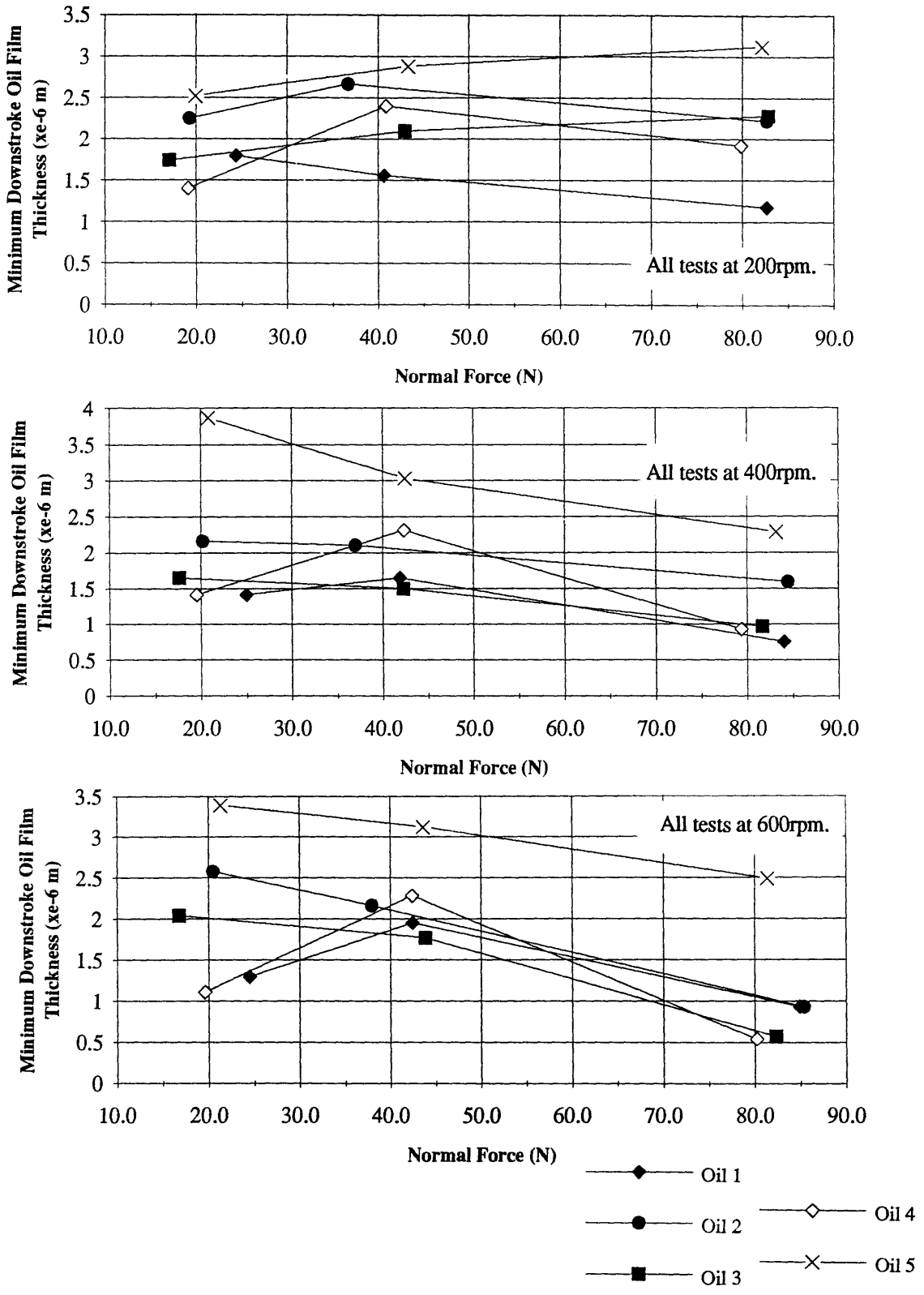

Figure 4-18: Downstroke Minimum Oil Film Thickness vs. Normal Load, along lines of constant Viscosity for three Engine Speeds.

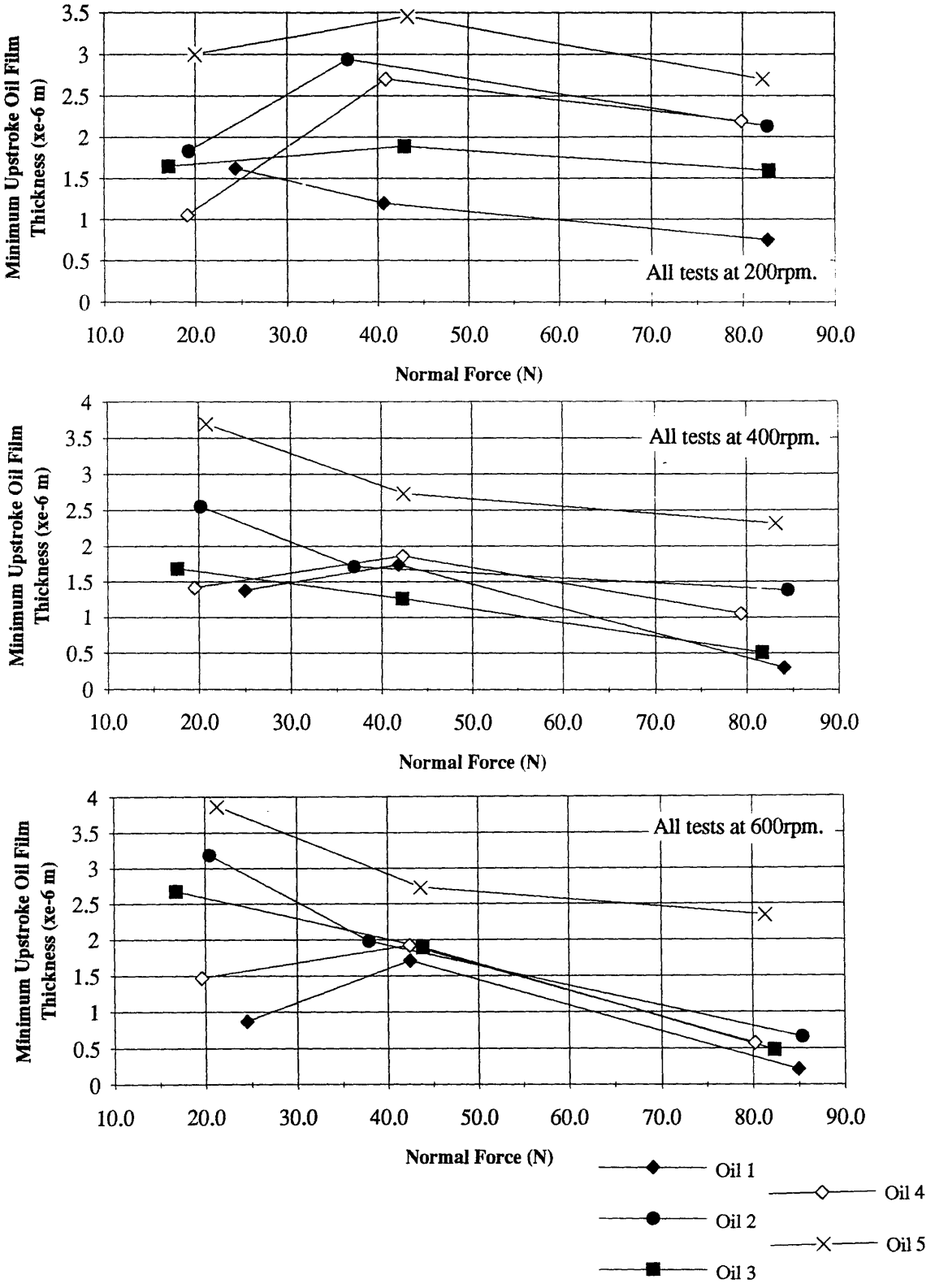

Figure 4-19: Upstroke Minimum Oil Film Thickness vs. Normal Load, along lines of constant Viscosity for three Engine Speeds.

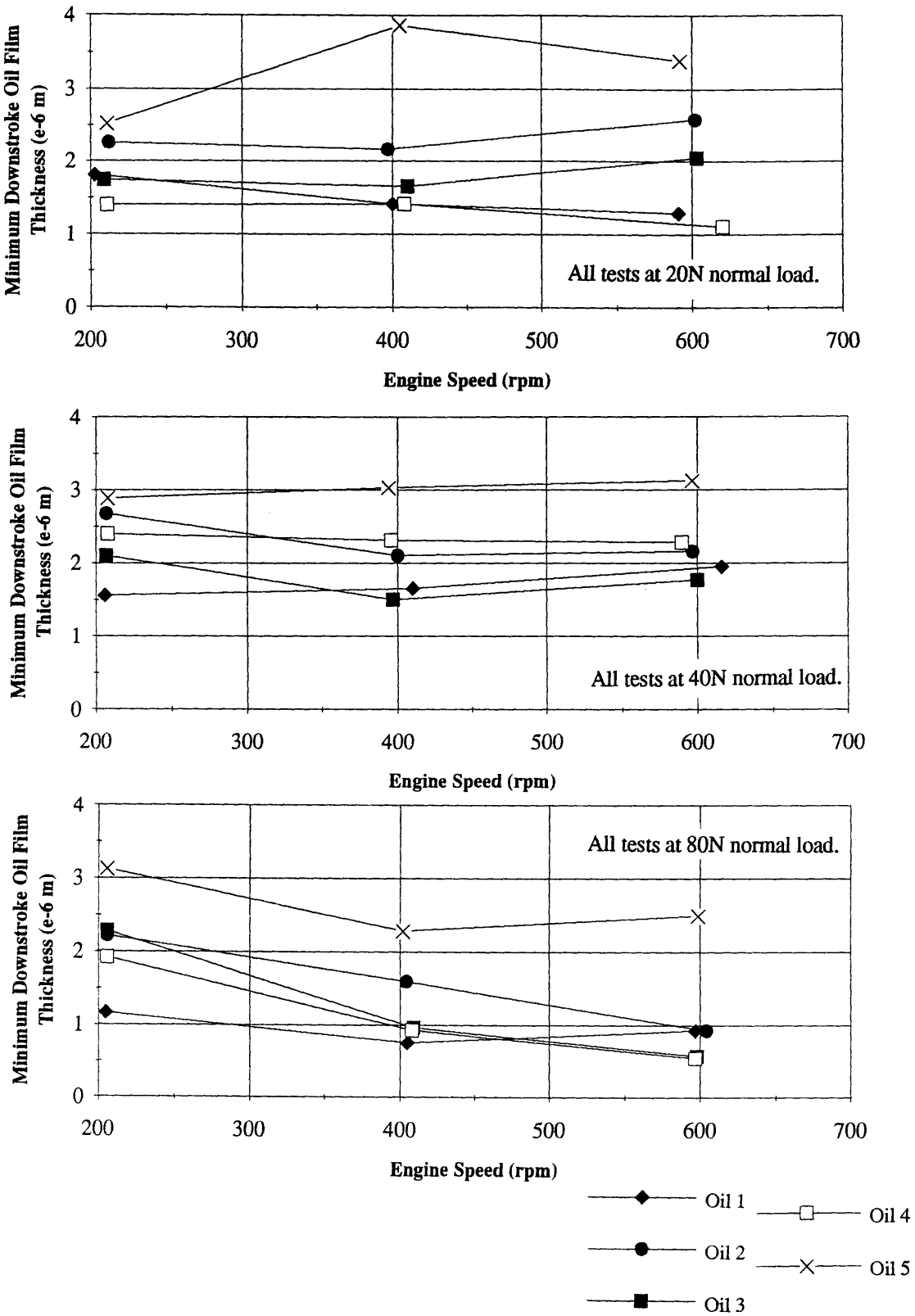

Figure 4-20: Downstroke Minimum Oil Film Thickness vs. Engine Speed, along lines of constant Viscosity for three Normal Loads.

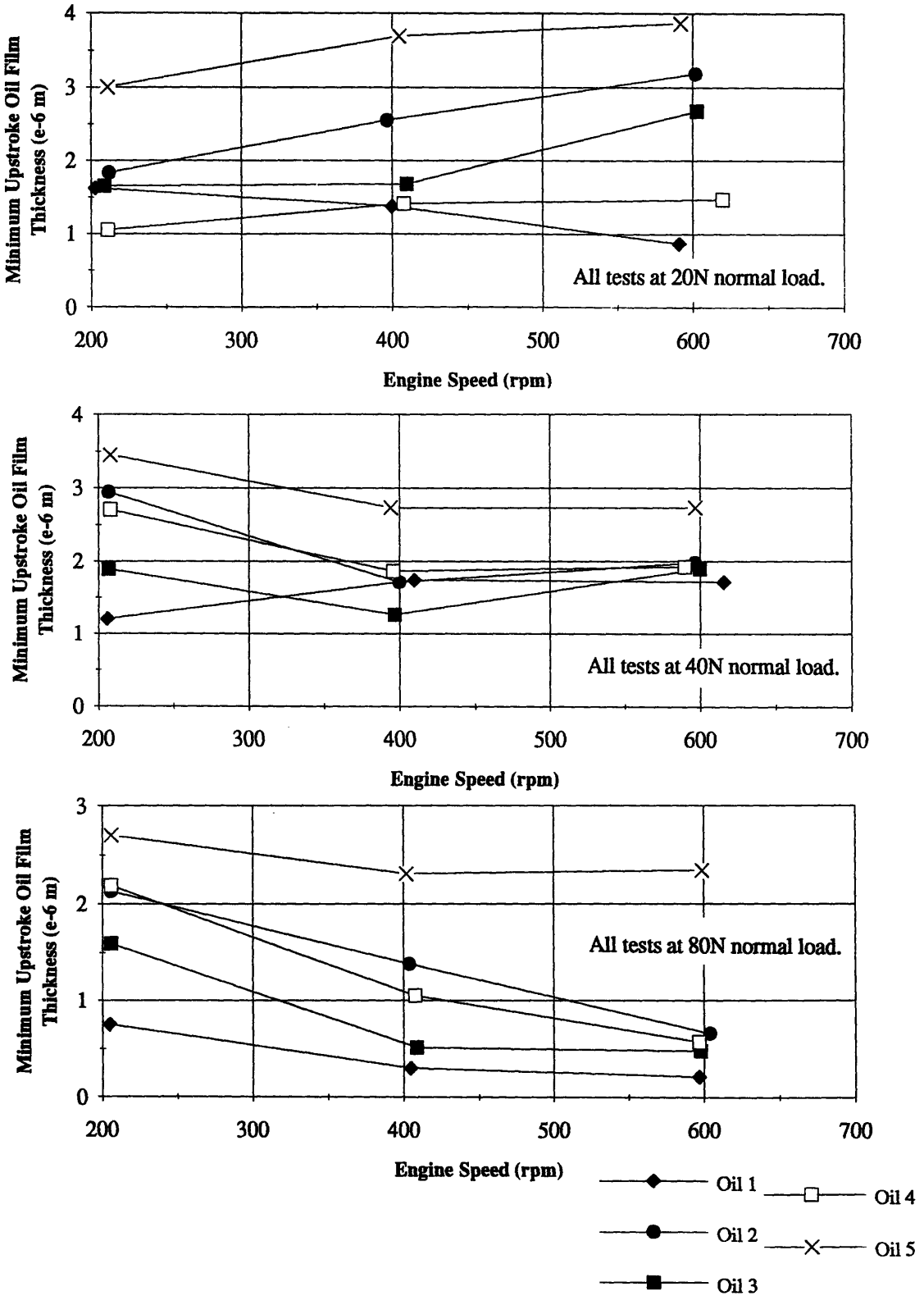

Figure 4-21: Upstroke Minimum Oil Film Thickness vs. Engine Speed, along lines of constant Viscosity for three Normal Loads.

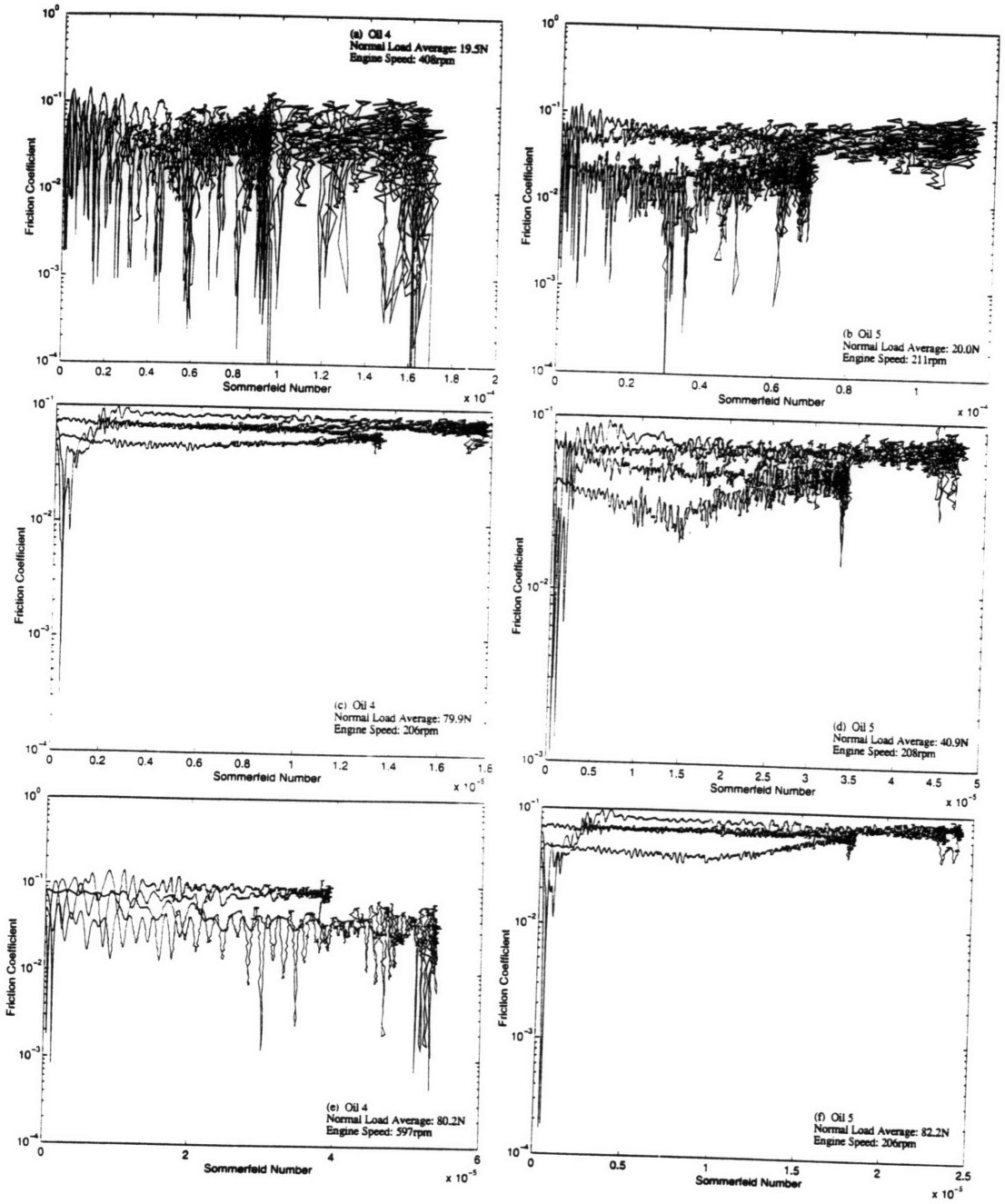

Figure 4-22: Stribeck Diagram for Six Test Conditions

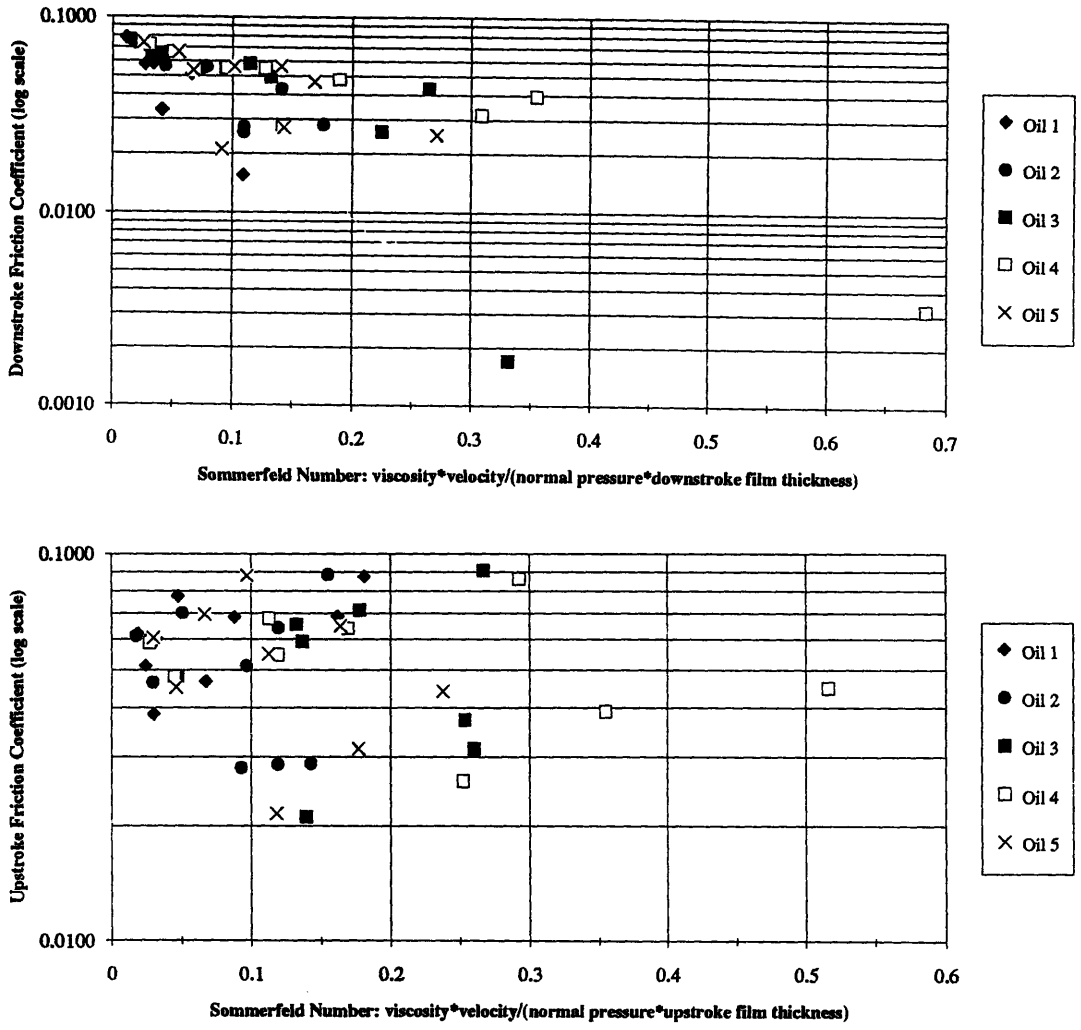

Figure 4-23: Stribeck Diagrams for Up- and Downstroke, Complete Data Collection.

have not been achieved on the downstroke. Figure 4-25 shows the upstroke Stribeck diagrams by oil type. The friction coefficient does not vary with the Sommerfeld Number. That is, the best match to the data is a horizontal line. This, combined with the low friction coefficient values, is perhaps more promising, since it may signal mixed lubrication and a proximity to hydrodynamic lubrication transition.

4.3 Repeatability

As mentioned earlier, ten cycles of data were gathered and averaged to eliminate noise. Individual traces were examined to check for repeatability and to ensure that

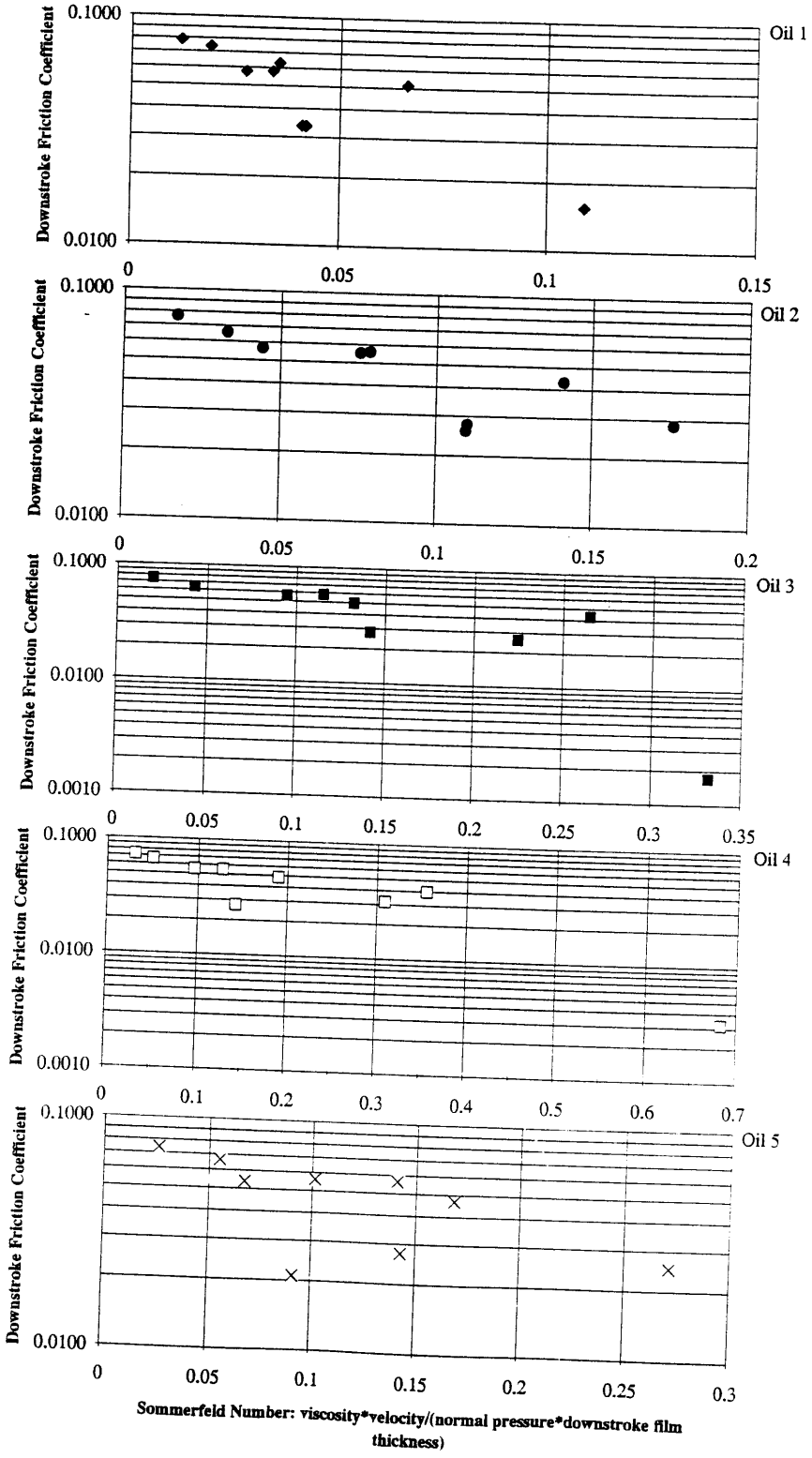

Figure 4-24: Downstroke Stribeck Diagrams by Oil Type.

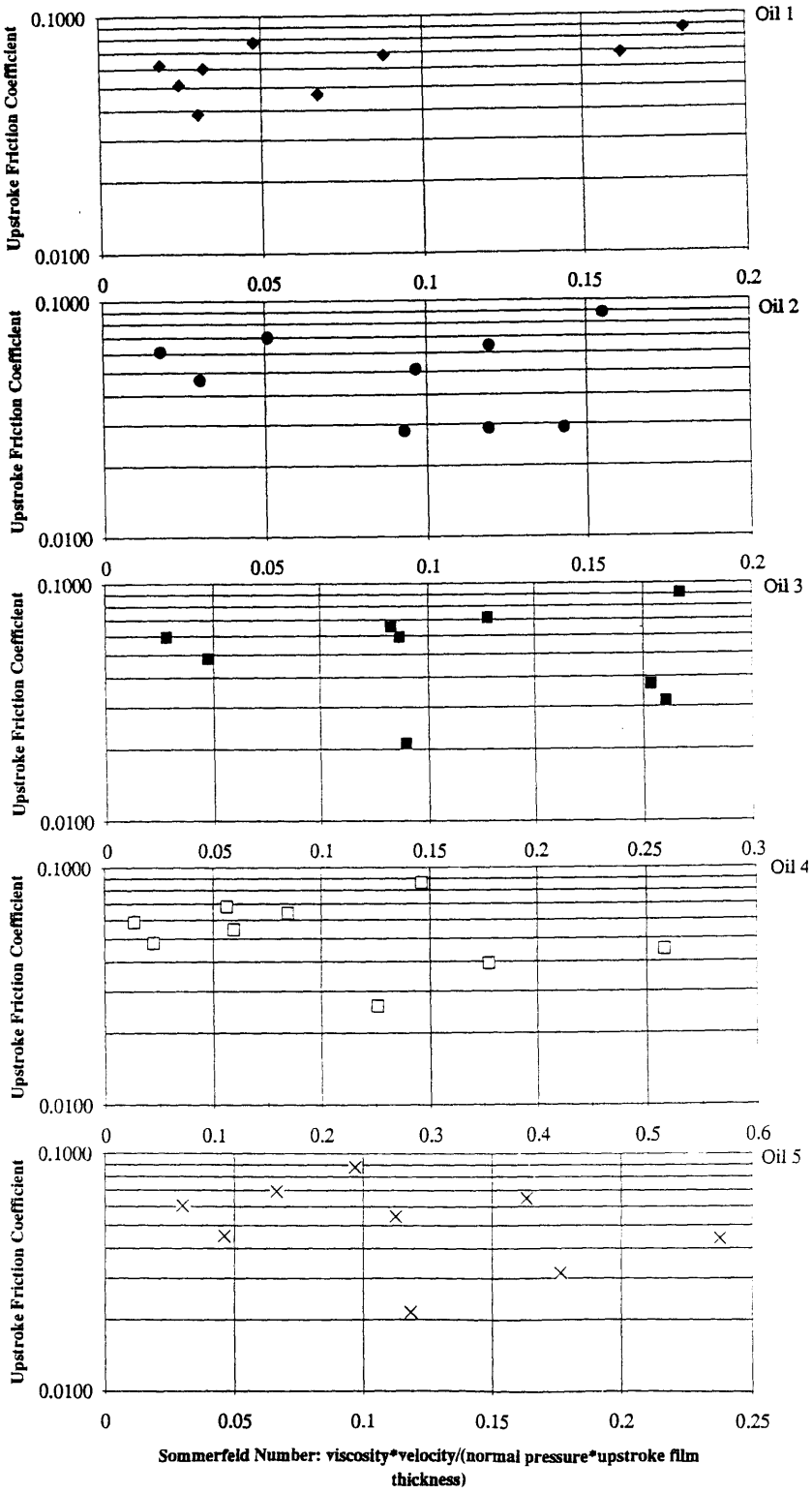

Figure 4-25: Upstroke Stribeck Diagrams by Oil Type.

characteristics found in single traces were not being averaged out. The specific concern was that the ring profile might be flooded and the groove distinguishable for a single trace. Figure 4-26 shows the first, second, fifth and tenth cycles of the oil film thickness traces, as well as the averaged cycle.

The individual traces do not vary significantly from the average or from each other in general shape or width, although there is some noise which is averaged out. On the tenth subring region trace, there are indications of the ring groove, indicating some flooding of the groove. However, this is indistinguishable from the noise and therefore unreliable. Figure 4-27 shows four successive traces of friction and normal forces, indicating that both are repeatable and that there are no individual characteristics to a particular trace. There is a large amount of noise present in the individual normal force traces, which confirms the necessity of averaging over many cycles.

4.4 Verification of Experimental Procedure

To summarize, the procedure followed in using the oil feed system was to allow the oil film thickness to stabilize for a few minutes after pulsing the oil, as described earlier in the oil thinning traces. This procedure was verified by three additional data sets, in which the oil feed was varied. The first had regular oil pulsing of 4 millisecond pulse width and 1 second pulse spacing. The second was taken simultaneously with a single oil pulse and the third was taken six seconds after the single oil pulse. The goal of the second and third collection was to provide data for oil behavior while the oil film thickness is unstable. Figure 4-28 shows the results of oil film thickness and friction behavior for the three tests and typical results, for comparison. All the tests were performed using oil 4, at a normal load of approximately 19 N and engine speed of approximately 211 rpm. There are no changes in the friction coefficient trace, but the oil film thickness curve does change with oil flooding. The regularly pulsed oil curve and the curve at time zero are similar, but at six seconds after the oil pulse, the curve shape has changed, reflecting the increased oil presence on the liner and ring holder. The lowest row presents the most lubricant-starved condition, two minutes

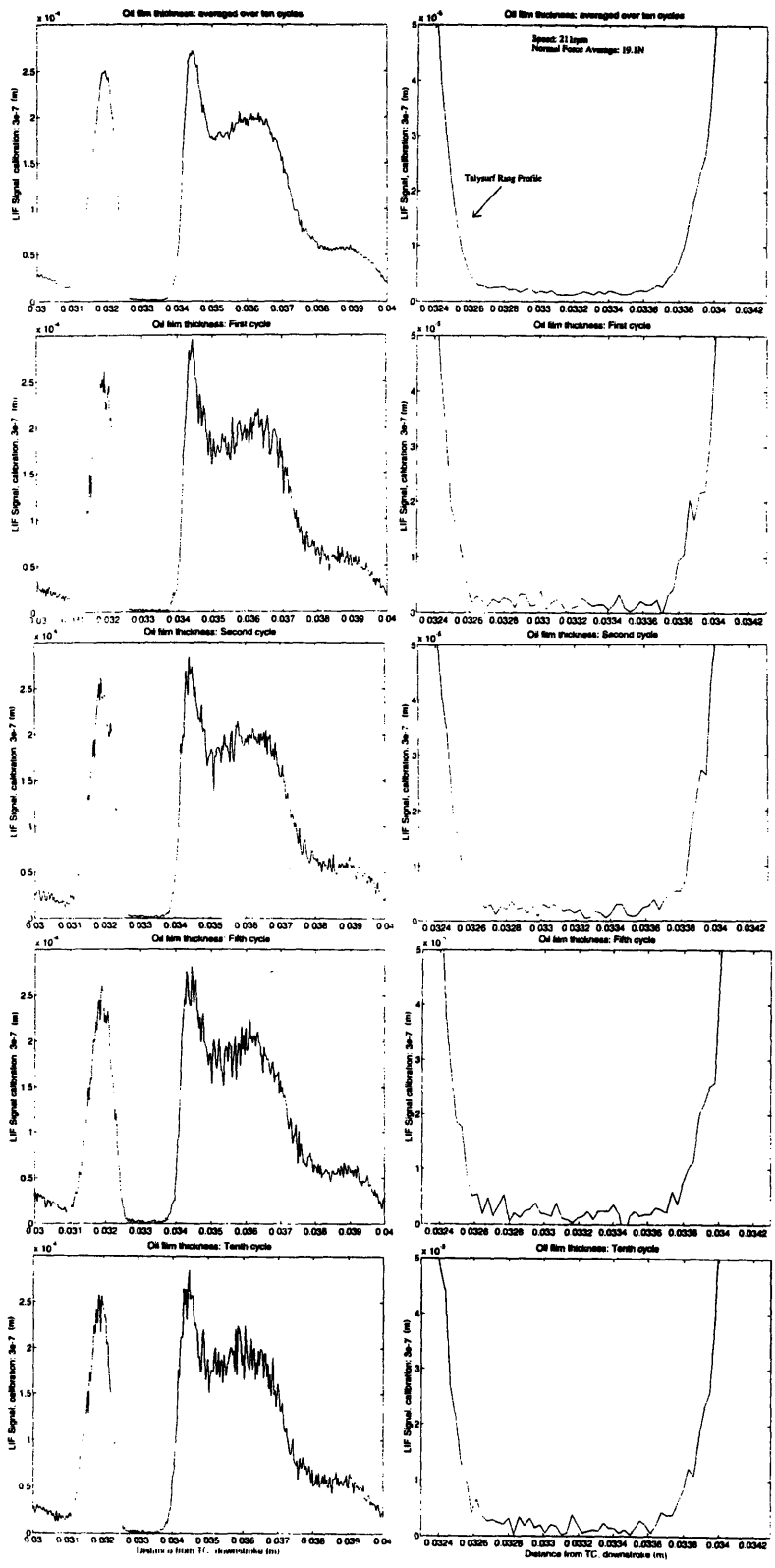

oil 4 (10W50)

low speed

low load

Figure 4-26: Oil Film Thickness Single Traces

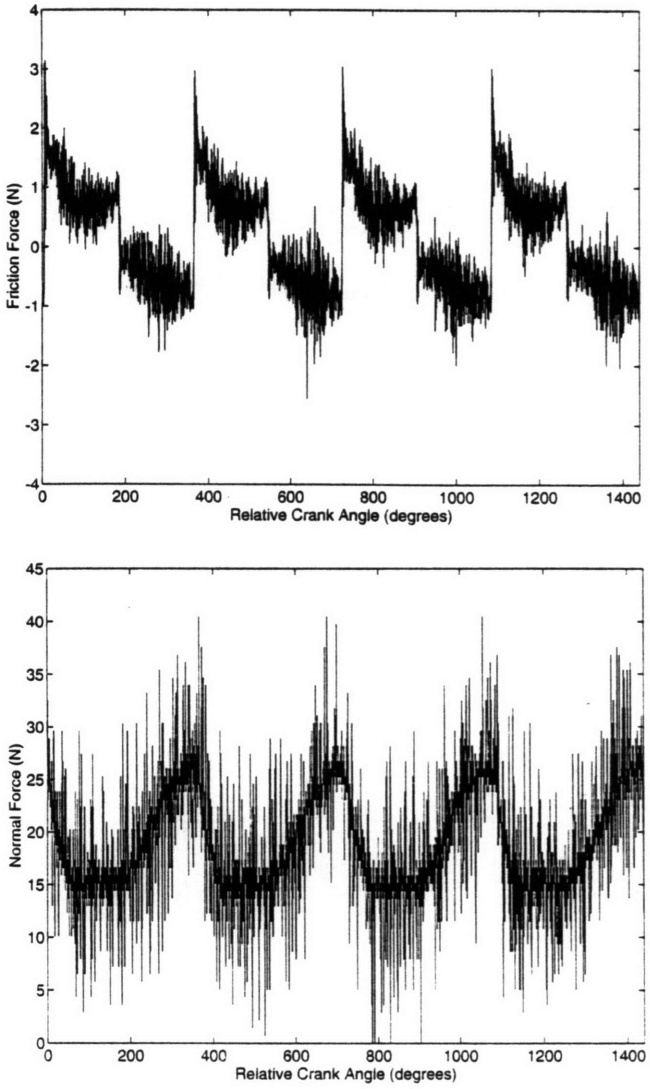

Both graphs are from the data set: oil 4 (10W50) at low load and low speed.

Figure 4-27: Four Successive Traces of Friction and Normal Forces

after the oil pulse. Here, the volume of oil around the ring has diminished, perhaps due to reduction from the motion and vibration of the ring holder and the scraping of the oil from the liner by the ring. Additionally, the film thickness in the subring region is substantially lower for the lowest row, indicating that the oil film thickness has been thinned by the motion of the ring against the liner. There is no change in the fit of the oil profile to that of the Talysurf ring profile. Even the most flooded condition does not exhibit a ring groove from which to calibrate.

It may also be instructive to examine individual cycles of the two tests taken under unstable oil film conditions. This is shown in Figure 4-29. For the data set taken simultaneously with the single oil pulse, there are minor changes in shape from one cycle to the next. The oil thickness following the ring increases, perhaps reflecting an increased volume of oil on the ring holder, which has changed the profile of oil around the ring. The film thickness under the ring does not change substantially from the first to the tenth cycle for either data set. In the second data set, taken six seconds after the single oil pulse, there are also slight changes in the shape of the volume of oil as it adjusts to the oil input.

The oil pulsing data for the first test was also collected and is shown in Figure 4-30. The pulsing occurred three times during the ten measured cycles, during the second cycle, the sixth cycle and at the beginning of the tenth cycle. The first three oil film thickness downstroke cycles are given, for comparison before, during and after the oil pulse. There are few noticeable differences in the oil film behavior from the change in oil feed, except for the shape of the oil film behind the ring (from 0.035 to 0.04m). Figure 4-31 shows the second, third and fourth cycles, both down and upstroke, temporally relative to the oil pulse. This confirms that the oil thickness curve does not change dramatically with a small addition of oil.

The data was found to be very repeatable within a cycle, normal load and temperature variations were observed and accounted for, results were presented for friction and oil film thickness and trends were observed. The results and patterns presented seem reasonable when compared to common knowledge in this field.

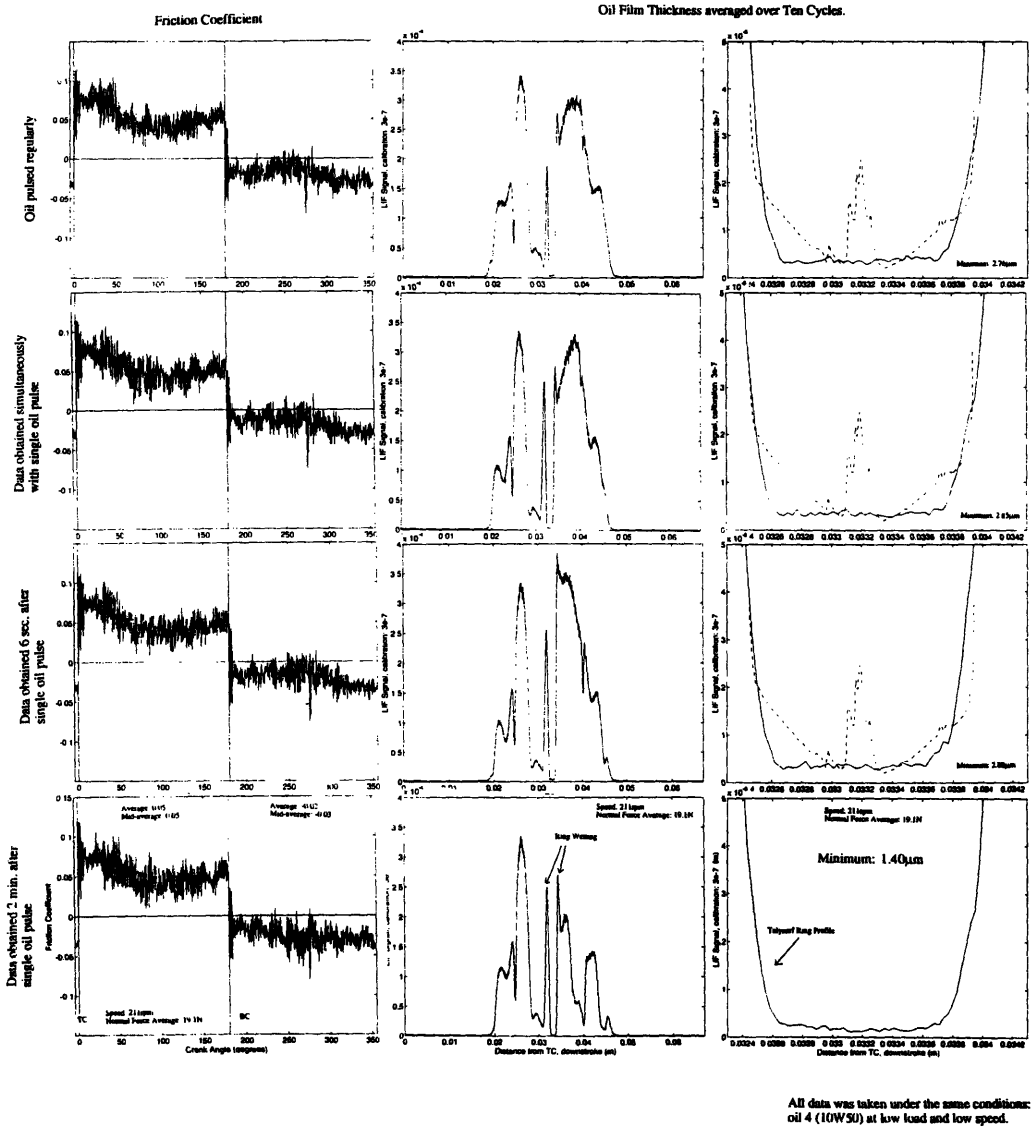

Figure 4-28: Oil Film Thickness and Friction Behavior for Experimental Procedure Verification.

Oil Pulsing and Measurement simultaneous

Measurement 6 seconds after oil pulse.

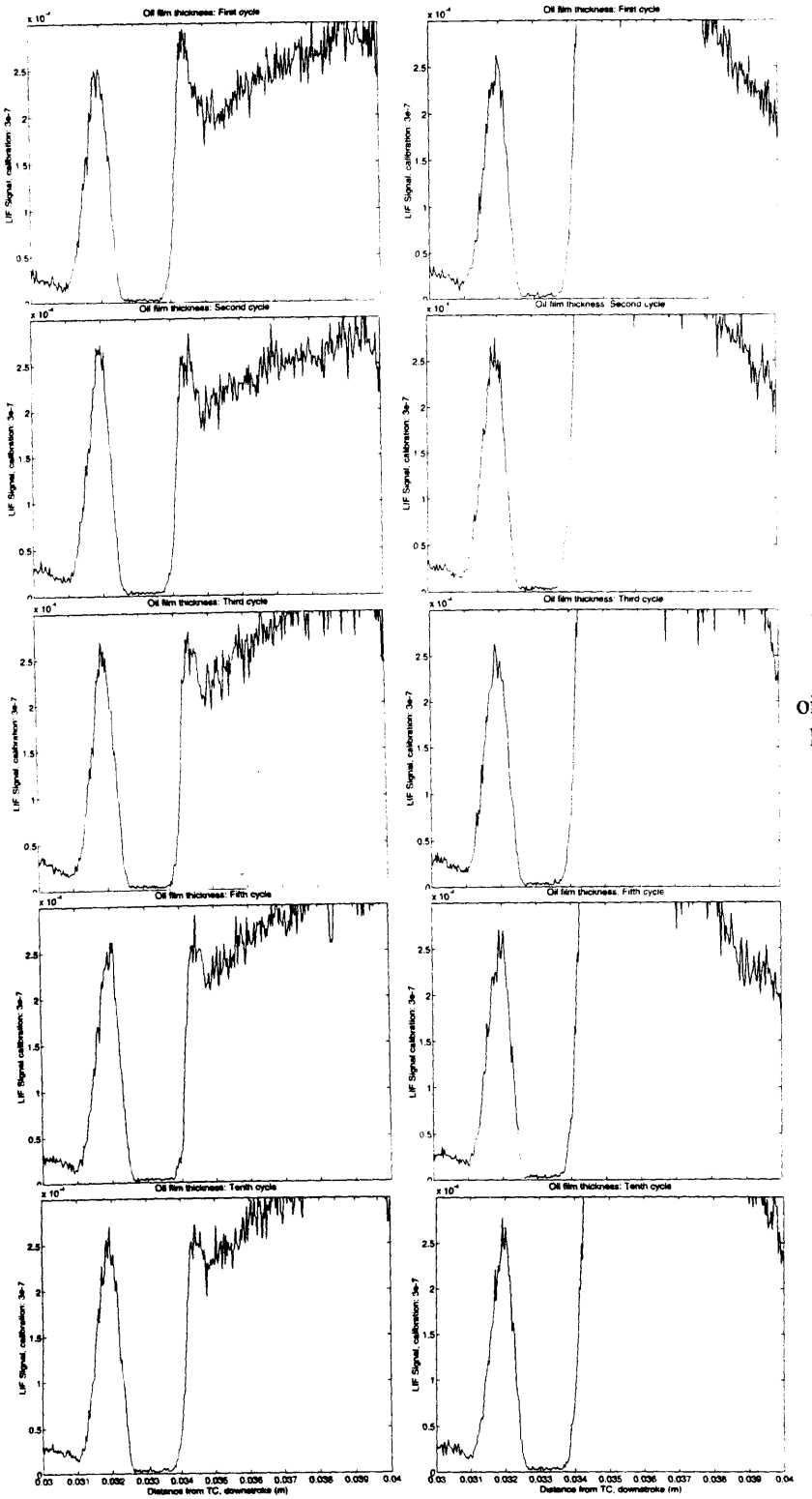

All data was taken under the same conditions: oil 4 (10W50) at low load and low speed.

Figure 4-29: Individual Cycles of Oil Film Thickness Measurements

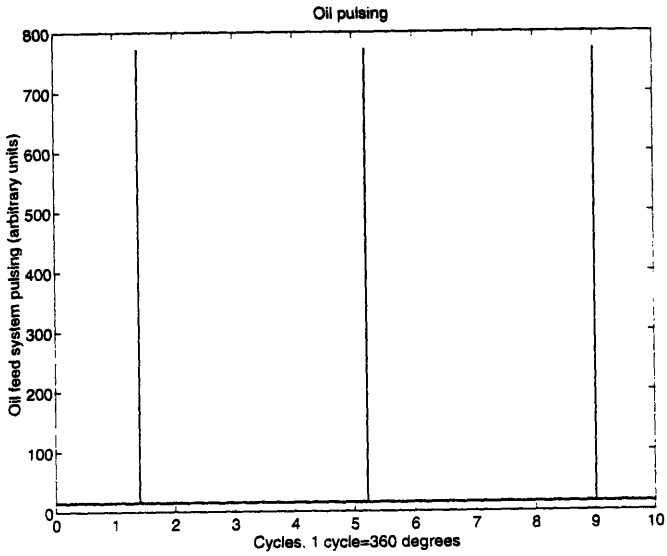

(a) Oil Pulsing during Data Collection

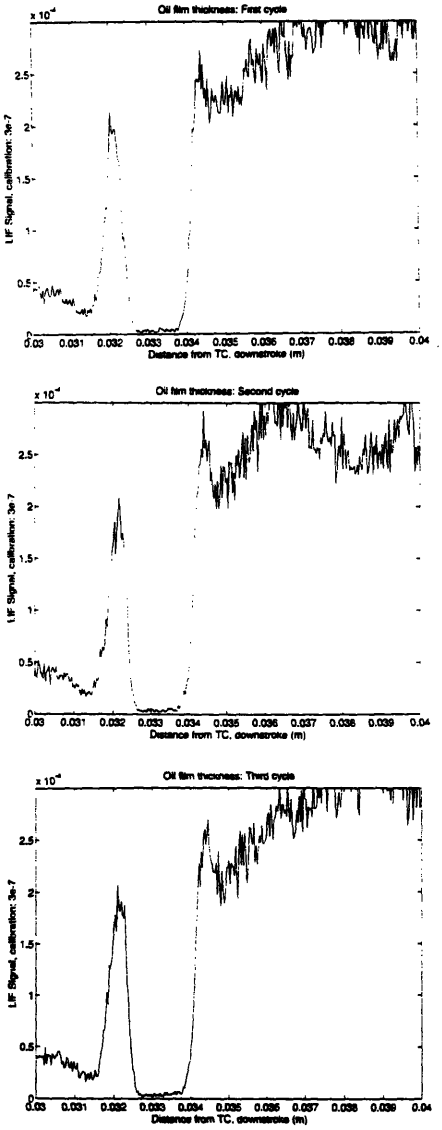

(b) First Three Cycles of Downstroke Oil Film Thickness. All data are for oil 4, at low load and low speed.

Figure 4-30: Effect of Oil Pulsing on Oil Film Thickness Traces.

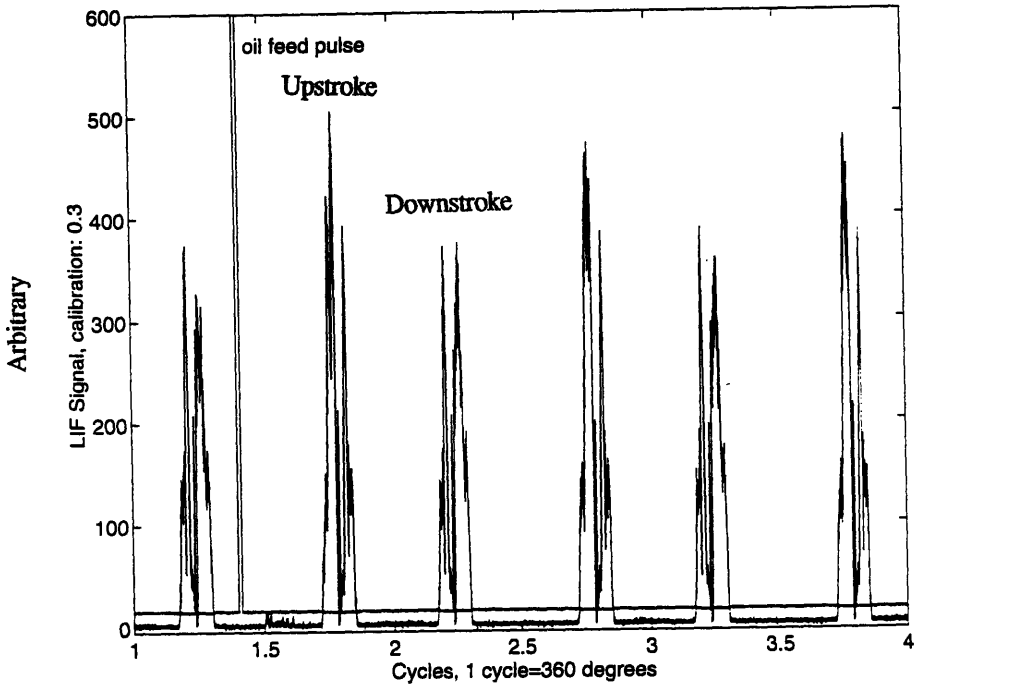

Figure 4-31: Changes in Oil Film Thickness under Oil Pulsing.

Chapter 5

Comparison of Data with Theoretical and Current Research Results

This chapter compares the experimental results obtained with both those gathered by research peers and with theoretical results, in order to facilitate evaluation of the data from this test apparatus.

5.1 Current Research

The works referred to herein have all been previously reviewed in the Introduction to this thesis. Figure 5-1 diagrams friction force results from a fixed sleeve engine friction measurement assembly. Part (a) shows typical firing and motoring results for friction force at 1,000 rpm and part load. The motoring trace is very similar in shape to the friction force results shown in Figure 4-4, one of which is given in part (c). Part (b) shows the friction force results as the rings were successively removed. The dashed trace showing the top ring and piston friction force, is dissimilar in shape to the top ring friction force shown in (c). This may be due to the presence of friction from the piston skirt itself, which isn't present in the current test apparatus. The magnitude of the friction force is also difficult to compare, because of the presence of

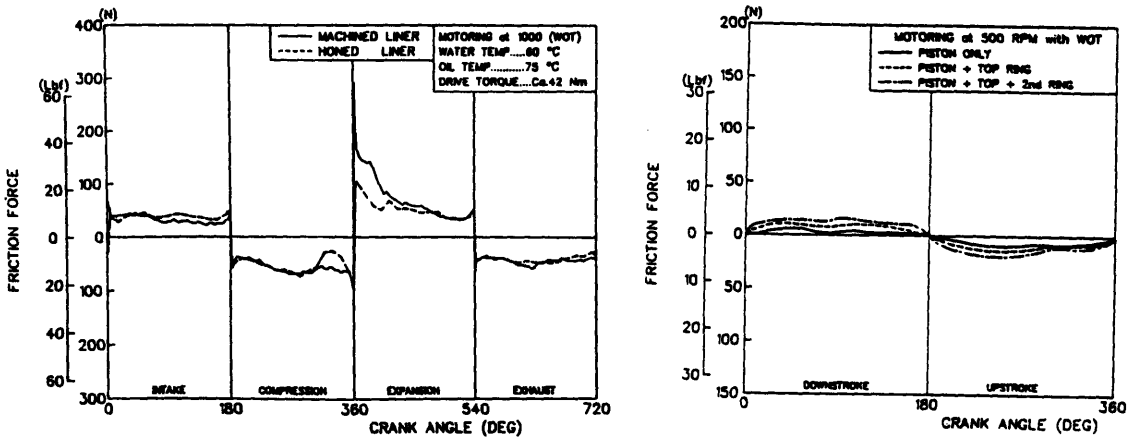

(a) & (b) Source: SAE Paper 880571

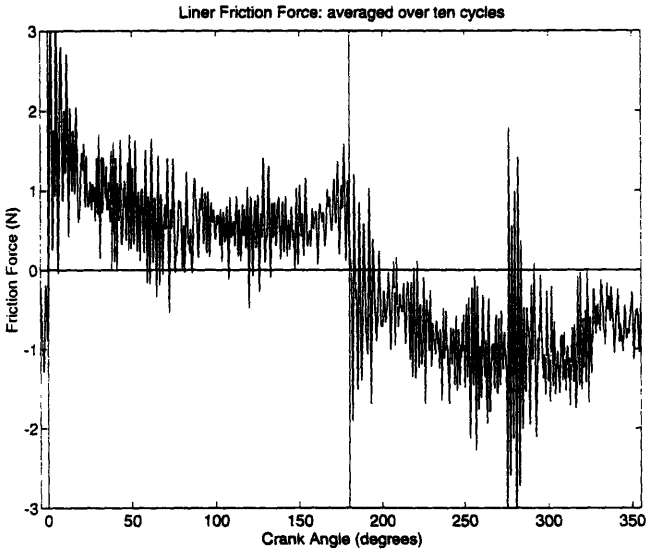

(c)

Oil 10W50
Engine Speed 408rpm
Normal Load 19N

Figure 5-1: Comparison of Friction Force Results.

the piston and the utilization of the complete ring, rather than a ring segment. In Figure 5-2, friction coefficient results from the Slone et. al. [*ibid.*] wear simulator are placed next to a friction coefficient graph gained under similar conditions of speed, load and temperature. The wear simulator has two-thirds the friction coefficient of the M.I.T. test apparatus and the traces are dissimilar in curvature. The M.I.T. test rig graph shows a mild spike at endstroke and a flat, steady friction coefficient trace while the graph in (a) shows a lot of fluctuation and noise and a much higher friction coefficient at endstroke.

The Stribeck diagram results for the instantaneous Sommerfeld Number, $\frac{\mu U}{\sigma h_0}$, cannot be compared, since there are no other simultaneous measurements of friction and

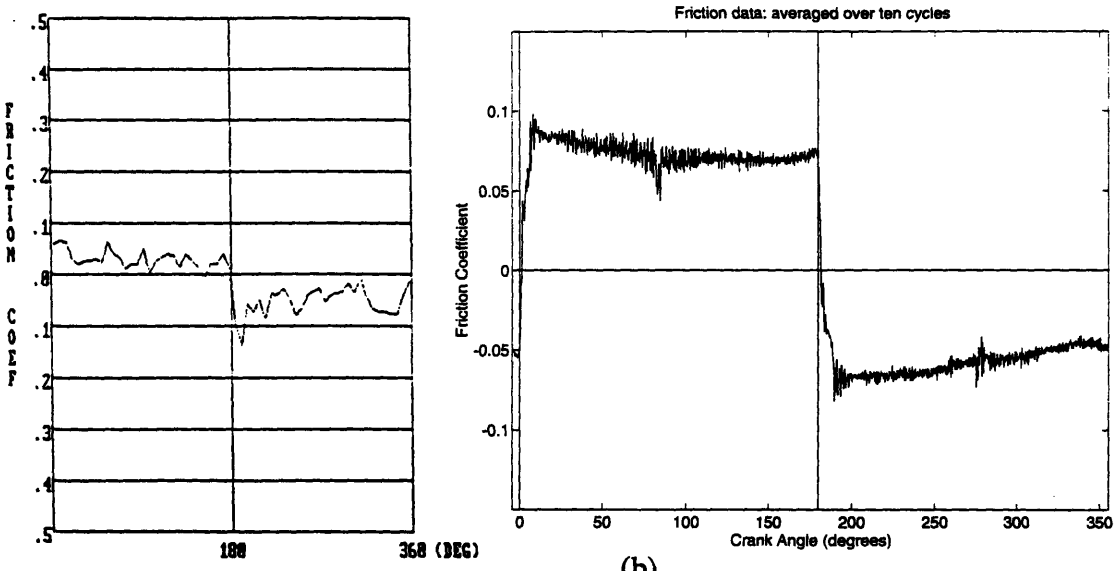

(a) Source: SAE Paper 890146

Normal Load 85.4N
Engine Speed 268rpm
Temperature 35°C
Average Friction Coefficient 0.04

(b)

Oil 10W50
Normal Load 80N
Engine Speed 206rpm
Temperature 35°C
Average Friction Coefficient 0.06

Figure 5-2: Comparison of Friction Coefficient Results.

oil film thickness known to the author. However, a single cycle Stribeck diagram, using ring width as the sliding pad dimension is available from Ting [*ibid.*], shown in Figure 5-3, for comparison with Figure 4-22. Trace 3 of part(b) and the M.I.T. graph are for similar oils (both oils used are SAE50), speeds of approximately 200 rpm, and normal loads of approximately 80 N. The friction coefficient values are similar between the graphs, with a friction coefficient of 0.1 at the endstroke and approximately 0.6 at midstroke. However, the M.I.T. trace does not have the 50% drop in friction coefficient between mid- and endstroke that is characteristic of the Ting trace.

A comparison with the oil film thickness measurement results of Grice et. al. [*ibid.*], obtained using the capacitance method, is given in Figure 5-4. The range of engine speeds is different and the measurements were made further from midstroke than in the experiments reported herein. However, the top ring, diagrammed in (b) as ring 1u, shows non-monotonic variation with speed and, like the graph in (a), it is difficult to discern a clear relationship between film thickness and engine speed. This is in

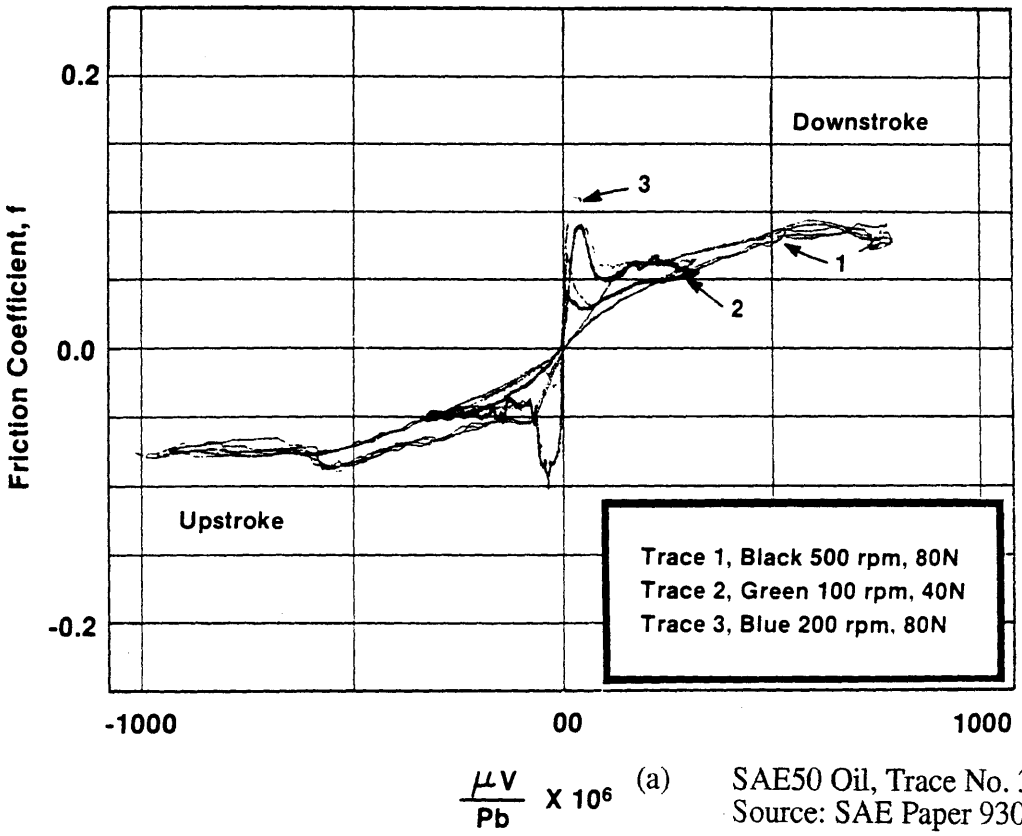

(a) SAE50 Oil, Trace No. 3
Source: SAE Paper 930686

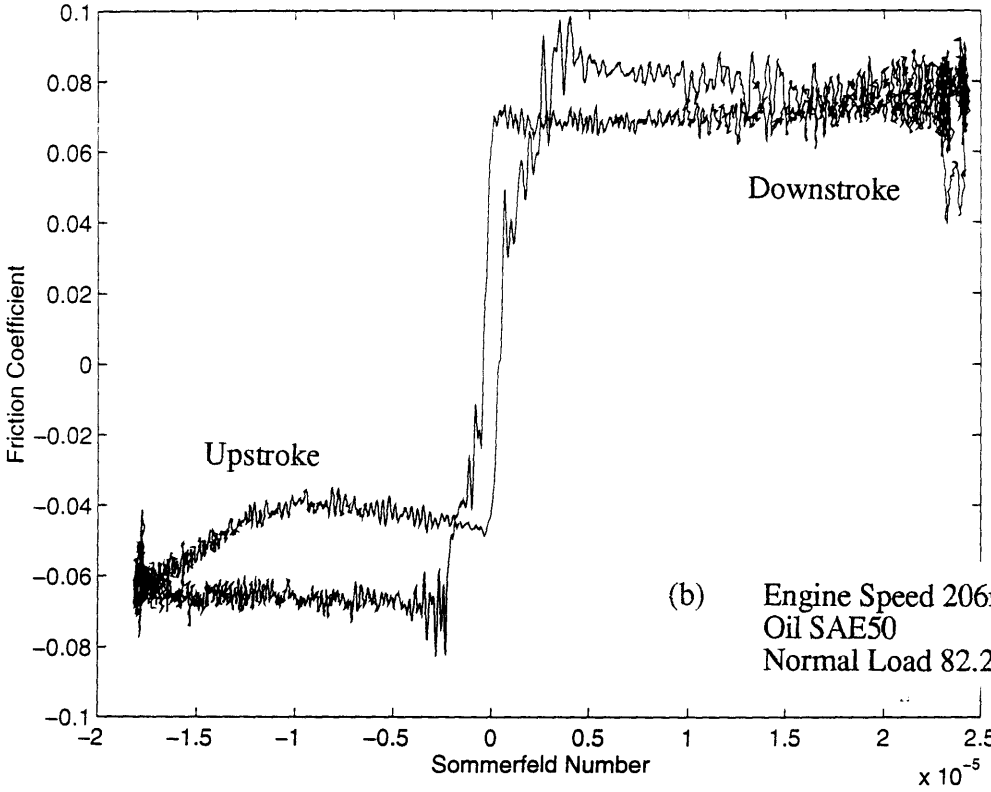

(b) Engine Speed 206rpm
Oil SAE50
Normal Load 82.2N

Figure 5-3: Comparison of Single Cycle Stribeck Diagrams.

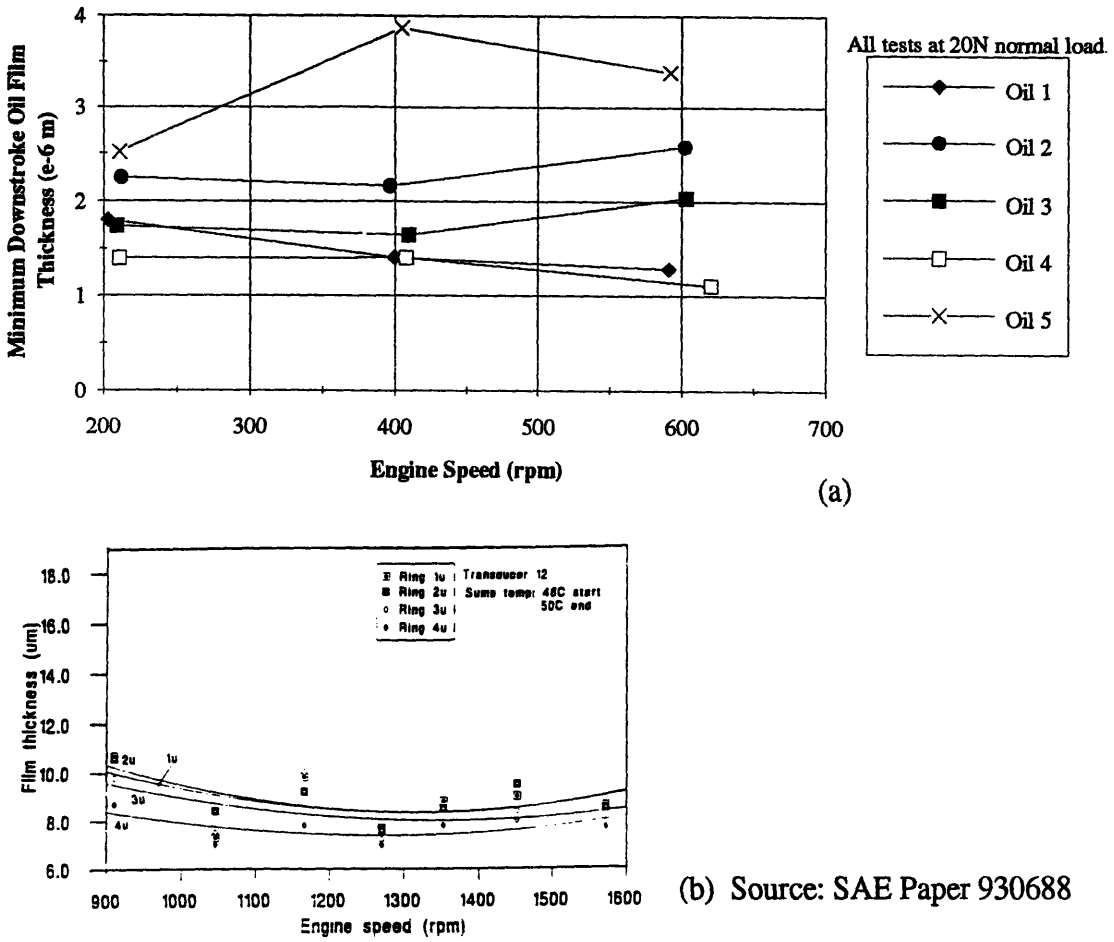

Figure 5-4: Comparison of Oil Film Thickness Measurements.

agreement with the results of Deutsch [*ibid.*], who using the M.I.T. L.I.F. equipment, found minimum film thickness to be relatively independent of speed. Deutsch's top ring minimum oil film thicknesses, for motored conditions, were in the range of 5 to 6 μm and from 2 to 4 μm for fired conditions. The range of minimum oil film thicknesses obtained using the M.I.T. test rig have been from 0.2 to 4 μm, which, while of the same order of magnitude, are lower and are closer to the Brown [*ibid.*] results of 0.5 to 2 μm top ring oil film thicknesses for full ring pack lubrication. This again places doubt on the L.I.F. signal calibration . Additionally, Deutsch found minimum oil film thickness to decrease with increasing viscosity, which is diametrically opposite to the trends observed from the test apparatus.

5.2 Theoretical Analysis and Comparison

A simplified theory of ring/liner lubrication will be presented in this section and compared to experimental results. The theory was developed by Tian [19].

There has been considerable work in the area of modeling engine lubrication. The difficulty of this task arises from the complexity of the internal combustion engine environment. The friction behavior is affected by: the ring/liner sliding speed, which is maximum close to midstroke and zero at ring reversal, oil properties, which vary with the large temperature fluctuations resulting from combustion and heat transfer, the ring/liner normal force, metallurgical behavior of the ring and liner coatings, which vary with engine longevity, oil feed, which includes the amount of oil splashed onto the liner and the spreading of the oil layer by the rings themselves. However, for the test apparatus described herein, many of these factors can be simplified or neglected and a rough model of friction can be developed for correlation with experimental results.

The lubricant flow between the ring and liner is modeled as flow between two flat sliding plates. Figure 5-5 shows the actual ring curvature used in the test apparatus. Part (b) of the figure is the model of the ring/oil/liner interface. The following assumptions allow for development of a simple model: (1) the ring/liner friction behavior is isolated to midstroke, for uniform and maximum speed, (2) hydrodynamic lubrication is prevalent, where the oil film under the ring has pressure to maintain a separation between the surfaces and the friction occurs between the ring and the oil film and the liner and the oil film, rather than surface to surface contact of the ring and liner, (3) a uniform pressure is present on the surface of the oil film and (4) that there is enough oil on the liner to assume that the ring is fully wetted and there is no cavitation under the ring or, the leading edge is fully flooded. The first assumption is met by the collecting of film thickness data at midstroke and the fourth is easily met by the oil feed system of this apparatus. The use of a single ring in the rig means that the pressure outside the region under the ring is atmospheric pressure and therefore uniform. The second assumption is the most difficult to meet.

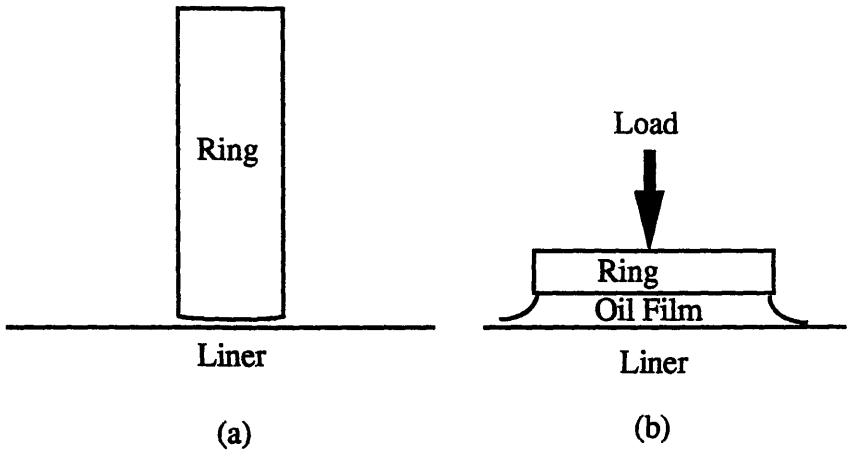

Figure 5-5: Actual and Model Ring/Liner Interaction.

The simplified Reynolds equation in one dimension, at midstroke, can be applied to this test apparatus.

$$\frac{\partial}{\partial x}\left[\frac{h^3}{\mu}\frac{\partial P}{\partial x}\right] = 6U\frac{\partial h}{\partial x} \tag{5.1}$$

where $h(x)$ is oil film thickness, μ is oil viscosity, P is pressure, U is sliding velocity and x is the direction along the liner. These variables are diagrammed in Figure 1-2. Viscosity is assumed constant. The boundary conditions are,

$$P(x_1) = P(x_2) = P_{ATM} \tag{5.2}$$

$$\frac{dP}{dx}(x_2) = 0 \tag{5.3}$$

$$h(x) = h_0 + \frac{x^2}{2a} \tag{5.4}$$

The first boundary condition assumes that the pressure outside the subring region is equal to the atmospheric pressure around the ring and the second boundary condition is the Reynolds exit condition. Further information about the Reynolds equation and boundary condition can be found in [20]. The third boundary condition assumes that, in the subring region, no gaseous voids or cavitation is present and the oil

profile follows that of the ring, represented by a parabolic profile. Additionally, the ring load, W, is assumed to be supported by the pressure generated under the ring.

$$W = \int_{x_1}^{x_2} P(x)dx \tag{5.5}$$

This is termed the load condition. Integrating the Reynolds equation and applying the above conditions yields, after some algebraic manipulation and integration by parts,

$$\int_{x_1}^{x_2} \frac{h(x) - h(x_2)}{h^3(x)}dx = 0 \tag{5.6}$$

$$6\mu U \int_{x_1}^{x_2} \frac{(x - x_1)[h(x) - h(x_2)]}{h^3(x)}dx + W = 0 \tag{5.7}$$

Using the following non-dimensional variables,

$$x = \bar{x}B \tag{5.8}$$

$$h_0 = \bar{h}_0 \frac{B^2}{2a} \tag{5.9}$$

yields:

$$h(x) = \frac{B^2}{2a}\bar{h}(\bar{x}) \tag{5.10}$$

$$\bar{h}(\bar{x}) = \bar{h}_0 + \bar{x}^2 \tag{5.11}$$

Equations 5.6 and 5.7 can now be rewritten in terms of the dimensionless variables $\bar{h}_0$ and $\bar{x}_2$.

$$\int_{\bar{x}_1}^{\bar{x}_2} \frac{\bar{h}(\bar{x}) - \bar{h}(\bar{x}_2)}{\bar{h}^3(\bar{x})}d\bar{x} = 0 \tag{5.12}$$

$$\int_{\bar{x}_1}^{\bar{x}_2} \frac{(\bar{x} - \bar{x}_1)[\bar{h}(\bar{x}) - \bar{h}(\bar{x}_2)]}{\bar{h}^3(\bar{x})}d\bar{x} + \frac{W}{6\mu U}\left(\frac{B}{2a}\right)^2 = 0 \tag{5.13}$$

The preceding two equations demonstrate that $\bar{h}_0$ and $\bar{x}_2$ are functions of geometric parameters and operating conditions.

$$\bar{h}_0 = F_1\left[\frac{\mu U}{W}\left(\frac{2a}{B}\right)^2\right] \tag{5.14}$$

$$\bar{x}_2 = F_2\left[\frac{\mu U}{W}\left(\frac{2a}{B}\right)^2\right] \tag{5.15}$$

A similar analysis can be performed for the dimensionless friction coefficient, by first considering the ring shear stress.

$$\mu\frac{\partial u}{\partial y}|_{y=h(x)} = -\mu\frac{U}{h} + \frac{dP}{dx}\frac{h}{2} \tag{5.16}$$

Substitution for the pressure gradient from the derivation of equation 5.6 yields the following.

$$\mu\frac{\partial u}{\partial y}|_{y=h(x)} = \mu U\frac{[2h(x) - 3h(x_2)]}{h^2(x)} \tag{5.17}$$

If the left hand side term is integrated over the subring liner distance, it can be thought of as the pressure due to shear forces, which, when divided by the pressure due to normal forces, is the friction coefficient.

$$C_f = \frac{\int_{x_1}^{x_2}\mu\frac{\partial u}{\partial y}|_{y=h(x)}dx}{W} = \mu\frac{\frac{U}{W}}{\frac{B}{2a}}\int_{\bar{x}_1}^{\bar{x}_2}\frac{[2\bar{h}(\bar{x}) - 3\bar{h}(\bar{x}_2)]}{\bar{h}^2(\bar{x})}d\bar{x} \tag{5.18}$$

This gives the coefficient of friction as a function of similar parameters as $\bar{h}_0$ and $\bar{x}_2$.

$$C_f = \frac{\mu\frac{U}{W}}{\frac{B}{2a}}F_3\left[\frac{\mu U}{W}\left(\frac{2a}{B}\right)^2\right] \tag{5.19}$$

The Sommerfeld Number is re-defined as:

$$SN_{MOD} = \frac{\mu U}{W}\left(\frac{2a}{B}\right)^2 \tag{5.20}$$

and $\frac{2a}{B}$ is called the ring geometry parameter. Tian [*ibid.*] used a numerical method to obtain power laws relating $\bar{h}_0$, $\bar{x}_2$ and C_f to the modified Sommerfeld Number, for the test apparatus ring geometry. The relationships are graphed in Figure 5-6.

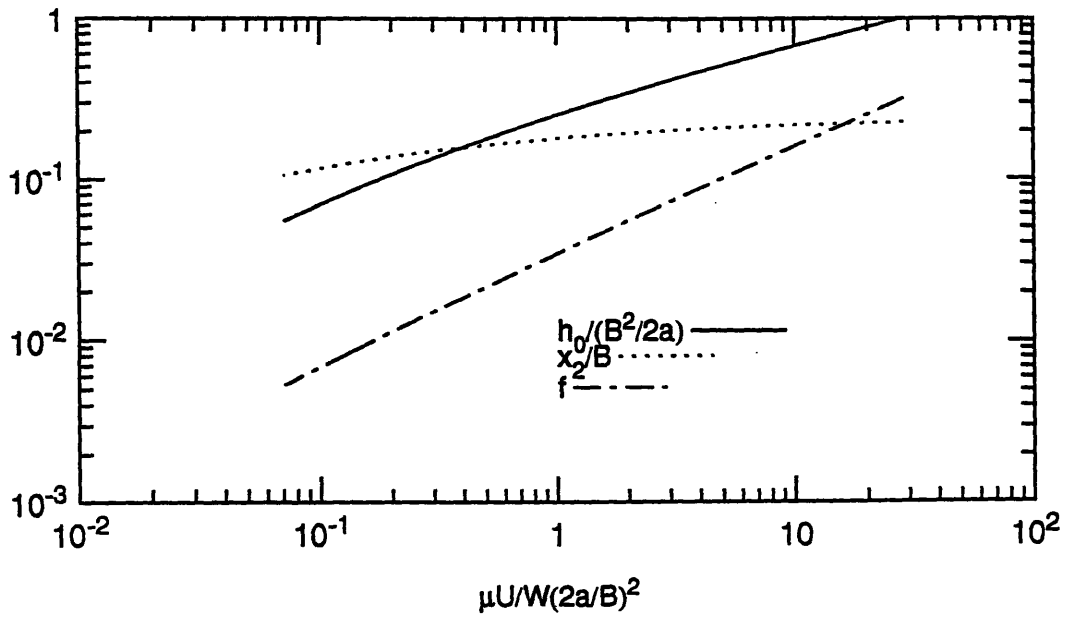

Figure 5-6: Friction Coefficient, Film Thickness and Ring Wetting Dimensionless Variables graphed against the modified Sommerfeld Number.

$$C_f = 2.05 \frac{\left(\frac{\mu U}{W}\right)^{0.68}}{\left(\frac{B}{2a}\right)^{0.36}} \tag{5.21}$$

$$\bar{h}_0 = 0.25 \left[\frac{\mu U}{W}\left(\frac{2a}{B}\right)^2\right]^{0.528} \tag{5.22}$$

$$\bar{x}_2 = 0.178 \left[\frac{\mu U}{W}\left(\frac{2a}{B}\right)^2\right]^{0.162} \tag{5.23}$$

The power law relating the friction coefficient to the modified Sommerfeld Number was slightly modified to obtain:

$$C_f = 2 \frac{\left(\frac{\mu U}{W}\right)^{\frac{2}{3}}}{\left(\frac{B}{2a}\right)^{\frac{1}{3}}} \tag{5.24}$$

The results of this theoretical model are compared with the data results in Figure 5-7, which shows one cycle of data of the friction coefficient graphed against the modified Sommerfeld Number on a logarithmic scale. The friction traces are from midstroke to top center, and are taken from the data sets which appeared most

likely to demonstrate hydrodynamic lubrication. Although the values of the modified Sommerfeld Number differ by an order of magnitude between theory and experiment, they exhibit a similar power law relationship. This implies that the power law model developed in the theoretical analysis suitably models the experimental behavior and only differs from actual measurements by an offset. Moreover, the figure suggests that the assumptions used in the theory, including the assumption of hydrodynamic lubrication, are applicable to this test apparatus.

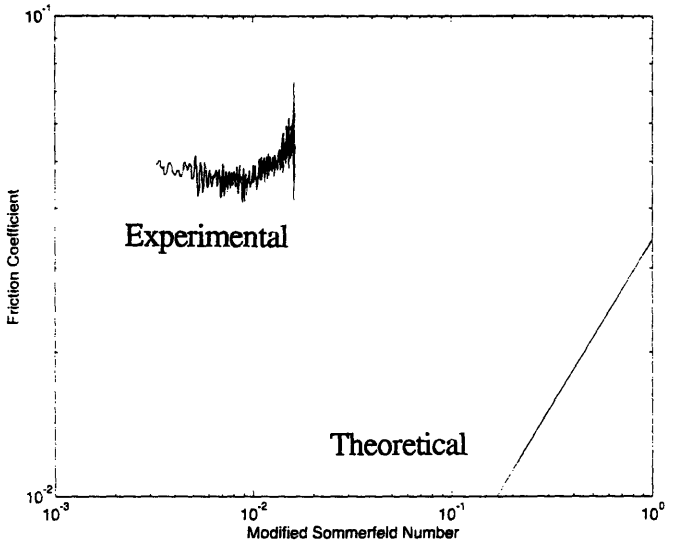

(a) Oil 10W50
Engine Speed 206rpm
Normal Load 79.9N

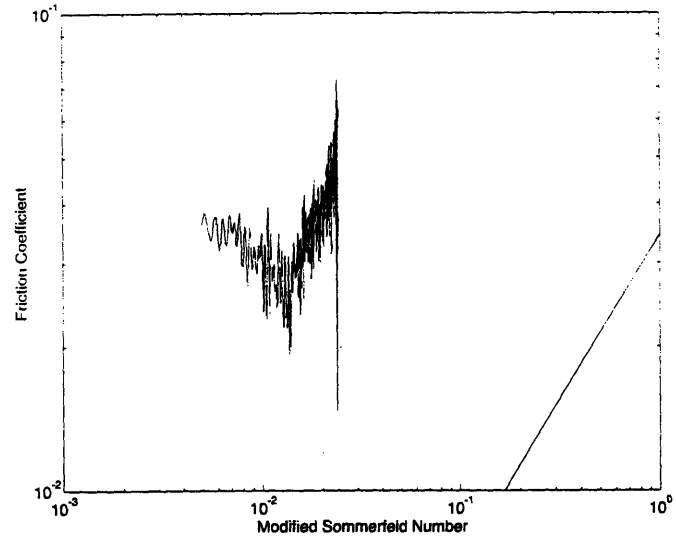

(b Oil SAE50
Engine Speed 208rpm
Normal Load 40.9N

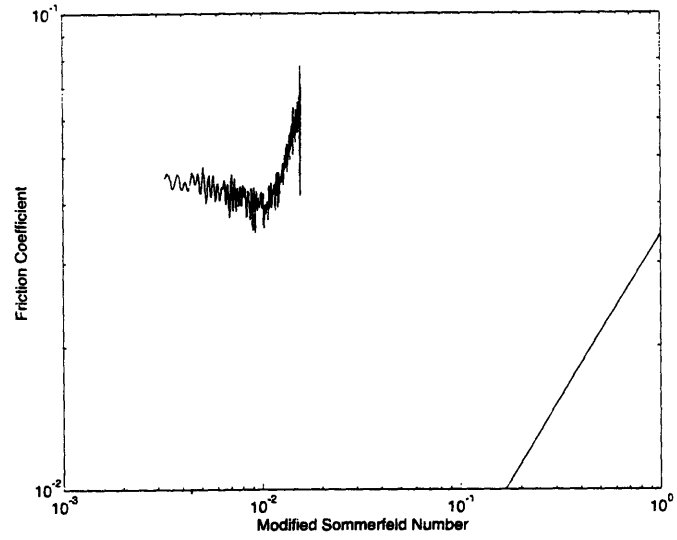

(c) Oil SAE50
Engine Speed 206rpm
Normal Load 82.2N

Figure 5-7: Friction Coefficient graphed against the modified Sommerfeld Number.

Chapter 6

Conclusions

6.1 Research Summary

The following research was presented in this thesis:

(i) The design and construction of a novel test apparatus for simultaneous friction and oil film thickness measurements was detailed. The corresponding instrumentation and experimental procedure were described. The advantages of this rig include: a realistic stroke length and ring motion, realistic engine-like geometry of a vertical stationary liner and reciprocating ring, ability to isolate single ring effects, variation of the normal load to simulate ring elastic pressure or gas pressure, use of actual engine specimens and an oil feed system allowing oil flow control.

(ii) Preliminary results and consequent issues were presented. The most serious problems included: ring conformance to liner curvature, oil film thickness calibration, friction effects of L.I.F. windows and the ability to operate the engine at a sufficiently high speed to enable measurements well into the hydrodynamic regime.

(iii) A test matrix was presented, which included test conditions of five oils of differing viscosity, three ring normal forces and three engine speeds. Resulting friction coefficients and oil film thicknesses were presented, as well as liner temperatures.

(iv) The data was found to be highly repeatable, but the friction coefficient noise increased with speed. The results for high speed and low load were difficult to interpret. The oil film thickness was calibrated using the ring width. The friction coefficient

varied from 0.01 to 0.1 and the oil film thickness varied from 0.2 to 0.4 μm.

(v) The following general patterns were observed. Minimum oil film thickness increased with viscosity and, for some oils, decreased with normal force. Minimum oil film thickness did not appear to vary with engine speed. In most cases, the friction coefficient increased with normal force and decreased with engine speed, displaying lubrication behavior indicative of mixed lubrication.

(vi) The Stribeck Diagram was generated and, for downstroke, the friction coefficient decreases with increasing Sommerfeld Number, indicating conditions of mixed lubrication.

6.2 Suggestions for Future Research

There are two changes to the test apparatus which have potential to improve the quality of the results. The first is the redesign of the normal force transducer mounting for reduced normal load variation and the second is improvement of the L.I.F. signal calibration. The latter is extremely important. Two alternatives to the current calibration technique are calibration from marks on the ring holder or construction of a calibration cell.

Due to time constraints, the following were not fully addressed in this thesis: the error of the friction coefficient and oil film thickness results, the current surface finish condition of the liner sample after approximately fifty hours of operation, further investigation of the oil thinning to understand at what stage the rig lubricant conditions correlate to those of an internal combustion engine, the exact location of the quartz windows with respect to the liner sample curvature and noise effects on the friction force transducer.

In addition, the test apparatus has two weaknesses which prevent it from simulating a production engine lubrication environment, and perhaps inhibit transition to the hydrodynamic lubrication regime. These are temperature and engine speed. The liner temperature could be increased by enclosing the rig in an oven, similar to the one constructed by Slone et. al. [*ibid*]. The difficulties associated with this are: mounting

of the oven on the test bed, insulation of the instrumentation and clear passage for the L.I.F. instrumentation. The engine speed range can be easily increased by changing the driving system pulley arrangement. However, the speed should be increased slowly and carefully, to avoid seize-up or scuffing from engine failure as a result of the heavy reciprocator inertial load on the engine piston. A counterbalance for the engine crankshaft would be difficult to construct, due to the limited crankcase volume.

Further experiments on this simultaneous oil film thickness and friction test apparatus could include: use of worn ring and liner samples or special ring and liner coatings, utilization of reduced-friction oils or installation of the second ring. It is also possible to redesign the ring holder to fit two rings.

Bibliography

[1] John B. Heywood. *Internal Combustion Engine Fundamentals.* McGraw-Hill, Inc., New York, 1988.

[2] L. L. Ting. Development of a Reciprocating Test Rig for Tribological Studies of Piston Engine Moving Components - Part I: Rig Design and Piston Ring Friction Coefficient Measuring Method. *SAE Paper 930685*, 1993.

[3] Hideki Yoshida, Kazunori Kusama, and Junichi Sagawa. Effects of Surface Treatments on Piston Ring Friction Force and Wear. *SAE Paper 900589*, 1990.

[4] A. Gauthier, B. Constans, H. Perrin, and F. Roux. Lubricants Effects on Piston/Rings/Liner Friction in an Instrumented Single Cylinder Diesel Engine. *SAE Paper 872034*, 1987.

[5] Young-Gon Ku and Donald J. Patterson. Piston and Ring Friction by the Fixed Sleeve Method. *SAE Paper 880571*, 1988.

[6] L. L. Ting. Development of a Reciprocating Test Rig for Tribological Studies of Piston Engine Moving Components - Part II: Measurements of Piston Ring Friction Coefficients and Rig Test Confirmation. *SAE Paper 930686*, 1993.

[7] Susan E. Hartfield-Wünsch, Simon C. Tung, and Chester J. Rivard. Development of a Bench Wear Test for the Evaluation of Engine Cylinder Components and the Correlation with Engine Test Results. *SAE Paper 932693*, 1993.

[8] Ralph Slone, Donald J. Patterson, Kevin M. Morrison, and George B. Schwartz. Wear of Piston Rings and Liners by Laboratory Simulation. *SAE Paper 890146*, 1989.

[9] Neil Grice and Ian Sherrington. An Experimental Investigation into the Lubrication of Piston Rings in an Internal Combustion Engine - Oil Film Thickness Trends, Film Stability and Cavitation. *SAE Paper 930688*, 1993.

[10] Yutaro Wakuri, Shinsuke Ono, Mitsuhiro Soejima, and Kenmei Masuda. Oil-Film Behaviour of Reciprocating Slider with Circular Profile (Optical Measurement of Oil Film Separation Boundary). *Bulletin of the JSME*, 24(194):1462–1469, 1981.

[11] L.L. Ting. Development of a Laser Fluorescence Technique for Measuring Piston Ring Oil Film Thickness. *ASME Society Paper 79-Lub-2*, 1979.

[12] Eric Deutsch. Piston Ring Friction Analysis from Oil Film Thickness Measurements. Master's thesis, Massachusetts Institute of Technology, 1994.

[13] D.P. Hoult, S.A. Billian, J.P. Lux, and V.W. Wong. Calibration of Laser Fluorescence Measurements of Lubricant Film Thickness in Engines. *SAE Paper 881587*, 1988.

[14] B.T. Shaw II, D.P. Hoult, and V.W. Wong. Development of Engine Lubricant Film Thickness Diagnostics Using Fiber Optics and Laser Fluorescence. *SAE Paper 920651*, 1992.

[15] J.P. Lux. Lubricant Film Thickness Measurements in a Diesel Engine. Master's thesis, Massachusetts Institute of Technology, 1989.

[16] M.A. Brown, H. McCann, and D.M. Thompson. Characterization of the Oil Film Behaviour Between the Liner and Piston of a Heavy-Duty Diesel Engine. *SAE Paper 932784*, 1993.

[17] Leon Bronchtein. *Laser Fluorescence Fiber Optic Technique For Engine Oil Film Thickness Measurement*, 1992. M.I.T. Sloan Automotive Laboratory manual.

[18] Byron T. Shaw II. Direct Observation of the Oil Consumption Mechanism of a Production Single-Cylinder Diesel Engine. Master's thesis, Massachusetts Institute of Technology, 1992.

[19] Tian Tian. A note on hydrodynamic friction coefficient and minimum film thickness of piston ring with fully flooded leading edge. Intra-laboratory report, 1994.

[20] Alastair Cameron. *Basic Lubrication Theory.* John Wiley & Sons, Inc., New York, 1976.

Appendix A

Software used in Experimental Procedure

```
%Janice Dearlove: Rig for simultaneous measurement of
%friction and oil film thickness, feb. 27, 1994, updated august 1, 1994
%File for averaging and analyzing data from rig
%WARNING: set for a 7200 by 10 matrix only,
%ie: 10 cycles, REMEMBER TO CHANGE THE INPUT FILE NAME

%input data
load forlm.dat
frict= forlm(:,1);
norm=forlm(:,2);
lif=forlm(:,3);

%make crank angle vector and adjust for dead centers
%according to friction direction change
CA=0.05:0.05:360;
rsc=CA-4.625;

%calibration of friction force
calfrict=frict*0.024347;

%calibration of normal force
calnorm=norm*0.722178;

%calibration of lif signal
clif=lif*0.0000003;

%average data over ten cycles by reshaping matrices
avgfrict=reshape(calfrict,7200,10);
avgnorm=reshape(calnorm,7200,10);
avglif=reshape(clif,7200,10);
mnfrict=mean(avgfrict');
mnnorm=mean(avgnorm');
mnlif=mean(avglif');

%instantaneous friction coefficient
fco=mnnorm.\mnfrict;

%calculation of: average friction force, upstroke and downstroke
%               max, min and avg. normal force
%               average friction coefficient, upstroke and downstroke
%               lif signal min, upstroke and downstroke
frictdavg=mean(mnfrict(93:3692))
frictuavg=mean(mnfrict(3693:7200))
midfrictdavg=mean(mnfrict(692:3093))
midfrictuavg=mean(mnfrict(4292:6693))
normavg=mean(mnnorm)
normmax=max(mnnorm)
normmin=min(mnnorm)
cofrctdavg=mean(fco(93:3692))
cofrctuavg=mean(fco(3693:7200))
midcofrctdavg=mean(fco(692:3093))
midcofrctuavg=mean(fco(4292:6693))
lifdwnmin=min(mnlif(1692:1733))
lifupmin=min(mnlif(5652:5693))

%plotting friction force
plot(rsc,mnfrict)
hold
axis([-4.625 355.375 -3 3]);
title('Liner Friction Force: averaged over ten cycles');
xlabel('Crank Angle (degrees)');
ylabel('Friction Force (N)');
gtext('file:forlm.dat')
A=[0; 0; 0];
B=[-5.9; 0; 356];
plot(B,A,'g')
```

```
D=[-25;0;225];
plot(A,D,'r')
E=[180;180;180];
plot(E,D,'r')
print pic2.ps
hold

%plotting normal force
plot(rsc,mnnorm)
hold
axis([-4.625 355.375 0 30]);
xlabel('Crank Angle (degrees)');
ylabel('Normal Force (N)');
title('Liner Normal Force: averaged over ten cycles');
gtext('file:forlm.dat')
A=[0; 0; 0];
B=[-5.9; 0; 356];
plot(B,A,'g')
D=[-25;0;225];
plot(A,D,'r')
E=[180;180;180];
plot(E,D,'r')
print pic3.ps
hold

%plotting friction coefficient
plot(rsc,fco)
hold
axis([-4.625 355.375 -0.15 0.15]);
title('Friction data: averaged over ten cycles');
xlabel('Crank Angle (degrees)');
ylabel('Friction Coefficient');
gtext('file:forlm.dat')
A=[0; 0; 0];
B=[-5.9; 0; 356.1];
plot(B,A,'g')
D=[-25;0;225];
plot(A,D,'r')
E=[180;180;180];
plot(E,D,'r');
print pic4.ps
hold

%plotting lif trace vs. crank angle
plot(rsc,mnlif)
hold
axis([-4.625 355.375 0 0.0004]);
title('Oil film thickness: averaged over ten cycles');
xlabel('Crank Angle (degrees)');
ylabel('LIF Signal, calibration: 3e-7');
gtext('file:forlm.dat')
A=[0; 0; 0];
B=[-5.9; 0; 356.1];
plot(B,A,'g')
D=[-25;0;225];
plot(A,D,'r')
E=[180;180;180];
plot(E,D,'r')
print pic5.ps
hold

plot(rsc,mnlif)
axis([79 83 0 0.00005])
title('Oil film thickness: averaged over ten cycles');
xlabel('Crank Angle (degrees)');
ylabel('LIF Signal, calibration: 3e-7');
```

```
gtext('file:forlm.dat')
print pic17.ps

plot(rsc,mnlif)
axis([277 281 0 0.00005])
title('Oil film thickness: averaged over ten cycles');
xlabel('Crank Angle (degrees)');
ylabel('LIF Signal, calibration: 3e-7');
gtext('file:forlm.dat')
print pic18.ps

%conversion of crank angles to linear distance from TC
stroke=0.067;
aa=stroke/2;
l=0.11309;
bb=aa+l;
ti=3600;
for i=1:ti
 theta(i)=(rsc(i)*pi)/180;
 dif(i)=bb-((aa*cos(theta(i)))+sqrt((l^2)-((aa^2)*(sin(theta(i)))^2)));
end

%plot of downstroke lif signal vs. distance from TC in two scales
newlif=mnlif(1:3600);
plot(dif,newlif)
axis([0 0.067 0 0.0004]);
title('Oil film thickness: averaged over ten cycles');
xlabel('Distance from TC, downstroke (m)');
ylabel('LIF Signal, calibration: 3e-7');
gtext('file:forlm.dat')
print pic8.ps

axis([0 0.067 0 0.00005])
gtext('file:forlm.dat')
print pic6.ps

axis([0.03 0.04 0 0.0003])
gtext('file:forlm.dat')
print pic16.ps

%plot of subring area, downstroke, with overlaid ring profile
plot(dif,newlif)
axis([0.0323 0.0343 0 0.00005]);
title('Oil film thickness: averaged over ten cycles');
xlabel('Distance from TC, downstroke (m)');
ylabel('LIF Signal, calibration: 3e-7');
gtext('file:forlm.dat')
hold
ringanal
print pic9.ps
hold

%plot first cycle of lif signal for comparison to average
onesigd=clif(1:3600);
plot(dif,onesigd)
axis([0.03 0.04 0 0.0003])
title('Oil film thickness: First cycle');
xlabel('Distance from TC, downstroke (m)');
ylabel('LIF Signal, calibration: 3e-7');
gtext('file:forlm.dat')
print pic1.ps

axis([0.0323 0.0343 0 0.00005])
gtext('file:forlm.dat')
print pic7.ps
```

```
%plot second cycle of lif signal for comparison to average
twosigd=clif(7201:10800);
plot(dif,twosigd)
axis([0.03 0.04 0 0.0003])
title('Oil film thickness: Second cycle');
xlabel('Distance from TC, downstroke (m)');
ylabel('LIF Signal, calibration: 3e-7');
gtext('file:forlm.dat')
print pic10.ps

axis([0.0323 0.0343 0 0.00005])
gtext('file:forlm.dat');
print pic11.ps

%plot fifth cycle of lif signal for comparison to average
fvesigd=clif(28801:32400);
plot(dif,fvesigd)
axis([0.03 0.04 0 0.0003])
title('Oil film thickness: Fifth cycle');
xlabel('Distance from TC, downstroke (m)');
ylabel('LIF Signal calibration: 3e-7');
gtext('file:forlm.dat')
print pic12.ps

axis([0.0323 0.0343 0 0.00005])
gtext('file:forlm.dat')
print pic13.ps

%plot tenth cycle of lif signal for comparison to average
tensigd=clif(64801:68400);
plot(dif,tensigd)
axis([0.03 0.04 0 0.0003])
title('Oil film thickness: Tenth cycle');
xlabel('Distance from TC, downstroke (m)');
ylabel('LIF Signal, calibration: 3e-7');
gtext('file:forlm.dat')
print pic14.ps

axis([0.0323 0.0343 0 0.00005])
gtext('file:forlm.dat')
print pic15.ps

%plot of all several friction and normal force traces
allCA=0.05:0.05:1440;
sevfrict=calfrict(1:28800);
sevnorm=calnorm(1:28800);
plot(allCA,sevfrict)
xlabel('Relative Crank Angle (degrees)');
ylabel('Friction Force (N)');
title('Liner Friction Force, shown over four cycles');
axis([0 1440 -4 4]);
gtext('file:forlm.dat')
print pic19.ps

plot(allCA,sevnorm)
xlabel('Relative Crank Angle (degrees)');
ylabel('Normal Force (N)');
title('Liner Normal Force, shown over four cycles');
axis([0 1440 0 45]);
gtext('file:forlm.dat')
print pic20.ps
```

Appendix B

Experimental Data

This appendix includes the data sheets for the test matrix given in Table 4.1. The following conditions are applicable to the entire data set.

Date: July 31, 1994

L.I.F. window: right side (viewed from the ring)

Ring groove: ring 1, location b

Oil thinning data observed on ring downstroke.

Oil feed system: controlled single pulse.

Test Number	1
Oil Number	1
Engine speed (rpm)	203
Liner Temp. (°C)	29

Friction Force downstroke average (N)	1.2913
Friction Force upstroke average (N)	-1.0052
Friction Force mid-downstroke average (N)	1.1654
Friction Force mid-upstroke average (N)	-1.0650
Normal Force average (N)	24.4089
Normal Force maximum (N)	35.1701
Normal Force minimum (N)	17.8378
Coefficient of friction downstroke average	0.0601
Coefficient of friction upstroke average	-0.0365
Coefficient of friction mid-downstroke average	0.0576
Coefficient of friction mid-upstroke average	-0.0385
Minimum oil film thickness, downstroke (m)	1.8E-06
Minimum oil film thickness, upstroke (m)	1.62E-06

Oil thinning data:	
Time (s)	Delta y
0	3.5
15	3.3
30	3.5
45	2.8
60	2.7
90	2.8
120	2.8
180	2.6
time of data collection:	2.5 min

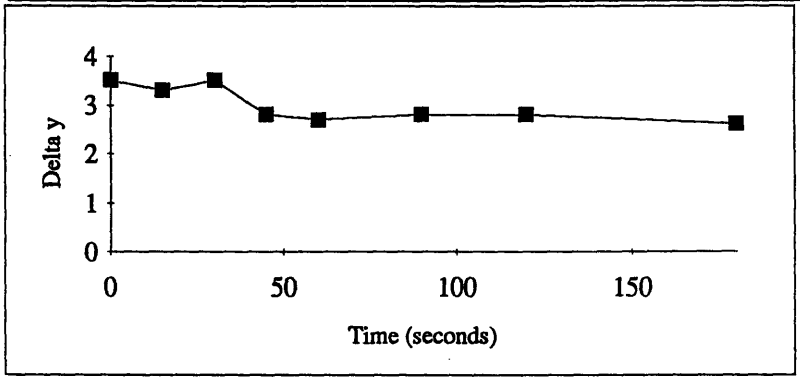

Test Number	2
Oil Number	1
Engine speed (rpm)	400
Liner Temp. (°C)	30

Friction Force downstroke average (N)	1.1931
Friction Force upstroke average (N)	-1.2346
Friction Force mid-downstroke average (N)	1.0619
Friction Force mid-upstroke average (N)	-1.3615
Normal Force average (N)	25.0122
Normal Force maximum (N)	33.9424
Normal Force minimum (N)	18.1267
Coefficient of friction downstroke average	0.0543
Coefficient of friction upstroke average	-0.0441
Coefficient of friction mid-downstroke average	0.0514
Coefficient of friction mid-upstroke average	-0.0466
Minimum oil film thickness, downstroke (m)	1.41E-06
Minimum oil film thickness, upstroke (m)	1.38E-06

Oil thinning data:	
Time (s)	Delta y
0	3.0
15	2.7
30	2.5
45	2.6
60	2.6
90	2.5
120	2.5
150	2.4
time of data collection:	2.5 min

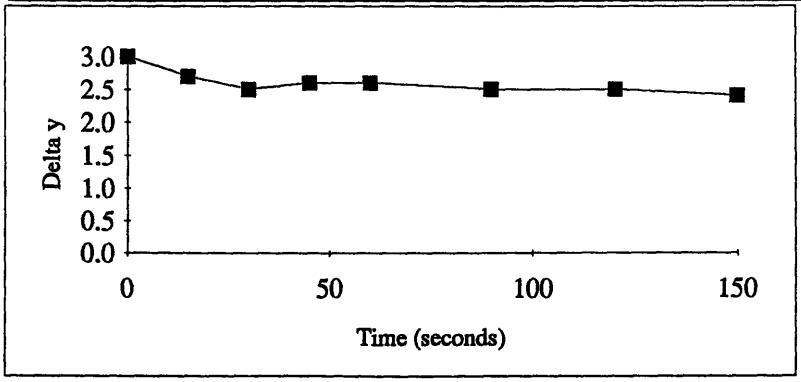

Test Number	3
Oil Number	1
Engine speed (rpm)	591
Liner Temp. (°C)	30

Friction Force downstroke average (N)	0.4388
Friction Force upstroke average (N)	-1.8648
Friction Force mid-downstroke average (N)	0.3020
Friction Force mid-upstroke average (N)	-2.0615
Normal Force average (N)	24.4913
Normal Force maximum (N)	38.3477
Normal Force minimum (N)	13.2159
Coefficient of friction downstroke average	0.0185
Coefficient of friction upstroke average	-0.0663
Coefficient of friction mid-downstroke average	0.0155
Coefficient of friction mid-upstroke average	-0.0688
Minimum oil film thickness, downstroke (m)	1.29E-06
Minimum oil film thickness, upstroke (m)	8.7E-07

Oil thinning data:	
Time (s)	Delta y
0	3.0
15	2.8
30	2.7
45	2.8
60	2.7
90	2.7
120	2.6
time of data collection:	2.5 min

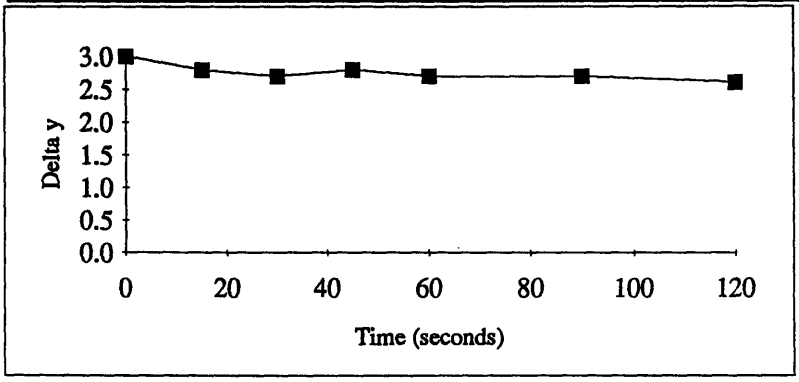

Test Number	4
Oil Number	1
Engine speed (rpm)	206
Liner Temp. (°C)	31

Friction Force downstroke average (N)	2.6227
Friction Force upstroke average (N)	-2.2471
Friction Force mid-downstroke average (N)	2.4948
Friction Force mid-upstroke average (N)	-2.3734
Normal Force average (N)	40.6607
Normal Force maximum (N)	54.3800
Normal Force minimum (N)	31.4870
Coefficient of friction downstroke average	0.0745
Coefficient of friction upstroke average	-0.0490
Coefficient of friction mid-downstroke average	0.0737
Coefficient of friction mid-upstroke average	-0.0512
Minimum oil film thickness, downstroke (m)	1.56E-06
Minimum oil film thickness, upstroke (m)	1.2E-06

Oil thinning data:	
Time (s)	Delta y
0	2.8
5	3.5
15	3.1
30	3.4
45	2.9
60	2.7
90	2.8
120	2.7
time of data collection:	2.5 min

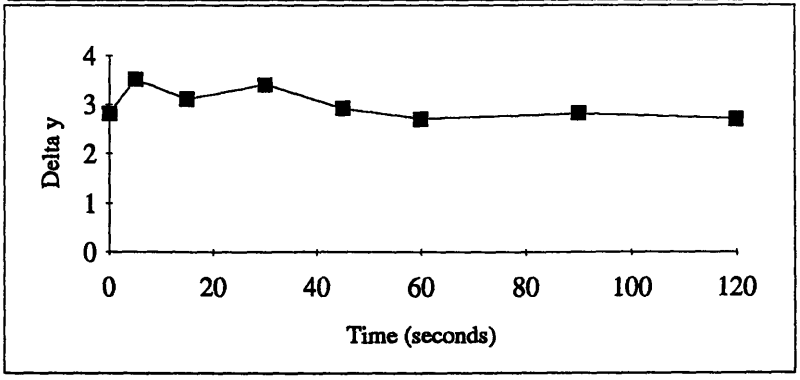

Test Number	5
Oil Number	1
Engine speed (rpm)	410
Liner Temp. (°C)	32

Friction Force downstroke average (N)	2.1861
Friction Force upstroke average (N)	-2.6923
Friction Force mid-downstroke average (N)	2.0698
Friction Force mid-upstroke average (N)	-2.9044
Normal Force average (N)	41.9221
Normal Force maximum (N)	51.5635
Normal Force minimum (N)	34.4479
Coefficient of friction downstroke average	0.0590
Coefficient of friction upstroke average	-0.0577
Coefficient of friction mid-downstroke average	0.0579
Coefficient of friction mid-upstroke average	-0.0602
Minimum oil film thickness, downstroke (m)	1.65E-06
Minimum oil film thickness, upstroke (m)	1.74E-06

Oil thinning data:	
Time (s)	Delta y
0	2.7
15	2.9
30	3.0
45	2.9
60	2.8
90	2.7
120	2.7
150	2.6
time of data collection:	2.5 min

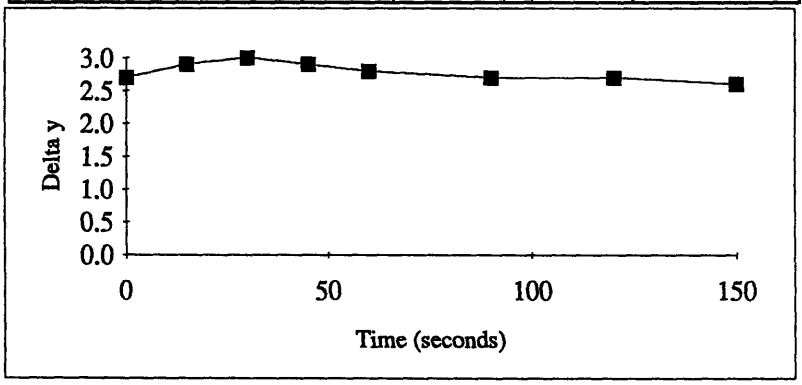

Test Number	6
Oil Number	1
Engine speed (rpm)	616
Liner Temp. (°C)	33

Friction Force downstroke average (N)	1.3190
Friction Force upstroke average (N)	-3.6601
Friction Force mid-downstroke average (N)	1.1627
Friction Force mid-upstroke average (N)	-3.8837
Normal Force average (N)	42.4663
Normal Force maximum (N)	56.4021
Normal Force minimum (N)	29.4649
Coefficient of friction downstroke average	0.0348
Coefficient of friction upstroke average	-0.0775
Coefficient of friction mid-downstroke average	0.0334
Coefficient of friction mid-upstroke average	-0.0777
Minimum oil film thickness, downstroke (m)	1.95E-06
Minimum oil film thickness, upstroke (m)	1.71E-06

Oil thinning data:	
Time (s)	Delta y
0	2.8
15	2.5
30	2.4
45	2.5
60	2.4
90	2.5
120	2.6
150	2.6
time of data collection:	2.5 min

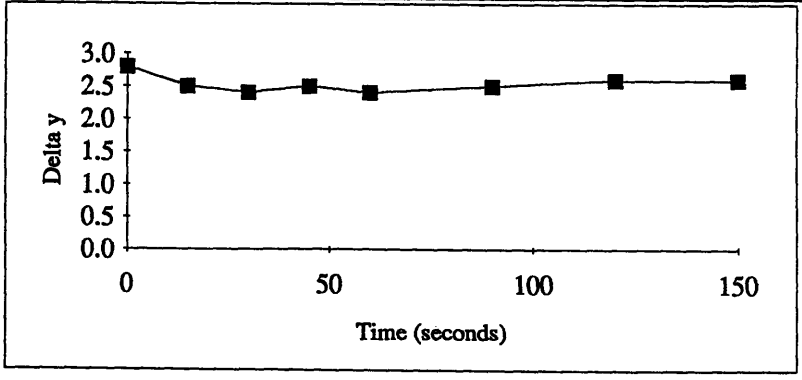

Test Number	7
Oil Number	1
Engine speed (rpm)	205
Liner Temp. (°C)	33

Friction Force downstroke average (N)	5.6049
Friction Force upstroke average (N)	-5.3636
Friction Force mid-downstroke average (N)	5.4999
Friction Force mid-upstroke average (N)	-5.8199
Normal Force average (N)	82.6949
Normal Force maximum (N)	105.7269
Normal Force minimum (N)	66.3682
Coefficient of friction downstroke average	0.0777
Coefficient of friction upstroke average	-0.0580
Coefficient of friction mid-downstroke average	0.0787
Coefficient of friction mid-upstroke average	-0.0621
Minimum oil film thickness, downstroke (m)	1.17E-06
Minimum oil film thickness, upstroke (m)	7.5E-07

Oil thinning data:	
Time (s)	Delta y
0	2.8
15	3.1
30	3.5
45	3.3
60	3.1
90	2.9
105	2.8
120	2.8
150	2.5
time of data collection:	2.5 min

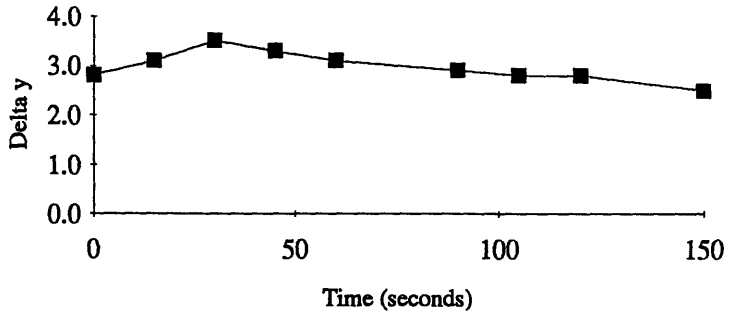

Test Number	8
Oil Number	1
Engine speed (rpm)	405
Liner Temp. (°C)	35

Friction Force downstroke average (N)	4.6248
Friction Force upstroke average (N)	-6.0506
Friction Force mid-downstroke average (N)	4.5278
Friction Force mid-upstroke average (N)	-6.5409
Normal Force average (N)	84.0241
Normal Force maximum (N)	99.9494
Normal Force minimum (N)	70.0513
Coefficient of friction downstroke average	0.0622
Coefficient of friction upstroke average	-0.0646
Coefficient of friction mid-downstroke average	0.0628
Coefficient of friction mid-upstroke average	-0.0684
Minimum oil film thickness, downstroke (m)	7.5E-07
Minimum oil film thickness, upstroke (m)	3.0E-07

Oil thinning data:	
Time (s)	Delta y
0	2.5
15	2.7
30	2.2
45	1.8
60	1.8
90	1.7
105	1.5
120	1.3
150	1.1
time of data collection:	2.5 min

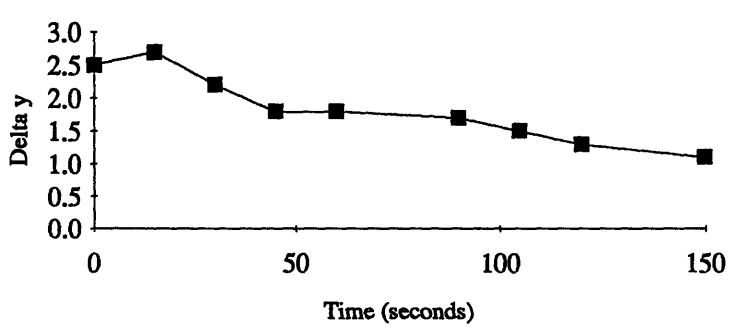

Test Number	9
Oil Number	1
Engine speed (rpm)	597
Liner Temp. (°C)	36

Friction Force downstroke average (N)	2.7277
Friction Force upstroke average (N)	-7.9645
Friction Force mid-downstroke average (N)	2.3834
Friction Force mid-upstroke average (N)	-8.4889
Normal Force average (N)	84.9477
Normal Force maximum (N)	107.5323
Normal Force minimum (N)	63.6239
Coefficient of friction downstroke average	0.0352
Coefficient of friction upstroke average	-0.0848
Coefficient of friction mid-downstroke average	0.0335
Coefficient of friction mid-upstroke average	-0.0874
Minimum oil film thickness, downstroke (m)	9.3E-07
Minimum oil film thickness, upstroke (m)	2.1E-07

Oil thinning data:	
Time (s)	Delta y
0	2.6
15	2.2
30	2.2
45	2.1
60	2.1
90	2.1
120	2.1
150	2.1
time of data collection:	2.5 min

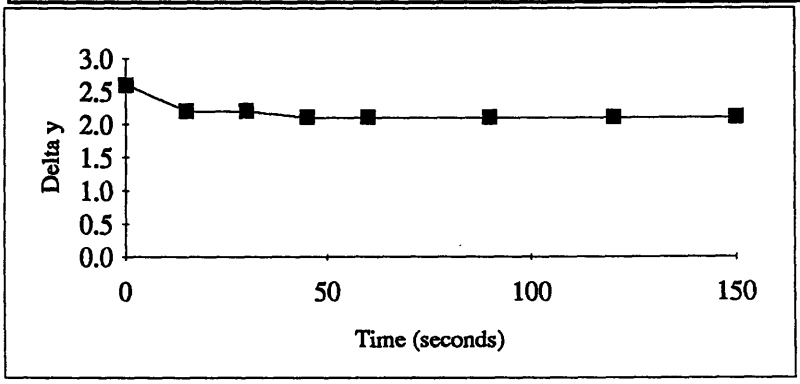

Test Number	10
Oil Number	2
Engine speed (rpm)	212
Liner Temp. (°C)	31

Friction Force downstroke average (N)	0.9186
Friction Force upstroke average (N)	-0.5321
Friction Force mid-downstroke average (N)	0.8533
Friction Force mid-upstroke average (N)	-0.6244
Normal Force average (N)	19.2929
Normal Force maximum (N)	28.0927
Normal Force minimum (N)	12.8548
Coefficient of friction downstroke average	0.0547
Coefficient of friction upstroke average	-0.0243
Coefficient of friction mid-downstroke average	0.0550
Coefficient of friction mid-upstroke average	-0.0281
Minimum oil film thickness, downstroke (m)	2.25E-06
Minimum oil film thickness, upstroke (m)	1.83E-06

Oil thinning data:	
Time (s)	Delta y
0	2.8
15	2.8
30	2.7
45	2.8
60	2.8
90	2.8
120	2.8
150	2.7
180	2.7
time of data collection:	3min 15sec

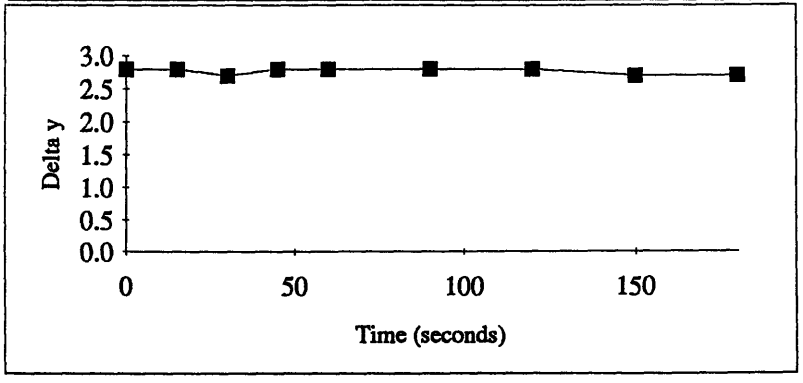

Test Number	11
Oil Number	2
Engine speed (rpm)	397
Liner Temp. (°C)	31

Friction Force downstroke average (N)	0.7774
Friction Force upstroke average (N)	-0.6122
Friction Force mid-downstroke average (N)	0.6924
Friction Force mid-upstroke average (N)	-0.6846
Normal Force average (N)	20.1808
Normal Force maximum (N)	28.1649
Normal Force minimum (N)	14.5158
Coefficient of friction downstroke average	0.0447
Coefficient of friction upstroke average	-0.0268
Coefficient of friction mid-downstroke average	0.0430
Coefficient of friction mid-upstroke average	-0.0287
Minimum oil film thickness, downstroke (m)	2.16E-06
Minimum oil film thickness, upstroke (m)	2.55E-06

Oil thinning data:	
Time (s)	Delta y
0	2.8
15	2.6
30	2.6
45	2.7
60	2.7
90	2.7
120	2.7
150	2.7
180	2.6
time of data collection:	3 min

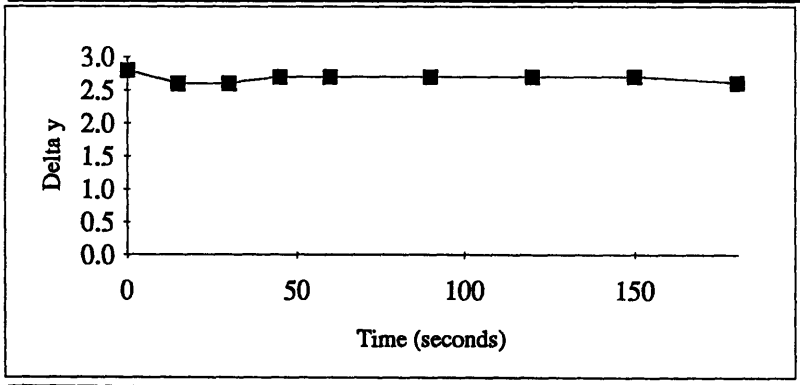

Test Number	12
Oil Number	2
Engine speed (rpm)	602
Liner Temp. (°C)	31

Friction Force downstroke average (N)	0.5107
Friction Force upstroke average (N)	-0.6968
Friction Force mid-downstroke average (N)	0.3999
Friction Force mid-upstroke average (N)	-0.7713
Normal Force average (N)	20.5027
Normal Force maximum (N)	32.2814
Normal Force minimum (N)	11.1938
Coefficient of friction downstroke average	0.0300
Coefficient of friction upstroke average	-0.0277
Coefficient of friction mid-downstroke average	0.0282
Coefficient of friction mid-upstroke average	-0.0289
Minimum oil film thickness, downstroke (m)	2.58E-06
Minimum oil film thickness, upstroke (m)	3.18E-06

Oil thinning data:	
Time (s)	Delta y
0	2.9
15	2.9
30	2.8
45	3.1
60	2.8
90	2.9
120	2.8
150	2.9
180	3.1
210	2.9
240	2.9
time of data collection:	4 min

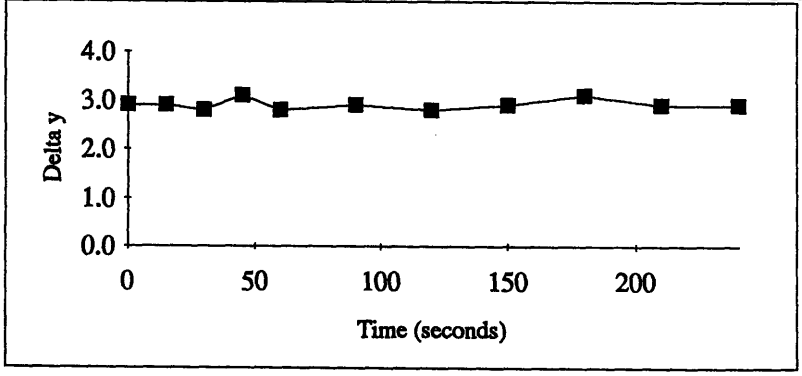

Test Number	13
Oil Number	2
Engine speed (rpm)	207
Liner Temp. (°C)	31

Friction Force downstroke average (N)	2.1266
Friction Force upstroke average (N)	-1.8109
Friction Force mid-downstroke average (N)	2.0183
Friction Force mid-upstroke average (N)	-1.9210
Normal Force average (N)	36.7078
Normal Force maximum (N)	48.8192
Normal Force minimum (N)	28.6705
Coefficient of friction downstroke average	0.0660
Coefficient of friction upstroke average	-0.0444
Coefficient of friction mid-downstroke average	0.0655
Coefficient of friction mid-upstroke average	-0.0464
Minimum oil film thickness, downstroke (m)	2.67E-06
Minimum oil film thickness, upstroke (m)	2.94E-06

Oil thinning data:	
Time (s)	Delta y
0	2.9
15	3.2
30	2.9
45	2.9
60	2.8
90	2.8
120	2.9
150	2.9
time of data collection:	2.5 min

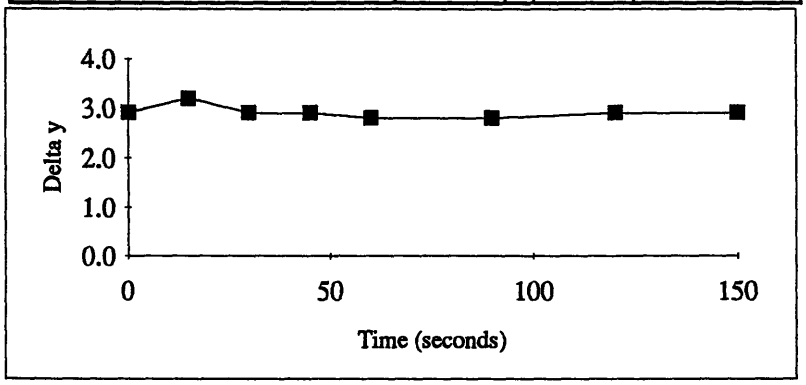

Test Number	14
Oil Number	2
Engine speed (rpm)	400
Liner Temp. (°C)	32

Friction Force downstroke average (N)	1.8700
Friction Force upstroke average (N)	-2.0013
Friction Force mid-downstroke average (N)	1.7616
Friction Force mid-upstroke average (N)	-2.1782
Normal Force average (N)	36.9855
Normal Force maximum (N)	47.2304
Normal Force minimum (N)	28.9593
Coefficient of friction downstroke average	0.0572
Coefficient of friction upstroke average	-0.0488
Coefficient of friction mid-downstroke average	0.0559
Coefficient of friction mid-upstroke average	-0.0511
Minimum oil film thickness, downstroke (m)	2.1E-06
Minimum oil film thickness, upstroke (m)	1.71E-06

Oil thinning data:	
Time (s)	Delta y
0	3.0
15	2.8
30	2.7
45	2.6
60	2.7
90	2.7
120	2.7
150	2.7
time of data collection:	2.5 min

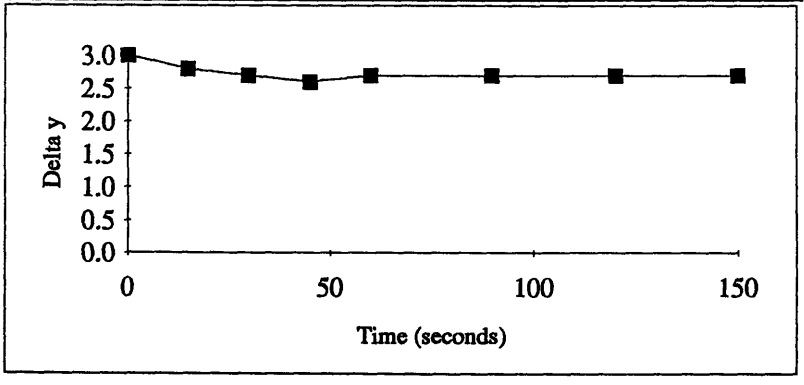

Test Number	15
Oil Number	2
Engine speed (rpm)	597
Liner Temp. (°C)	33

Friction Force downstroke average (N)	0.9966
Friction Force upstroke average (N)	-2.7503
Friction Force mid-downstroke average (N)	0.8055
Friction Force mid-upstroke average (N)	-2.8695
Normal Force average (N)	37.9706
Normal Force maximum (N)	51.3469
Normal Force minimum (N)	26.7206
Coefficient of friction downstroke average	0.0290
Coefficient of friction upstroke average	-0.0654
Coefficient of friction mid-downstroke average	0.0257
Coefficient of friction mid-upstroke average	-0.0642
Minimum oil film thickness, downstroke (m)	2.16E-06
Minimum oil film thickness, upstroke (m)	1.98E-06

Oil thinning data:	
Time (s)	Delta y
0	3.0
15	2.8
30	2.8
45	2.8
60	2.9
75	2.9
90	3.0
120	3.0
150	3.0
time of data collection:	2.5 min

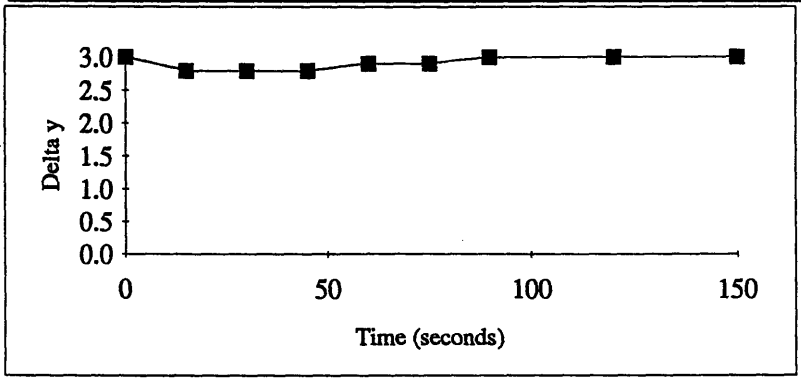

Test Number	16
Oil Number	2
Engine speed (rpm)	206
Liner Temp. (°C)	33

Friction Force downstroke average (N)	5.4710
Friction Force upstroke average (N)	-5.2857
Friction Force mid-downstroke average (N)	5.3954
Friction Force mid-upstroke average (N)	-5.7030
Normal Force average (N)	82.6821
Normal Force maximum (N)	105.2936
Normal Force minimum (N)	66.9459
Coefficient of friction downstroke average	0.0754
Coefficient of friction upstroke average	-0.0574
Coefficient of friction mid-downstroke average	0.0765
Coefficient of friction mid-upstroke average	-0.0612
Minimum oil film thickness, downstroke (m)	2.22E-06
Minimum oil film thickness, upstroke (m)	2.13E-06

Oil thinning data:	
Time (s)	Delta y
0	3.0
15	2.8
30	2.8
45	2.8
60	2.8
90	2.9
120	2.8
150	2.8
180	2.8
time of data collection:	3 min

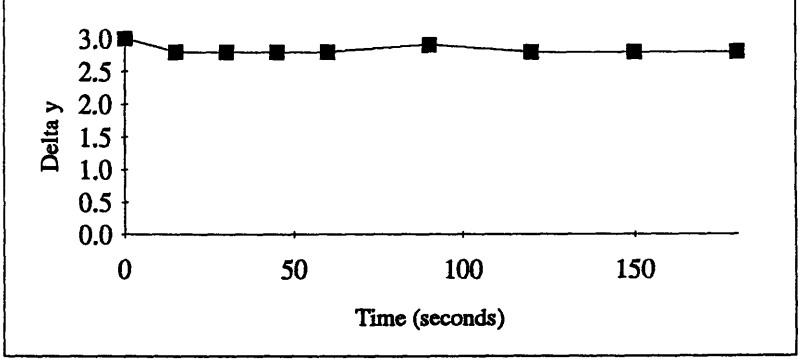

Test Number	17
Oil Number	2
Engine speed (rpm)	404
Liner Temp. (°C)	35

Friction Force downstroke average (N)	4.2091
Friction Force upstroke average (N)	-6.3098
Friction Force mid-downstroke average (N)	4.1308
Friction Force mid-upstroke average (N)	-6.7336
Normal Force average (N)	84.5015
Normal Force maximum (N)	100.1661
Normal Force minimum (N)	70.5568
Coefficient of friction downstroke average	0.0563
Coefficient of friction upstroke average	-0.0670
Coefficient of friction mid-downstroke average	0.0566
Coefficient of friction mid-upstroke average	-0.0701
Minimum oil film thickness, downstroke (m)	1.59E-06
Minimum oil film thickness, upstroke (m)	1.38E-06

Oil thinning data:	
Time (s)	Delta y
0	2.7
15	2.7
30	2.8
45	2.7
60	2.6
90	2.5
120	2.4
150	2.5
time of data collection:	2.5 min

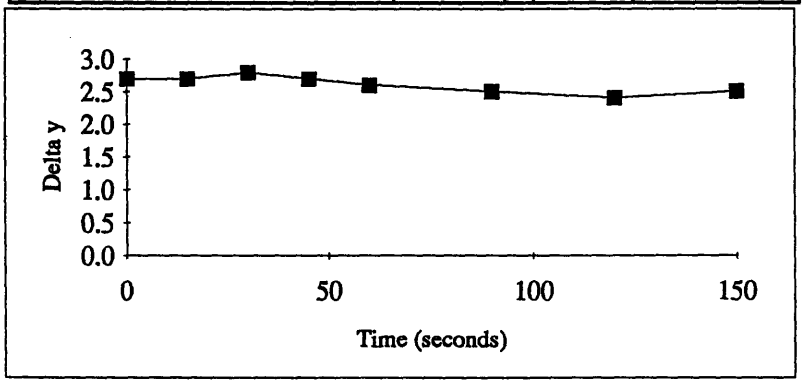

Test Number	18
Oil Number	2
Engine speed (rpm)	604
Liner Temp. (°C)	36

Friction Force downstroke average (N)	2.3298
Friction Force upstroke average (N)	-8.1244
Friction Force mid-downstroke average (N)	1.9968
Friction Force mid-upstroke average (N)	-8.6097
Normal Force average (N)	85.4089
Normal Force maximum (N)	101.7549
Normal Force minimum (N)	67.1626
Coefficient of friction downstroke average	0.0297
Coefficient of friction upstroke average	-0.0865
Coefficient of friction mid-downstroke average	0.0274
Coefficient of friction mid-upstroke average	-0.0883
Minimum oil film thickness, downstroke (m)	9.3E-07
Minimum oil film thickness, upstroke (m)	6.6E-07

Oil thinning data:	
Time (s)	Delta y
0	2.6
15	2.5
30	2.5
45	2.4
60	2.4
90	2.4
120	2.5
150	2.4
time of data collection:	2.5 min

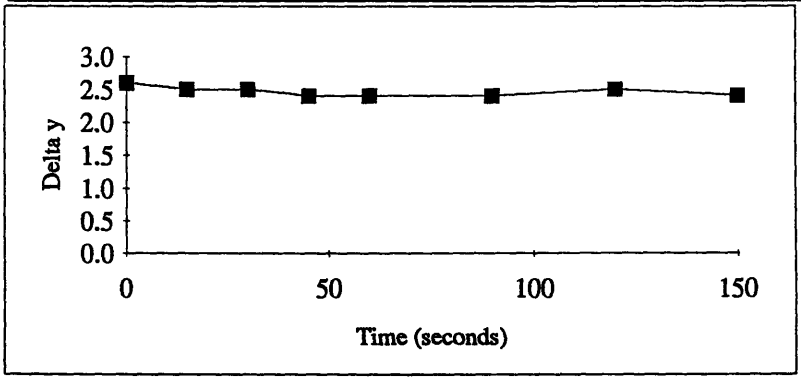

Test Number	19
Oil Number	3
Engine speed	209
Liner Temp.	32
Time (s)	Delta y
0	2.9
5	3.8
15	2.8
30	2.8
45	2.9
60	2.9
90	2.8
105	3.1
120	3.3
150	3.3
180	3.2
210	3.2
240	3.2
300	2.8
330	2.8
360	2.8
390	2.8
collct. time: 5.5 min	

Friction Force downstroke average (N)	0.7534
Friction Force upstroke average (N)	-0.3731
Friction Force mid-downstroke average (N)	0.6618
Friction Force mid-upstroke average (N)	-0.4476
Normal Force average (N)	17.1025
Normal Force maximum (N)	25.2040
Normal Force minimum (N)	11.1215
Coefficient of friction downstroke average	0.0517
Coefficient of friction upstroke average	-0.0169
Coefficient of friction mid-downstroke average	0.0496
Coefficient of friction mid-upstroke average	-0.0211
Minimum oil film thickness, downstroke (m)	1.74E-06
Minimum oil film thickness, upstroke (m)	1.65E-06

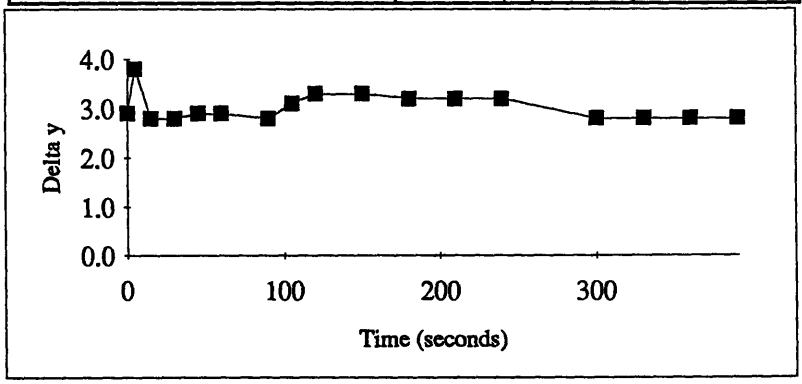

Test Number	20
Oil Number	3
Engine speed (rpm)	410
Liner Temp. (°C)	32

Friction Force downstroke average (N)	0.6541
Friction Force upstroke average (N)	-0.5817
Friction Force mid-downstroke average (N)	0.5937
Friction Force mid-upstroke average (N)	-0.7153
Normal Force average (N)	17.6708
Normal Force maximum (N)	25.7818
Normal Force minimum (N)	11.8437
Coefficient of friction downstroke average	0.0448
Coefficient of friction upstroke average	-0.0260
Coefficient of friction mid-downstroke average	0.0431
Coefficient of friction mid-upstroke average	-0.0315
Minimum oil film thickness, downstroke (m)	1.65E-06
Minimum oil film thickness, upstroke (m)	1.68E-06

Oil thinning data:	
Time (s)	Delta y
0	4.0
15	2.6
30	2.5
45	2.5
60	2.4
90	2.3
120	2.4
150	2.4
time of data collection:	2.5 min

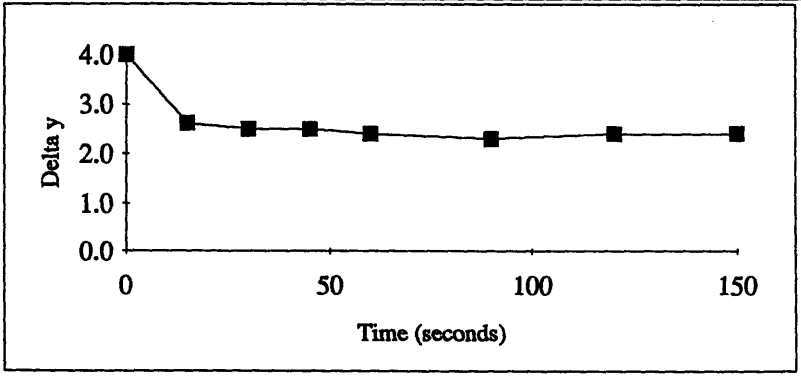

Test Number	21
Oil Number	3
Engine speed (rpm)	603
Liner Temp. (°C)	32

Friction Force downstroke average (N)	0.1044
Friction Force upstroke average (N)	-0.7916
Friction Force mid-downstroke average (N)	-0.0201
Friction Force mid-upstroke average (N)	-0.7855
Normal Force average (N)	16.7764
Normal Force maximum (N)	33.9424
Normal Force minimum (N)	8.1606
Coefficient of friction downstroke average	0.0012
Coefficient of friction upstroke average	-0.0351
Coefficient of friction mid-downstroke average	-0.0017
Coefficient of friction mid-upstroke average	-0.0372
Minimum oil film thickness, downstroke (m)	2.04E-06
Minimum oil film thickness, upstroke (m)	2.67E-06

Oil thinning data:	
Time (s)	Delta y
0	3.0
15	3.4
30	3.2
45	3.0
60	3.0
90	3.0
120	2.8
150	3.0
180	3.0
time of data collection:	3 min

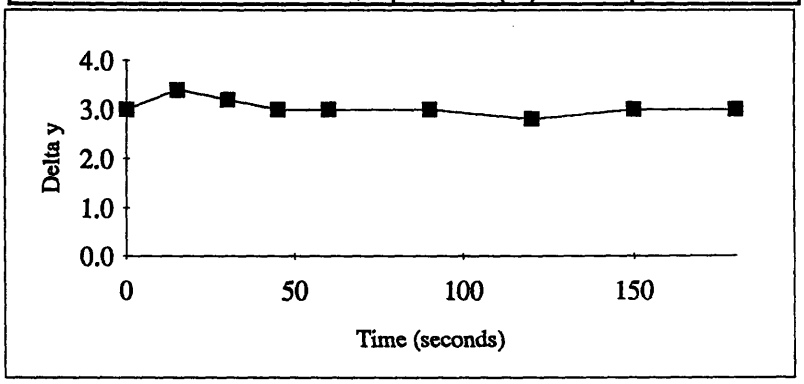

Test Number	22
Oil Number	3
Engine speed (rpm)	207
Liner Temp. (°C)	33

Friction Force downstroke average (N)	2.5043
Friction Force upstroke average (N)	-2.2349
Friction Force mid-downstroke average (N)	2.3502
Friction Force mid-upstroke average (N)	-2.3304
Normal Force average (N)	42.9746
Normal Force maximum (N)	54.3800
Normal Force minimum (N)	34.6645
Coefficient of friction downstroke average	0.0659
Coefficient of friction upstroke average	-0.0468
Coefficient of friction mid-downstroke average	0.0637
Coefficient of friction mid-upstroke average	-0.0482
Minimum oil film thickness, downstroke (m)	2.1E-06
Minimum oil film thickness, upstroke (m)	1.89E-06

Oil thinning data:	
Time (s)	Delta y
0	4.0
15	2.8
30	2.8
45	2.6
60	2.6
90	3.3
120	3.0
150	2.8
180	3.0
210	2.8
240	2.8
270	2.8
time of data collection:	4.5 min

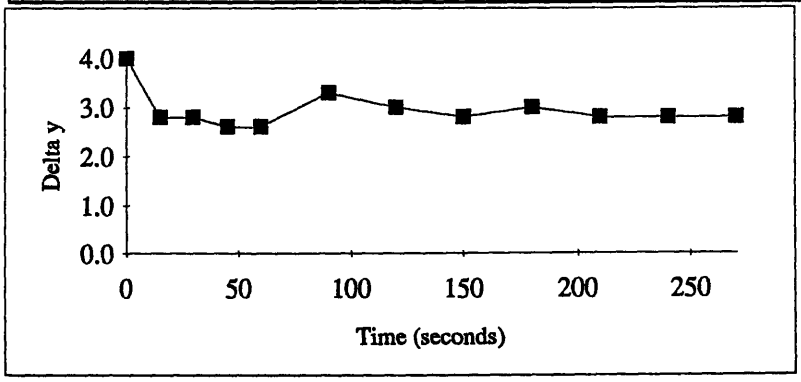

Test Number	23
Oil Number	3
Engine speed (rpm)	397
Liner Temp. (°C)	34

Friction Force downstroke average (N)	2.2749
Friction Force upstroke average (N)	-2.6735
Friction Force mid-downstroke average (N)	2.1572
Friction Force mid-upstroke average (N)	-2.8613
Normal Force average (N)	42.3037
Normal Force maximum (N)	51.2746
Normal Force minimum (N)	34.2312
Coefficient of friction downstroke average	0.0602
Coefficient of friction upstroke average	-0.0570
Coefficient of friction mid-downstroke average	0.0581
Coefficient of friction mid-upstroke average	-0.0593
Minimum oil film thickness, downstroke (m)	1.5E-06
Minimum oil film thickness, upstroke (m)	1.26E-06

Oil thinning data:	
Time (s)	Delta y
0	2.8
15	2.6
30	2.6
45	2.5
60	2.4
90	2.2
120	2.0
150	2.0
180	2.0
210	2.0
time of data collection:	3.5 min

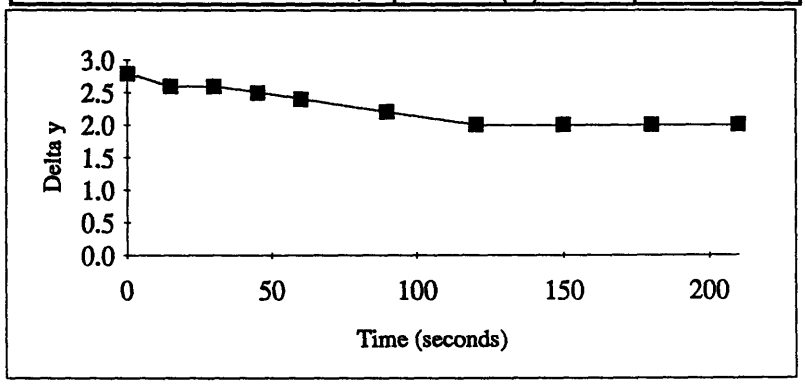

Test Number	24
Oil Number	3
Engine speed (rpm)	600
Liner Temp. (°C)	34

Friction Force downstroke average (N)	1.2995
Friction Force upstroke average (N)	-3.2743
Friction Force mid-downstroke average (N)	1.0397
Friction Force mid-upstroke average (N)	-3.3548
Normal Force average (N)	43.9173
Normal Force maximum (N)	56.5465
Normal Force minimum (N)	29.8982
Coefficient of friction downstroke average	0.0325
Coefficient of friction upstroke average	-0.0673
Coefficient of friction mid-downstroke average	0.0280
Coefficient of friction mid-upstroke average	-0.0656
Minimum oil film thickness, downstroke (m)	1.77E-06
Minimum oil film thickness, upstroke (m)	1.89E-06

Oil thinning data:	
Time (s)	Delta y
0	3.0
15	3.2
30	3.0
45	3.0
60	3.0
90	2.6
120	2.6
150	2.6
time of data collection:	2.5 min

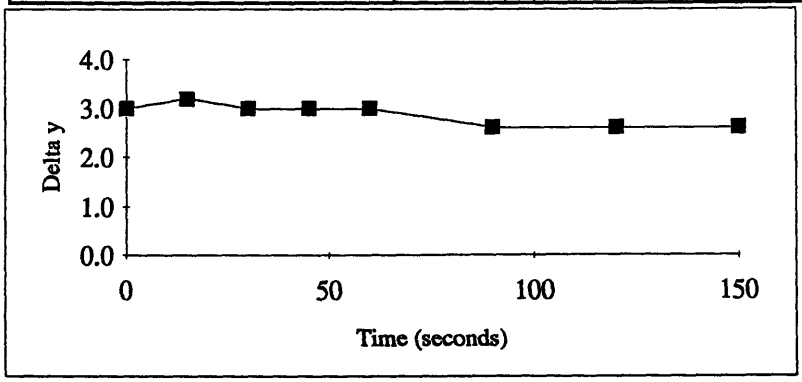

Test Number	25
Oil Number	3
Engine speed (rpm)	206
Liner Temp. (°C)	35

Friction Force downstroke average (N)	5.4084
Friction Force upstroke average (N)	-5.2038
Friction Force mid-downstroke average (N)	5.2984
Friction Force mid-upstroke average (N)	-5.5427
Normal Force average (N)	82.8678
Normal Force maximum (N)	106.0157
Normal Force minimum (N)	67.4514
Coefficient of friction downstroke average	0.0745
Coefficient of friction upstroke average	-0.0562
Coefficient of friction mid-downstroke average	0.0750
Coefficient of friction mid-upstroke average	-0.0594
Minimum oil film thickness, downstroke (m)	2.28E-06
Minimum oil film thickness, upstroke (m)	1.59E-06

Oil thinning data:	
Time (s)	Delta y
0	3.0
7	3.5
15	2.8
30	2.8
45	2.7
60	2.7
90	2.7
120	2.7
time of data collection:	2 min

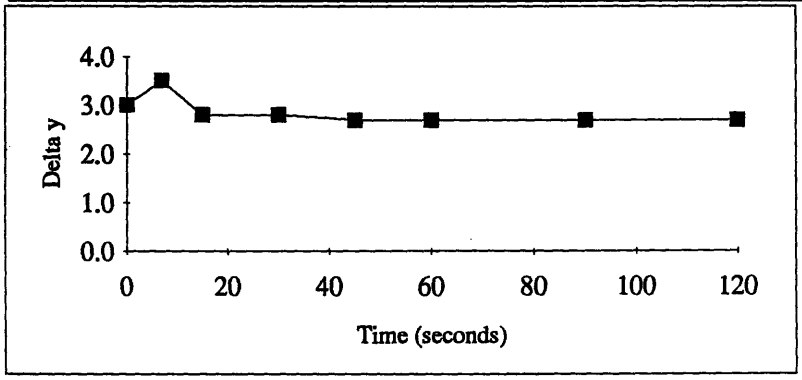

Test Number	26
Oil Number	3
Engine speed (rpm)	409
Liner Temp. (°C)	35

Friction Force downstroke average (N)	4.0868
Friction Force upstroke average (N)	-6.2233
Friction Force mid-downstroke average (N)	3.9701
Friction Force mid-upstroke average (N)	-6.6009
Normal Force average (N)	81.6980
Normal Force maximum (N)	95.9052
Normal Force minimum (N)	68.4625
Coefficient of friction downstroke average	0.0562
Coefficient of friction upstroke average	-0.0687
Coefficient of friction mid-downstroke average	0.0557
Coefficient of friction mid-upstroke average	-0.0715
Minimum oil film thickness, downstroke (m)	9.6E-07
Minimum oil film thickness, upstroke (m)	5.1E-07

Oil thinning data:	
Time (s)	Delta y
0	2.5
15	2.6
30	2.5
45	2.4
60	2.4
90	2.4
120	2.4
150	2.4
time of data collection:	2.5 min

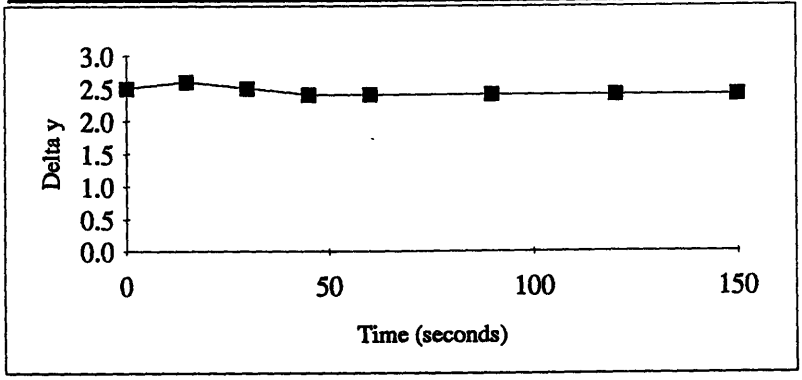

Test Number	27
Oil Number	3
Engine speed (rpm)	598
Liner Temp. (°C)	37

Friction Force downstroke average (N)	2.2015
Friction Force upstroke average (N)	-8.0388
Friction Force mid-downstroke average (N)	1.8421
Friction Force mid-upstroke average (N)	-8.4873
Normal Force average (N)	82.3616
Normal Force maximum (N)	98.5051
Normal Force minimum (N)	64.6349
Coefficient of friction downstroke average	0.0290
Coefficient of friction upstroke average	-0.0890
Coefficient of friction mid-downstroke average	0.0260
Coefficient of friction mid-upstroke average	-0.0906
Minimum oil film thickness, downstroke (m)	5.7E-07
Minimum oil film thickness, upstroke (m)	4.8E-07

Oil thinning data:	
Time (s)	Delta y
0	2.5
15	2.8
30	2.8
45	2.8
60	2.8
90	2.6
105	2.4
120	2.4
150	2.2
180	2.2
time of data collection:	3 min

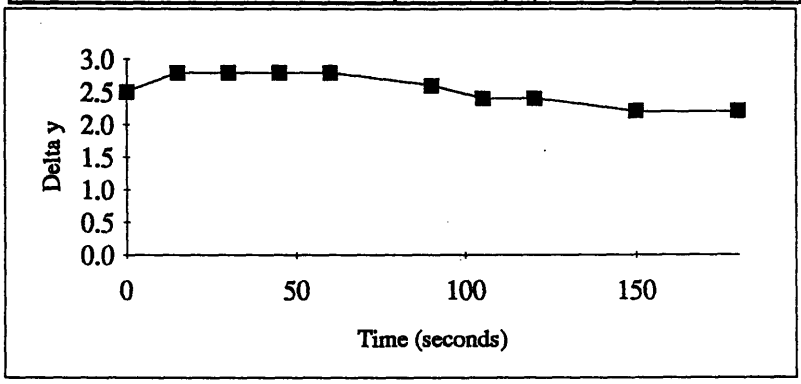

Test Number	28
Oil Number	4
Engine speed (rpm)	211
Liner Temp. (°C)	32

Friction Force downstroke average (N)	0.8818
Friction Force upstroke average (N)	-0.5596
Friction Force mid-downstroke average (N)	0.7478
Friction Force mid-upstroke average (N)	-0.5896
Normal Force average (N)	19.1013
Normal Force maximum (N)	29.0316
Normal Force minimum (N)	12.4215
Coefficient of friction downstroke average	0.0529
Coefficient of friction upstroke average	-0.0248
Coefficient of friction mid-downstroke average	0.0483
Coefficient of friction mid-upstroke average	-0.0260
Minimum oil film thickness, downstroke (m)	1.4E-06
Minimum oil film thickness, upstroke (m)	1.05E-06

Oil thinning data:	
Time (s)	Delta y
0	3
10	3.5
15	2.8
30	2.4
45	2.4
60	2.4
90	2.4
120	2.4
time of data collection:	120 sec.

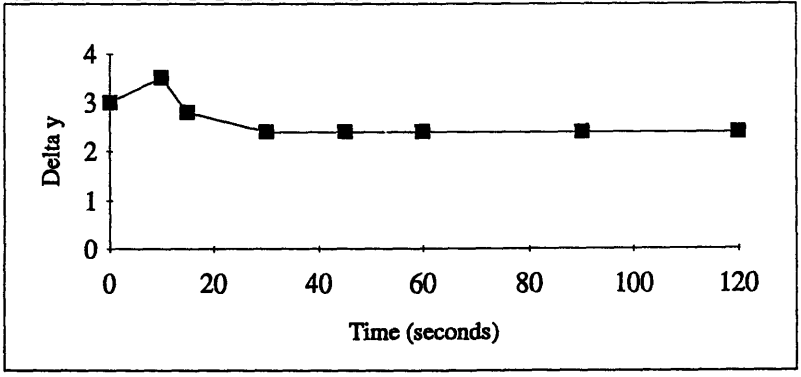

Test Number	29
Oil Number	4
Engine speed (rpm)	408
Liner Temp. (°C)	32

Friction Force downstroke average (N)	0.7432
Friction Force upstroke average (N)	-0.8041
Friction Force mid-downstroke average (N)	0.6151
Friction Force mid-upstroke average (N)	-0.9452
Normal Force average (N)	19.5417
Normal Force maximum (N)	27.2983
Normal Force minimum (N)	13.4325
Coefficient of friction downstroke average	0.0447
Coefficient of friction upstroke average	-0.0347
Coefficient of friction mid-downstroke average	0.0396
Coefficient of friction mid-upstroke average	-0.0392
Minimum oil film thickness, downstroke (m)	1.41E-06
Minimum oil film thickness, upstroke (m)	1.41E-06

Oil thinning data:	
Time (s)	Delta y
0	2.5
15	2.4
30	2.3
45	2.3
60	2.3
90	2.3
120	2.2
time of data collection:	120 sec.

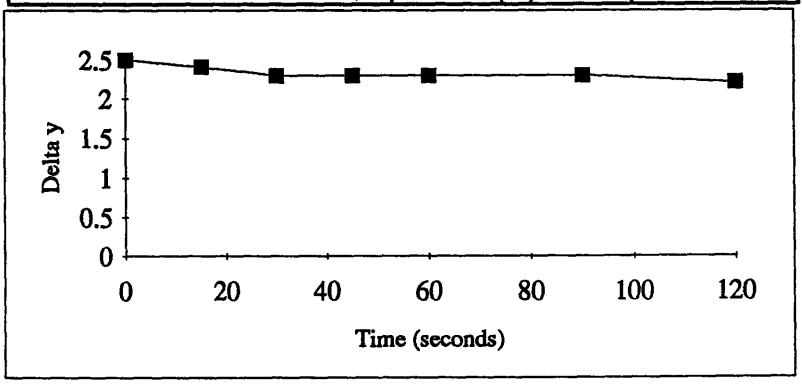

Test Number	30
Oil Number	4
Engine speed (rpm)	620
Liner Temp. (°C)	32

Friction Force downstroke average (N)	0.1805
Friction Force upstroke average (N)	-0.9694
Friction Force mid-downstroke average (N)	0.0460
Friction Force mid-upstroke average (N)	-1.1471
Normal Force average (N)	19.5914
Normal Force maximum (N)	36.6144
Normal Force minimum (N)	7.2940
Coefficient of friction downstroke average	0.0074
Coefficient of friction upstroke average	-0.0368
Coefficient of friction mid-downstroke average	0.0032
Coefficient of friction mid-upstroke average	-0.0450
Minimum oil film thickness, downstroke (m)	1.11E-06
Minimum oil film thickness, upstroke (m)	1.47E-06

Oil thinning data:	
Time (s)	Delta y
0	3.0
15	3.0
30	3.0
45	3.0
60	3.0
90	2.8
120	2.8
time of data collection:	2 min

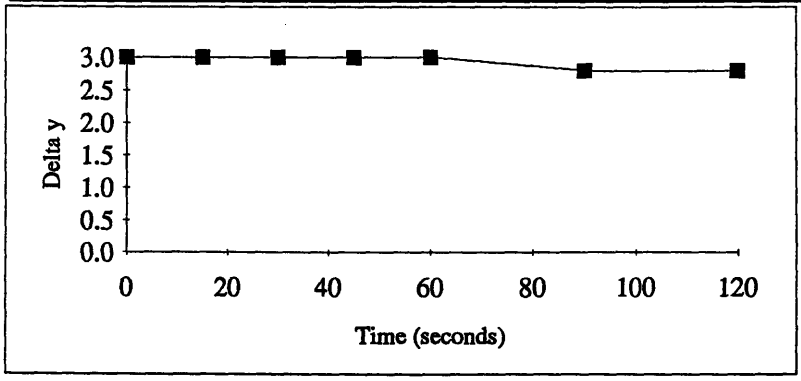

Test Number	31
Oil Number	4
Engine speed (rpm)	208
Liner Temp.	32
Oil thinning data:	
Time (s)	Delta y
0	2.6
10	3.5
15	2.8
30	2.6
45	2.6
60	2.6
90	2.6
120	3.2
150	3.2
180	2.6
210	3.2
240	3.4
270	2.6
300	2.6
time of data collection:	5 min

Friction Force downstroke average (N)	2.4473
Friction Force upstroke average (N)	-2.1152
Friction Force mid-downstroke average (N)	2.3132
Friction Force mid-upstroke average (N)	-2.1993
Normal Force average (N)	40.8944
Normal Force maximum (N)	53.8745
Normal Force minimum (N)	32.2814
Coefficient of friction downstroke average	0.0680
Coefficient of friction upstroke average	-0.0466
Coefficient of friction mid-downstroke average	0.0666
Coefficient of friction mid-upstroke average	-0.0480
Minimum oil film thickness, downstroke (m)	2.4E-06
Minimum oil film thickness, upstroke (m)	2.7E-06

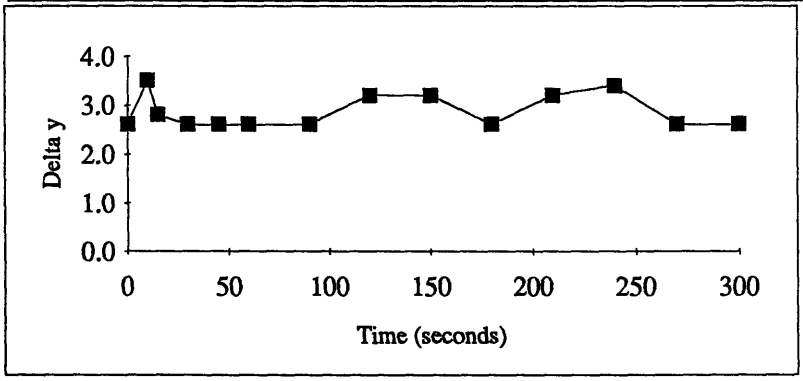

Test Number	32
Oil Number	4
Engine speed (rpm)	396
Liner Temp. (°C)	33
Oil thinning data:	
Time (s)	Delta y
0	2.4
15	2.4
30	2.4
45	2.4
60	2.4
90	2.4
120	2.4
time of data collection:	2 min

Friction Force downstroke average (N)	2.1412
Friction Force upstroke average (N)	-2.4844
Friction Force mid-downstroke average (N)	2.0111
Friction Force mid-upstroke average (N)	-2.6607
Normal Force average (N)	42.3631
Normal Force maximum (N)	51.7802
Normal Force minimum (N)	34.8090
Coefficient of friction downstroke average	0.0569
Coefficient of friction upstroke average	-0.0528
Coefficient of friction mid-downstroke average	0.0550
Coefficient of friction mid-upstroke average	-0.0547
Minimum oil film thickness, downstroke (m)	2.31E-06
Minimum oil film thickness, upstroke (m)	1.86E-06

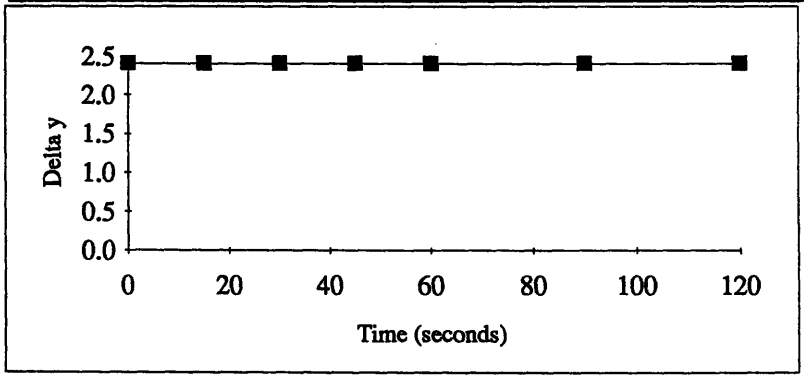

Test Number	33
Oil Number	4
Engine speed (rpm)	590
Liner Temp. (°C)	34

Friction Force downstroke average (N)	1.2336
Friction Force upstroke average (N)	-3.1121
Friction Force mid-downstroke average (N)	0.9659
Friction Force mid-upstroke average (N)	-3.1754
Normal Force average (N)	42.4090
Normal Force maximum (N)	54.4522
Normal Force minimum (N)	29.2482
Coefficient of friction downstroke average	0.0322
Coefficient of friction upstroke average	-0.0660
Coefficient of friction mid-downstroke average	0.0271
Coefficient of friction mid-upstroke average	-0.0640
Minimum oil film thickness, downstroke (m)	2.28E-06
Minimum oil film thickness, upstroke (m)	1.92E-06

Oil thinning data:	
Time (s)	Delta y
0	3.5
15	3.0
30	2.8
45	2.8
60	2.8
90	2.8
120	2.8
time of data collection:	2 min

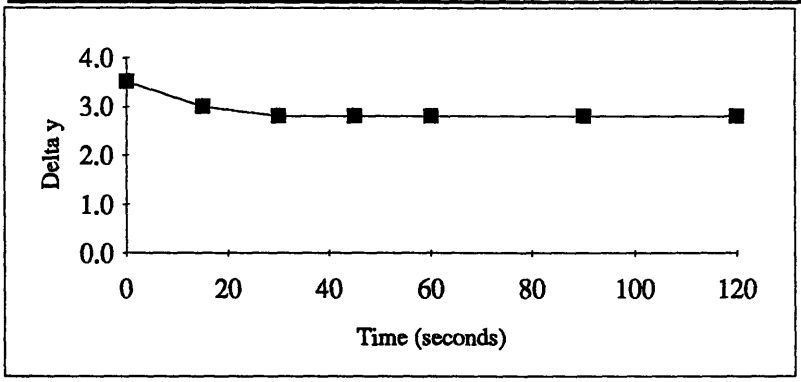

Test Number	34
Oil Number	4
Engine speed (rpm)	206
Liner Temp. (°C)	35

Friction Force downstroke average (N)	5.0969
Friction Force upstroke average (N)	-4.9508
Friction Force mid-downstroke average (N)	4.9737
Friction Force mid-upstroke average (N)	-5.2282
Normal Force average (N)	79.8714
Normal Force maximum (N)	103.4159
Normal Force minimum (N)	64.1294
Coefficient of friction downstroke average	0.0720
Coefficient of friction upstroke average	-0.0560
Coefficient of friction mid-downstroke average	0.0721
Coefficient of friction mid-upstroke average	-0.0587
Minimum oil film thickness, downstroke (m)	1.92E-06
Minimum oil film thickness, upstroke (m)	2.19E-06

Oil thinning data:	
Time (s)	Delta y
0	2.8
10	3.4
15	2.8
30	2.6
45	2.6
60	2.6
90	2.6
120	3.2
150	2.6
180	3.0
210	3.0
240	2.6
time of data collection:	4 min

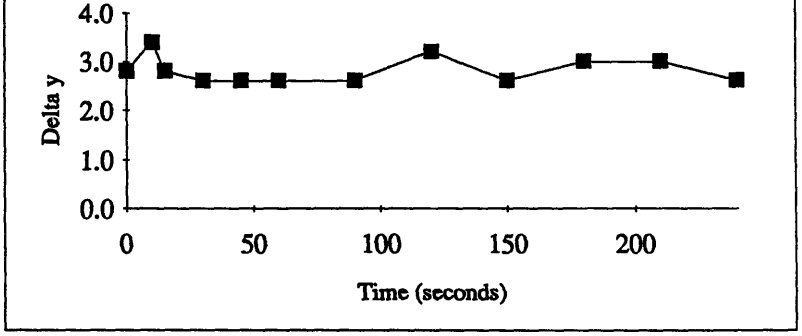

Test Number	35
Oil Number	4
Engine speed (rpm)	408
Liner Temp. (°C)	35

Friction Force downstroke average (N)	4.0252
Friction Force upstroke average (N)	-5.7128
Friction Force mid-downstroke average (N)	3.8527
Friction Force mid-upstroke average (N)	-6.0390
Normal Force average (N)	79.3556
Normal Force maximum (N)	92.2221
Normal Force minimum (N)	67.1626
Coefficient of friction downstroke average	0.0564
Coefficient of friction upstroke average	-0.0655
Coefficient of friction mid-downstroke average	0.0548
Coefficient of friction mid-upstroke average	-0.0681
Minimum oil film thickness, downstroke (m)	9.3E-07
Minimum oil film thickness, upstroke (m)	1.05E-06

Oil thinning data:	
Time (s)	Delta y
0	2.4
15	2.4
30	2.4
45	2.4
60	2.4
90	2.4
120	2.4
time of data collection:	2 min

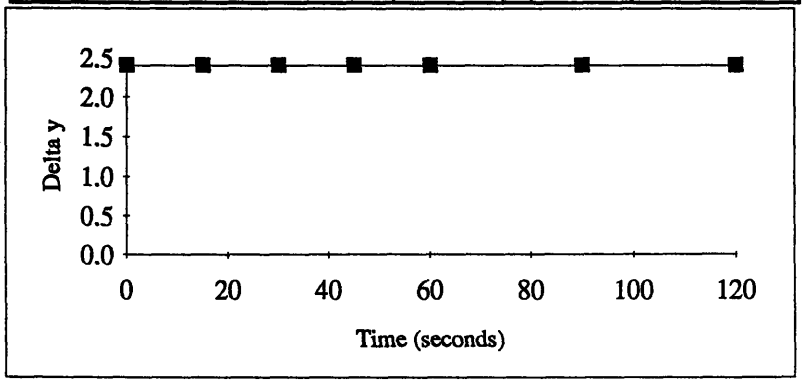

Test Number	36
Oil Number	4
Engine speed (rpm)	597
Liner Temp. (°C)	37

Friction Force downstroke average (N)	2.5435
Friction Force upstroke average (N)	-7.4038
Friction Force mid-downstroke average (N)	2.1933
Friction Force mid-upstroke average (N)	-7.8464
Normal Force average (N)	80.1963
Normal Force maximum (N)	95.4719
Normal Force minimum (N)	62.3240
Coefficient of friction downstroke average	0.0345
Coefficient of friction upstroke average	-0.0842
Coefficient of friction mid-downstroke average	0.0316
Coefficient of friction mid-upstroke average	-0.0861
Minimum oil film thickness, downstroke (m)	5.4E-07
Minimum oil film thickness, upstroke (m)	5.7E-07

Oil thinning data:	
Time (s)	Delta y
0	2.4
15	2.6
30	2.5
45	2.4
60	2.4
90	2.4
120	2.4
time of data collection:	2 min

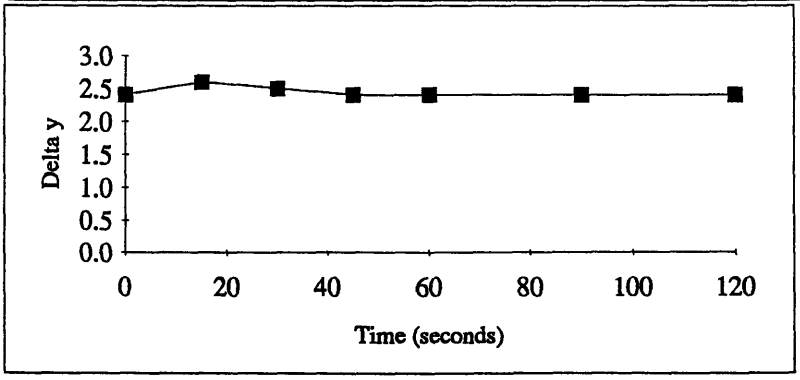

Test Number	37
Oil Number	5
Engine speed (rpm)	211
Liner Temp. (°C)	32

Friction Force downstroke average (N)	0.9632
Friction Force upstroke average (N)	-0.4487
Friction Force mid-downstroke average (N)	0.8941
Friction Force mid-upstroke average (N)	-0.5047
Normal Force average (N)	19.9628
Normal Force maximum (N)	28.1649
Normal Force minimum (N)	13.5769
Coefficient of friction downstroke average	0.0566
Coefficient of friction upstroke average	-0.0196
Coefficient of friction mid-downstroke average	0.0563
Coefficient of friction mid-upstroke average	-0.0215
Minimum oil film thickness, downstroke (m)	2.52E-06
Minimum oil film thickness, upstroke (m)	3.00E-06

Oil thinning data:	
Time (s)	Delta y
0	2.8
5	3.9
15	2.9
30	2.9
45	2.9
60	2.6
90	2.5
120	2.5
150	2.5
time of data collection:	2.5 min

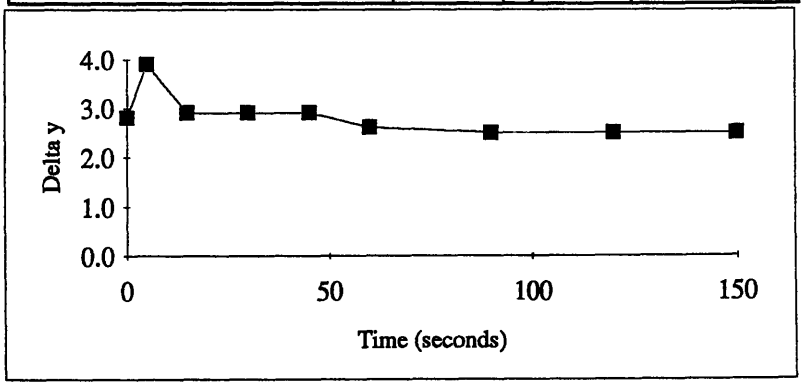

Test Number	38
Oil Number	5
Engine speed (rpm)	405
Liner Temp. (°C)	32

Friction Force downstroke average (N)	0.8088
Friction Force upstroke average (N)	-0.7225
Friction Force mid-downstroke average (N)	0.7619
Friction Force mid-upstroke average (N)	-0.8085
Normal Force average (N)	20.8418
Normal Force maximum (N)	29.3926
Normal Force minimum (N)	14.3713
Coefficient of friction downstroke average	0.0465
Coefficient of friction upstroke average	-0.0299
Coefficient of friction mid-downstroke average	0.0467
Coefficient of friction mid-upstroke average	-0.0315
Minimum oil film thickness, downstroke (m)	3.87E-06
Minimum oil film thickness, upstroke (m)	3.69E-06

Oil thinning data:	
Time (s)	Delta y
0	2.5
15	2.6
30	2.5
45	2.6
60	2.7
90	2.6
120	2.3
150	2.2
180	2.2
time of data collection:	3 min

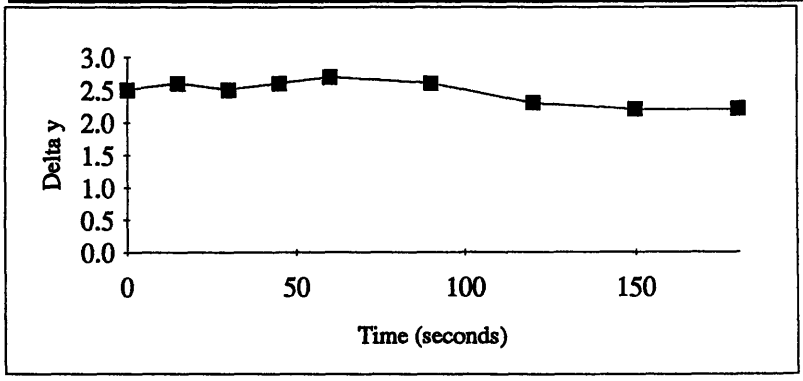

Test Number	39
Oil Number	5
Engine speed (rpm)	592
Liner Temp. (°C)	33

Friction Force downstroke average (N)	0.4615
Friction Force upstroke average (N)	-1.0115
Friction Force mid-downstroke average (N)	0.3921
Friction Force mid-upstroke average (N)	-1.1982
Normal Force average (N)	21.3209
Normal Force maximum (N)	34.6645
Normal Force minimum (N)	10.2549
Coefficient of friction downstroke average	0.0251
Coefficient of friction upstroke average	-0.0398
Coefficient of friction mid-downstroke average	0.0250
Coefficient of friction mid-upstroke average	-0.0440
Minimum oil film thickness, downstroke (m)	3.39E-06
Minimum oil film thickness, upstroke (m)	3.87E-06

Oil thinning data:	
Time (s)	Delta y
0	2.7
15	2.8
30	2.9
45	2.9
60	2.9
90	2.9
120	2.8
time of data collection:	2 min

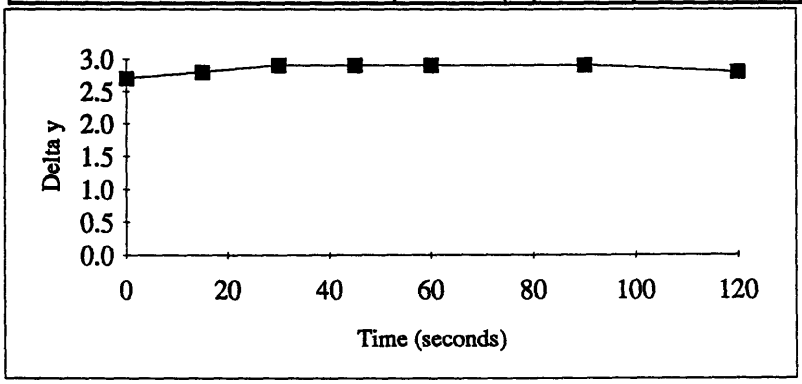

Test Number	40
Oil Number	5
Engine speed (rpm)	208
Liner Temp. (°C)	33

Friction Force downstroke average (N)	2.5487
Friction Force upstroke average (N)	-2.0495
Friction Force mid-downstroke average (N)	2.4647
Friction Force mid-upstroke average (N)	-2.1886
Normal Force average (N)	43.3001
Normal Force maximum (N)	54.8133
Normal Force minimum (N)	34.9534
Coefficient of friction downstroke average	0.0665
Coefficient of friction upstroke average	-0.0428
Coefficient of friction mid-downstroke average	0.0664
Coefficient of friction mid-upstroke average	-0.0451
Minimum oil film thickness, downstroke (m)	2.88E-06
Minimum oil film thickness, upstroke (m)	3.45E-06

Oil thinning data:	
Time (s)	Delta y
0	2.7
15	2.9
30	2.6
45	2.5
60	2.3
90	2.7
120	2.7
150	2.6
180	2.5
210	2.6
time of data collection:	3.5 min

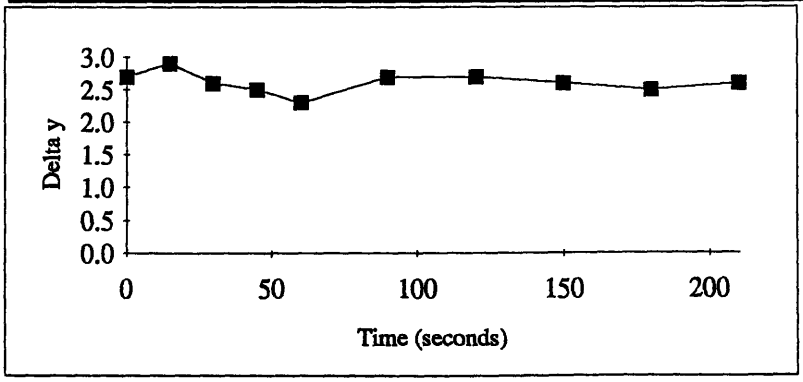

Test Number	41
Oil Number	5
Engine speed (rpm)	394
Liner Temp. (°C)	33

Friction Force downstroke average (N)	2.1228
Friction Force upstroke average (N)	-2.4664
Friction Force mid-downstroke average (N)	2.0481
Friction Force mid-upstroke average (N)	-2.6679
Normal Force average (N)	42.4845
Normal Force maximum (N)	52.7190
Normal Force minimum (N)	34.8090
Coefficient of friction downstroke average	0.0561
Coefficient of friction upstroke average	-0.0525
Coefficient of friction mid-downstroke average	0.0560
Coefficient of friction mid-upstroke average	-0.0549
Minimum oil film thickness, downstroke (m)	3.03E-06
Minimum oil film thickness, upstroke (m)	2.73E-06

Oil thinning data:	
Time (s)	Delta y
0	2.7
7	3.0
15	2.4
30	2.6
45	2.6
60	2.5
90	2.6
120	2.5
time of data collection:	2 min

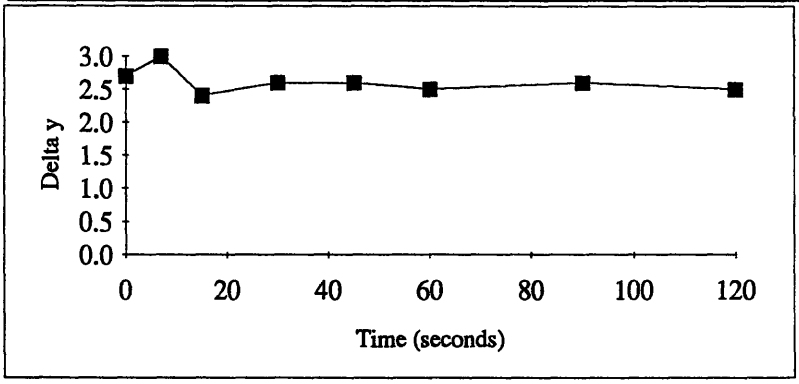

Test Number	42
Oil Number	5
Engine speed (rpm)	597
Liner Temp. (°C)	34

Friction Force downstroke average (N)	1.1635
Friction Force upstroke average (N)	-3.1172
Friction Force mid-downstroke average (N)	0.9984
Friction Force mid-upstroke average (N)	-3.2848
Normal Force average (N)	43.6803
Normal Force maximum (N)	55.6077
Normal Force minimum (N)	33.2202
Coefficient of friction downstroke average	0.0296
Coefficient of friction upstroke average	-0.0649
Coefficient of friction mid-downstroke average	0.0272
Coefficient of friction mid-upstroke average	-0.0650
Minimum oil film thickness, downstroke (m)	3.12E-06
Minimum oil film thickness, upstroke (m)	2.73E-06

Oil thinning data:	
Time (s)	Delta y
0	2.6
15	2.9
30	2.9
45	2.9
60	2.9
90	2.8
120	2.8
time of data collection:	2 min

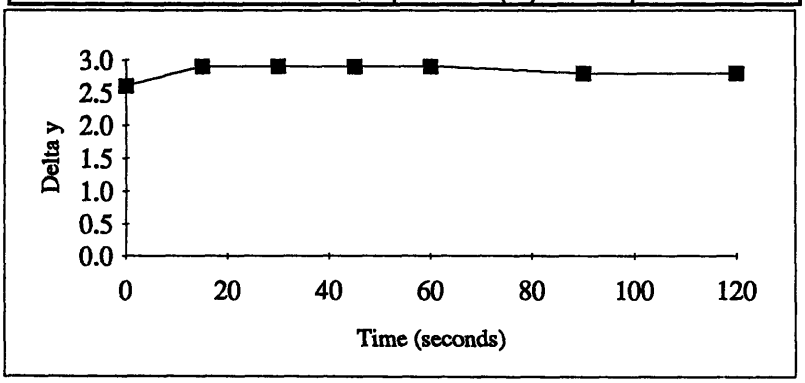

Test Number	43
Oil Number	5
Engine speed (rpm)	206
Liner Temp. (°C)	35

Friction Force downstroke average (N)	5.2995
Friction Force upstroke average (N)	-5.1500
Friction Force mid-downstroke average (N)	5.2390
Friction Force mid-upstroke average (N)	-5.5586
Normal Force average (N)	82.1559
Normal Force maximum (N)	103.4881
Normal Force minimum (N)	66.9459
Coefficient of friction downstroke average	0.0728
Coefficient of friction upstroke average	-0.0567
Coefficient of friction mid-downstroke average	0.0740
Coefficient of friction mid-upstroke average	-0.0605
Minimum oil film thickness, downstroke (m)	3.12E-06
Minimum oil film thickness, upstroke (m)	2.7E-06

Oil thinning data:	
Time (s)	Delta y
0	2.5
15	2.4
30	2.5
45	2.9
60	2.8
90	2.5
120	2.4
150	2.4
time of data collection:	2.5 min

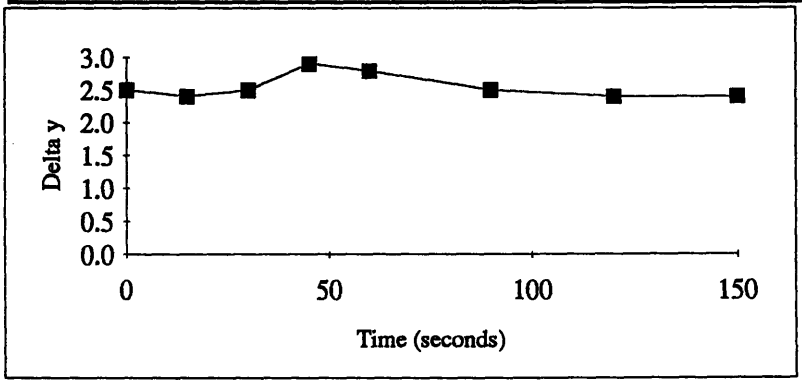

Test Number	44
Oil Number	5
Engine speed (rpm)	402
Liner Temp. (°C)	36

Friction Force downstroke average (N)	3.9903
Friction Force upstroke average (N)	-6.1175
Friction Force mid-downstroke average (N)	3.9432
Friction Force mid-upstroke average (N)	-6.4825
Normal Force average (N)	83.2251
Normal Force maximum (N)	97.6385
Normal Force minimum (N)	69.6180
Coefficient of friction downstroke average	0.0534
Coefficient of friction upstroke average	-0.0669
Coefficient of friction mid-downstroke average	0.0538
Coefficient of friction mid-upstroke average	-0.0696
Minimum oil film thickness, downstroke (m)	2.28E-06
Minimum oil film thickness, upstroke (m)	2.31E-06

Oil thinning data:	
Time (s)	Delta y
0	2.5
15	2.6
30	2.4
45	2.3
60	2.3
90	2.2
120	2.0
time of data collection:	2 min

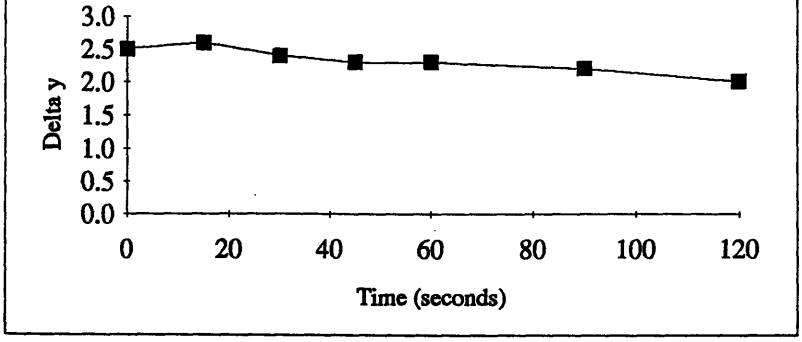

Test Number	45
Oil Number	5
Engine speed (rpm)	599
Liner Temp. (°C)	38

Friction Force downstroke average (N)	1.8232
Friction Force upstroke average (N)	-7.6366
Friction Force mid-downstroke average (N)	1.4972
Friction Force mid-upstroke average (N)	-8.0556
Normal Force average (N)	81.3911
Normal Force maximum (N)	96.1219
Normal Force minimum (N)	66.5126
Coefficient of friction downstroke average	0.0241
Coefficient of friction upstroke average	-0.0860
Coefficient of friction mid-downstroke average	0.0210
Coefficient of friction mid-upstroke average	-0.0878
Minimum oil film thickness, downstroke (m)	2.49E-06
Minimum oil film thickness, upstroke (m)	2.34E-06

Oil thinning data:	
Time (s)	Delta y
0	2.5
15	2.7
30	2.6
45	2.6
60	2.7
90	2.6
120	2.6
150	2.5
time of data collection:	2.5 min

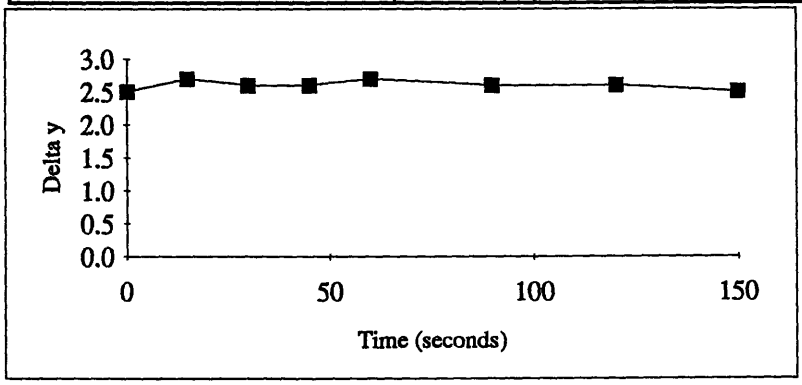

Appendix C

Friction Coefficient Results

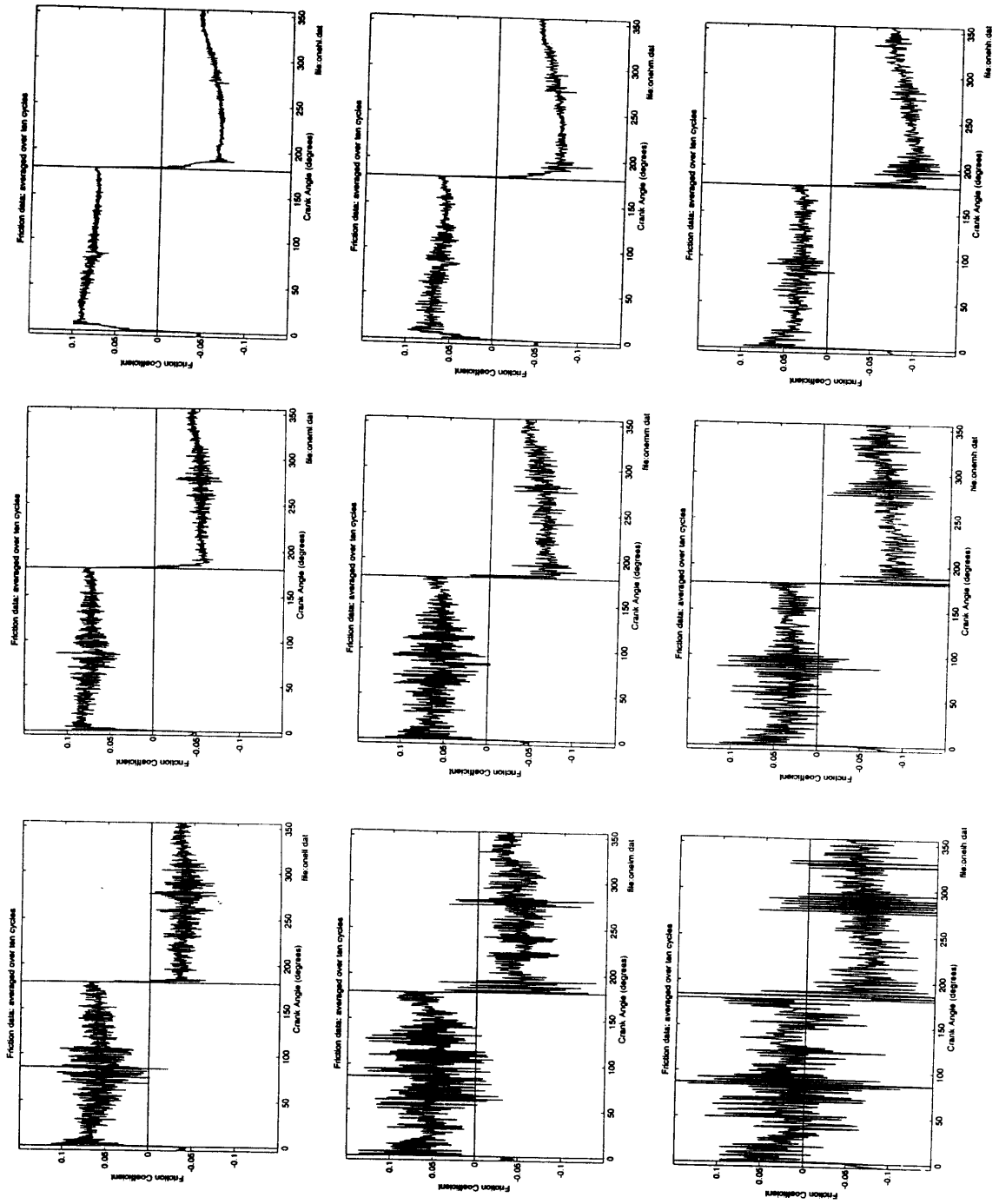
Friction data: averaged over ten cycles
Friction Coefficient
Crank Angle (degrees)
file:oneh1.dat
file:oneh2.dat
file:oneh3.dat
file:onem1.dat
file:onem2.dat
file:onem3.dat
file:onel1.dat
file:onel2.dat
file:onel3.dat

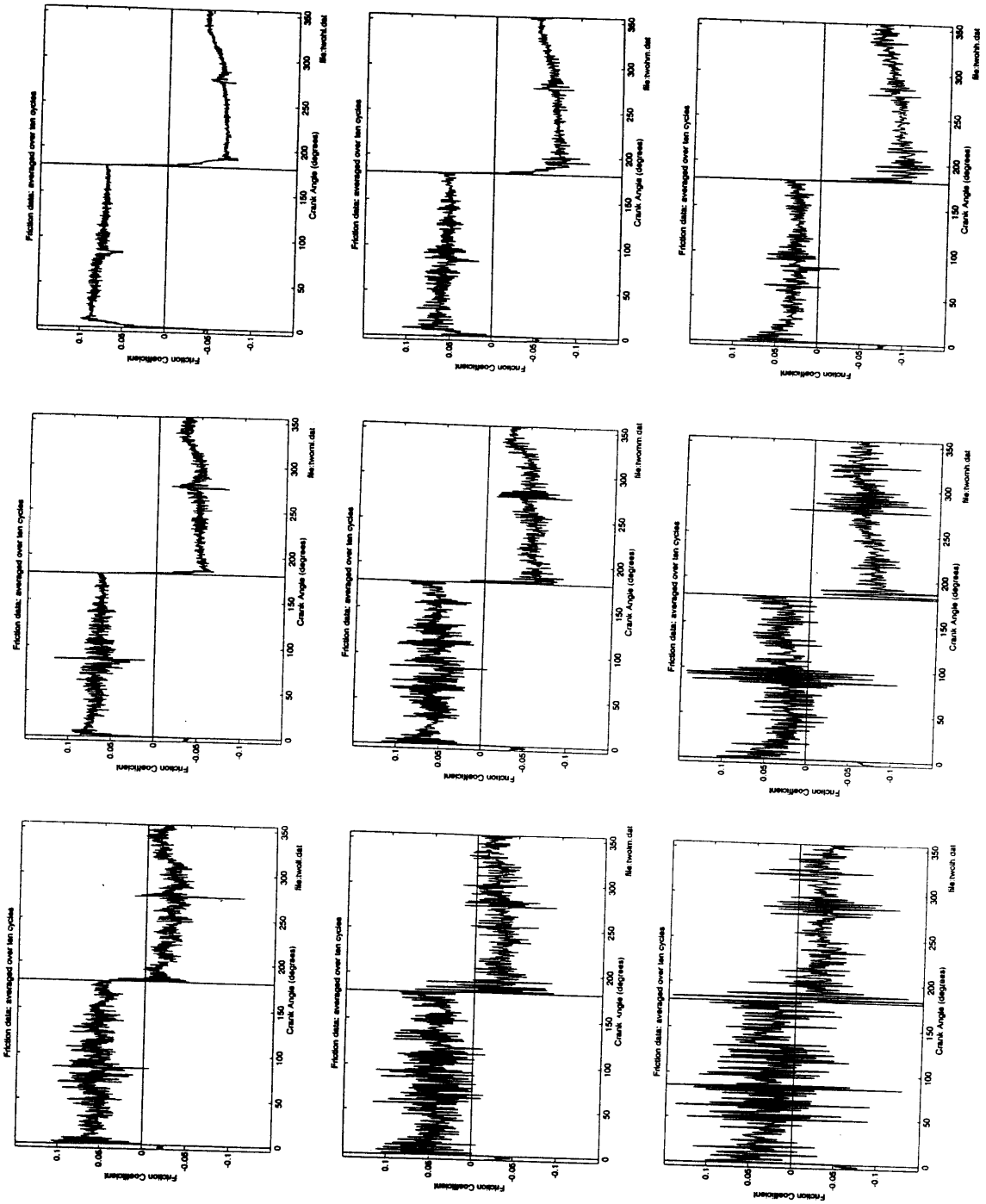
Friction data: averaged over ten cycles
Friction Coefficient
Crank Angle (degrees)
file:twoll.dat
file:twolm.dat
file:twolh.dat
file:twoml.dat
file:twomm.dat
file:twomh.dat
file:twohl.dat
file:twohm.dat
file:twohh.dat

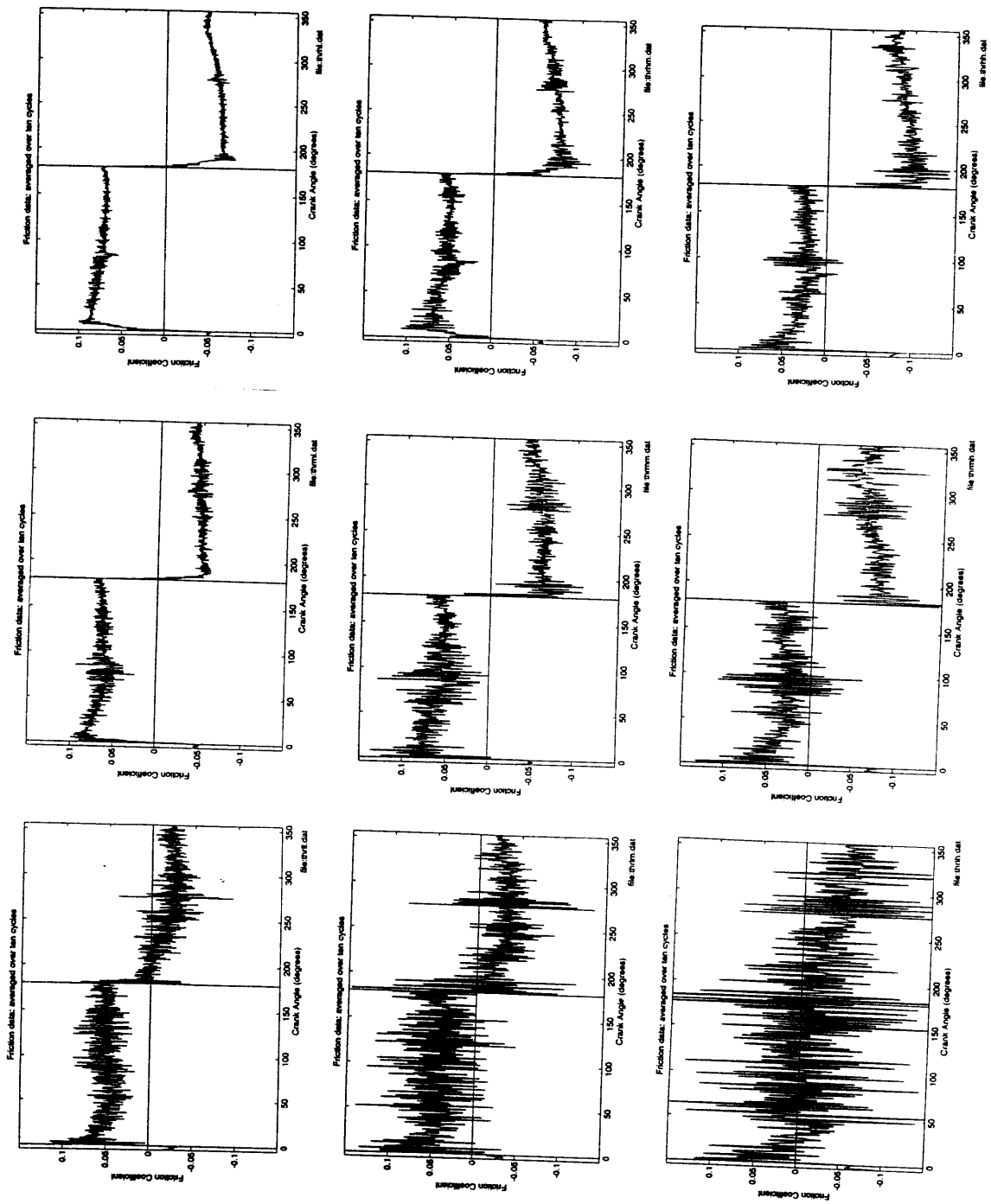
Friction data: averaged over ten cycles
Friction Coefficient
Crank Angle (degrees)
file:thrht.dat
file:thrhm.dat
file:thrhh.dat
file:thrmt.dat
file:thrmm.dat
file:thrmh.dat
file:thrlt.dat
file:thrlm.dat
file:thrlh.dat

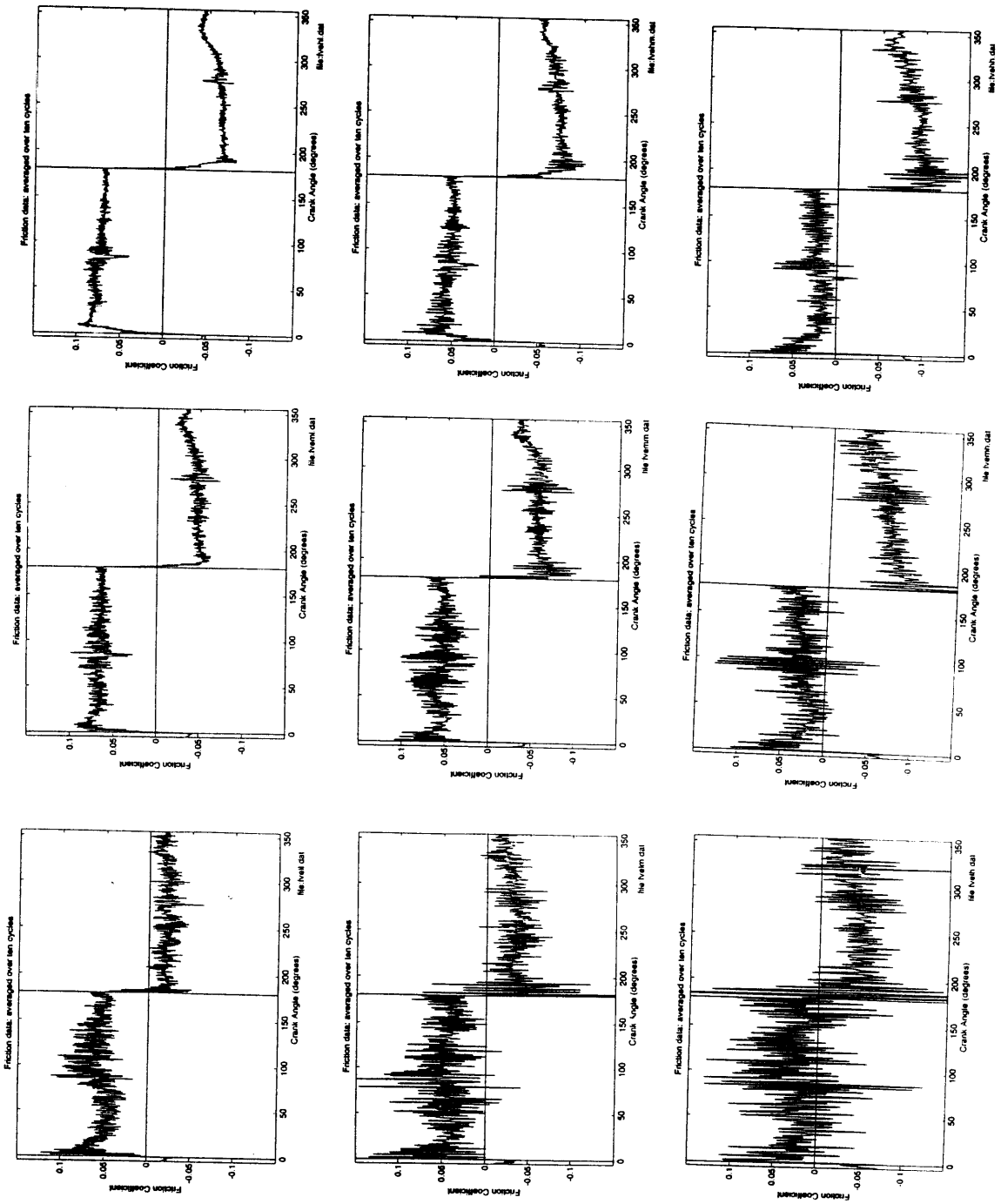
Friction data: averaged over ten cycles
Friction Coefficient
Crank Angle (degrees)
file:hvelt.dat
file:hvelm.dat
file:hvelh.dat
file:hvemt.dat
file:hvemm.dat
file:hvemh.dat
file:hveht.dat
file:hvehm.dat
file:hvehh.dat

Appendix D

Oil Film Thickness Results

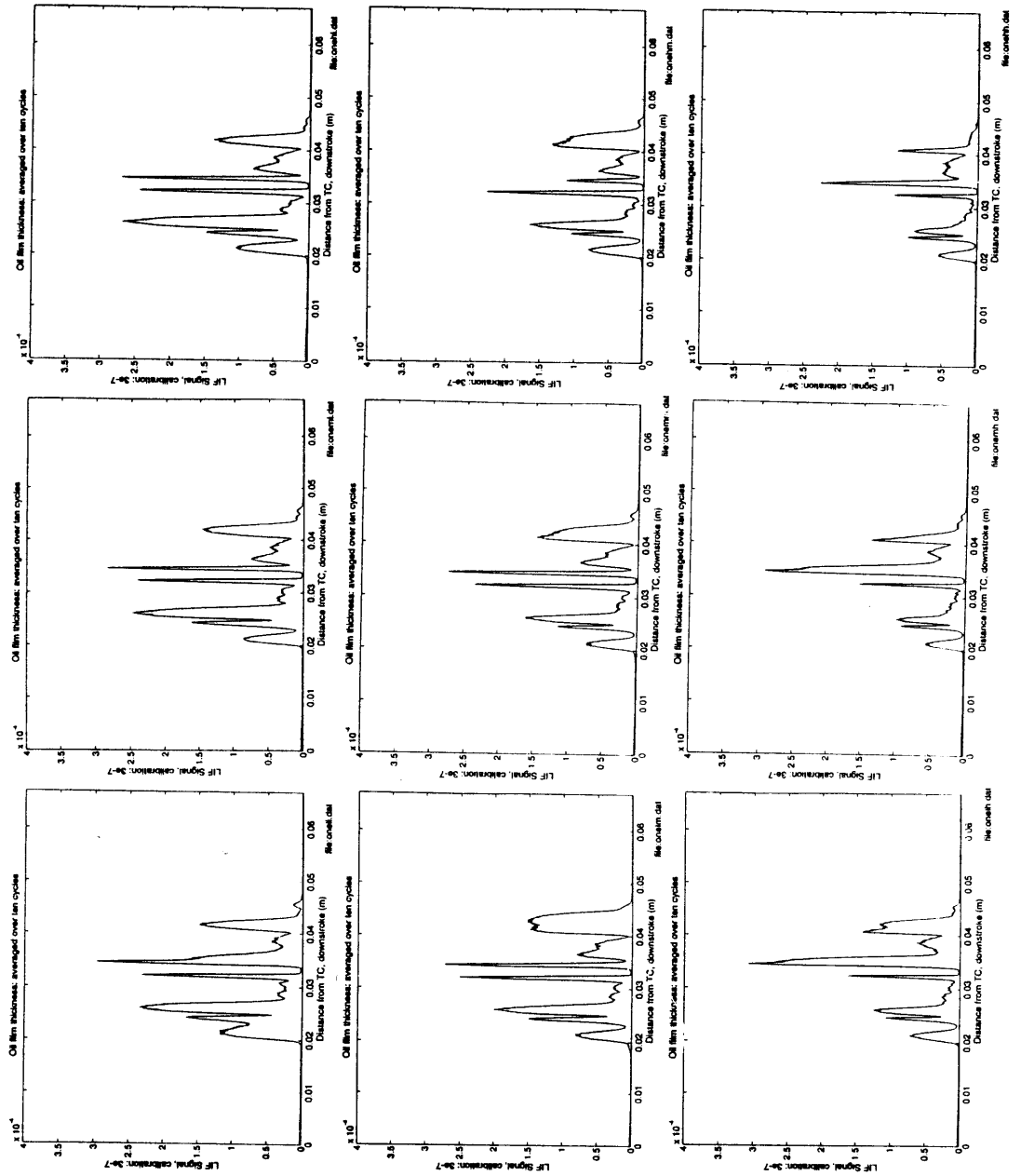
Oil film thickness: averaged over ten cycles
LIF Signal, calibration: 3e-7
Distance from TC, downstroke (m)
file:oneln.dat
file:onelm.dat
file:onelh.dat

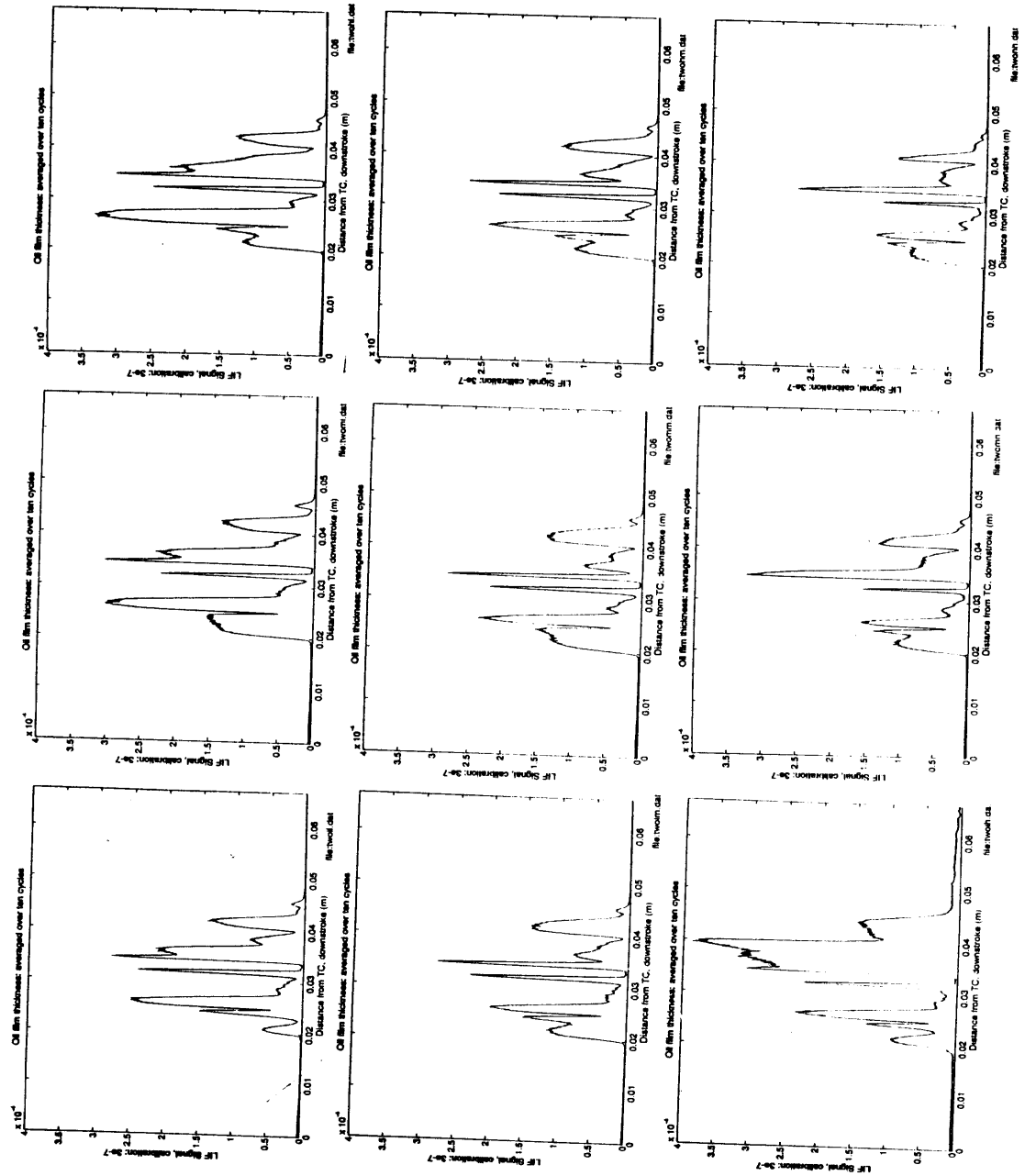
Oil film thickness: averaged over ten cycles
LIF Signal, calibration: 3e-7
Distance from TC, downstroke (m)
file:twoil.dat
file:twoml.dat
file:twomm.dat
file:twoln.dat

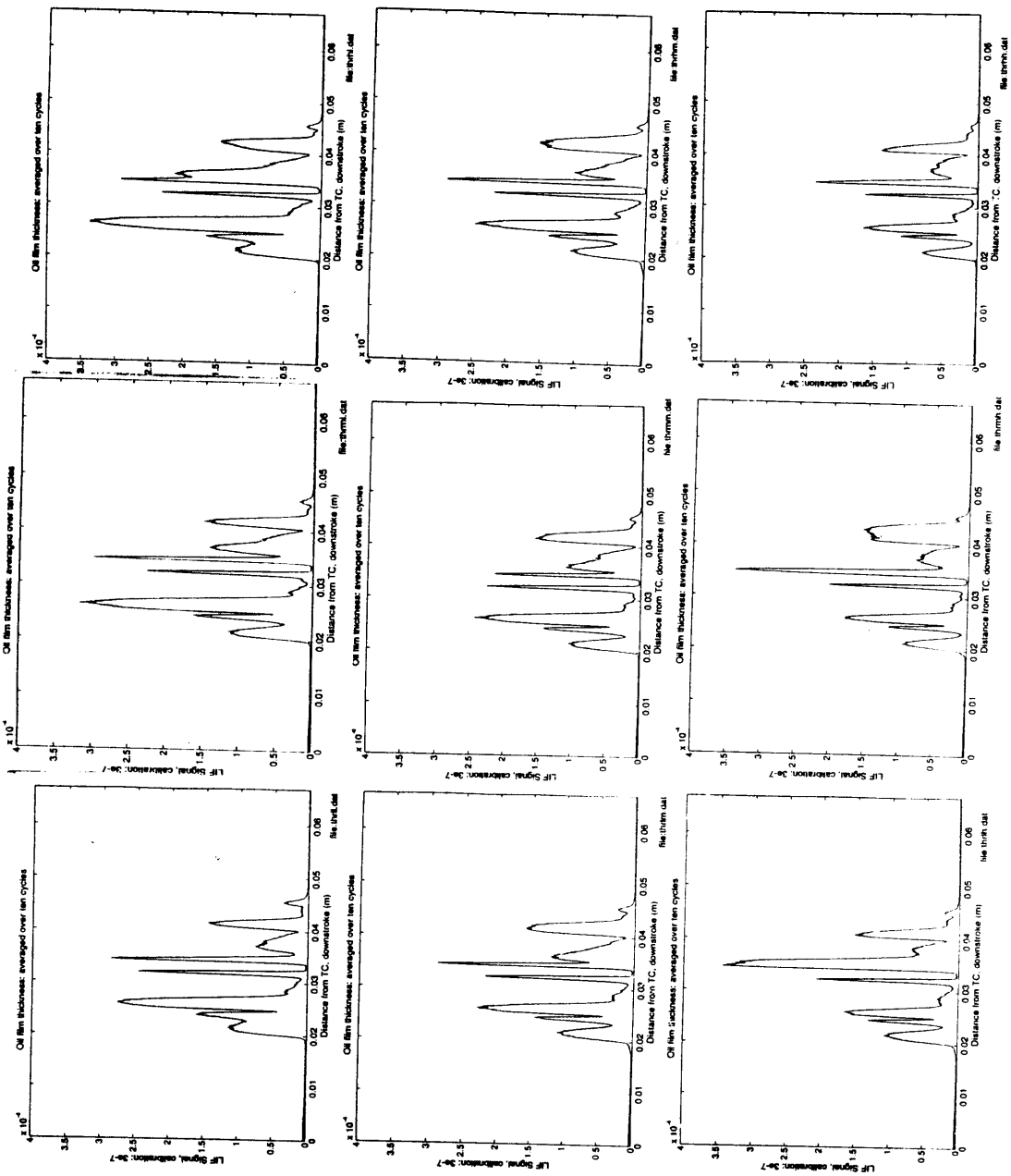
Oil film thickness: averaged over ten cycles
Distance from TC, downstroke (m)
LIF Signal, calibration: 3e-7
file:thrhh.dat
file:thrmh.dat
file:thrml.dat
file:thmhh.dat
file:thmmh.dat
file:thmml.dat
file:thrhh.dat
file:thrmh.dat
file:thrml.dat

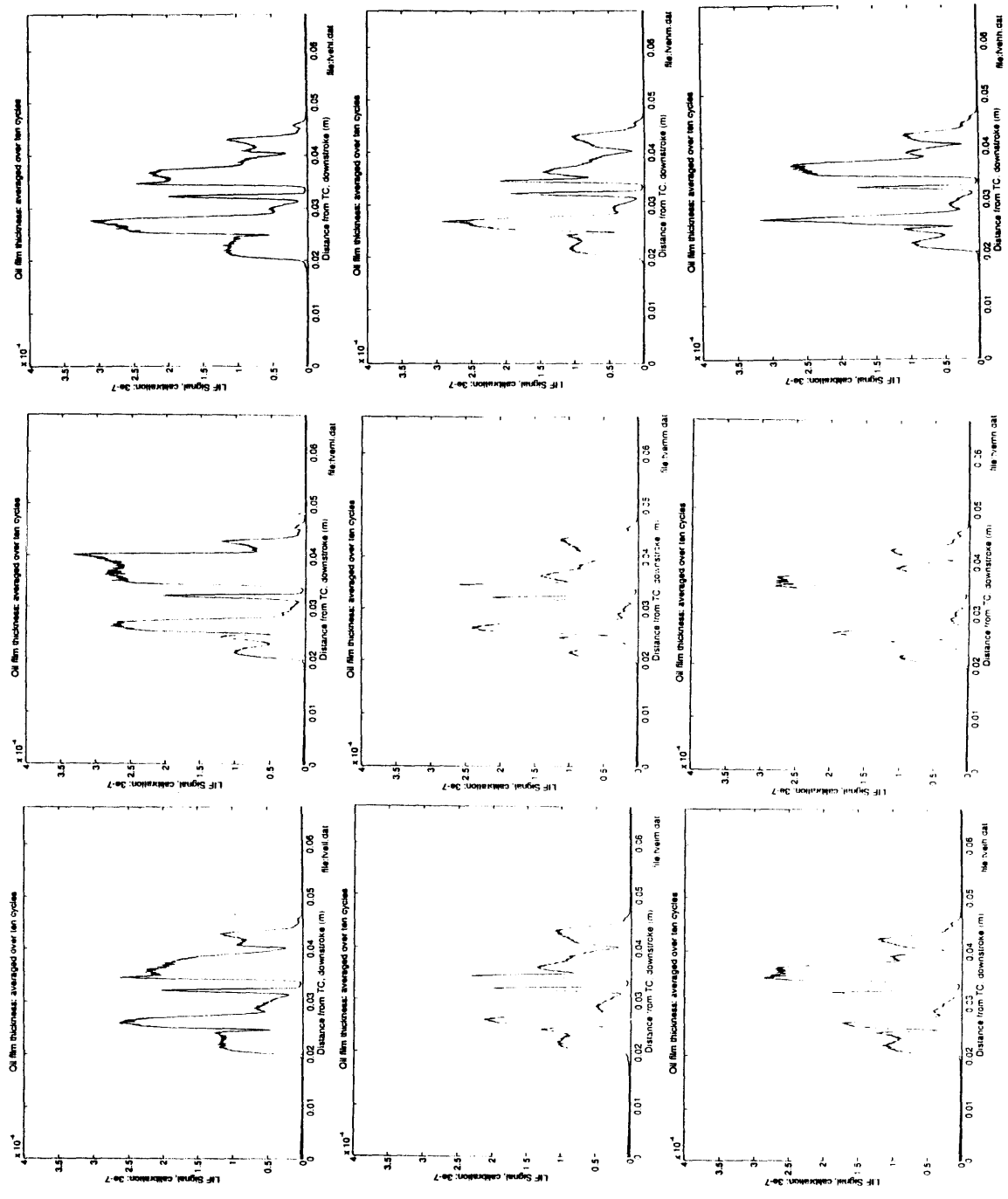
Oil film thickness: averaged over ten cycles
LIF Signal, calibration: 3e-7
Distance from TC, downstroke (m)
file:fvent.dat